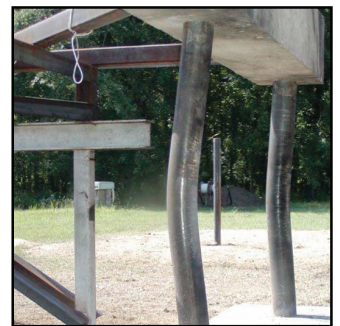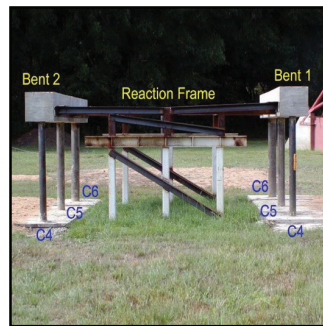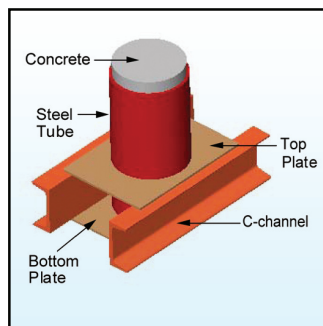# Experimental Investigation of Blast Performance of Seismically Resistant Concrete-Filled Steel Tube Bridge Piers

by

Shuichi Fujikura, Michel Bruneau and Diego Lopez-Garcia

NOTICE

Experimental Investigation of Blast Performance of Seismically Resistant Concrete-Filled Steel Tube Bridge Piers

by

Shuichi Fujikura,[1] Michel Bruneau[2] and Diego Lopez-Garcia[3]

1   Graduate Student, Department of Civil, Structural and Environmental Engineering, University at Buffalo, The State University of New York
2   Professor, Department of Civil, Structural and Environmental Engineering, University at Buffalo, The State University of New York
3   Assistant Professor, Departamento de Ingenieria Estructural y Geotecnica, Pontificia Universidad Catolica de Chile; Formerly Graduate Student, Department of Civil, Structural and Environmental Engineering, University at Buffalo, The State University of New York

MCEER
University at Buffalo, The State University of New York
Red Jacket Quadrangle, Buffalo, NY 14261
Phone: (716) 645-3391; Fax (716) 645-3399
E-mail: *mceer@buffalo.edu*; WWW Site: *http://mceer.buffalo.edu*

Preface

The Multidisciplinary Center for Earthquake Engineering Research (MCEER) is a national center of excellence in advanced technology applications that is dedicated to the reduction of earthquake losses nationwide. Headquartered at the University at Buffalo, State University of New York, the Center was originally established by the National Science Foundation in 1986, as the National Center for Earthquake Engineering Research (NCEER).

Comprising a consortium of researchers from numerous disciplines and institutions throughout the United States, the Center's mission is to reduce earthquake losses through research and the application of advanced technologies that improve engineering, pre-earthquake planning and post-earthquake recovery strategies. Toward this end, the Center coordinates a nationwide program of multidisciplinary team research, education and outreach activities.

MCEER's research is conducted under the sponsorship of two major federal agencies, the National Science Foundation (NSF) and the Federal Highway Administration (FHWA), and the State of New York. Significant support is also derived from the Federal Emergency Management Agency (FEMA), other state governments, academic institutions, foreign governments and private industry.

The Center's Highway Project develops improved seismic design, evaluation, and retrofit methodologies and strategies for new and existing bridges and other highway structures, and for assessing the seismic performance of highway systems. The FHWA has sponsored three major contracts with MCEER under the Highway Project, two of which were initiated in 1992 and the third in 1998.

Of the two 1992 studies, one performed a series of tasks intended to improve seismic design practices for new highway bridges, tunnels, and retaining structures (MCEER Project 112). The other study focused on methodologies and approaches for assessing and improving the seismic performance of existing "typical" highway bridges and other highway system components including tunnels, retaining structures, slopes, culverts, and pavements (MCEER Project 106). These studies were conducted to:

- assess the seismic vulnerability of highway systems, structures, and components;
- develop concepts for retrofitting vulnerable highway structures and components;
- develop improved design and analysis methodologies for bridges, tunnels, and retaining structures, which include consideration of soil-structure interaction mechanisms and their influence on structural response; and
- develop, update, and recommend improved seismic design and performance criteria for new highway systems and structures.

The 1998 study, "Seismic Vulnerability of the Highway System" (FHWA Contract DTFH61-98-C-00094; known as MCEER Project 094), was initiated with the objective of performing studies to improve the seismic performance of bridge types not covered under Projects 106 or 112, and to provide extensions to system performance assessments for highway systems. Specific subjects covered under Project 094 include:

- development of formal loss estimation technologies and methodologies for highway systems;
- analysis, design, detailing, and retrofitting technologies for special bridges, including those with flexible superstructures (e.g., trusses), those supported by steel tower substructures, and cable-supported bridges (e.g., suspension and cable-stayed bridges);
- seismic response modification device technologies (e.g., hysteretic dampers, isolation bearings); and
- soil behavior, foundation behavior, and ground motion studies for large bridges.

In addition, Project 094 includes a series of special studies, addressing topics that range from non-destructive assessment of retrofitted bridge components to supporting studies intended to assist in educating the bridge engineering profession on the implementation of new seismic design and retrofitting strategies.

The objective of this research is to develop and validate a multi-hazard bridge pier concept. A multi-column pier-bent with concrete-filled steel tube (CFST) columns is investigated experimentally to assess the adequacy of such a system under blast loading. This report describes the development of the multi-hazard pier concept, design of the prototype bridge pier under blast and seismic loading, specimen design, experimental set-up, and experimental results. Additionally, the results from the blast experiments are compared with the results from simplified method of analysis considering an equivalent SDOF system with elastic-perfectly-plastic behavior. It is found that the prototype bridge CFST columns can be designed to provide both satisfactory seismic performance and adequate blast resistance. It is also shown that the CFST columns exhibit ductile behavior under blast load in a series of tests at 1/4 scale. Maximum deformation of the columns was calculated using simplified analysis considering a factor to account for the reduction of pressures on the circular column and determined from this experimental program.

ABSTRACT

The terrorist threat on bridges, and on the transportation system as a whole, has been recognized by the engineering community and public officials since recent terrorist attacks. There are some similarities between seismic and blast effects on bridge structures: both major earthquakes and terrorist attacks/accidental explosions are rare events that can induce large inelastic deformations in the key structural components of bridges. Since many bridges are (or will be) located in areas of moderate or high seismic activity, and because many bridges are potential terrorist targets, there is a need to develop structural systems capable of performing equally well under both events.

The objective of this research is to present the development and experimental validation of a multi-hazard bridge pier concept, i.e., a bridge pier system capable of providing an adequate level of protection against collapse under both seismic and blast loading. A multi-column pier-bent with concrete-filled steel tube (CFST) columns is the proposed concept. The work presented here experimentally investigates the adequacy of such a system under blast loading.

This report describes development of the multi-hazard pier concept, design of the prototype bridge pier under blast and seismic loading, specimen design, experimental set-up, and experimental results. Additionally, the results from the blast experiments are compared with the results from simplified method of analysis considering an equivalent SDOF system having an elastic-perfectly-plastic behavior.

It is found that prototype bridge CFST columns can be designed to provide both satisfactory seismic performance and adequate blast resistance. It is also shown that the CFST columns exhibited a ductile behavior under blast load in a series of tests at 1/4 scale. Maximum deformation of the columns could be calculated using simplified analysis considering a factor to account for the reduction of pressures on the circular column and determined from this experimental program.

ACKNOWLEDGMENTS

TABLE OF CONTENTS

TABLE OF CONTENTS (Continued)

TABLE OF CONTENTS (Continued)

LIST OF FIGURES

LIST OF FIGURES (Continued)

LIST OF FIGURES (Continued)

LIST OF FIGURES (Continued)

LIST OF FIGURES (Continued)

LIST OF TABLES

NOTATIONS

A_c	Core concrete area
A_f	Projected area normal to wind
A_g	Peak ground acceleration
B	Cap-beam width
b_f	Flange width of C-channel
c	(1) Damping coefficient (2) speed of sound
c_0	Speed of sound in air at ambient pressure
C	Stiffness coefficient of medium
C_d	Drag coefficient
C_f	Force coefficient
$C_{r\alpha}$	Peak reflected pressure coefficient
d	Depth of C-channel
D	Column diameter
E_c	Secant elastic modulus of concrete
E_s	Elastic modulus of steel
EI_e	Equivalent flexural stiffness
F	Wind load
f_c'	Static compressive strengths of concrete
F_d	Drag force
f_{dc}'	Ultimate compressive strengths of concrete
f_{dy}	Dynamic yield stress of steel
f_{du}	Dynamic ultimate stress of steel
f_p	Yield stress of plate
F_p	In-plane force
f_s	Stress of steel plate
f_u	Static ultimate stress of steel
f_y	Static yield stress of steel
G	Gust-effect factor
H	(1) Column height (2) plate height
i	Unit positive impulse
I	Importance of the facility

NOTATIONS (Continued)

I_c	Moment of inertia of core concrete section
I_D	Equivalent moment of inertia of deck
i_{eq}	Equivalent uniform impulse per unit area
I_{eq}	Equivalent uniform impulse per unit length
$i_r/W^{1/3}$	Scaled unit reflected impulse
i_s^+	Positive impulse
i_s^-	Negative impulse
I_s	Moment of inertia of steel tube section
K	Stiffness
k^*	Generalized stiffness
K_e	Equivalent stiffness
k_c	Stiffness of column
K_E	Equivalent elastic stiffness
K_L	(1) Load factor (2) total stiffness of column in longitudinal direction
K_{LM}	Load-mass factor
K_M	Mass factor
K_P	Stiffness of pier-bent
K_S	Stiffness factor
KE	Kinetic energy
L	(1) Total height of column (2) Total span length
l_p	Plate length
m	Unit mass
m^*	Generalized mass
m_D	Mass of a deck per unit length
M	Total mass
M_e	Equivalent total mass
M_p	Plastic moment capacity of column
O	Likelihood that terrorists will attack the asset
p	(1) External load per unit length (2) maximum pressure
P	(1) Load (2) axial force
p_0	Ambient air pressure
P_e	Equivalent load

NOTATIONS (Continued)

p_{eq}	Equivalent peak pressure
p_r	Peak reflected pressure, reflected overpressure or peak positive normal reflected pressure
P_r	(1) Reflected overpressure, peak positive normal reflected pressure (2) axial design strength
P_{rc}	Factored compressive strength of concrete section
P_{ro}	Factored compressive strength of CFST columns
p_s	Peak overpressure
P_s^+	Peak side-on overpressure, peak overpressure or peak incident pressure
P_s^-	Peak underpressure
P_{so}	Peak incident pressure or peak positive incident pressure
q_s	Peak dynamic pressure
q_z	Velocity pressure
R	(1) Distance from explosion center (2) resistance of column
r_e	Yield resistance of column
R_e	Equivalent resistance of column
r_u	Ultimate resistance of column
R_u	Strength per unit length of column
S_A	Pseudo-acceleration response spectrum
S_D	Elastic displacement response of bridge
T	Natural period of a bridge
T^+	Positive phase duration of blast pressure
T^-	Negative phase duration of blast pressure
t	Thickness of steel tube
t_0	Duration of positive phase of blast pressure
t_a	Arrival time of blast wave
t_d	Duration of positive phase of blast pressure
t_f	Flange thickness of C-channel
t_m	Time at which maximum deflection occurs
t_p	Thickness of plate
U	Strain energy
u_s	Particle velocity behind wave front

NOTATIONS (Continued)

U_s	Blast wavefront velocity
V	Likely damage resulting from various terrorist threats
V_e	Elastic lateral force capacity of column
Z	(1) Scaled distance (2) plastic modulus of C-channel
W	Explosive charge weight
W_{int}	Internal work
W_p	Explosive charge weight
WD	Work done by load
x	Deflection
$\dot{x}$	Velocity
$\ddot{x}$	Acceleration
x_0	Maximum deflection
$\dot{x}_0$	Maximum velocity
X_e	Yield deflection of column
X_E	Equivalent maximum elastic deflection
X_m	Maximum deflection
X_p	(1) Horizontal distance between center of an explosive charge weight and a pier (2) Plastic deflection
X_{test}	Maximum residual deformation from test
X_u	Displacement capacity of column
z	Height of column
Z	(1) Scaled distance (2) plastic modulus of steel tube
α'	Critical angle of incident blast wave
α_I	Angle of incident blast wave
$\alpha_{I \cdot crit}$	Critical angle of incident blast wave
α_R	Angle of reflected blast wave
β	Shape factor
δ	Normalized deflected shape of column
Δ_u	Displacement demand
Δ_y	Elastic displacement capacity of column
ε	Strain of steel plate
ε_u	Rupture strain

NOTATIONS (Continued)

ϕ_p	Strength factor
θ_u	Rotation capacity of column
μ	Displacement ductility demand
ρ	(1) Density of medium (2) triple point
ρ_0	Density of air at ambient pressure
ρ_s	Air density behind wavefront
σ_{max}	Maximum normal stress of steel plate
ψ	Deformation shape

ABBREVIATIONS

AASHTO   American Association of State Highway and Transportation Officials
BEL   Bridge Explosive Loading
CFST   Concrete-Filed Steel Tube
DIF   Dynamic Increase Factor
FHWA   Federal Highway Administration
FRP   Fiber-Reinforced Plastic

SECTION 1
INTRODUCTION

1.1 Motivation for Research

Recent terrorist attacks such as the one on the Alfred P. Murrah Federal Building in Oklahoma City (1995) and the one on the tallest towers of the World Trade Center in New York City (2001) are examples of the fact that the destruction of civil engineering structures has become one of the means employed by terrorists to achieve their objectives. Although bridge structures in North America have not been attacked so far, the terrorist threats received by the state of California to its main suspension bridges and the detailed shots of the Golden Gate and Brooklyn bridges found among the possessions of terrorists captured in Spain indicate that bridge structures are definitely being considered as potential targets by terrorist organizations (Williamson and Winget 2005). While much focus of these threats has been on large landmark bridges due to their symbolic nature, the destruction of regular bridges along routes that are key lifelines to specific regional economies is also foreseeable due to the significant disruption these attacks can create and the possibly simpler logistics in their planning. The terrorist threat on bridges, and on the transportation system as a whole, has been recognized by the engineering community and public officials, which resulted in the recent publication of a number of documents addressing this concern (see, for instance, FHWA 2003).

One of the courses of action by which terrorists might seek the destruction of bridge structures consists of detonating an explosive device (Williamson and Winget 2005). The explosion creates an atmospheric blast wave, which in turn induces pressures of significant magnitude on structural members. Since these pressures (usually referred to as "blast loads") are typically not accounted for in the design process, intentional explosions can result in significant damage in structural members, which in turn might result in partial or total collapse of the structure.

There is a need to develop bridge structural systems capable of providing an adequate level of protection against intentional blast loads. However, due to the limited resources available to reduce the vulnerability of the transportation system, the characteristics of such systems (e.g.,

1

size, structural configuration, materials and cost) should not be significantly different from those of the systems typically being used in bridge structures.

Any blast-resistant structural system must also be able to perform satisfactorily under all of the other loads acting on bridge structures, including those due to other extreme events, such as earthquakes. In this regard, it is interesting to note that there are some important similarities between seismic and blast effects on bridge structures: both major earthquakes and terrorist attacks are rare events, and, due to economic considerations, most of the energy imparted to structural members by these events is dissipated through inelastic deformations rather than elastically absorbed. Given the fact that: (a) current codes require that bridge structures be designed for some level of seismic action in most regions across the US; and (b) blast and seismic loads often control the design, there is a need for structural systems capable of performing equally well under both seismic and blast loads.

The objective of this research project is to develop and experimentally validate such a multi-hazard bridge pier concept, i.e., a bridge pier system capable of providing an adequate level of protection against collapse under both seismic and blast loading, and whose structural, construction and cost characteristics are not significantly different from those of the pier systems currently found in typical highway bridges in the US. As will be shown later in this report, the proposed pier system is a pier-bent where concrete-filled steel tube columns frame into beams made up of C-shape steel sections embedded in the fiber-reinforced concrete foundation and pier cap.

1.2   Scope of Research

The multi-hazard bridge pier-bent concept proposed in this study is intended for use in typical highway bridges only. Although the terrorist threat to this type of bridges is usually assumed to be of lesser magnitude than that assigned to large signature bridges, the threat, especially to the ones strategically located, is nevertheless real and worthy of consideration (Winget et al. 2005). In fact, terrorist groups might prefer to attack typical highway bridges because their destruction requires less effort (in terms of necessary expertise, amount of explosives and need to account for surveillance) than that required to destroy a large signature bridge.

There are many possible courses of action by which terrorists might intend to destroy a bridge structure. The bridge pier-bent concept proposed in this study was developed considering only one type of terrorist threat: the detonation of explosives located inside a small vehicle placed below the deck at close distance to the pier (details will be explained in the next section). Other possible courses of action, such as the detonation of hand-placed explosives and collisions using large vehicles, were not considered.

1.3   Organization of This Report

Following this introduction, a review of research related to blast-resistant design of bridges is discussed in Section 2. The development of the bridge pier concept proposed in this study, along with details of the assumed blast scenario, is presented in Section 3. The design of the test specimens is presented in Section 4, along with a description of the intended test program. Next, experimental observations are summarized in Section 5. Test results are presented in Section 6, along with a comparison with theoretical predictions. Conclusions are summarized in Section 7, which also includes some recommendations for future research.

Finally, note that for security reasons, some key details of this blast-related study is withhold from this report. More specifically, the numerical values of some key quantities are not provided. Instead, results are presented in terms of parameters. The values of all of these parameters will be listed in a special Appendix, which will be made available to selected individuals.

SECTION 2
LITERATURE REVIEW

2.1   General

There are three widely used documents dealing with blast resistant design available in the public domain; *Design of Structures to Resist Nuclear Weapons Effects* (ASCE Manual 42 1985), *Structures to Resist the Effects of Accidental Explosions* (USDA 1990) and *Design of Blast Resistant Buildings in Petrochemical Facilities* (ASCE 1997). The target structures in these documents have been mission-critical structures such as army facilities, governmental buildings and petrochemical facilities. The current knowledge of structural design for blast-resistance is limited to buildings rather than bridges. Moreover, bridge engineers and planners have typically not considered designing for bridges against blast loading before the tragedies of September 11th. Therefore, there are no comprehensive design guidelines and specifications for bridges subjected to blast loading. Furthermore, little research is available on this topic and all of it is very recent and still on-going.

In this section, airblast effects are reviewed to summarize the physical effect of explosion. Then, the simplified method used for the analysis of structures subjected to blast loads, where the structure is considered as an SDOF system, is presented. Finally, structural element behavior under blast loading is presented followed by recent research on blast-resistant design of bridges.

2.2   Airblast Effects

This section is a brief review of blast effects of freely expanding shocks in air. Although the response of structure under blast loading is of primary concern in this report, it is important to know the characteristics of the shock wave itself as a result of an explosion (before it strikes a structure). Blast scaling law and blast wave parameters are described followed by a description of the characteristics of reflected wave and the effects of free air and surface bursts.

2.2.1. Blast Scaling Law

When experimentally investigating the effect of explosions on structures (or for other purposes), full scale testing is desirable. However, such full scale (or even large scale) tests are expensive. Several scaling laws have been proposed to expand the applicability of the experiments conducted at different scales (Baker 1973).

The most common scaling law is Hopkinson or "cube-root" scaling law. Hopkinson (1915) stated that "self-similar blast (shock) waves are produced at identical scaled distances when two explosive charges of similar geometry and the same explosive, but of different size, are detonated in the same atmosphere" (quoted by Baker 1973). The scaled distance, Z, is given by:

$$Z = \frac{R}{W^{1/3}} \tag{2-1}$$

where R is the distance from the center of the explosion and W is the explosive charge weight. According to this law, a same pressure occurs at given distances from the explosions with identical charge shapes and identical charge-to-surface geometries in identical ambient conditions if the explosions are at the same scaled distances. This law has been empirically confirmed by many researchers over the years for a variety of explosive charges ranging from a few pounds up to thousand pounds (Baker 1973).

2.2.2. Blast Wave Parameters

When explosive materials detonate, shock waves are created. The shock wave in the air is a traveling front of abruptly higher pressure and temperature moving at high speed, the magnitude of which is a function of the size of the explosion. High pressures are created by the compression of air itself triggered initially by the expansion in volume of the exploding mass. This high-pressure disturbance in the air can cause the damage of structures. The shock wave front expands outward from the center of the detonation with the pressure of the compressed air decaying with increasing distance.

Figure 2-1 shows an ideal blast wave profile for a blast wave in free air, where t_a is the arrival time of the blast wave and p_0 is the ambient pressure of the air when the explosion takes place. The blast wave has two phases over its duration; the positive and negative phase. Parameters that define the positive phase are the peak side-on overpressure, P_s^+, (also called peak
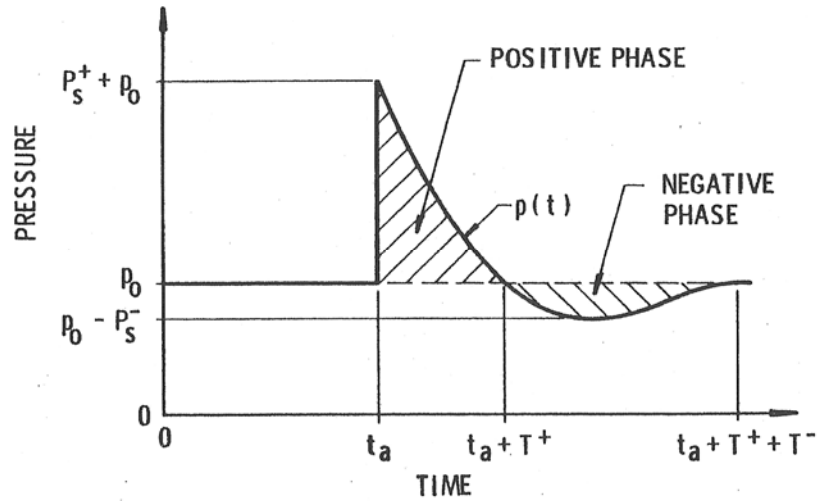
Figure 2-1   Ideal Blast Wave Profile (Baker 1973)

overpressure or peak incident pressure, and this overpressure is the maximum pressure reached above the ambient pressure at the point of interest), the positive phase duration, T^+, and the associated positive impulse, i_s^+. This positive impulse is equal to the area beneath the pressure-time curve in the positive phase. Likewise, P_s^-, T^- and i_s^- are identically defined for the negative phase except that P_s^- is called peak underpressure. In most studies of structural response to blast loading, only the blast parameters associated with the positive phase are considered since those in the negative phase are generally negligible. Note that the impulse is a useful parameter in assessing the effect of blast on the structures, as will be shown later (Baker 1973).

Brode (1955) theoretically showed that the peak overpressure, p_s (same as P_s^+ in Figure 2-1), in the near field and in the medium to far field can be expressed by the equations below:

$$p_s = \frac{6.7}{Z^3} + 1 \ \text{ bar} \ \ (p_s > 10 \text{ bar, near field}) \tag{2-2}$$

$$p_s = \frac{0.975}{Z} + \frac{1.455}{Z^2} + \frac{5.85}{Z^3} - 0.019 \ \text{ bar} \ \ (0.1 < p_s < 10 \text{ bar, medium to far field}) \tag{2-3}$$

In these equations, Z is the scaled distance defined by Equation 2-1, where the distance from the center of the explosion is in meters and the explosive charge weight is in kilograms. The predicted values in the near field do not match the experimental results very well due to the complexity of the flow process in the near field range (Smith and Hetherington 1994).

In addition, a number of other wavefront parameters can be important to determine the blast load on a structure, such as the peak reflected pressure, p_r, blast wavefront velocity, U_s, the particle velocity behind the wave front, u_s, air density behind the wavefront, ρ_s, and peak dynamic pressure, q_s, depending on whether the blast is a free air burst or a surface burst as will be shown in the following sections. In practice, p_s, p_r and U_s are typically expressed in normalized format, which makes it possible to plot them on graphs expressed in terms of scale distance. Such graphs are presented in the following sections.

The theoretical basis to characterize normal shocks in ideal gasses can be derived from Rankine-Hugoniot conditions (Rankine 1870) based on the conservation of mass, energy and momentum at the shock wave front (Glasstone, S. and Dolan, P.J. ed. 1977). The resulting parameters of U_s, u_s, and ρ_s in air, defined above and predicted by this theory, are given by the equations below:

$$U_s = \sqrt{1 + \frac{6p_s}{7p_0}} \cdot c_0 \tag{2-4}$$

$$u_s = \frac{5p_s}{7p_0} \cdot \frac{1}{\sqrt{1 + 6p_s/7p_0}} \cdot c_0 \tag{2-5}$$

$$\rho_s = \frac{6p_s + 7p_0}{p_s + 7p_0} \cdot \rho_0 \tag{2-6}$$

where p_0 is the ambient air pressure ahead of the blast wave, ρ_0 is the density of air at ambient pressure ahead of the blast wave, and c_0 is the speed of sound in air at ambient pressure.

The dynamic pressure, q_s, is important to calculate the drag force due to a moving shock wave. When the shock wave moves around a structure, the structure experiences a drag force, F_d, defined by:

$$F_d = q_s C_d \tag{2-7}$$

where q_s is the peak dynamic pressure and C_d is the drag coefficient which depends on the shape of the structure (Glasstone, S. and Dolan, P.J. ed. 1977). The dynamic pressure in air is the pressure produced by the wind behind the blast wavefront. This dynamic pressure is given by Bernoulli's equation:

$$q_s = \frac{1}{2} \rho_s u_s{}^2 \tag{2-8}$$

From Equations 2-5, 2-6 and 2-8, the resulting dynamic pressure is given by:

$$q_s = \frac{5}{2} \cdot \frac{p_s{}^2}{p_s + 7p_0} \tag{2-9}$$

2.2.3. Reflected Wave with Normal Reflection

If a shock wave strikes an infinitely rigid wall at an angle normal to the direction of the wave propagation, a reflected overpressure develops on the surface immediately. The moving air molecules of the blast wave are brought to rest and compressed on the wall, which induces a reflected overpressure. Hence, the reflected overpressure is considerably greater than the incident overpressure (Smith and Hetherington 1994). The peak reflected overpressure, p_r, for air derived from Rankine-Hugoniot conditions (and described in many books such as Glasstone, S. and Dolan, P.J. ed. 1977) is given by:

$$p_r = 2p_s + \frac{12}{5} q_s \tag{2-10}$$

where p_s and q_s are defined previously. Substituting Equation 2-9 into Equation 2-10 gives:

$$p_r = 2p_s \left(\frac{7p_0 + 4p_s}{7p_0 + p_s} \right) \tag{2-11}$$

By inspection of Equation 2-11, it is seen that p_r ranges from 2 times of p_s when $p_s \ll p_0$, to 8 times of p_s when $p_s \gg p_0$ (when $p_s = 0$, $p_r = 0$ because of the discontinuity at this point). The ratio of p_r/p_s is defined as the peak reflected pressure coefficient, $C_{r\alpha}$. However, in some instances, p_r could be 20 times p_s due to gas dissociation effects that are chemical processes in which molecules split into smaller molecules caused by a change in physical condition and that occur at very close range (Mays and Smith 1995).

2.2.4. Reflected Wave with Oblique Reflection

Oblique reflection is classified under two categories: regular reflection and Mach reflection, depending on the incident angle and shock strength (Baker et al. 1983). Regular reflection is illustrated in Figure 2-2, where α_I is the angle of incident blast wave with respect to the wall and α_R is the angle of reflected blast wave. Note that, for a given strength of p_r, there exists a

9
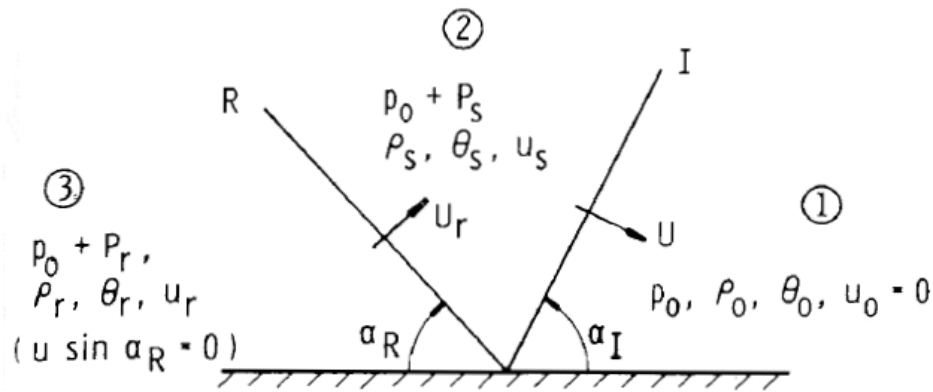
Figure 2-2   Regular Reflection (Baker et al. 1983)

limiting angle of incidence, $\alpha_{I\text{-}crit}$, above which regular reflection cannot occur but Mach reflection occurs instead. Also, for each gas, there is an angle α' above which the reflected pressure is greater than the normal reflected pressure ($\alpha_I = 0$). This angle α' is approximately 40° for air.

Figure 2-3 illustrates the geometry of the Mach reflection process. As stated above, the Mach reflection process occurs when the angle of incidence, α_I , exceeds a limiting value of $\alpha_{I\text{-}crit}$. This process develops due to the interaction between the incident and reflected blast waves (Bulson 1997). When the incident wave strikes a rigid surface, the reflected shock wave travels faster than the incident wave because the reflected overpressure is much greater than the incident overpressure. When the reflected wave overtakes the incident wave after the reflection, the reflected wave merges with the incident wave forming a single outward traveling front wave, called the Mach stem. The intersection of these three shock waves is called the triple point whose path is shown as ρ in Figure 2-3. Note that, since the shock wave velocity is a function of the overpressure as defined in Equation 2-4, the wave travels faster when the overpressure is greater. Incidentally, the shock wave is different from the sound wave. In general, the speed of sound c is given as:

$$c = \sqrt{\frac{C}{\rho}} \tag{2-12}$$

10
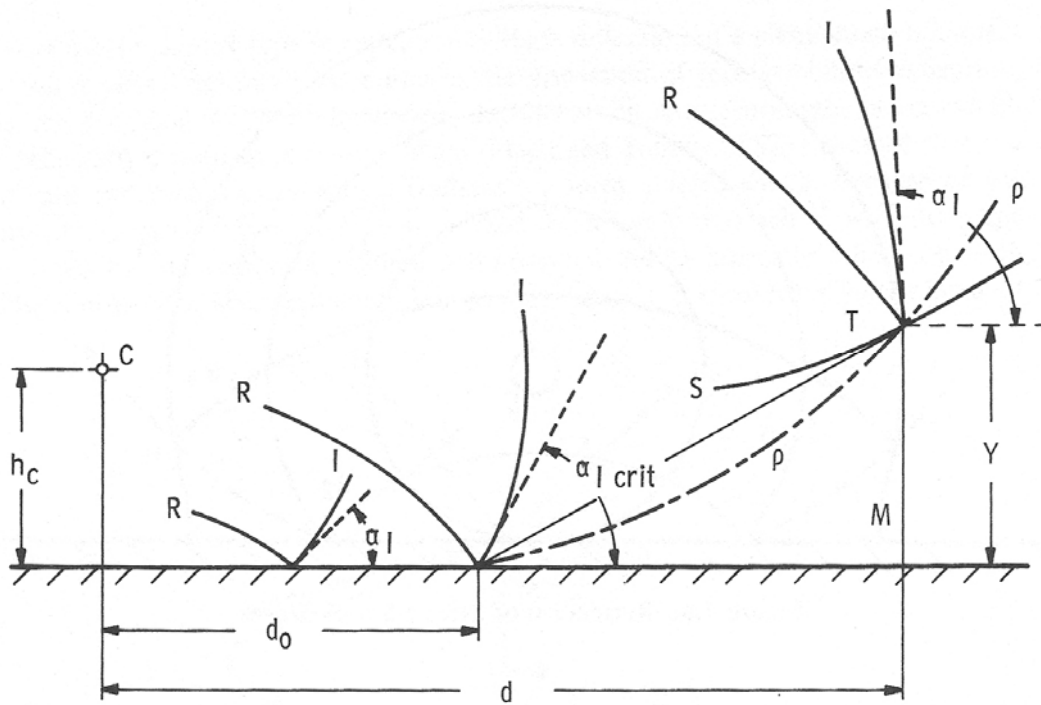
Figure 2-3   Mach Reflection (Baker 1973)

where C and ρ are the stiffness coefficient and density of the medium, respectively. For air, C equals 1.420 x 10^5 kg m^{-1} s^{-2} and ρ is 1.204 kg m^{-3}. Therefore, the speed of sound does not depend on the intensity of the sound but the properties of the medium.

If the shock wave strikes on the structure at an oblique incidence, the reflected peak pressure is a function of the incident pressure and the incident angle. Figure 2-4 (USDA 1990) shows the effect of the angle of incidence, α_I, on the peak reflected pressure expressed as a peak reflected pressure coefficient, $C_{r\alpha}$, defined previously. The peak reflected pressure, p_r, is calculated by multiplying the peak reflected pressure coefficient, $C_{r\alpha}$, by the peak incident pressure, p_{so}. For example, when the peak incident pressure, p_{so} is 3000 psi and the angle of incidence, α_I is 20 degrees, the reflected pressure coefficient, $C_{r\alpha}$ results in 10 according to Figure 2-4. Note that the value of $C_{r\alpha}$ in Figure 2-4 exceeds the theoretical maximum coefficient of 8 predicted by Equation 2-11 (α_I=0) as described in Section 2.2.3.
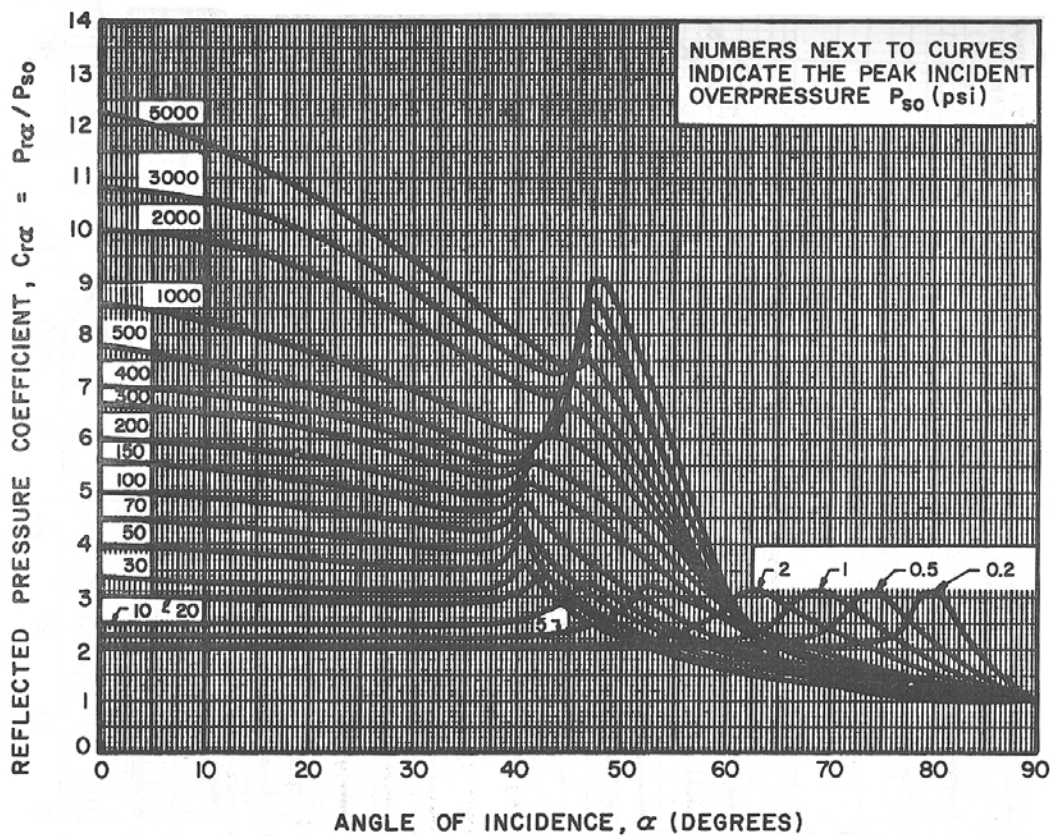
Figure 2-4   Reflected Pressure Coefficient Versus Angle of Incidence (USDA 1990)

2.2.5. Free Air Bursts

When a shock wave strikes a structure as a result of a free-air burst (or spherical explosion), there are no amplification of the initial shock wave pressures between the explosive charge and the structure. The situation corresponds to that shown in Figure 2-5 (USDA 1990). As mentioned above, the blast wave parameter values can be normalized and plotted against scale distance (as shown in Figure 2-6 for spherical explosions). For the purpose of the current research, peak positive incident pressure (or peak overpressure), P_{so}, peak positive normal reflected pressure (or peak reflected pressure), P_r and positive normal reflected impulse (or reflected impulse), i_r are important parameters in this figure. For example, when the explosive charge and the standoff distance are, respectively, 100 lb of TNT and 4.64 ft, the scaled distance, Z, would be 1. At this scaled distance, the peak overpressure, P_{so}, peak reflected pressure, P_r and scaled unit reflected impulse, $i_r/W^{1/3}$, respectively, are 800 psi, 7,000 psi and 200 psi-

12

ms/lb$^{1/3}$ according to Figure 2-6. Note that the peak reflected pressure is larger than the peak overpressure by an order of magnitude. The peak reflected pressure, P_r, rapidly drops with scaled distance. For instance, when the scaled distance increases by 10 times from 1 to 10, the peak reflected pressure decreases from 7,000 psi to 15 psi. The peak overpressure, P_{so}, and the scaled unit reflected impulse, $i_r/W^{1/3}$, similarly drop with scaled distance. As expressed in a log- log scale, these variations are somewhat linear.
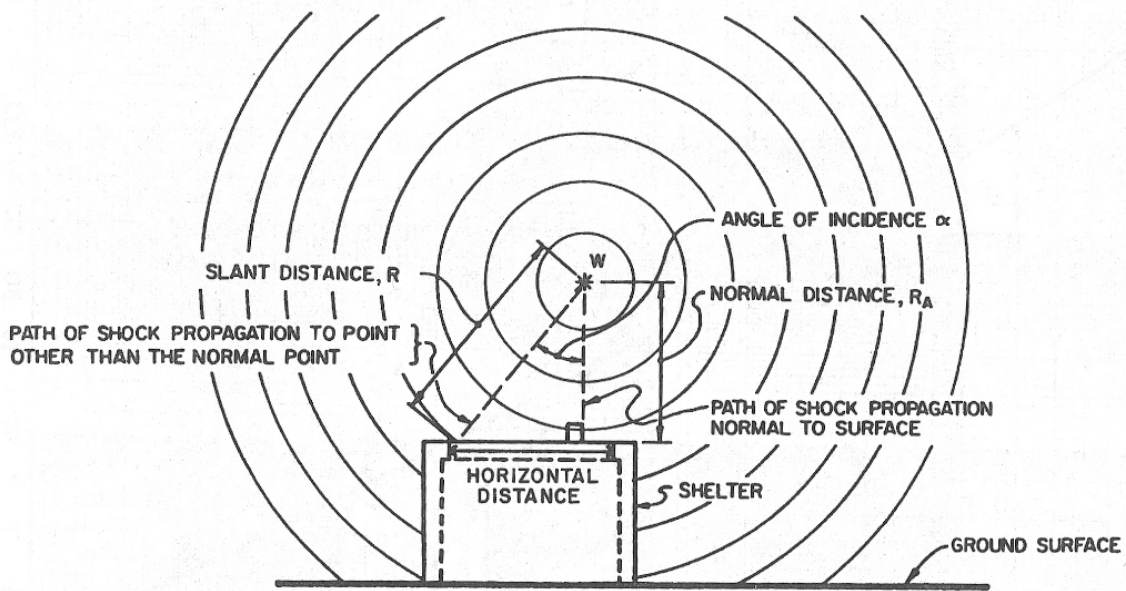
Figure 2-5   Free-air Burst Blast Environment (USDA 1990)

Figure 2-6   Shock Wave Parameters for Spherical TNT Explosion in Free Air (USDA 1990)

2.2.6. Surface Bursts

When the charge is in contact with the ground or close to the ground surface, the explosion is considered to be a surface burst (Figure 2-7). In such case, the initial shock is amplified at the point of detonation, forming a single wave similar to the reflected wave of the airburst, and the shape is essentially hemispheric (USDA 1986). USDA (1990) presented shock wave parameters for this hemispherical explosion in free air as shown in Figure 2-8. The way to use this figure is identical to what was previously explained for Figure 2-6. Note that all of the parameters for surface bursts are larger than those for the corresponding free-air bursts, typically by a factor of 1.8; in other words, a hemispherical explosion releases a shock wave having 1.8 times larger energy than the corresponding spherical explosion (Smith and Hetherington 1994). Note that this factor would be 2.0 if a hemispherical explosion perfectly reflected on the ground such that no energy was absorbed by the ground. To calculate this factor, when the scaled distance, $Z = 1$, the factor of scaled unit reflected impulse, $i_r/W^{1/3}$, for example, is 1.75 (the values of $i_r/W^{1/3}$ for free-air bursts and surface bursts are 200 and 350 psi-ms/lb$^{1/3}$, respectively).
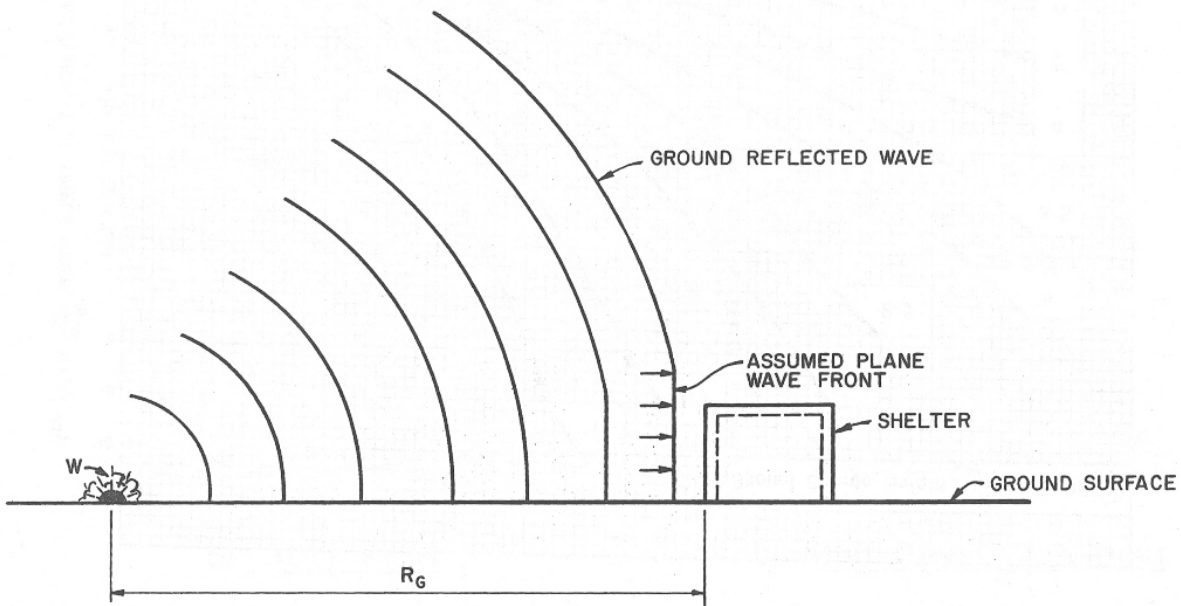
Figure 2-7   Surface Burst Blast Environment (USDA 1990)

CHARGE SURFACE

$\frac{L_W}{W^{1/3}}$, P_r, P_{so}, $\frac{i_r}{W^{1/3}}$, $\frac{i_s}{W^{1/3}}$, U

$\frac{t_A}{W^{1/3}}$, $\frac{t_o}{W^{1/3}}$

SCALED DISTANCE $Z_e = R_e/W^{1/3}$

P_r
P_{so}
$i_r/W^{1/3}$
$t_o/W^{1/3}$
$i_s/W^{1/3}$
U
$t_A/W^{1/3}$
$L_W/W^{1/3}$
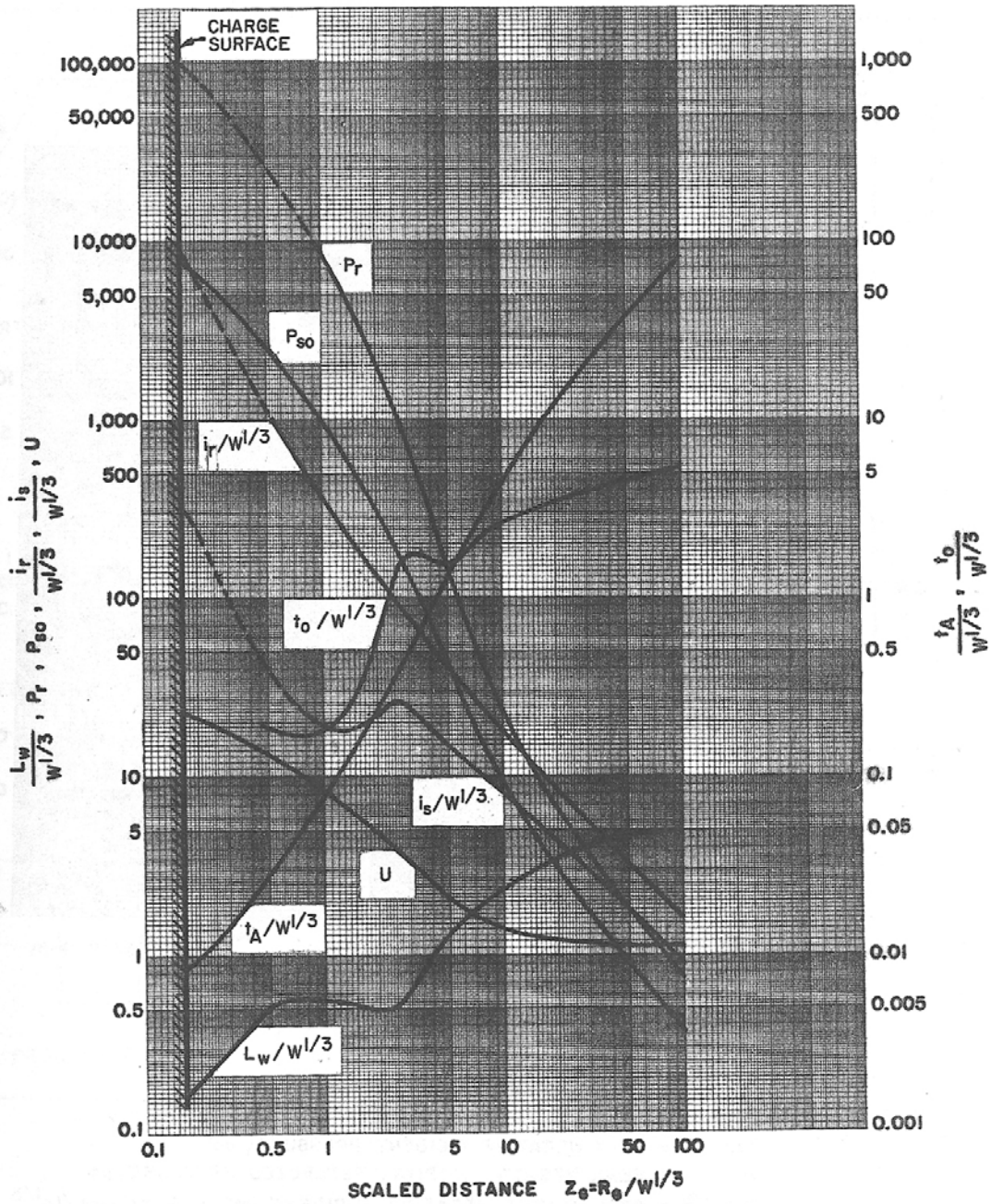
P_{so} = PEAK POSITIVE INCIDENT PRESSURE, psi
P_r = PEAK POSITIVE NORMAL REFLECTED PRESSURE, psi
$i_s/W^{1/3}$ = SCALED UNIT POSITIVE INCIDENT IMPULSE, psi-ms/lb$^{1/3}$
$i_r/W^{1/3}$ = SCALED UNIT POSITIVE NORMAL REFLECTED IMPULSE, psi-ms/lb$^{1/3}$
$t_A/W^{1/3}$ = SCALED TIME OF ARRIVAL OF BLAST WAVE, ms/lb$^{1/3}$
$t_o/W^{1/3}$ = SCALED POSITIVE DURATION OF POSITIVE PHASE, ms/lb$^{1/3}$
U = SHOCK FRONT VELOCITY, ft/ms
W = CHARGE WEIGHT, lbs
$L_W/W^{1/3}$ = SCALED WAVE LENGTH OF POSITIVE PHASE, ft/lb$^{1/3}$

Figure 2-8   Shock Wave Parameters for Hemispherical TNT Explosion in Free Air (USDA 1990)

16

2.3 Simplified Blast Analysis by Equivalent SDOF System

2.3.1. General

The simplified analysis procedure described below is commonly used in blast resistant design. Smith and Hetherington (1994), and Mays and Smith (1995) provide good descriptions of the method. The analysis procedure considers an equivalent SDOF system having an elastic-perfectly-plastic behavior, and assumes that all the energy imparted to the system by the blast loading is converted into internal strain energy.

Structural response under blast loading depends on the response time of the structure relative to the duration of the explosion. USDA (1990) categorized the relationship between these two parameters into three design ranges, which are impulsive load, pressure-time load (also called dynamic load) and pressure load (also called quasi-static load), as shown in Figure 2-9. The ranges are defined by the relationship between the time to reach maximum deflection, t_m, and the blast load time duration of positive phase, t_0. For terrorist attack scenarios such as those

PRESSURE DESIGN RANGE	HIGH	LOW	VERY LOW
DESIGN LOAD	IMPULSE	PRESSURE-TIME	PRESSURE
INCIDENT PRESSURE	$\gg 100$ psi	< 100 psi	< 10 psi
PRESSURE DURATION	SHORT	INTERMEDIATE	LONG
RESPONSE TIME	LONG	INTERMEDIATE	SHORT
RELATIONSHIP OF t_m/t_0	$t_m/t_0 > 3$	$3 > t_m/t_0 > 0.1$	$t_m/t_0 < 0.1$
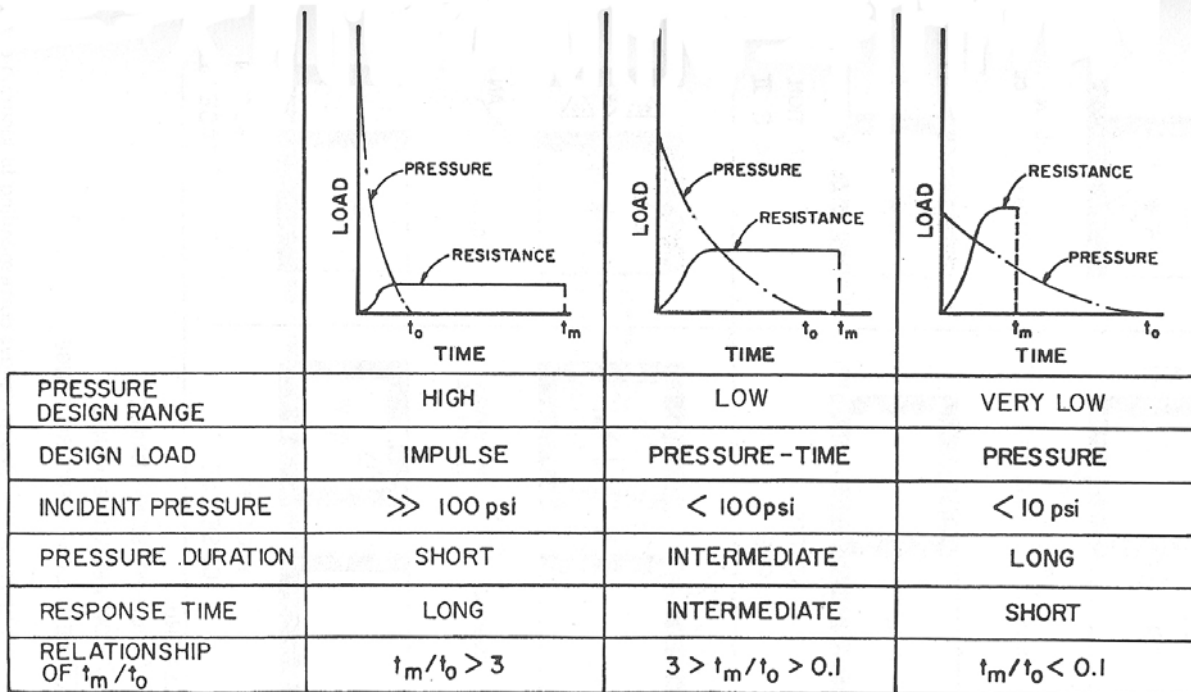
Figure 2-9   Parameters Defining Pressure Design Ranges (USDA 1990)

considered in this report with severe explosion-induced pressures at relatively close range, the design falls within the impulsive loading category. Therefore, the energy imparted to the structural system by blast loading is considered an impulsive loading.

The following describes the concept of simplified blast analysis using an equivalent SDOF system subjected to impulsive loading. First, the equivalent SDOF system used to represent the real structure and its response are described. Next, an equivalent resistance function is introduced simplifying the resistance function of the real structure into an elastic-perfectly-plastic function. Finally, the method to calculate the maximum displacement under blast loading is described.

2.3.2. Equivalent SDOF System

The key assumption of this analysis method is that real structures or components, which are multi-degree of freedom systems, can be represented by a SDOF lumped-mass system (often called an equivalent SDOF system). Figure 2-10 shows a fix-fix supported column as an example of an actual structural system and its equivalent SDOF system. Although this equivalent system can not provide the detailed response of the structure, it is enough to calculate the response at one particular point of the structure; typically the point where the maximum

(a) Real Structural System   **(b) Equivalent SDOF System**
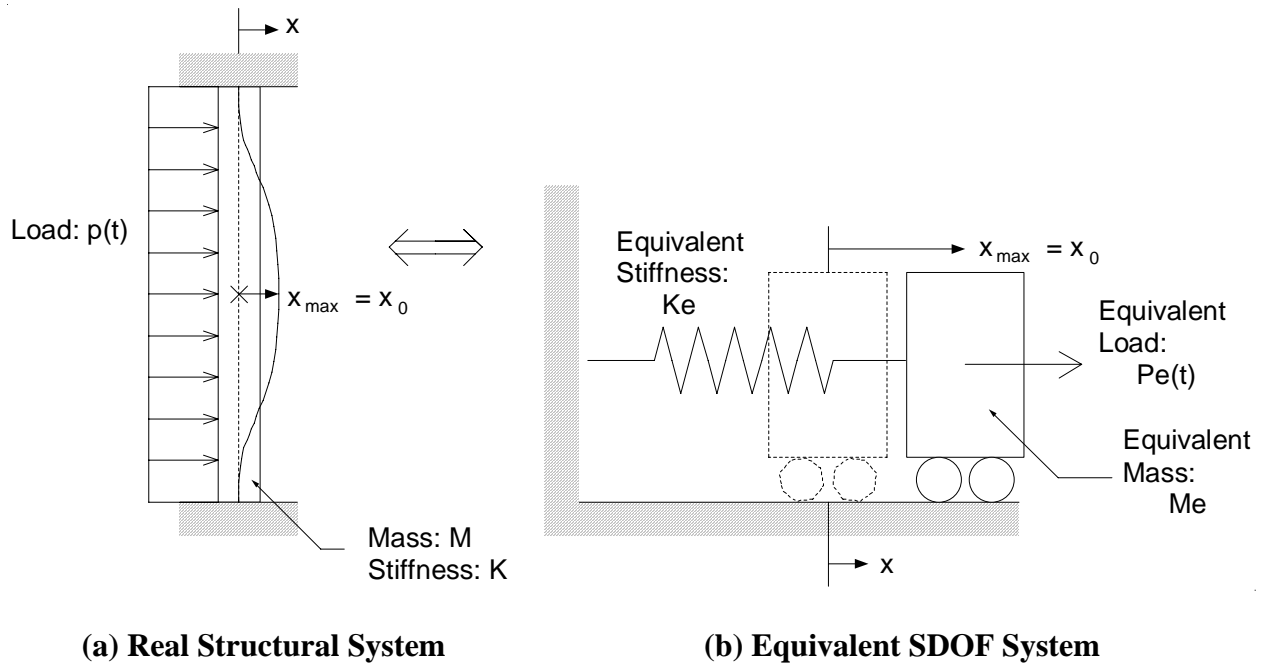
Figure 2-10   Real and Equivalent SDOF System

deformation occurs in the system is chosen for design.

The equation of motion for an SDOF system is given by:

$$M\ddot{x} + c\dot{x} + Kx = P(t) \tag{2-13}$$

The damping component $c\dot{x}$ is typically neglected when calculating response under blast loading since one cycle of response develops. Ignoring this term is also a conservative approach for design purposes. Thus, Equation 2-13 simplifies to:

$$M\ddot{x} + Kx = P(t) \tag{2-14}$$

The equation of motion for an equivalent SDOF system as shown in Figure 2-10 is written as:

$$M_e\ddot{x} + K_e x = P_e(t) \tag{2-15}$$

where M_e is the equivalent mass, K_e is the equivalent stiffness and $P_e(t)$ is the equivalent load. To express Equation 2-15 in terms of the mass, M, stiffness, K, and load, $P(t)$ of the real structure, the load factor, K_L, the mass factor, K_M, and the stiffness factor, K_S are introduced and defined as:

$$K_L = \frac{P(t)_e}{P(t)} \tag{2-16}$$

$$K_M = \frac{M_e}{M} \tag{2-17}$$

$$K_S = \frac{K_e}{K} \tag{2-18}$$

The procedure to calculate these factors will be described later in this section. Using these factors, Equation 2-15 is rewritten as:

$$K_M M\ddot{x} + K_S Kx = K_L P(t) \tag{2-19}$$

Since the resistance of an element which comes from the stiffness is the internal force tending to restore the structure to its original position, the maximum resistance is the total load. Therefore, the stiffness factor must always equal to the load factor. They are set as equal in practical analysis ($K_L = K_S$).

A load-mass factor is then defined as:

$$K_{LM} = \frac{K_M}{K_L} \tag{2-20}$$

19

Thus, dividing each terms in Equation 2-19 by K_L gives:

$$K_{LM} \, M \, \ddot{x} + K \, x = P(t) \qquad (2\text{-}21)$$

The resulting Equation 2-21 shows that the equation of motion of the equivalent system is directly obtained from the original equation of motion by multiplying the mass by the load-mass factor.

Load factor, K_L, and mass factor, K_M, are obtained by equating the energies of the real structure and the equivalent SDOF system. The strain energy, U, the kinetic energy, KE, and the work done by the load, WD, in the equivalent SDOF system are, respectively, evaluated by:

$$U = \frac{1}{2} K_e \, x_0^{\,2} \qquad (2\text{-}22)$$

$$KE = \frac{1}{2} M_e \, \dot{x}_0^{\,2} \qquad (2\text{-}23)$$

$$WD = P_e(t) \, x_0 \qquad (2\text{-}24)$$

where x_0 and $\dot{x}_0$ are, respectively, the maximum deformation and velocity of the system.

Figure 2-11 is used for the following example to illustrate how these factors are calculated for a fix-fix supported column. The column undergoes plastic deformation forming plastic hinges at
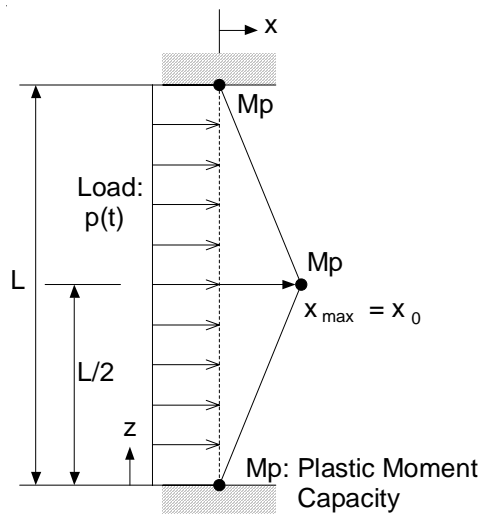
Figure 2-11   Plastic Deformation of Fix-Fix Supported Column

the top and bottom of the fixed supports and the center of the column, and the plastic
deformations are given by:

$$x(z) = \delta(z) \, x_0 = \begin{cases} \dfrac{2 \, z}{L} \, x_0 & \text{for } 0 < z < \dfrac{L}{2} \\ \left(2 - \dfrac{2 \, z}{L} \right) x_0 & \text{for } \dfrac{L}{2} < z < L \end{cases} \tag{2-25}$$

where $\delta(z)$ is a shape function. The load factor, K_L, is obtained by setting the external work done
by the equivalent load, $P_e(t)$, equal to the one done by the external load on the actual structure,
$p(t)$. This equivalency is calculated by:

$$WD = \int_0^L P(t) x(z) \, dx = \frac{1}{2} \, p(t) x_0 \tag{2-26}$$

Equating Equation 2-24 and Equation 2-26 gives the load factor, K_L, as:

$$K_L = \frac{P_e(t)}{P(t)} = 0.5 \tag{2-27}$$

The mass factor, K_M, is evaluated by setting the kinetic energy of the equivalent SDOF system
equal to the one of the actual structure. This is expressed by:
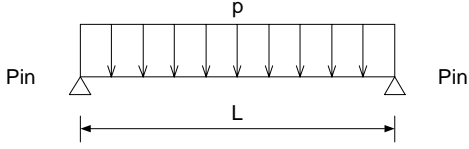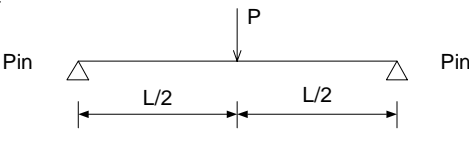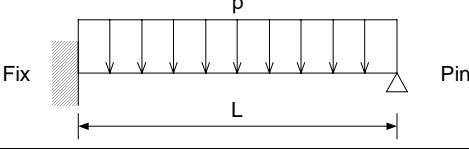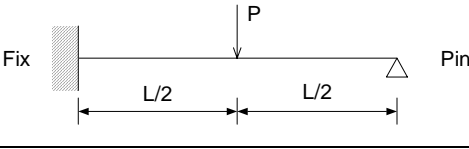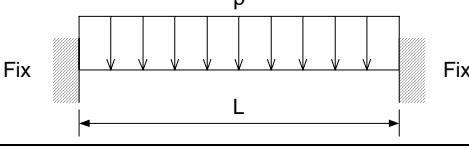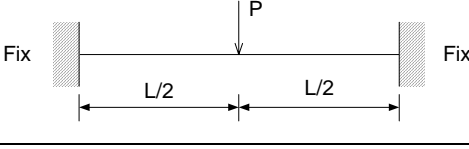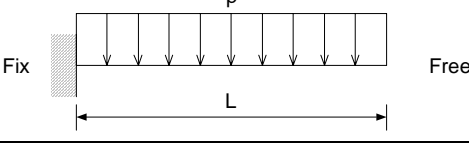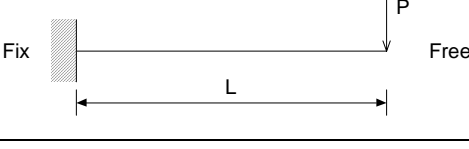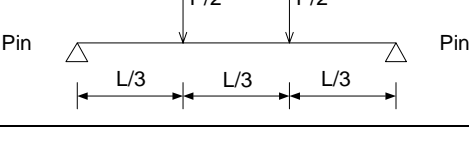
$$KE = \frac{1}{2} \int_0^L m(z) \, \dot{x}(z)^2 \, dz = \frac{1}{2} m \, \dot{x}_0^2 \int_0^L \delta(z)^2 \, dz = \frac{1}{6} m \, L \, \dot{x}^2 = \frac{1}{6} M \, \dot{x}^2 \tag{2-28}$$

Equating Equation 2-23 and Equation 2-28 gives the mass factor K_M as:

$$K_M = \frac{M_e}{M} = \frac{1}{3} \tag{2-29}$$

Similarly, load and mass factors for one various single span structural members subjected to
various boundary conditions and load conditions are summarized in Table 2-1.

Table 2-1   Transformation Factors for Beam Elements (USDA 1990)

Edge Conditions and Loading Diagrams	Range of Behavior	Load Factor K_L	Mass Factor K_M	Load-Mass Factor K_{LM}
Pin — p (uniform) — Pin, L	Elastic	0.64	0.50	0.78
	Elasto-Plastic	-----	-----	-----
	Plastic	0.50	0.33	0.66
Pin — P (at L/2) — Pin	Elastic	1.0	0.49	0.49
	Elasto-Plastic	-----	-----	-----
	Plastic	1.0	0.33	0.33
Fix — p (uniform) — Pin, L	Elastic	0.58	0.45	0.78
	Elasto-Plastic	0.64	0.50	0.78
	Plastic	0.50	0.33	0.66
Fix — P (at L/2) — Pin	Elastic	1.0	0.43	0.43
	Elasto-Plastic	1.0	0.49	0.49
	Plastic	1.0	0.33	0.33
Fix — p (uniform) — Fix, L	Elastic	0.53	0.41	0.77
	Elasto-Plastic	0.64	0.50	0.78
	Plastic	0.50	0.33	0.66
Fix — P (at L/2) — Fix	Elastic	1.0	0.37	0.37
	Elasto-Plastic	-----	-----	-----
	Plastic	1.0	0.33	0.33
Fix — p (uniform) — Free, L	Elastic	0.40	0.26	0.65
	Elasto-Plastic	-----	-----	-----
	Plastic	0.50	0.33	0.66
Fix — P (at Free end), L	Elastic	1.0	0.24	0.24
	Elasto-Plastic	-----	-----	-----
	Plastic	1.0	0.33	0.33
Pin — P/2, P/2 (at L/3, L/3, L/3) — Pin	Elastic	0.87	0.52	0.60
	Elasto-Plastic	-----	-----	-----
	Plastic	1.0	0.56	0.56

2.3.3. Equivalent Resistance Function

The various stages of response, from elastic to plastic response, are shown for a one span fix-fix supported column in Figure 2-12. The corresponding resistance-deflection function, $R(x)$, is shown in Figure 2-13 as plastic hinging progresses in the system up to the plastic collapse mechanism. In these figures, r_e is the yield resistance and r_u is the ultimate resistance, and X_e and X_p are the corresponding yield and ultimate displacements. In order to calculate the maximum plastic deflection using the equivalent energy concept, the actual resistance function, $R(x)$, is simplified to a bilinear force-displacement relationship and corresponding equivalent resistance function, $R_e(x)$. The equivalent resistance function is determined such that the area under the dotted curve, ODB, in Figure 2-13 is equal to the area under the solid curve, OAB, where K_E is the equivalent elastic stiffness and X_E is the equivalent maximum elastic deflection. They are given by:

$$X_E = X_e + X_p \left(1 - \frac{r_e}{r_u} \right) \tag{2-30}$$

$$K_E = \frac{r_u}{X_E} \tag{2-31}$$

The ultimate resistance and the equivalent elastic stiffness depend on the boundary conditions and loading conditions. Tables 2-2 and 2-3 summarize the ultimate, elastic, and elasto-plastic resistances for beam elements, and equivalent elastic stiffness, respectively (USDA 1990).

(a) Original Structure   **(b) Yielding State**   **(c) Ultimate State**
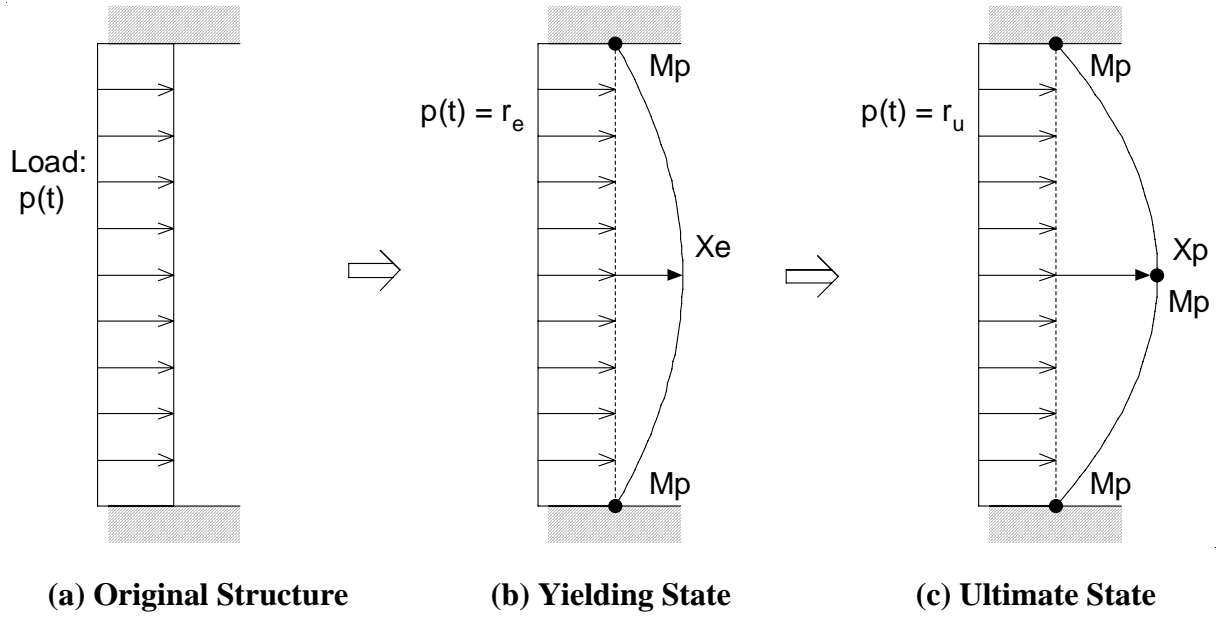
Figure 2-12   **Progress of Column Collapse for Fix-Fix Supported Column**
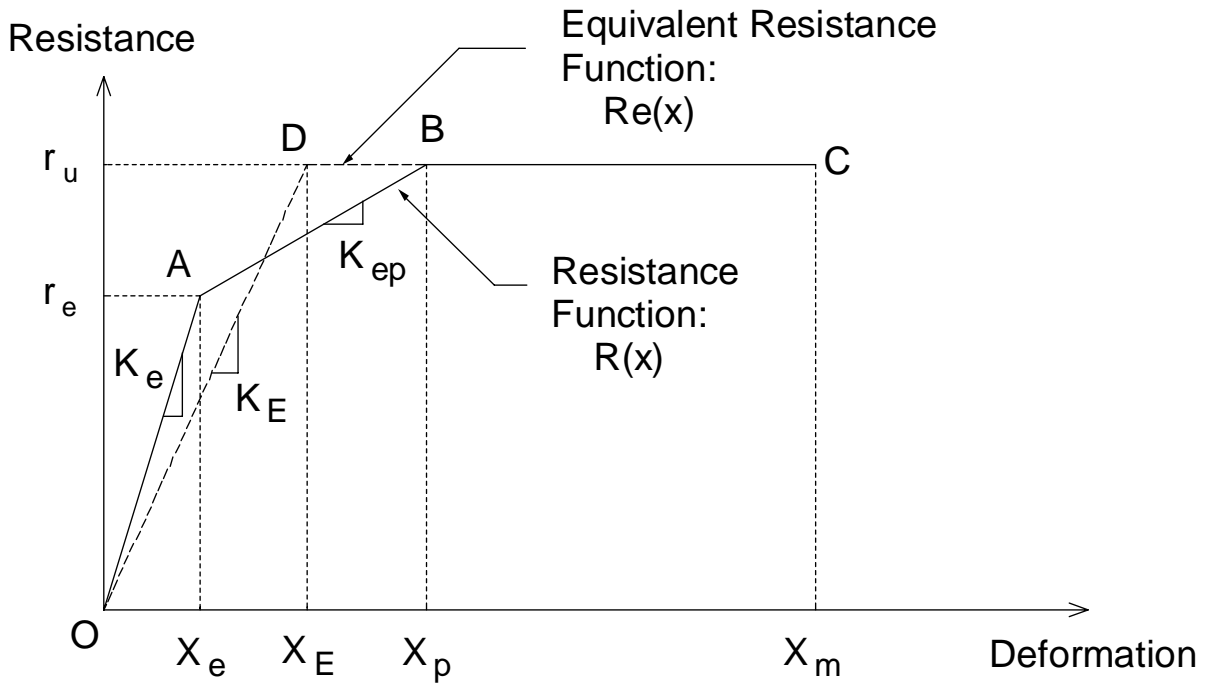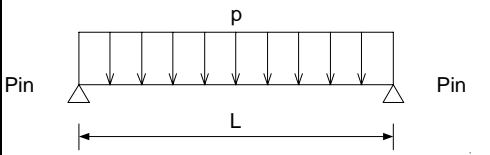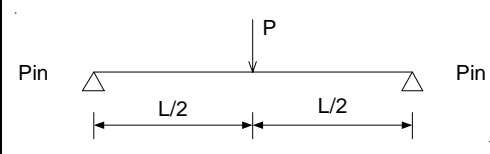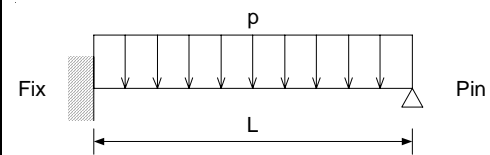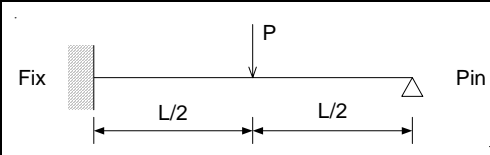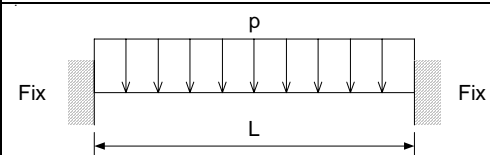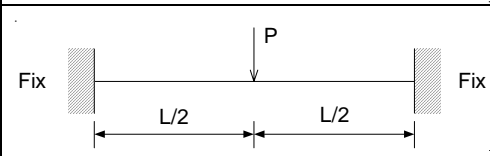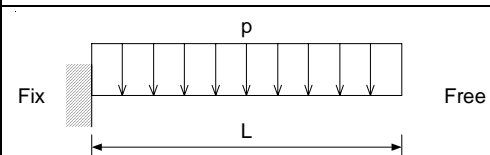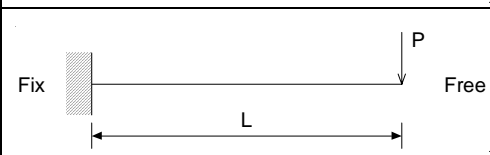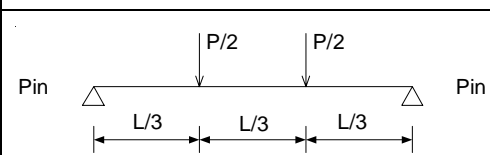
Figure 2-13   **Idealized Resistance-Deflection Function (USDA 1990)**

Table 2-2   Ultimate, Elastic and Elasto-Plastic Unit Resistances for Beam Elements (USDA 1990)

Edge Conditions and Loading Diagrams	Ultimate Resistance, R_u, r_u	Elastic Resistance, R_e, r_e	Elasto-Plastic Resistance, R_{ep}, r_{ep}
Pin — Pin, distributed load p, span L	$r_u = \dfrac{8M_p}{L^2}$	r_u	-----
Pin — Pin, point load P at center, $L/2$, $L/2$	$R_u = \dfrac{4M_p}{L}$	R_u	-----
Fix — Pin, distributed load p, span L	$r_u = \dfrac{4(M_N + 2M_P)}{L^2}$	$\dfrac{8M_N}{L^2}$	r_u
Fix — Pin, point load P, $L/2$, $L/2$	$R_u = \dfrac{2(M_N + 2M_p)}{L}$	$\dfrac{16M_N}{3L}$	R_u
Fix — Fix, distributed load p, span L	$r_u = \dfrac{8(M_N + M_P)}{L^2}$	$\dfrac{12M_N}{L^2}$	r_u
Fix — Fix, point load P, $L/2$, $L/2$	$R_u = \dfrac{4(M_N + M_p)}{L}$	$\dfrac{8M_N}{L}$	R_u
Fix — Free, distributed load p, span L	$r_u = \dfrac{2M_N}{L^2}$	r_u	-----
Fix — Free, point load P at end, span L	$R_u = \dfrac{M_N}{L}$	R_u	-----
Pin — Pin, two point loads $P/2$, $L/3$, $L/3$, $L/3$	$R_u = \dfrac{6M_p}{L}$	R_u	-----

M_N: Ultimate Negative Unit Moment Capacity, M_p: Ultimate Positive Unit Moment Capacity

Table 2-3   Elastic, Elasto-Plastic and Equivalent Elastic Stiffness for Beam Elements (USDA 1990)

Edge Conditions and Loading Diagrams	Elastic Stiffness, K_e	Elasto-Plastic Stiffness, K_{ep}	Equiv. Elastic Stiffness, K_E
Pin — p (uniform load), Pin, L	$\dfrac{384EI}{5L^4}$	-----	$\dfrac{384EI}{5L^4}$
Pin — P at center, Pin, L/2, L/2	$\dfrac{48EI}{L^3}$	-----	$\dfrac{48EI}{L^3}$
Fix — p (uniform load), Pin, L	$\dfrac{185EI}{L^4}$	$\dfrac{384EI}{5L^4}$	$\dfrac{160EI}{L^4}$ *
Fix — P at center, Pin, L/2, L/2	$\dfrac{107EI}{L^3}$	$\dfrac{48EI}{L^3}$	$\dfrac{106EI}{L^3}$ *
Fix — p (uniform load), Fix, L	$\dfrac{384EI}{L^4}$	$\dfrac{384EI}{5L^4}$	$\dfrac{307EI}{L^4}$ *
Fix — P at center, Fix, L/2, L/2	$\dfrac{192EI}{L^3}$	$\dfrac{48EI}{L^3}$ **	$\dfrac{192EI}{L^3}$ *
Fix — p (uniform load), Free, L	$\dfrac{8EI}{L^4}$	-----	$\dfrac{8EI}{L^4}$
Fix — P at end, Free, L	$\dfrac{3EI}{L^3}$	-----	$\dfrac{3EI}{L^3}$
Pin — P/2, P/2, Pin, L/3, L/3, L/3	$\dfrac{56.4EI}{L^3}$	-----	$\dfrac{56.4EI}{L^3}$

* Valid only if $M_N = M_p$, ** Valid only if $M_N < M_p$

2.3.4. Response to Impulsive Loading

Using the equivalent SDOF analysis method, the maximum response to an impulsive load is obtained by assuming that all the energy imparted to the system by the blast loading is converted into internal strain energy. The blast load is idealized as a triangular shape function defined by the maximum blast pressure, p, and positive time duration, t_d, as shown in Figure 2-14. The impulse, i, is given by:

$$i = \frac{p\,t_d}{2} \tag{2-32}$$

The kinetic energy delivered by the impulsive load is given by:

$$KE = \frac{i^2}{2M_e} = \frac{i^2}{2K_{LM}\,m} \tag{2-33}$$

The strain energy stored in the equivalent elastic system mentioned in Section 2.3.3 is given by:

$$U = \frac{r_u X_E}{2} + r_u \left(X_m - X_E \right) \tag{2-34}$$

Therefore, equating Equation 2-33 and Equation 2-34 gives the maximum deformation of the equivalent SDOF system due to impulsive-type blast loading as:

$$X_m = \frac{1}{2} \left(\frac{i^2}{K_{LM}\; m\; r_u} + X_E \right) \tag{2-35}$$
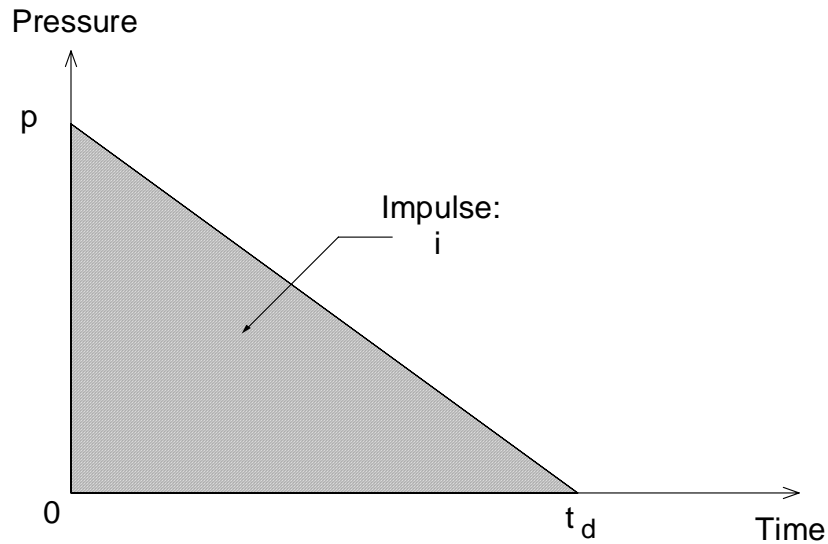
Figure 2-14   Idealized Blast Load

2.4   Structural Element Behavior under Blast Loading

2.4.1. Dynamic Strength Increase

A structural element under blast loading develops a higher strength than one subjected to a static loading. This increase in strength is a function of the strain rate developing in the materials. Figure 2-15 (USDA 1990) shows typical stress-strain curves for concrete and steel. The solid lines and dotted lines respectively represent the stress-strain curves under static loading rates (according to ASTM standards loading rates) and rapid loading rates. The symbols in these
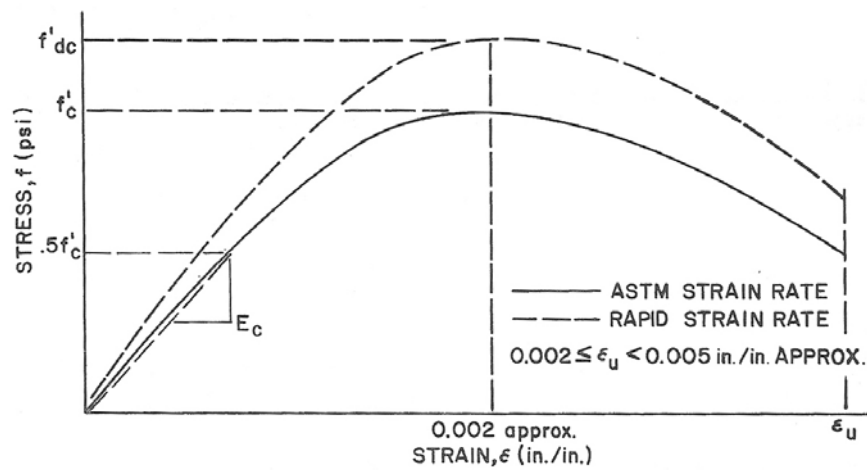
(a) Stress-strain Curves for Concrete
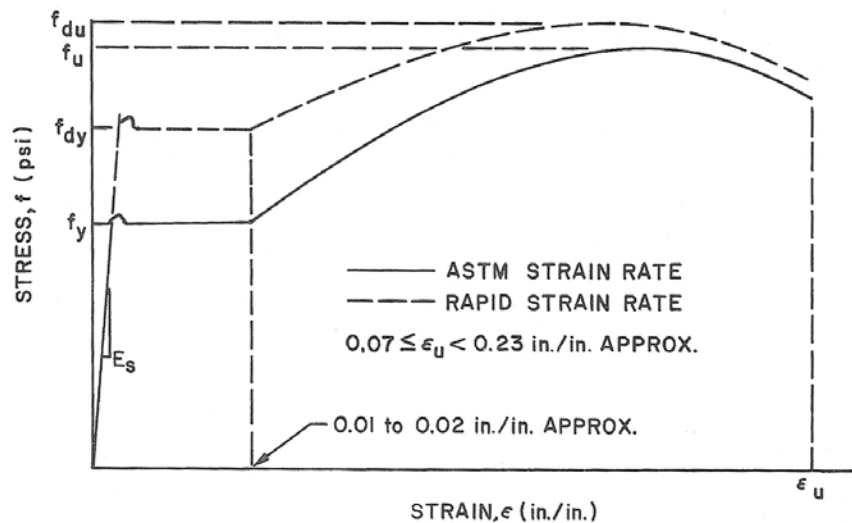
(b) Stress-strain Curves for Steel

Figure 2-15   Typical Stress-strain Curves for Concrete and Steel (USDA 1990)

figures are defined as follows: f_c' and f_{dc}' are the static and dynamic ultimate compressive strengths of concrete, respectively. f_y, f_{dy}, f_u and f_{du} are, respectively, the static yield, dynamic yield, static ultimate and dynamic ultimate stress of steel. E_s, E_c and ε_u are the elastic modulus of steel, the secant elastic modulus of concrete and the rupture strain, respectively. Qualitatively, the increase in the yield strength of steel and the compressive strength of the concrete under blast load increase more substantially due to strain rate than the ultimate strength of steel. Also, the secant elastic modulus of concrete increases due to the strain rate effect, whereas the elastic modulus of the steel is insensitive to the loading rate.

In designing structure or its members subjected to blast loads, these increases in yield and ultimate strengths are typically considered using a dynamic increase factor (DIF). The DIF is defined as the ratio of the dynamic strength to the static strength. The typical DIF values for concrete, reinforcing bars and structural steel are presented in Table 2-4 (Mays and Smith 1995).

2.4.2. Response Deformation Limits

Once structural response is obtained by the analysis techniques presented previously (such as the simplified analysis described in Section 2.3), the damage level associated with this response needs to be evaluated. Conrath et al. (1999) described various states of damage for a number of structural elements as a function of a number of deformation or strain quantities based on observations in experiments and numerical simulations, as shown in Table 2-5. For instance, for a steel beam, light, moderate and severe damage are defined as a midspan deformation due to

Table 2-4   Dynamic Increase Factors for Design of Reinforced Concrete and Structural Steel Elements (Mays and Smith 1995)

Type of stress	Concrete	Reinforcing bars		Structural steel	
	f_{dc}'/f_c'	f_{dy}/f_y	f_{du}/f_y	f_{dy}/f_y *	f_{du}/f_y
Bending	1.25	1.20	1.05	1.20	1.05
Shear	1.00	1.10	1.00	1.20	1.05
Compression	1.15	1.10	---	1.10	---

* Minimum specified f_y for grade 50 steel or less may be enhanced by the average strength increase factor of 1.10.

bending of 5, 12 and 25 %, respectively, of the span, and a deformation in shear of 2, 4 and 8 %, respectively. The values in Table 2-5 based on observations in experiments and numerical simulations would be appropriate for post-event assessment and, although not necessarily recommended to provide a safe design, could be used in a performance-based design interested in achieving various stages of damage under ultimate conditions.

Table 2-5   Typical Failure Criteria for Structural Elements (Conrath et al. 1999)

Element Type	Material Type	Type of Failure	Criteria	Light Damage	Moderate Damage	Severe Damage
Beams	Reinforced Concrete ($\rho >$ 0.5%/face)	Global Bending/ Membrane Response	Ratios of Center-line Deflection to Span, δ/L	4%	8%	15%
		Shear	Average Shear Strain Across Section, γ_v	1%	2%	3%
	Steel	Bending/ Membrane	δ/L	5%	12%	25%
		Shear	δ/L	2%	4%	8%
Slabs	Reinforced Concrete ($\rho >$ 0.5%/face)	Bending/ Membrane	δ/L	4%	8%	15%
		Shear	γ_v	1%	2%	3%
Columns	Reinforced Concrete ($\rho >$ 0.5%/face)	Compression	Shortening/ Height	1%	2%	4%
	Steel	Compression	Shortening/ Height	2%	4%	8%
Load-Bearing Walls	Reinforced Concrete ($\rho >$ 0.5%/face)	Compression	Shortening/ Height	1%	2%	4%
Shear Walls	Reinforced Concrete ($\rho >$ 0.5%/face)	Shear	Average Shear Strain Across Section	1%	2%	3%

2.4.3. Local Failures

In case of small standoff distances or severe fragment loading, local failures are expected in members made from some materials, such as reinforced concrete. These failures can take the form of breaching, spalling and scabbing. These local failures are material failures rather than structural failures. The structural elements composed of steel are not likely to be subjected to breaching (Conrath et al. 1999) although other types of local failures are possible. "Breaching" is a local failure with an opening also known as a local shear failure, which is common for slabs. "Spalling" and "scabbing" are often used to describe the same phenomenon for localized damage of concrete elements. These are the results of a tension failure in the concrete normal to its free surface (USDA 1990), and generally result in chipping and pitting of the concrete surface. Also, breaching is commonly used as a term to describe these phenomena.

2.5   Blast-resistant Design of Bridges

2.5.1. Recommendations by the Blue Ribbon Panel

A Blue Ribbon Panel (BRP) consisting of professionals from practice, academia and government agencies, recommended policies and actions to reduce the probability of catastrophic structural damage to bridges and tunnels subjected to terrorist attacks (FHWA 2003). The BRP provided seven overarching recommendations addressing institutional, fiscal and technical issues. The institutional recommendations focus on the roles and responsibilities of agencies and organizations such as the FHWA and AASHTO for transportation security, and address interagency coordination, outreach and communication strategies and clarification of legal responsibility. The fiscal recommendations are related to new funding sources for bridge/tunnel security and funding eligibility. Although institutional and fiscal dimensions are essential to support implementation of the technical recommendations, the focus of this BRP report was primarily on technical recommendations, namely addressing needed technical expertise and research, development and implementation.

A significant conclusion of the BRP is that security solutions must be "engineered" on the basis of technical expertise. Prioritization and risk assessment are the two key processes proposed for this purpose. The prioritization method should be based on subjective or empirical criteria, and is typically carried out in two steps. First step is a data-driven approach to rank bridges using

31

some commonly accepted criteria and data mostly coming from the National Bridge Inventory, and second step considers additional data from the bridge owners that addresses particular characteristics of the facilities and the services (issues of potential for mass casualty based on Average Daily Traffic, alternative routes, etc.). The risk assessment procedure is recommended to be performed for the bridges identified at the highest priority as a result of the prioritization processes. The following equation recommended for calculating the risk exposure of a given bridge is suggested (adapted from one used for the purpose of seismic retrofit):

$$R = O \times V \times I \tag{2-36}$$

where O (Occurrence) is the likelihood that terrorists will attack the asset, V (Vulnerability) is the likely damage resulting from various terrorist threats and I (Importance) is the importance of the facility. Countermeasures may be designed to reduce these factors and in-turn reduce the risk exposure of the facility. For example, if the vulnerability factor is high, this factor can be lessened by hardening the facility. A case study illustrating how such a risk assessment procedure can be used for bridges and tunnels is presented using this equation in Appendix C of the BRP report (FHWA 2003).

The panel also identified the need for further research and development to create empirically validated computational tools, design methods, and hardening technologies for design against terrorist attacks. In particular, new knowledge is needed on how to assess performance of critical elements under credible extreme loads; validate and calibrate computational methods and modeling with experiments to better understand structural behavior from blast and thermal loads; determine the residual functionality of bridge and tunnel systems and their tolerance for extreme damage; and develop mitigation measures and hardening technologies.

2.5.2. Risk Assessment and Management of Bridges for Terrorist Attacks

Williamson and Winget (2005) investigated methods to mitigate the risk of terrorist attack for critical bridges, mainly using information obtained from the literature (such as USDA 1990, USDJ 1995, ASCE 1997, Abramson 1999, SAIC 2002 and USDHS 2002) and a panel of experts in blast-resistant design and bridge construction. Cost-effective security measures are proposed to be the result of a risk assessment and management process such as the one shown in Figure 2-16. The risk assessment and management processes were, respectively, simplified from a threat point-of view by dividing bridges into categories based on bridge type, criticality

32
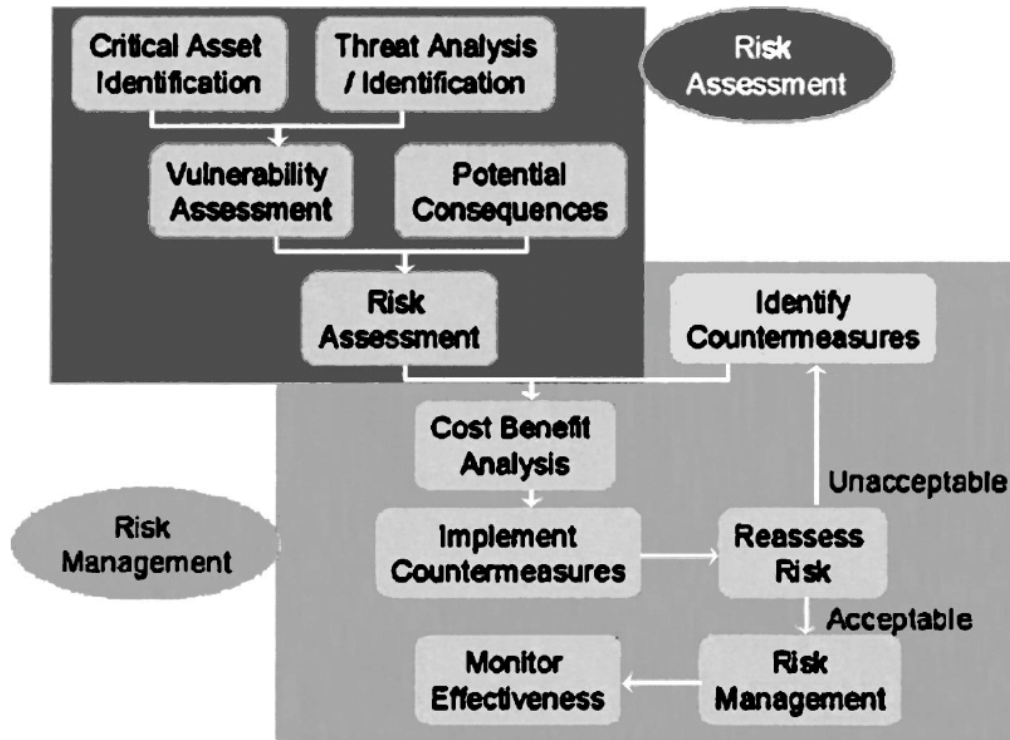
Figure 2-16   Risk Assessment and Management Processes (Williamson and Winget 2005)

(importance of a particular bridge) and associated threats. The threat analysis aims to determine the tactics most likely to be used by terrorists, and the analysis should consider both strategic vulnerabilities of the entire transportation system and of a specific bridge. Table 2-6 provides examples of suggested bridge protection levels as a function of bridge importance categories, following a procedure similar to the Government Services Administration's building classification procedure (USDJ 1995). This approach is intended to assist in prioritizing the allocation of resources. Williamson and Winget discussed a number of possible ways to enhance security ranging from deterrence, prevention and mitigation security measures; planning and coordination measures; information control measures; site layout measures; access control/deterrent measures; and deception measures. Then, threat-level-based security measures (Table 2-7) were developed to provide courses of action to react rapidly to increased threat levels, and possible temporary measures to increase security.

Table 2-6   Example of Bridge Protection Categories (Williamson and Winget 2005)

Category			Protection measures	
Criticality category	Bridge importance	Protection level	Concrete girder bridge (<75 m span over land)	Cable stayed bridge (>100 m span over water)
All	All	Basic	Planning, coordination, and information control measures	
1	Very Important (criticality=91–100)	Maximum protection	CAT 2 and 3 measures Real-time CCTV Emergency telephones No parking under bridge Boundary penetration sensors below deck Steel jacketing around columns Additional rebar in top face of girder Additional measures based on threat level	CAT 2 and 3 measures Real-time CCTV Emergency telephones "Bridge out" warning system actuated by span failure detectors Intrusion detection systems inside tower Reinforce tower walls and use standoff barriers around towers Anchorages covered with protective armor plates Additional measures based on threat level
2	Important (criticality=71–90)	Some protection	CAT 3 measures Pier protection (concrete barricade)	CAT 3 measures Dummy CCTV cameras Pier protection (dolphins)
3	Slightly important (criticality=51–70)	Minimal protection	Improved lighting above deck	Improved lighting above and below deck Keyless entry systems on towers
4	Unimportant (criticality=0–50)	No additional protection	None	None

Note: CAT=category, and CCTV=closed circuit television. This table is only an example demonstrating bridge protection categories. It is not based on a cost–benefit assessment and is not intended to be all-inclusive or serve as a recommendation for specific protection measures.

Table 2-7   Example of Threat Level Based Security Measures (Williamson and Winget 2005)

Threat level to bridges	Additional security measures (for Category 1 bridges in affected area)
Severe	Restrict access with guards, barriers, and vehicle searches All other measures listed below
High	Increase frequency of patrols and checks Conduct unscheduled exercise of emergency response plan Postpone nonessential maintenance Coordinate with National Guard or law enforcement for possible closure and vehicle searches once severe level is reached All other measures listed below
Elevated	Implement regularly scheduled police patrols All other measures listed below
Guarded	Review and update emergency response procedures Increase frequency of periodic checks of cameras, fences, etc. All other measures listed below
Low	Monitor security systems in place (including periodic checks) Disseminate threat information to personnel Regular refinement and exercising of emergency operations plan Emergency responder training Continually updating threat and vulnerability assessments

Note: This table is only an example of additional bridge protection measures based on the current threat level. It should be modified based on available resources, specific threats, and risk tolerance.

Possible blast effects on bridges were also discussed for diverse structural components such as decks, girders, bents and columns, and footings. They commented that when explosions are placed underneath a bridge, the girders and deck systems are subjected to large uplift forces which can be amplified in the confined area between the girders and the abutments. In addition to these uplift forces, the blast pressure may create cratering and spalling of the concrete deck which translate into a reduction of the capacity of the girders in case of the concrete superstructures or composite steel superstructures. For explosions below the deck, bents and columns can be subjected to large deformations, shear, or flexural failure. The loss of the cover concrete can reduce the capacity of the column, particularly when the explosion is at small standoff distance. When this force in the column is transferred to the footing, the footing may also be damaged. Finally, Williamson and Winget proposed a set of design objectives (which they called performance-based standards for bridges) as shown in Table 2-8 that vary as a

Table 2-8   Performance-Based Standards for Bridges (Williamson and Winget 2005)

Performance based design standards for bridges (terrorist threats)

Category 1 (very important) Concept: Each structural element is designed to withstand two separate cases, large loads with repairable damage and smaller loads with negligible damage
    Design loads: Case 1 (small loads)
        "Most likely" threat scenarios using the following at-worst possible locations for each structural element being deigned:
            Medium-sized truck bomb for vehicle delivered bomb scenarios
            Backpack-sized bomb for hand emplaced explosive scenarios
            Average-sized truck collision for vehicle impact scenarios
    Acceptable damage: Case 1 (small loads)
        Local deck failure, support system still intact with negligible damage, truss/cables/piers still capable of supporting design loads
        when considering structural redundancy, no unrepairable foundation instabilities and no span loss
        Steel girders <5% maximum deflection to length ratio, reinforced concrete girders <4%
    Design loads: Case 2 (large loads)
        "Most likely" threat scenarios using the following at-worst possible locations for each structural element being deigned:
            Large-sized truck bomb for vehicle delivered bomb scenarios
            Large suitcase-sized bomb for hand emplaced explosive scenarios
            Large truck collision for vehicle impact scenarios
    Acceptable damage: Case 2 (large loads)
        Local deck failure, support system still intact with minor damage, not capable of supporting design loads but easily repairable,
        no unrepairable foundation instabilities and no span loss
        Steel girders <12% maximum deflection to length ratio, reinforced concrete girders <8%

Category 2 (important) Concept: Designed to withstand smaller loads with repairable damage
    Design loads: Same as Category 1, Case 1
    Acceptable damage: Same as Category 1, case 1

Category 3 (slightly important) Concept: Designed to withstand smaller loads with repairable damage
    Design loads: Same as Category 1, Case 1
    Acceptable damage: No more than one span loss (no progressive collapse)

Category 4 (unimportant)
    No standard

Note: Design explosive loads for some Category 1 bridges may need to be increased based on a detailed threat assessment. Specific charge weights were omitted for security reasons.

function of the importance of the bridge. That performance-based set of objectives qualified the terrorist threats against bridges in terms of small or large design loads, and described the acceptable level of damage subjected to these loads. Note that the ductility limits in these standards were referenced from the ones proposed by Conrath et al. (1999) and previously presented in Table 2-5.

2.5.3. Analysis and Design of Bridges for Terrorist Attacks

Winget et al. (2005) analyzed and designed a bridge subjected to blast loads generated by the computer program BlastX (distribution limited to U.S. Government agencies and their contractors). To account for the effects of spalling and cratering concrete, reductions in the cross-sectional area of the columns were calculated using empirical equations for spall and breach developed by Marchand and Plenge (1998, distribution limited to U.S. Government agencies and their contractors). The flexural response of the structural components was calculated on the basis of an equivalent SDOF dynamic analysis, using the program, SPAn32 version 1.2.6.9. (USACE-OD 2002). The external loads were considered as equivalent uniformly distributed loads automatically obtained from the pressure time-history calculated by BlastX. The baseline bridge in these analyses is shown in Figure 2-17, which consists of AASHTO Type IV prestressed concrete girders, three columns per pier bent and a reinforced concrete deck. The threat explosive weights considered ranged from 45 kg (large hand-placed explosions) to 1,800 kg (light, single rear-axle delivery vehicles). The prestressed concrete girders, cap beam and deck were analyzed considering the two scenarios of a truck bomb above or below the deck, based on a preliminary vulnerability assessment. The reinforced concrete piers were analyzed considering two different scenarios, namely a below-deck vehicle bomb and hand-placed charges in contact with the pier. The bridge structural system was characterized as uncoupled components having an elastic-perfectly-plastic behavior for each component as shown in Figure 2-18.
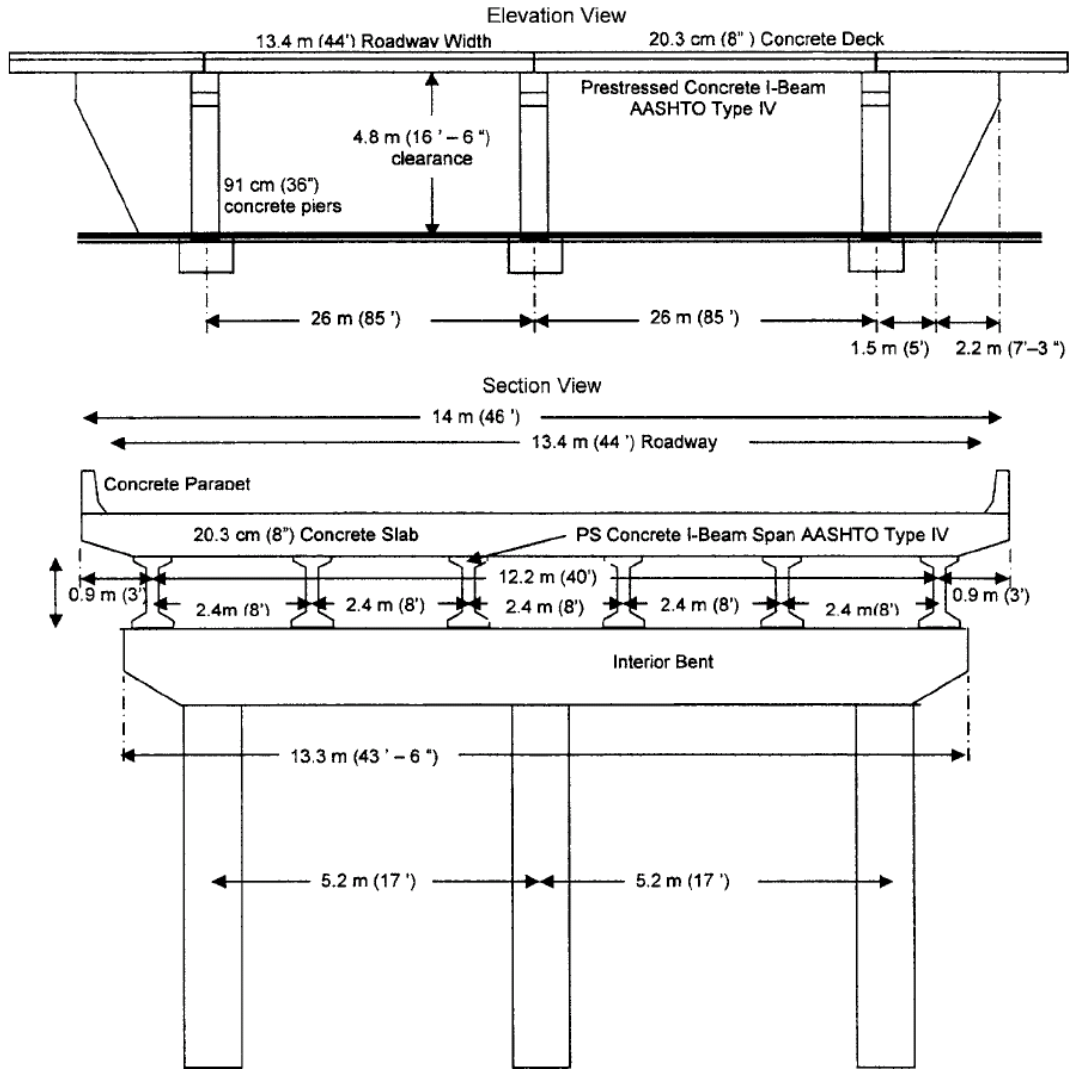
Figure 2-17   Baseline Bridge Plans (Winget et al. 2005)
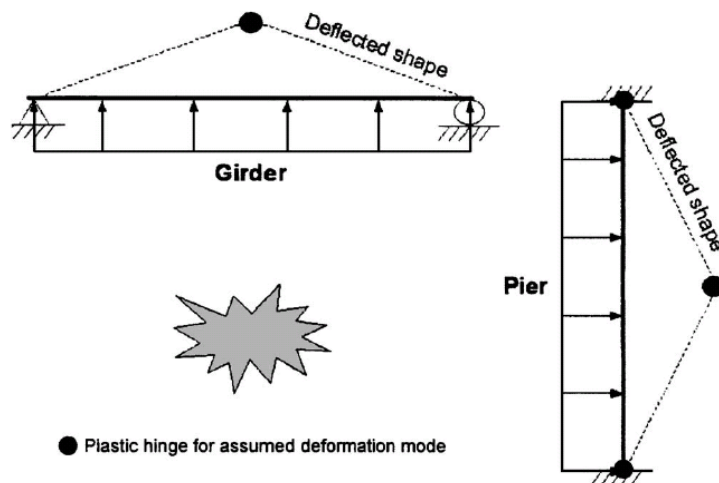
Figure 2-18   Dynamic Structural Models (Winget et al. 2005)

It was found that charges placed closer to a structural element tended to produce the most localized damage, however, when a truck bomb was placed below the deck, there was a region below the deck where increasing the height of the charge resulted in less damage due to the Mach region. As discussed in a previous section, the reflected pressure has a higher pressure and travels faster than the incident pressure. When the reflected shock wave overtakes the incident shock wave, these waves merge and create a single shock wave, so called a Mack front that has a much higher pressure than the incident shock wave (Figure 2-19). As such, there exists an area (the Mach region shown in Figure 2-19) where these waves do not merge at a certain explosion height. This phenomenon likely happens at the higher explosion heights. Charges detonated under the bridge and near sloped abutments were shown more likely to produce higher levels of damage than explosions at mid-span above the deck. This was due to the development of high pressures from the incident and reflected pressures in the confined area between the deck and the abutment, even though the explosion above deck at mid-span had a smaller standoff distance.

For the reinforced concrete piers, the resulting pressures from BlastX were reduced by a factor of 0.8 to account for the curved column surface, based on the changing angle of incidence. The breaching failure of the concrete resulted in governing the ultimate performance especially for large truck bombs detonated at limited standoff distances or for hand–placed charges. It was observed that significant impulse reductions occurred for every foot of standoff distance provided up to 6 m. The protective benefit of retrofit options, such as FRP wraps and steel jacketing, were mentioned and recommended on the basis of the anticipated breaching resistance of the steel jackets and the diagonal shear resistance of the FRP wraps. However, these recommendations were based on judgment and the behavior of the proposed retrofit systems were not analytically modeled nor experimentally verified by Winget et al. (2005).
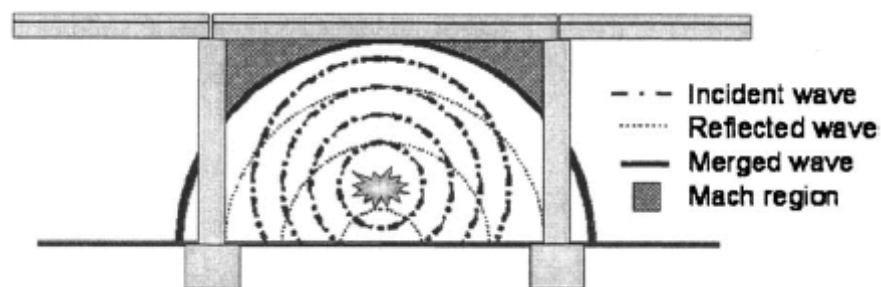
Figure 2-19   Vertical Mach Front (Winget et al. 2005)

SECTION 3

APPROACHES FOR BLAST DESIGN OF BRIDGE PIERS AND SELECTION OF CONCEPT

3.1   Description of the Assumed Blast Scenario

As mentioned in the former section, the terrorist action considered in this research consists of detonating the explosives located inside a car vehicle placed below the deck at a close distance of the pier. This scenario is schematically illustrated in Figure 3-1. The horizontal distance X_p between the center of an explosive charge and the pier, referred to as either blast distance or standoff distance in the literature, was set based on what is found in typical highway bridges (the exact value is not indicated here for the reasons mentioned in Section 1.3). The vertical distance between the center of an explosive charge and the ground was set equal to 1 meter based simply on the geometry of typical car vehicles.

Because of its very nature, it is virtually impossible to accurately predict the explosive charge weight to be used in a terrorist attack. Reasonable estimatess, however, can be made by taking
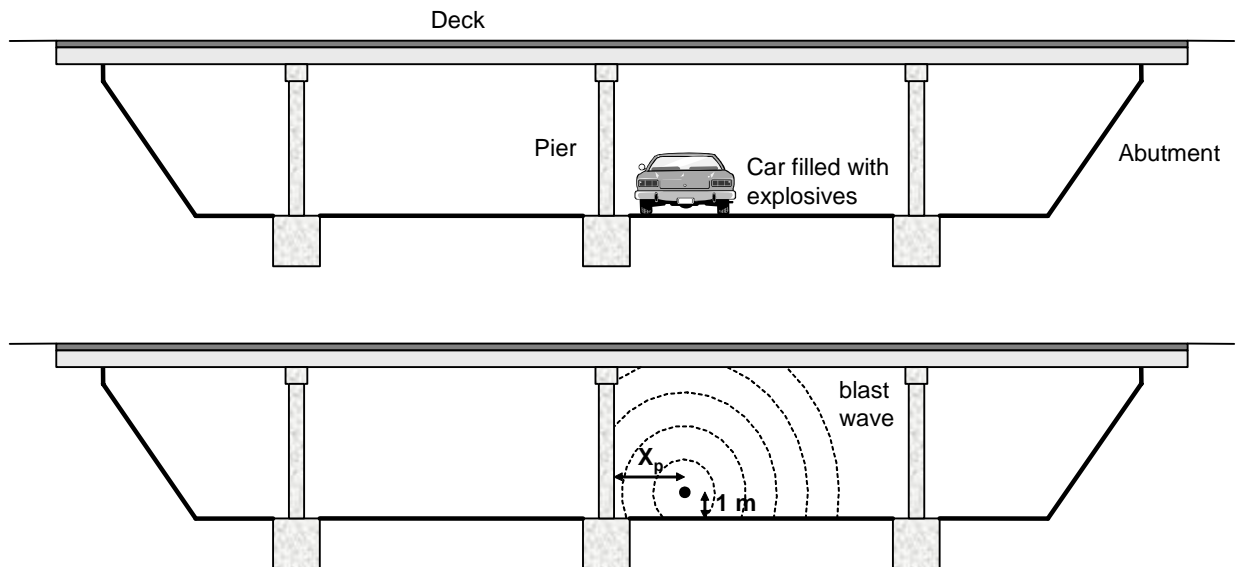
Figure 3-1   Schematics of the Assumed Blast Scenario

into account some characteristics of terrorist actions. For instance, there is clearly a relationship between the size of the vehicle used to carry the explosives and the maximum possible charge weight, especially when taking into account that the explosives will most likely be somehow hidden to avoid detection by simple visual inspection (Williamson and Winget 2005). Also, while high-tech explosives are expensive and difficult to handle (especially in large quantities), fertilizer-based explosives can be fabricated relatively easily using commercially available ingredients, which make them much more likely to be used. The explosive charge weight adopted in this study, referred to as W_p in this report, was set based on these and other considerations, and was found to be very similar to the blast weights predicted in FEMA (2003) and in FHWA (2003) for terrorist actions using car vehicles.

3.2   Development of the Multihazard Pier Concept

3.2.1. Description of the Bridge Structure

The pier concepts considered in this section were designed and analyzed assuming that they are part of a typical 3-span continuous highway bridge described in Dicleli and Bruneau (1996). The span lengths are 35 m, 25 m and 30 m (total length L = 90 m). The width of the deck is 16 m, the equivalent cross-section area of the deck is 0.592 m^2, the equivalent moment of inertia of the deck (with respect to a vertical axis passing through the centroid) is I_D = 13.9 m^4, the mass of the deck per unit length is m_D = 12.56 tons/m, and the height of the columns is H = 6 m. The total gravity load on each pier is assumed equal to 4098 kN.

3.2.2. Description of the Seismic Loading

The bridge structure described in the former subsection is assumed to be located in an area of moderate seismic activity. For analysis and design purposes, it is assumed that the corresponding pseudo-acceleration (S_A) response spectrum is given by:

$$S_A = \min\left\{ \left(1 + 18.75\,T\right) A_g \ , \ 2.50\,A_g \ , \ \frac{A_g}{T} \right\}$$

(3-1)

where A_g (peak ground acceleration) is assumed equal to 0.3 g, and T denotes natural period. The spectral shape of the response spectrum defined by Equation 3-1 (Figure 3-2) is typical of rock or very stiff soil foundations. Equation 3-1 is similar (but not identical) to the one implemented in AASHTO seismic codes for bridges, the difference being that here, the short
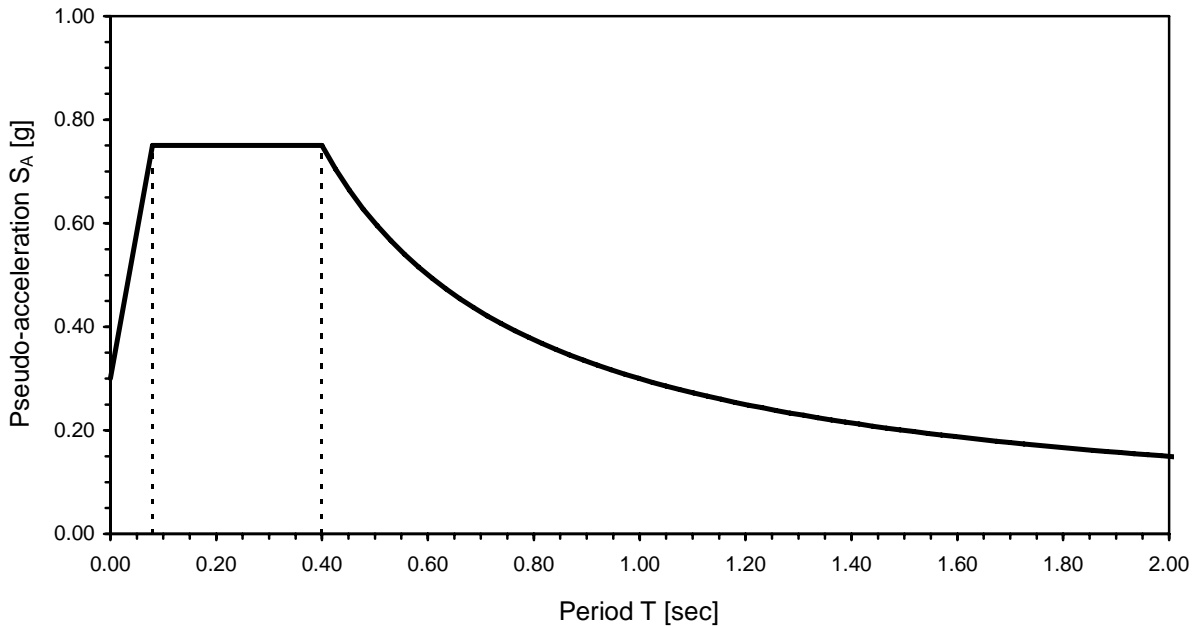
Figure 3-2 Pseudo-acceleration Response Spectrum for Seismic Analysis and Design

period range of the spectra is not taken as constant but rather varies as a function of T, and that the long period range varies as a function of $1/T$ instead of the more conservative $1/T^{2/3}$ in ASSHTO.

3.2.3. Steel Plate – Concrete Wall Pier Concept

This project intended to review a large number of existing systems known to provide satisfactory seismic performance, and identify from these systems which one would be most desirable to provide satisfactory blast resistance. This complete review is not presented here. However, although there was no preconceived notion of what would be the final selected system, there was an interest to investigate whether steel-plated walls of some sort would be effective for the current multihazard purpose. Therefore, prior to describing the final structural system identified and selected, a brief discussion of challenges in using wall designs is presented.

A concept relying on precast RC panels sandwiching a thin steel plate was considered as possibly adequate for both seismic and blast loading. The details for a possible implementation of this concept would remain to be worked out. However, the intent was to use steel plates framed by steel W-shape members to form a steel plate shear wall, a relatively novel type of structural system well suited for lateral seismic loading (Bruneau et al. 2005). The concrete

precast panels would be added only to provide inertia to resist gravity and blast loads (and possibly some of the seismic loads), while the steel plate shear wall was intended to resist seismic loading only. The concrete panels could also have prevented the steel plate from buckling, which would have enhanced the strength, stiffness and energy-dissipation capabilities of the steel plate shear wall.

Using the computer program BEL (USACE-ERDC 2004), it was found that the breaching and spalling threshold thicknesses for a 40 MPa concrete wall subjected to the explosive charge weight and distance assumed in this study are 635 mm (25") and 1219 mm (48"), respectively. This means that the concrete panels of the wall would have needed to be of considerable thickness in order to be able to resist the assumed blast load without substantially losing its ability to carry loads. Since the thickness of typical wall piers is 610 mm or 24" (FHWA 1969), the wall thickness that would be required for this multi-hazard application would have been significantly greater than that of typical wall piers, which made it unappealing. The implementation of wall piers having such a substantial thickness was judged unlikely, and attempts to further develop the wall pier concept were then abandoned.

3.2.4. Concrete-filled Steel Tube Columns Bridge Pier-bent Concept

Preliminary analysis and existing literature (e.g. Winget et al. 2005) indicate that breaching controls the design of substructure concrete members subjected to intentional blast loading. The behavior of concrete members under blast loading could be substantially improved if breaching could be somehow prevented. In that perspective, encasing concrete in a steel shell would seem to be an adequate approach to provide blast-resistant piers. The addition of steel jackets has been shown to be a viable strategy for the seismic retrofit of concrete bridge pier columns (Priestley et al. 1996), but using such a jacket alone was estimated to be insufficient to provide adequate resistance to the large shear forces that develop at the base of piers subjected to blast loads. As such, using a fully composite concrete-filled steel tube continuous onto the footing was deemed to be a more appropriate solution. Therefore, the second pier concept considered in this study is a multi-column pier-bent with concrete-filled steel tube (CFST) columns. Tests carried out by Marson and Bruneau (2004) showed that CFST columns subjected to cyclic loading exhibit good energy-dissipation capabilities and stable hysteretic behavior up to a drift level equal to 7%. A possible implementation of this concept is schematically shown in Figure 3-3a. The foundation

beam consists of concrete-embedded C-channels linked to the columns through steel plates. This connection concept is schematically illustrated in Figure 3-3b. This type of foundation beam performed successfully in the tests by Marson and Bruneau (2004) in that it allowed the composite column to develop its full moment capacity. Conceptually, the channels are designed to resist the full composite strength of the columns, and the concrete at the foundation beam does not need any reinforcement for strength purposes (fiber concrete is however recommended to prevent cracking of the concrete and subsequent water infiltration into the footing). However, the tests described in Marson and Bruneau (2004) were performed in the longitudinal direction of the foundation beam, and the concept would have to be slightly modified with additional concrete-embedded C-channels to provide equal resistance to loads acting in the short direction of the foundation.

3.3   Preliminary Analysis and Design of the Proposed Pier Concept

3.3.1. Analysis and Design for Blast Loading

Assuming that breaching and spalling are not design considerations for CFST columns (the tests described later in this report will show that this is indeed the case), the design of CFST columns subjected to blast loads is then governed by the magnitude of the allowable inelastic deformations under the expected blast pressures. No information was found in the literature on the behavior of CFST columns under blast loading, and thus no design guidance was found to estimate the size of the column necessary to resist an assumed blast load. It was therefore decided to calculate the inelastic response of all CFST columns possible considering all of the commercially available steel tube sections. For this purpose, a simplified analysis procedure was adopted, in part because it was judged that analysis refinements were not needed at this stage, and in part because little information was found about the actual distribution in space and time of blast pressures acting on circular columns subjected to short-distance blasts. The most cited reference on this topic (DTRA 1997) is of restricted circulation and could not be used in this research.

The simplified procedure adopted here for preliminary analysis is described in Mays and Smith (1995), and is essentially identical to the method presented in USDA (1990). In essence, the method considers an equivalent SDOF system having an elastic-perfectly-plastic behavior, and assumes that all the energy imparted to the system by the blast loading is converted into internal

43

strain energy. The detailed information was presented in Section 2.3. Under these conditions, the maximum deformation due to impulsive-type blast loading is given by:

$$X_m = \frac{1}{2} \left(\frac{I_{eq}^2}{K_{LM} \, m \, R_u} + X_E \right) \tag{3-2}$$

where I_{eq} is equivalent uniform impulse per unit length, K_{LM} is load-mass factor, m is the mass per unit length of the column, R_u is the strength per unit length of the column and X_E is the
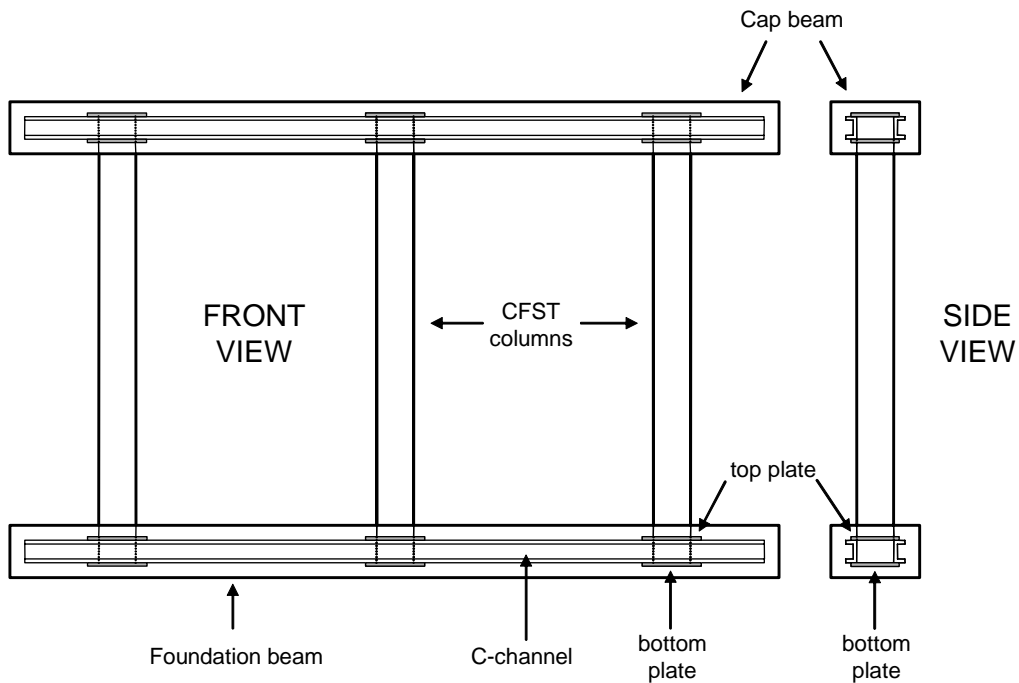
(a) General description
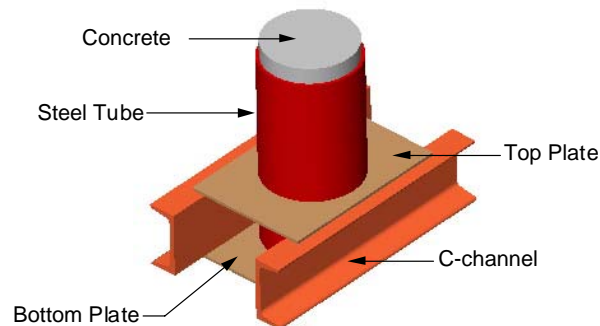
(b) Detail of the column-to-foundation beam connection

Figure 3-3   Multi-column Pier-bent Made up of Concrete-filled Steel Tube Columns

44

displacement at the onset of plastic behavior. In this analysis, I_{eq} was calculated by:

$$I_{eq} = \beta\, D\, i_{eq} \tag{3-3}$$

where i_{eq} is equivalent uniform impulse per unit area, D is column diameter and β is factor to account for the reduction of pressures on the column due to its circular shape. While no data could be found in the available literature on the actual blast pressure variation along the perimeter of circular sections, an estimate could be made by using data experimentally obtained for walls subjected to blast waves at different angles of incidence (Mays and Smith 1995). However, since the ratio of the pressure at a given angle of incidence to that at any other angle is not a constant but a function of the magnitude of the blast pressures, the value of β is then, strictly speaking, a function of both time and space (with respect to the coordinate system depicted in Figure 3-4, factor β is a function of space coordinate z). In order to simplify the analysis, it was decided to adopt a constant value of β which was calculated considering the level of peak blast pressures indicated by BEL for most of the height of the column. Values of
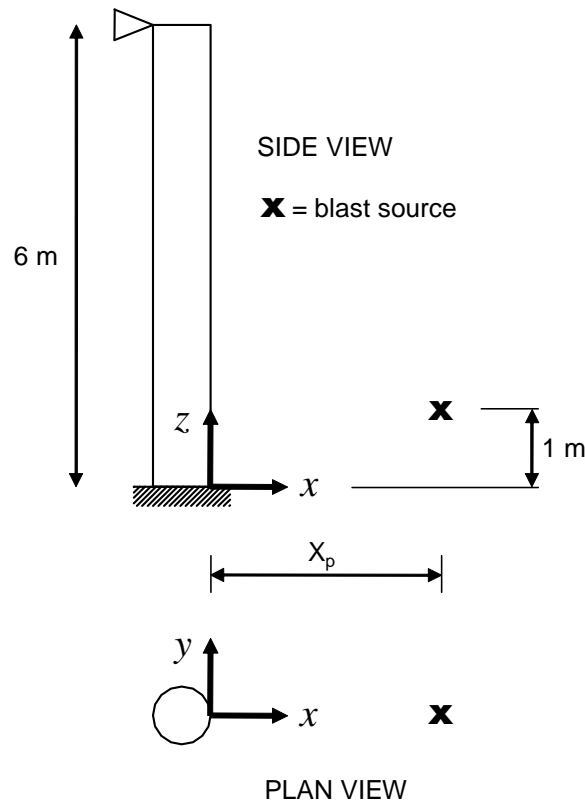
Figure 3-4   Coordinate System and Boundary Conditions for Simplified Analysis of CFST Columns

45

blast pressures at different angles of incidence were obtained using the public domain computer program AT-Blast (ARA 2004). The resulting value of β (= 0.85) turned out to be very similar to the value adopted by Winget et al. (2005) for a similar analysis (= 0.80). The quantity i_{eq} was calculated by:

$$i_{eq} = \frac{\int_0^H i(z)\,\delta(z)\,dz}{\int_0^H \delta(z)\,dz} \qquad (3\text{-}4)$$

where $i(z)$ indicates the variation of impulse per unit area along the height of the column and $\delta(z)$ is the normalized deflected shape of the column. In this analysis, $i(z)$ was assumed equal to the variation of total impulse (per unit area) along the height of the column. Values of $i(z)$ were calculated using the program BEL considering reflections of the blast wave on the deck and on the ground. The resulting values of $i(z)$ are qualitatively shown in Figure 3-5. Finally, reduction of blast impulse due to the clearing time (i.e., the time it takes for the blast wave to pass around the column) was not considered. Based on the analysis described in Winget et al. (2005), neglecting such pressure reduction due to "clearing time" is only slightly conservative.
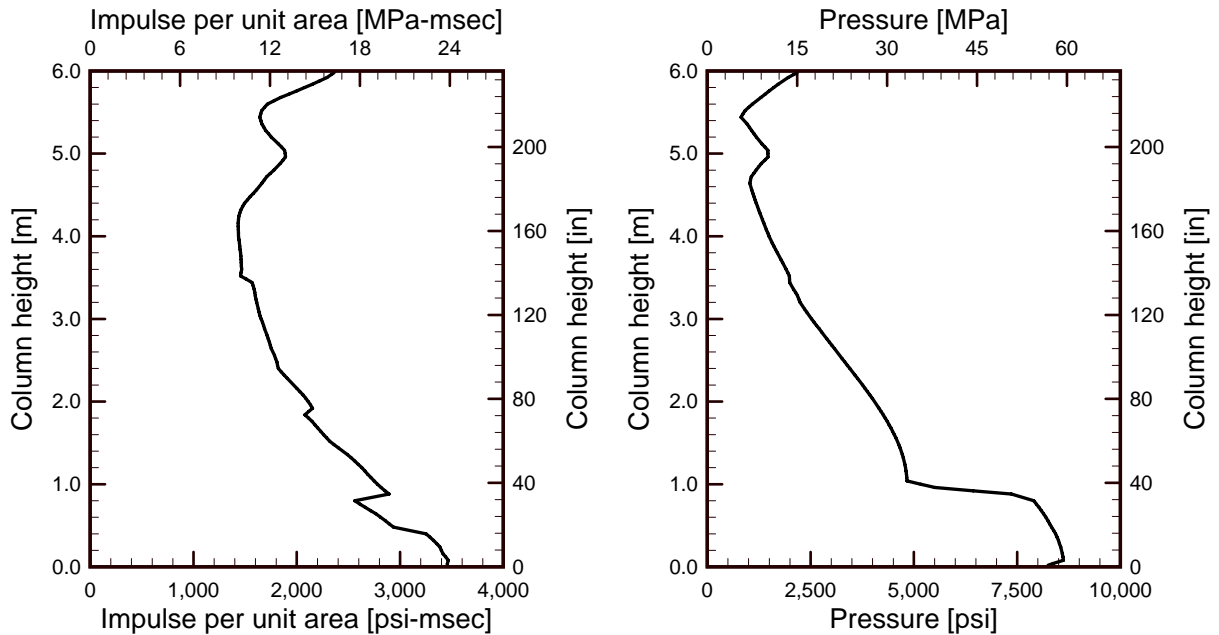
Figure 3-5   Variation of Total Impulse and Peak Pressure along Height of Column

The column was assumed fixed at the bottom but pinned at the top where bearings may not be able to prevent rotation of the cap beam about its longitudinal axis (Figure 3-4). For these boundary conditions, the normalized deflected shape for inelastic deformations after plastic hinging is given by (Figure 3-6):

$$\delta(z) = \begin{cases} \dfrac{2z}{H} & \text{for } 0 < z < \dfrac{H}{2} \\[3mm] 2 - \dfrac{2z}{H} & \text{for } \dfrac{H}{2} < z < H \end{cases}$$

(3-5)

which assumes that the in-span hinge develops at column mid-height (this assumption will be examined later in this report). For the deflected shape indicated by Equation 3-5, the load-mass factor (i.e., the factor that converts the actual, continuous system into an equivalent SDOF system – see Section 2.3) is $K_{LM} = 0.66$ and R_u is given by:

$$R_u = \frac{12\,M_p}{L^2}$$

(3-6)

where M_p is the plastic moment capacity of the column, which was calculated using the
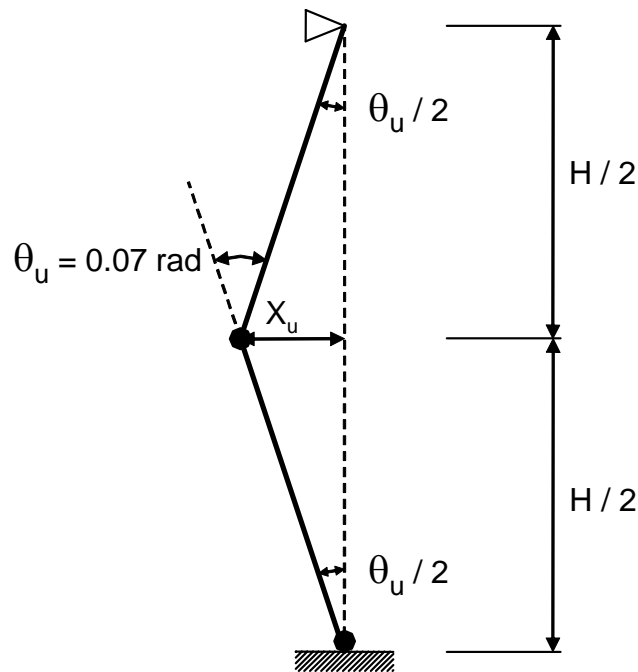
Figure 3-6   Plastic Deformations in Fixed-pinned Column under Blast Load

approximate equation presented in Bruneau and Marson (2004), i.e.:

$$M_p = \left(Z - 2\,t\,h_n^2\right) f_y + \left[\frac{2}{5}\left(\frac{D}{2} - t\right)^3 - \left(\frac{D}{2} - t\right) h_n^2\right] f_c' \qquad (3\text{-}7)$$

where Z and t are the plastic modulus and thickness of the steel tube section, f_y is the yield strength of steel, f_c' is the concrete strength and h_n is given by:

$$h_n = \frac{A_c\,f_c'}{2\,D\,f_c' + 4\,t\left(2\,f_y - f_c'\right)} \qquad (3\text{-}8)$$

where A_c is the core concrete area. It must be noted that no resistance factor was considered to calculate M_p. Finally, X_E is given by:

$$X_E = \frac{R_u}{K_e} \qquad (3\text{-}9)$$

where K_e, the elastic stiffness of the equivalent SDOF system, is given by:

$$K_e = \frac{160\,EI_e}{L} \qquad (3\text{-}10)$$

where, in turn, EI_e is the flexural stiffness of the column, which was calculated using the following equation:

$$EI_e = E_s\,I_s + 0.8\,E_c\,I_c \qquad (3\text{-}11)$$

where E_s, E_c are the Young's moduli of steel and concrete, and I_s, I_c are the moment of inertia of the steel tube section and core concrete section, respectively. Note that Equation 3-11 is from the Eurocode 4 (1994) and that the AISC Provisions (AISC 1999) do not provide an equation for EI_e (Bruneau and Marson 2004). At this preliminary stage, reductions of M_p due to axial load and P-Δ effects were not considered. It will be shown in the next subsection that this simplification does not introduce a significant error.

According to Mays and Smith (1995), Equation 3-2 is valid only if:

$$\frac{t_m}{t_d} > 3 \qquad (3\text{-}12)$$

where t_m, the time at which the deformation reaches X_m, is given by:

$$X_m = \frac{I_{eq}}{R_u} \qquad (3\text{-}13)$$

48

and t_d, the time at which blast pressures dissipate, is given by:

$$t_d = 2 \frac{i_{eq}}{p_{eq}} \qquad (3\text{-}14)$$

where, for consistency with Equation 3-4, p_{eq} was calculated by:

$$p_{eq} = \frac{\int_0^H p(z)\,\delta(z)\,dz}{\int_0^H \delta(z)\,dz} \qquad (3\text{-}15)$$

where $p(z)$ was assumed equal to the distribution of peak pressures along the height of the column. The distribution of peak pressures $p(z)$ along the height of the column indicated by BEL is shown in Figure 3-5. Note that Equation 3-14 is an approximation, since pressure time histories vary along the height of the column and t_d is, strictly speaking, also a function of coordinate z.

For the analysis, concrete strength, f_c', and Young's modulus, E_c, were assumed equal to 40 MPa and 30,000 MPa, respectively. Young's modulus of steel was assumed equal to 200,000 MPa (29,000 ksi). Steel tube sections considered in the analysis included AISC round hollow structural sections (HSS), AISC pipe sections and several other sections provided by US pipe manufacturers. Sections not complying with the minimum thickness (= $D(f_y/8E_s)^{0.5}$) and minimum area (= 0.01 β D^2) requirements for composite sections specified in AISC (1999) were not considered. Following AISC (2001), yield stress of steel was set equal to 290 MPa (42 ksi) for round HSS and equal to 240 MPa (35 ksi) for pipe sections. The above concrete strength and yield stress of steel were multiplied by 1.25 and 1.2, respectively, to account for strength magnification at large strain rates under impulsive conditions (Mays and Smith 1995). Finally, specific mass of concrete was assumed equal to 2400 kg/m^3, and that of steel was assumed equal to 7800 kg/m^3.

Marson and Bruneau (2004) experimentally demonstrated that CFST columns of the type considered here had a cyclic rotation capacity of 0.07 rad. Therefore, for the monolithic loading condition considered here, it was conservatively assumed that the rotation capacity, θ_u, of plastic hinges in CFST columns could be taken as 0.07 rad. For the assumed deflected shape of the column under blast load (Figure 3-6), it can be seen that the displacement capacity of the

49

column, X_u, measured at column mid-height (i.e., the displacement considered in the simplified method adopted for this analysis), is then equal to:

$$X_u = \frac{H}{2} \frac{\theta_u}{2} = 105 \text{ mm} \tag{3-16}$$

Given the lack of information about the behavior of CFST columns under blast loading, the value of X_u indicated by Equation 3-16 was taken only as representative of the magnitude of the probable displacement capacity rather than an exact measure. Furthermore, in hindsight, the maximum rotation capacity reported by Marson and Bruneau (2004) was developed at the base of a cantilever. Given that an in-span hinge can develop twice the plastic hinge length of a hinge at the base of a column, the mid-span plastic rotation capacity at this stage could have been taken as 0.14 rad. This will be investigated in later sections.

Displacement response of CFST columns under blast load is presented in Figure 3-7 in which solid contour lines indicate equal displacement response, X_m, and broken contour lines show equal cross-section area. The displacement response for the commercially available steel tube sections for which response is between 75 mm and 135 mm are shown in Figure 3-7 as individual data points (cases for which response falls outside that range are not plotted). The contours of X_m considered in the figure were selected to represent the range of estimated ultimate displacement capacity indicated by Equation 3-16. The plot shows that, for a fixed level of plastic rotation, the area of tube sections having a large D/t ratio is less than the area of tube sections having a small D/t ratio, hence material effectiveness was highest for piers having the highest diameter-to-thickness (D/t) ratio. For all of the sections shown in Figure 3-7, it was found that $X_m > X_E$ (i.e., confirming that the response is inelastic) and that $t_m/t_d > 7$ (i.e., use of Equation 3-2 is valid). It can be seen that, for a given level of displacement response, there are several available tube cross-sections providing the necessary plastic rotation capacity. Results in Figure 3-7 also show that, for the assumed blast load, the minimum thickness required is 0.5" for the range of diameters considered. Figure 3-7 also indicates that the required diameter of tube sections having this minimum thickness is in the range of 20"-24", which compares well with the typical 36" diameter of standard concrete piers. Results shown in Figure 3-7 indicate that CFST columns having practical dimensions are able to perform well under the assumed blast load, within the assumptions adopted for this analysis. Experimental work reported in subsequent

sections will allow revisiting some of these assumptions and enhancing the reliability of these analyses.
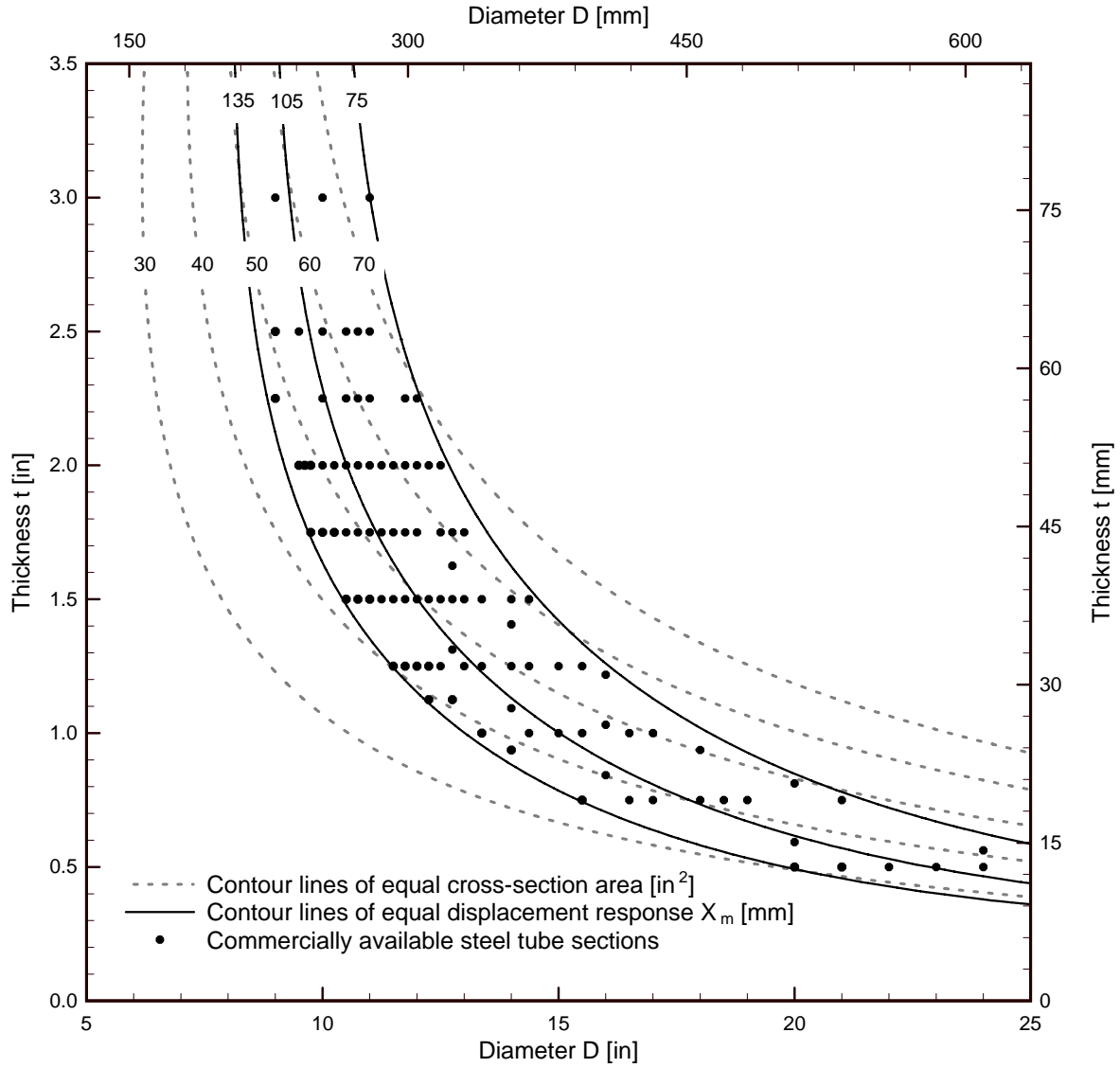
Figure 3-7   Displacement Response of CFST Columns under Blast Load

3.3.2. Analysis and Design for Seismic Loading

The seismic behavior of the proposed pier-bent concept will be examined considering only the 0.5" thick tube sections mentioned in the former subsection for diameters of 20" and 24". Larger diameter sections are deemed more desirable for practical applications. The area of the 0.5" thick tube cross-sections is less than that of all the other tube sections for which the level of blast response is similar (i.e., the 0.5" tube sections are the lightest ones). The 0.5" thick tube sections having diameters equal to 20"-24" are also produced by many suppliers.

Bruneau and Marson (2004) proposed that the ultimate combined P-M demand on CFST columns be given by:

$$\frac{P}{P_r} + \frac{P_{ro} - P_{rc}}{P_{rc}} \frac{M}{M_p} \leq 1 \tag{3-17}$$

subjected to:

$$\frac{M}{M_p} \leq 1 \tag{3-18}$$

In equation 3-17, P_r is the axial design strength, P_{ro} is the factored compressive strength of CFST columns calculated as indicated in Chapter I of the AISC Specifications (AISC 1999), i.e. $P_{ro} = 0.85\,(A_s f_y + 0.85\,A_c f_c')$ and $P_{rc} = 0.85\,A_c f_c'$. Equation 3-17 indicates that moment demand M can then be equal to the full plastic moment capacity M_p if the axial load P complies with:

$$P \leq \left(1 - \frac{P_{ro} - P_{rc}}{P_{rc}}\right) P_r \tag{3-19}$$

For the material properties indicated in the former subsection, Equation 3-19 gives $P \leq 4258$ kN for the 20" CFST column and $P \leq 7276$ kN for the 24" CFST column, considering an effective length factor equal to unity. Recalling that the total gravity load on the pier is 4098 kN (Section 2.2.1), then the selected pipe sections are able to develop their full plastic moment capacity M_p.

In the longitudinal direction, the seismic response of the selected CFST columns can be preliminarily assessed as follows. Assuming that the bearings supporting the end spans at the abutments do not restrain displacements in the longitudinal direction (conservative assumption), longitudinal stiffness and strength is then only provided by the pier. The bridge has 2 pier-bents,

and each pier-bent is assumed to have 3 CFST columns fixed at the foundation level. To account for uncertainty in the degree of fixity provided in the longitudinal direction by the cap-beam and its connection to the deck under blast loading, both fixed and pinned conditions are considered at the top of the columns. The actual condition will most likely be somewhere between those limits.

The stiffness of each column is given by:

$$k_c = \frac{\alpha \, EI_e}{H^3} \qquad (3\text{-}20)$$

where α is equal to 12 for a fixed-fixed column, or 3 for a fixed-pinned column. The total stiffness of the bridge in the longitudinal direction in this case is:

$$K_L = 6 \, k_c \qquad (3\text{-}21)$$

The total mass of the bridge is calculated as:

$$M = m_D \, L = 1130.40 \text{ tons} \qquad (3\text{-}22)$$

Assuming that the structure behaves as SDOF system, the natural period in the longitudinal direction is given by:

$$T = 2\pi \sqrt{\frac{M}{K_L}} \qquad (3\text{-}23)$$

The elastic displacement response of the bridge is given by:

$$S_D(T) = \frac{T^2 \, S_A(T)}{4 \, \pi^2} \qquad (3\text{-}24)$$

The elastic lateral force capacity of each column is given by:

$$V_e = \gamma \, \frac{M_p}{H} \qquad (3\text{-}25)$$

where γ is equal to 2 for a fixed-fixed column, or 1 for a fixed-pinned column. The elastic displacement capacity of each column is given by:

$$\Delta_y = \frac{V_e}{k_c} \qquad (3\text{-}26)$$

Numerical results for all cases considered here are summarized in Table 3-1. Since all the columns experience the same lateral displacement at the top, Δ_y is also the elastic displacement capacity of the bridge in the longitudinal direction.

Table 3-1   Seismic Analysis in Longitudinal Direction

$D = 20$"

Condition	EI_e [kN-m^2]	k_c [kN/m]	T [sec]	V_e [kN]	S_D [mm]	Δ_y [mm]	S_D / Δ_y
fixed-fixed	185,183	10,288	0.85	257	63	25	2.56
fixed-pinned	185,183	2,572	1.70	129	127	50	2.56

$D = 24$"

Condition	EI_e [kN-m^2]	k_c [kN/m]	T [sec]	V_e [kN]	S_D [mm]	Δ_y [mm]	S_D / Δ_y
fixed-fixed	349,447	19,414	0.62	369	46	19	2.47
fixed-pinned	349,447	4,853	1.24	180	92	37	2.47

Results are summarized in Table 3-1. Assuming that the "equal displacement rule" is applicable in this case (which is reasonable, since T is in all cases in the constant-velocity region of the spectrum), then S_D can be assumed equal to the inelastic displacement demand, and the S_D/Δ_y ratio can be assumed equal to the displacement ductility demand μ. It can be observed that, in all cases, the inelastic displacement demand is significantly less than the expected displacement capacity of the CFST columns (= 0.07 rad x 6 m = 420 mm). Resulting values of μ are well within the ductility capacity of CFST columns that can inferred from the results of the tests shown in Marson and Bruneau (2004).

The seismic response in the transverse direction can be preliminarily assessed as follows, assuming that the bearings at the abutments remain elastic and can restrain laterally the bridge spans. The deck is modeled as a flexural member pinned at the ends, and the pier-bents are modeled as springs of stiffness K_P (Figure 3-8). The stiffness of the pier-bents is simply given by:

$$K_P = 3\, k_c \qquad (3\text{-}27)$$
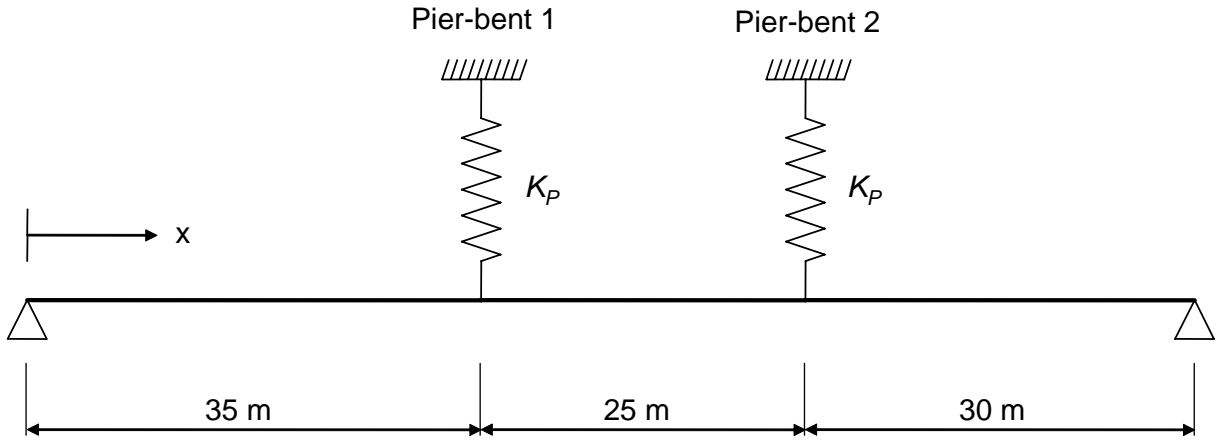
Figure 3-8   Seismic Analysis of Bridge in Transverse Direction

where k_c is the fixed-fixed stiffness of each column. The assumed deformed shape of the bridge is:

$$\psi(x) = \sin\left(\frac{\pi\, x}{L}\right) \tag{3-28}$$

If the mass of the piers is neglected, the generalized mass is given by:

$$m^* = \int_0^L m(x)\left[\psi(x)\right]^2 dx = \frac{m_D\, L}{2} = 565.20 \text{ tons} \tag{3-29}$$

and the generalized stiffness is given by:

$$k^* = \frac{\pi^4\, E_s\, I_D}{2\, L^3} + K_P\left[\psi(x_1)\right]^2 + K_P\left[\psi(x_2)\right]^2 \tag{3-30}$$

The natural period in the transverse direction is then given by:

$$T = 2\,\pi\,\sqrt{\frac{m^*}{k^*}} \tag{3-31}$$

For the value of T given by Equation 3-31, the spectral pseudo-acceleration S_A can be calculated with Equation 3-1, and the corresponding spectral displacement demand S_D can be calculated using Equation 3-24. The displacement demand on the pier-bent 1 (for which displacement demand is slightly greater due to bridge asymmetry) is given by:

$$\Delta_u = \Gamma\, S_D\, \psi(x_1) \tag{3-32}$$

where factor Γ is given by:

$$\Gamma = \frac{\int_0^L m(x)\, \psi(x)\, dx}{m^*} = \frac{4}{\pi} = 1.273 \tag{3-33}$$

Finally, the elastic displacement capacity of the pier-bent is calculated using Equation 3-26 for fixed-fixed columns.

Results are summarized in Table 3-2. In all cases, the Δ_u/Δ_y ratio is less than unity, which means that no inelastic deformations are expected in the columns. These results were obtained assuming that the bearings at the abutments have the necessary strength to remain elastic. If the bearings experience inelastic deformations, the displacement response would be greater than that indicated in Table 3-2. If the bearings instead provide no lateral stiffness, then the bridge behaves as a SDOF system, and its response is equal to that calculated in the longitudinal direction considering fixed-fixed columns. In all cases, response in the longitudinal direction would therefore govern the seismic design.

The above calculations show that, for the prototype considered, the tube sections selected to provide satisfactory performance for the considered blast load also provide adequate lateral load resistance for seismic loading.

Table 3-2   Seismic Analysis in Transverse Direction

D [in]	EI_e [kN m^2]	k_c [kN/m]	T [sec]	Δu [mm]	Δy [mm]	$\Delta u / \Delta y$
20	185,183	236,133	0.31	21	25	0.84
24	349,447	280,841	0.28	18	19	0.95

SECTION 4
EXPERIMENTAL DESIGN AND SETUP

4.1   General

This section describes the design and setup of a multi-column bent for experimental verification of its blast resistance. The proposed pier-bent design concept consisting of concrete-filled steel tube columns (CFST columns) linked by a cap-beam, as described in section 3.2, had much of the desired characteristics, was found possible using available tube sections and was selected for the purpose of these tests. As indicated in section 3.3, preliminary analyses showed this type of piers capable of providing high resistance and ductility against both blast and seismic loads.

Two identical multi-column bents, Bent 1 and Bent 2, were fabricated and a series of tests was performed at the U.S. Army Corps of Engineers Research Facility in Vicksburg, Mississippi. Due to constraints in the maximum possible blast charge weight that could be used at the test site and specimen cost considerations, test specimen dimensions were set to be 1/4 scale of the prototype bridge piers. Experimental specimens for column tests and a plate test are shown in Figure 4-1 and Figure 4-2 respectively. Each specimen consists of three piers with different diameters, D = 4", 5" and 6" (labeled hereafter as Column B1-C4, B1-C5 and B1-C6 for Bent 1 respectively, and, Column B2-C4, B2-C5 and B2-C6 for Bent 2 respectively), connected to steel beams embedded in the cap-beam and a foundation beam.

First, discussion of the column design and the plate design are presented followed by the foundation beam and cap-beam design. Next, materials used in the specimen fabrication are discussed and coupon test results are presented. Finally, the complete experimental setup is described.

4.2   Column Design

The selection of the column specimens was done according to the pier concept proposed in section 3.3 and considering the constraints of the test condition. As described in section 3.3.1, the prototype design pipe diameter is in the range of 20" – 24" with a minimum thickness of 0.5"

for the assumed blast load corresponding to a credible threat. Therefore, considering test specimen dimensions at a 1/4 scale, diameters of 4" (C4), 5" (C5) and 6" (C6) and thickness of 0.125" were selected as the column sections.

Side View

Plan View (1-1)

Plan View (2-2)

Plan View (3-3)
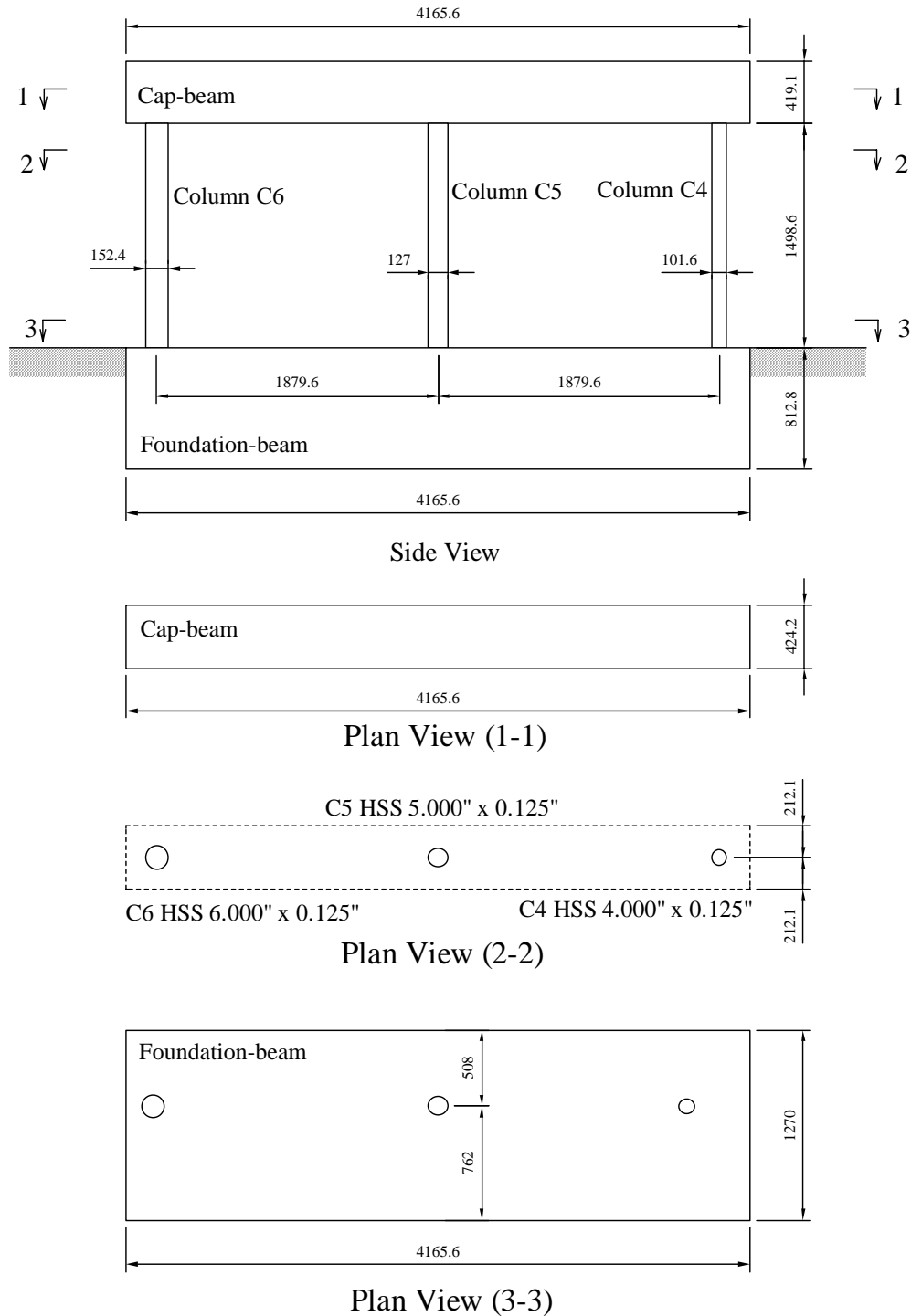
Figure 4-1   Experimental Specimen for Column Tests (Bent 1 and 2)
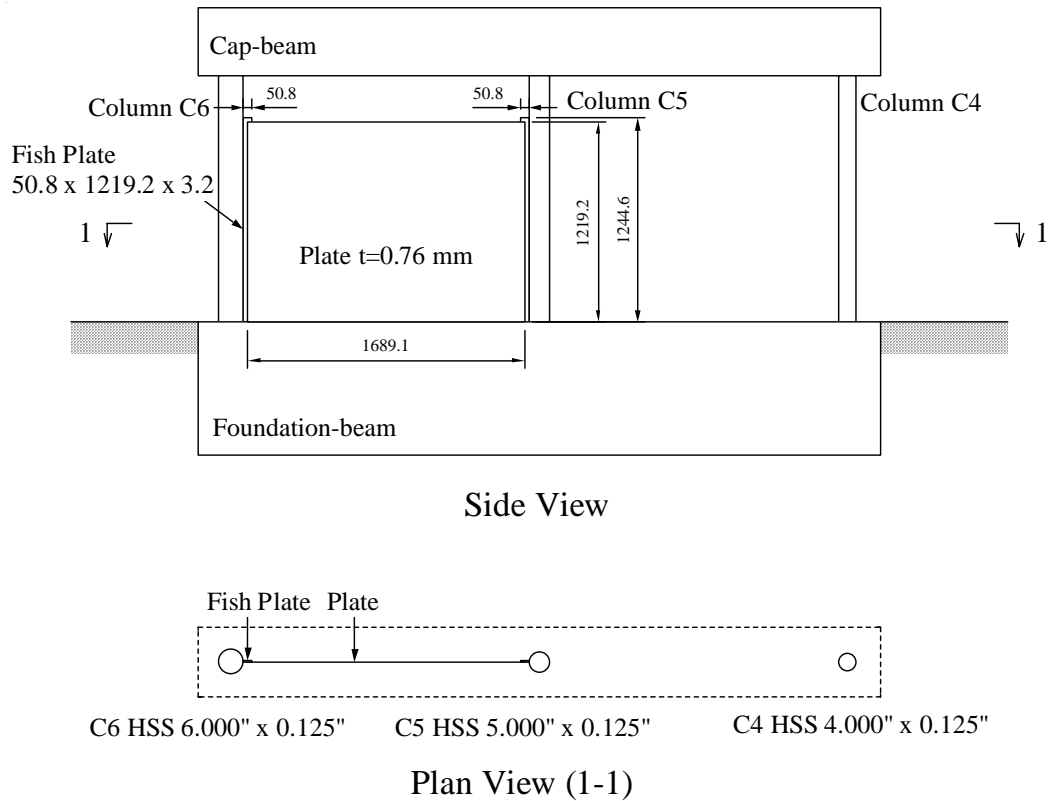
Figure 4-2   Experimental Specimen for Plate Test (Bent 2)

The plastic moment capacity of the column specimens was calculated using Equation 3-7 assuming steel yield strength, f_y, and concrete strength, f'_c, to be 42 ksi (290 MPa) and 5800 psi (40 MPa), respectively. Young's modulus was presumed to be 29,000 ksi (200,000 MPa) for steel and 4,350 ksi (30,000 MPa) for concrete. Furthermore, as recommended in the literature, concrete strength and yield stress of steel were multiplied by 1.25 and 1.2, respectively, to account for strength magnification under impulsive conditions (Mays and Smith 1995). The plastic moment capacity, M_p, of the column specimens resulted in 108.3 kip-in (12.2 kN-m), 169.4 kip-in (19.1 kN-m) and 242.2 kip-in (27.4 kN-m) for C4, C5 and C6 respectively. Calculations are presented in Appendix A.

4.3   Plate Design

Capacity design principles were used to size the plate. The intent was that the plate be able to reach its ultimate elongation before yielding of the columns to which the plate was welded. The structural response of the plate was idealized such that the plate dissipated all impulse provided

59

by the blast loading. The kinetic energy of the blast impulsive loading was assumed to be absorbed as internal plastic work of the plate, which is taken as the product of elongation and stress of the plate. For simplicity, the plate was assumed to elongate equally across the entire plate and the yield strength of the plate was assumed applied to the columns as a uniformly distributed load in order to check the capacity of the columns. The plate thickness was chosen based on the capacity of C5 since the capacity of C5 was smaller than the one of C6.

The blast impulse was calculated as an equivalent uniform impulse per unit area, i_{eq}, from Equation 2-4. The kinetic energy KE was given by:

$$KE = \frac{i_{eq}^{\,2}}{2 K_{LM} m}$$ (4-1)

where K_{LM} is the load-mass factor (0.66) and m is the mass per unit length of the plate. The internal work was calculated by:

$$W_{int} = \int f_s(\varepsilon) \cdot \varepsilon \cdot t_p \cdot H \cdot d\varepsilon$$ (4-2)

where $f_s(\varepsilon)$ is stress of plate at ε, ε is strain of plate, t_p is thickness of plate and H is height of plate. The required thickness of plate was obtained by setting $KE = W_{int}$, and a limit state of maximum plate elongation of 10 %.

Calculations for design of the steel plate, which was welded between Column B2-C5 and Column B2-C6, are presented in Appendix B. For these calculations, in addition to the material properties and dynamic strength magnification factors presented earlier, overstrength factors of 1.2 and 1.1 were considered for steel and concrete, respectively to account for the expected actual strength (based on AISC 2005 TABLE I-6-1 for steel, and discussions with concrete supplier). Note that the steel plate thickness of 22 gages (0.76 mm) and plate width of 48" (1219 mm) were selected in the final design because this was the thinnest sheet that could be easily obtained by the U.S. Army Corps of Engineers in small quantities. For this design, the maximum expected plate elongation became 8.6 % instead of the original target at 10 %.

4.4 Design of Foundation Beam

As mentioned in Section 3.2.4 and shown in Figure 3-3, the foundation beam consists of concrete-embedded C-channels linked to the columns through steel plates. For such a structural

scheme, it is assumed that the moment at the base of the columns is transmitted to the C-channels by in-plane forces acting in the corresponding steel plates (Marson and Bruneau 2004). The C-channels are assumed to work together as a single structural member, and possible contribution of the concrete to the strength of the foundation beam is conservatively neglected. Under these assumptions, each component of the foundation beam was designed as indicated in the next subsections.

4.4.1. Design of the C-channels

The moment demand on the C-channels was assumed equal to the plastic moment capacity M_p of the largest CFST column (i.e., Column C6). Since, according to AISC (2001), the yield stress of C-channels might be either 36 ksi or 50 ksi, a yield stress equal to 36 ksi was conservatively assumed. With $M_p = 242$ kip-in (Section 4.2), and taking into account the dynamic strength magnification factor for steel (= 1.2), the required plastic modulus for each channel was 2.80 in^3. C-channel C4x7.25, for which the plastic modulus Z is 2.84 in^3, the depth d is 4 in, the flange width b_f is 1.72 in, and the flange thickness t_f is 0.296 in, was then selected.

4.4.2. Design of the Top and Bottom Plates

By equilibrium considerations, the in-plane forces F_p acting on the top and bottom load-transfer
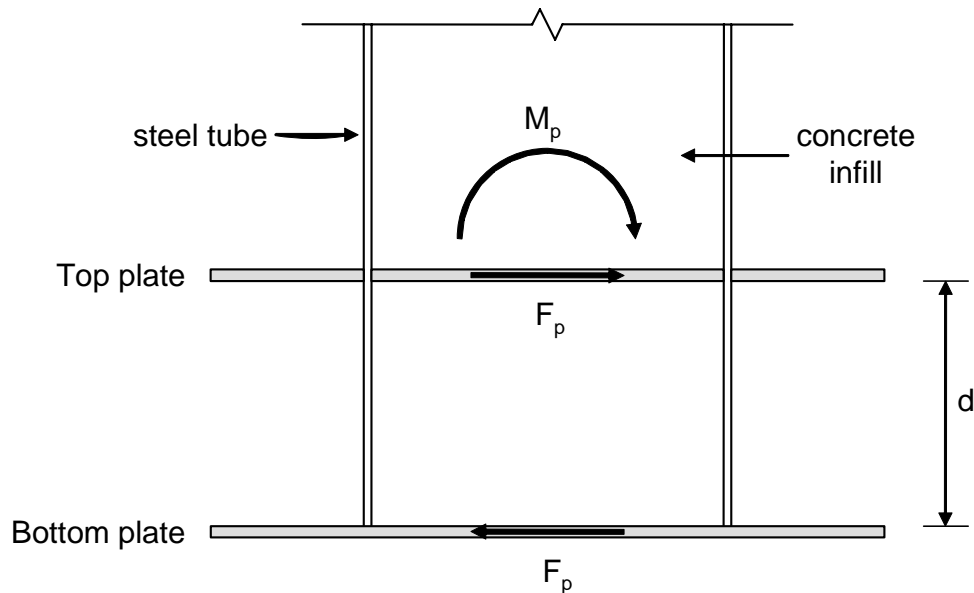
Figure 4-3   In-plane Forces in Steel Plates (for clarity, neither C-channels nor embedding concrete are shown)

61

plates (Figure 4-3) must be equal to the plastic moment capacity M_p of the corresponding CFST column divided by the distance between the axes of the plates. This distance is equal to the depth d of the C-channels plus the thickness of the plates t_p, but the latter term is conservatively ignored in design. Hence:

$$F_p = \frac{M_p}{d}$$ (4-3)

The dimensions of the top plate are shown in Figure 4-4. From geometric considerations, the width of the plate b_p is given by:

$$b_p = D + b_f$$ (4-4)

The plate thickness t_p and the plate length l_p were calculated based on the necessary length of the fillet welds and on the magnitude of the in-plane stresses in the plate, which in turn were calculated by considering the following simplifying assumptions.

The thickness of the plate t_p was calculated assuming that the force F_p induces stresses of equal magnitude and direction along the whole perimeter of the column (Figure 4-5). The magnitude
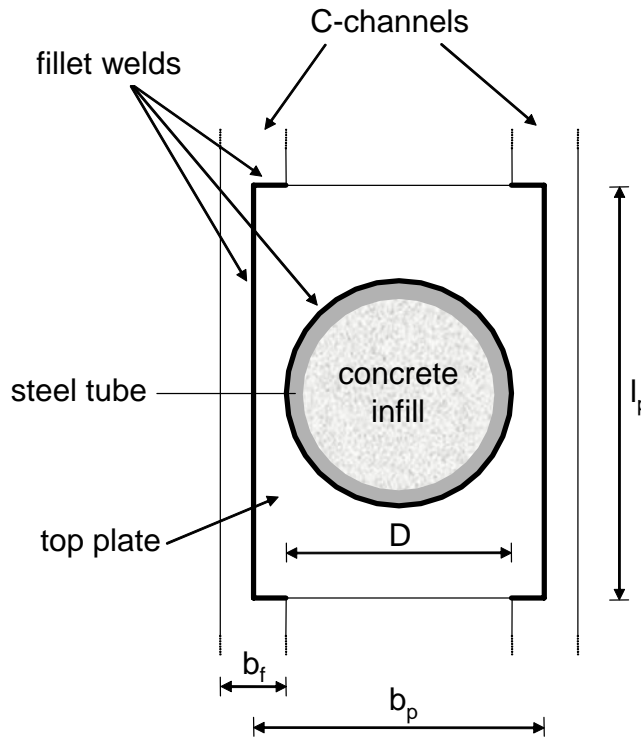
Figure 4-4   Plan View of Connection between CFST Column and Foundation Beam (for clarity, embedding concrete is not shown)

of these stresses is given by:

$$f = \frac{F_p}{\pi \ t_p \ D}$$

(4-5)

At point "1" shown in Figure 4-5, f is a pure shear stress, and must not exceed the shear strength of the plate, i.e.:

$$f \leq \phi_p \ 0.6 \ f_p$$

(4-6)

where ϕ_p is the strength factor (taken as 0.9 for both bending and shear in this case) and f_p is the yield stress of the plate. From Equations 4-5 and 4-6, the required plate thickness is then:

$$t_p \geq \frac{F_p}{\phi_p \ 0.6 \ \pi \ f_p \ D}$$

(4-7)

For f_p = 1.2 x 36 ksi (i.e., taking the dynamic strength magnification factor into account), Equation 4-7 gives in all cases (i.e., for Column C4, C5 and C6) values of t_p that are less than the minimum hot rolled steel plate thickness available (= 0.1875 in). Hence, this minimum plate thickness was selected and t_p was set equal to 0.1875 in for both top and bottom plates all subsequent calculations.

In-plane forces in the top plate are transmitted to the C-channels through the fillet welds along
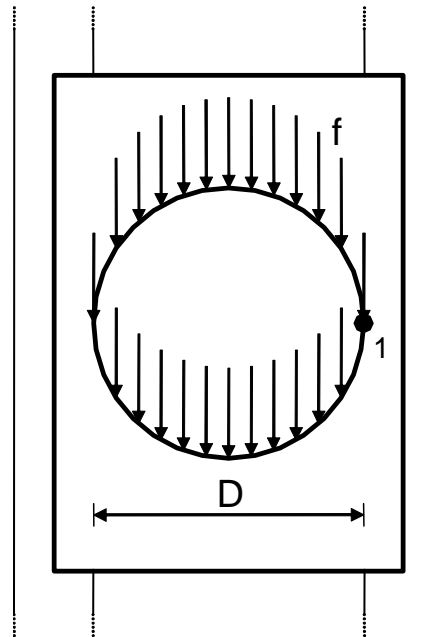
Figure 4-5   Stresses along Perimeter of Column

the longitudinal direction of the C-channels (Figure 4-4). The small transverse fillet welds shown were not considered in the calculations of the length of the fillet welds ($= l_p$). Note that no information was found in the literature about dynamic strength magnification factors for welds, and calculations were thus carried out conservatively using $f_w = 70$ ksi.

In-plane shear stresses in the plate were estimated assuming that the plate behaves as a beam simply supported by the fillet welds and subjected to a uniformly distributed load q equal to F_p/D (Figure 4-6). Under these assumptions, the maximum shear force in the "beam" is 0.50 F_p at the unloaded regions near the "supports" (i.e., between the border of the plate and the border of the column). Thus, the minimum value of l_p for which the maximum in-plane shear stresses acting on a plate rectangular cross-section of width t_p and height l_p do not exceed the allowable value $(= \phi_p \cdot 0.6 \cdot f_p)$ is given by:

$$l_p \geq \frac{1.5 \ F_p}{2 \ \phi_p \ 0.6 \ f_p \ t_p} \tag{4-8}$$

Finally, in-plane normal stresses in the plate were estimated assuming that the plate behaves as a beam simply supported by the fillet welds, but conservatively assuming the force F_p as concentrated load acting at beam mid-length (Figure 4-7). Under these assumptions, the maximum bending moment in the "beam" is $M_{max} = 0.25 \ F_p \ b_p$ at mid-length. The corresponding plate cross-section is assumed to consist of two equal rectangles of width t_p and height 0.5 (l_p - D) (Figure 4-8). The corresponding maximum normal stress is given by:
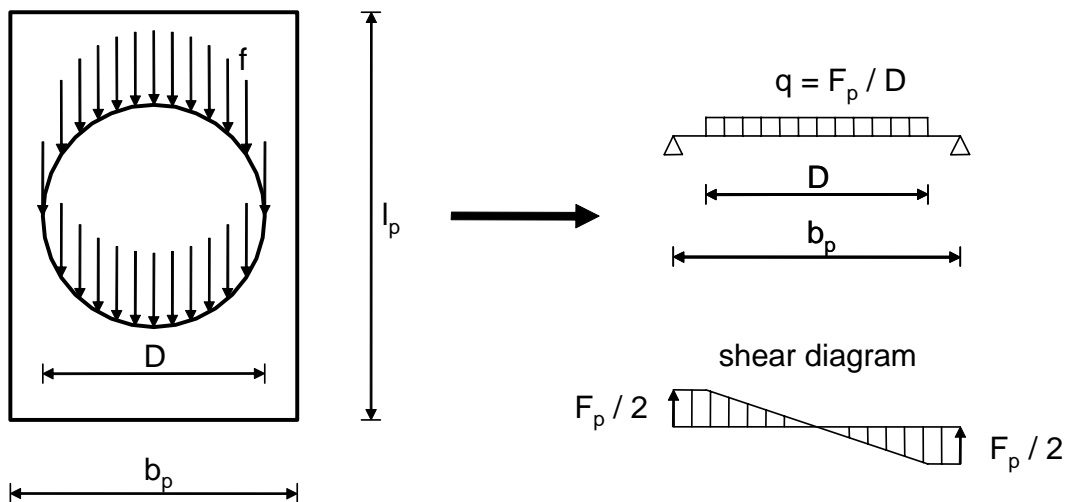
Figure 4-6   Estimation of Shear Forces in Top Plate

$$\sigma_{max} = \frac{6\,M_{max}\,l_p}{t_p\left(l_p^3 - D^3\right)} \le \phi_p\,f_p \qquad (4\text{-}9)$$

from which the required value of l_p can be obtain to limit normal stresses σ_{max} to the allowable

value (= $\phi_p\,f_p$).

In all cases (i.e., when designing the plates for Column C4, C5 and C6), Equation 4-9 governed

design for selecting the length of the plate l_p. This design approach could have been refined, but
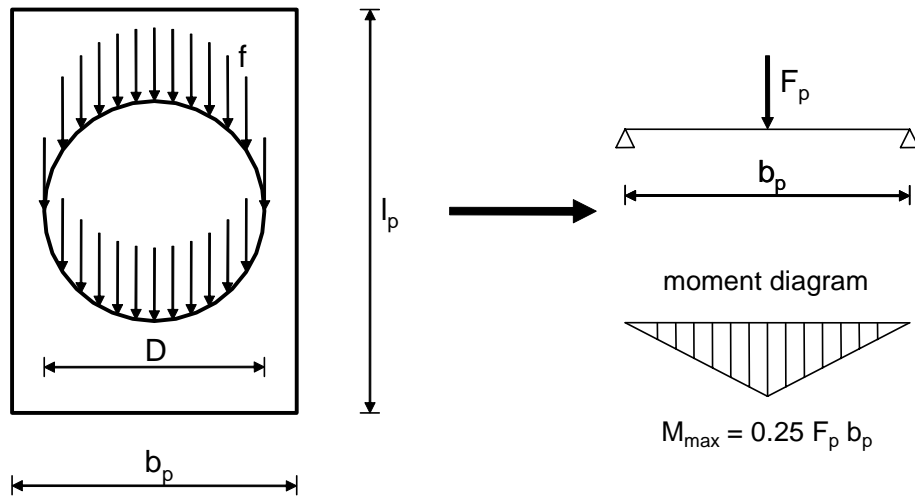
Figure 4-7   Estimation of Bending Moments in Top Plate
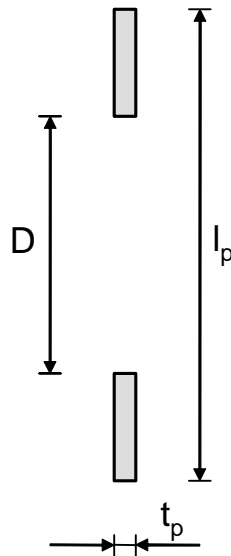
Figure 4-8   Cross-section of Top Plate at Location of Maximum Bending Moment

this was not deemed necessary given the small steel plate quantities required. Final dimensions of the steel plates are shown in Figure 4-9.

No specific calculations were performed for the bottom plates. Instead, the overall dimensions of the bottom plates were assumed equal to those of the corresponding top plate. Furthermore, the foundation beam was designed to prevent the rotation of the footings under the applied load. However, for simplicity and expediency in site construction, final dimensions of the foundation beam were significantly oversized as shown in Figure 4-1. It was also ensured that a minimum 2" thick cover concrete would be provided around all embedded steel.

4.5   Design of Cap-beam

The cap-beam was designed to remain elastic when subjected to blast pressures acting upwards on its underside. Blast pressures were obtained from the program BEL considering a blast weight equal to the maximum allowed at the test facility (W) located at a distance X from the column face and 0.25 m above the ground. Pressures were calculated along the longitudinal axis of the pier between column centerlines and assumed constant along the width of the beam.

Calculations were carried out following the same simplified method described in Section 3.3.1

PLATE PP6   PLATE PP5   PLATE PP4

(a) Top plates

PLATE P6   PLATE P5   PLATE P4

(b) Bottom plates
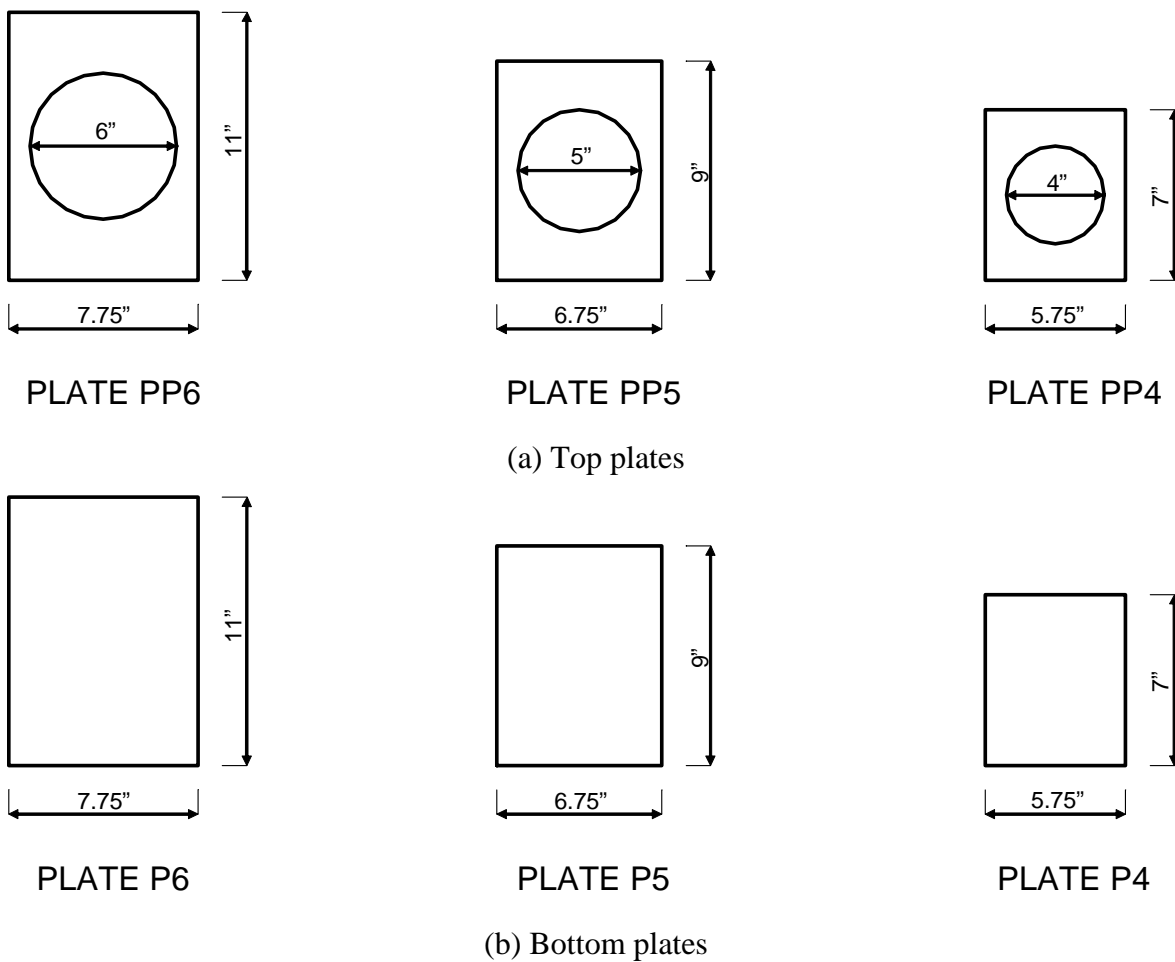
Figure 4-9   Plan Dimensions of Steel Plate

with the following differences. The beam was modeled as a fixed-fixed beam of length 1.875 m (i.e., the distance between the column centerlines). Since the beam was intended to remain elastic, the deformed shape of the beam (necessary to calculate equivalent uniform pressure and impulse) was assumed equal to that of a fixed-fixed beam subjected to a uniformly distributed load. The strength and stiffness of the beam were assumed equal to those of the C-channels acting together as a single structural member. Concrete contribution was neglected. The *mass* of the beam, however, was assumed equal to that of *both* the C-channels *and* concrete. Finally, for elastic behavior, maximum displacement under impulsive conditions is given by:

$$X_{max} = \frac{I_{eq}^2}{K_{LM} \ m \ R_u} \qquad (4\text{-}10)$$

where, as in Section 3.3.1, I_{eq} = equivalent uniform impulse per unit length, K_{LM} = load-mass factor, m is the mass per unit length of the beam and R_u is the strength per unit length of the beam. In this analysis, I_{eq} was calculated by:

$$I_{eq} = B \ i_{eq} \qquad (4\text{-}11)$$

where i_{eq} = equivalent uniform impulse per unit area and B = width of the beam. The quantity i_{eq} was calculated with Equation 3-4 considering values of $i(z)$ equal to the distribution of *total* impulse (per unit area) along the length of the beam (these values were calculated using the program BEL) and considering $\delta(z)$ as the *elastic* deflected shape of a fixed-fixed beam subjected to a uniformly distributed load. The corresponding value of K_{LM} is 0.77 and R_u is given by:

$$R_u = \frac{12 \ M_p}{L^2} \qquad (4\text{-}12)$$

where M_p is the plastic moment capacity of the C-channels acting together as a single unit. The selected section (C12x30) was found by trial and error considering A36 steel. A sizable level of conservatism is recognized in this approach to design the cap-beam, but was deemed acceptable given that the focus of the testing program is on the design and performance of the CFST. Final dimensions of the cap-beam (Figure 4-1) were determined considering a 2" thick cover concrete.

4.6   Experimentally Obtained Material Properties

Actual material properties (as opposed to values assumed for design reported earlier) were only obtained after completion of the test program. These are reported in this section. Note that no

coupon tests were performed on the material used for the connection plates and channels used in the foundation and cap beam since they were expected to remain in the elastic range during the tests. All weld metal was specified as E6010 electrode. Normal weight concrete with design strength of 40 MPa (5800 psi) was used in the circular columns. Fiber reinforced concrete was intended to be used for the cap-beam and the foundation beam to control cracking, which was deemed desirable against spalling of the concrete due to either earthquake or blast loading. However, as it was discovered after the fact, regular concrete was accidentally used for the cap beam and foundation beam instead of fiber reinforced concrete.

4.6.1. Steel Circular Column

The steel for all circular columns, HSS 4.000x0.125 (Column C4), HSS 5.000x0.125 (Column C5) and HSS 6.000x0.125 (Column C6), was specified to be ASTM A500 Grade B steel with a minimum yield stress of 290 MPa (42 ksi) and a minimum elongation at fracture of 23 % in 50.8 mm (2 in). Coupons were cut out from the specimens after the blast tests. Since the columns were partially damaged due to the tests (as described in the subsequent chapters), coupons were cut off from sides of the columns that were subjected to less strain (and presumably remained elastic). The measured coupon thicknesses of coupons taken from C4, C5 and C6 columns were 3.1 mm (0.121 in), 3.0 mm (0.117 in) and 2.8 mm (0.111 in) respectively. Coupons for tension testing were fabricated conforming to ASTM standards (ASTM A370). Mean coupon test results are shown in Figure 4-10, Figure 4-11 and Figure 4-12 for C4, C5 and C6 columns, respectively. The measured yield strengths of the steel tubes were 357 MPa (51.7 ksi), 254 MPa (36.8 ksi), 419 MPa (60.7 ksi) and the measured Young's modulus were 188,041MPa (27,266 ksi), 178,793 MPa (25,925 ksi), 196,179MPa (28,446 ksi) for C4, C5 and C6 columns, respectively.
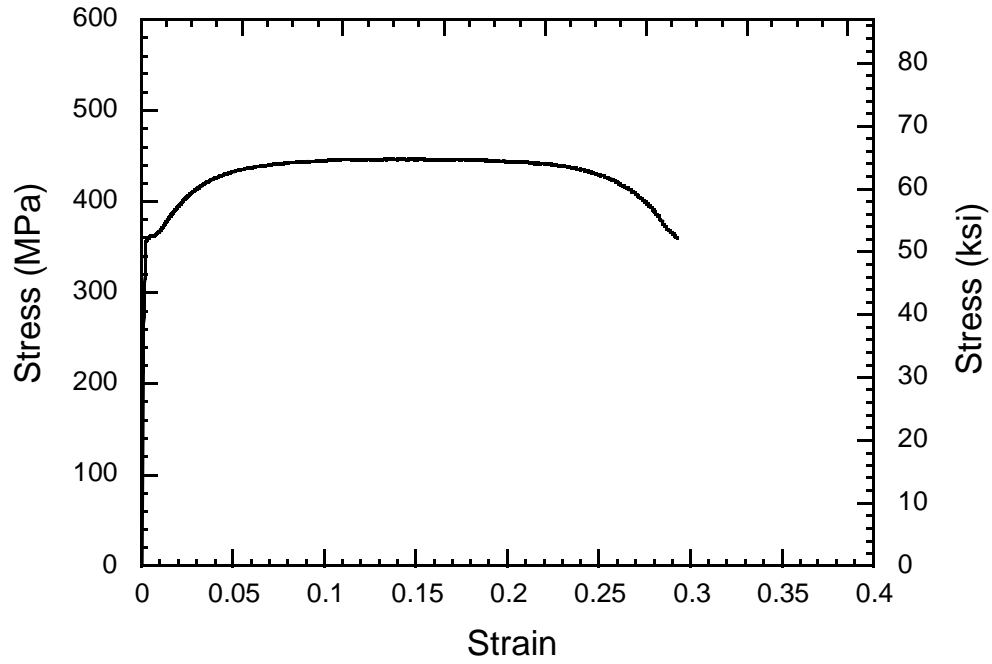
Figure 4-10   Stress-Strain Curve for Column C4
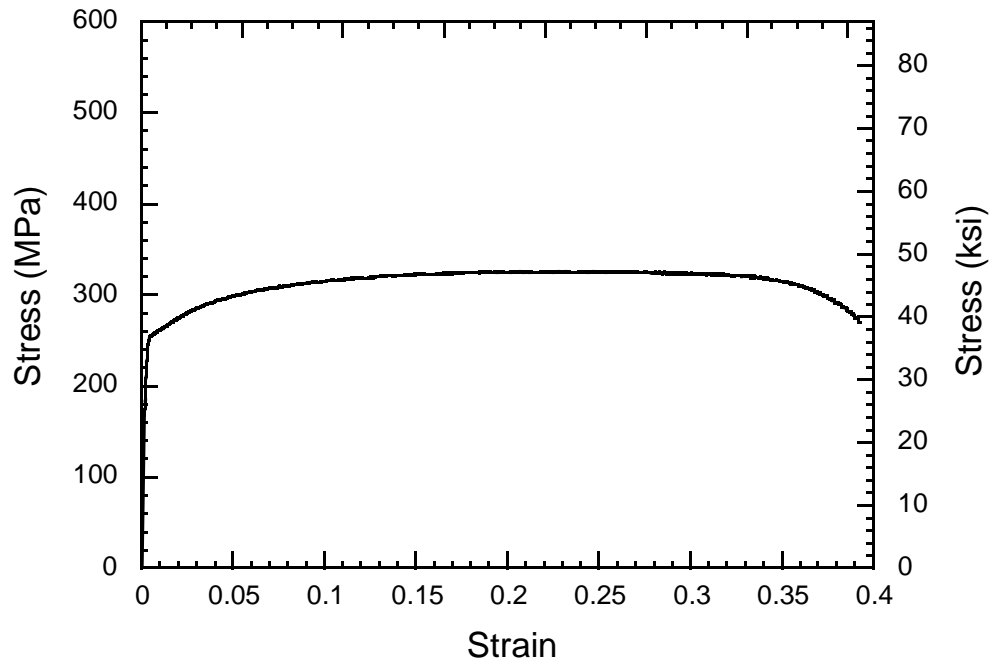
Figure 4-11   Stress-Strain Curve for Column C5
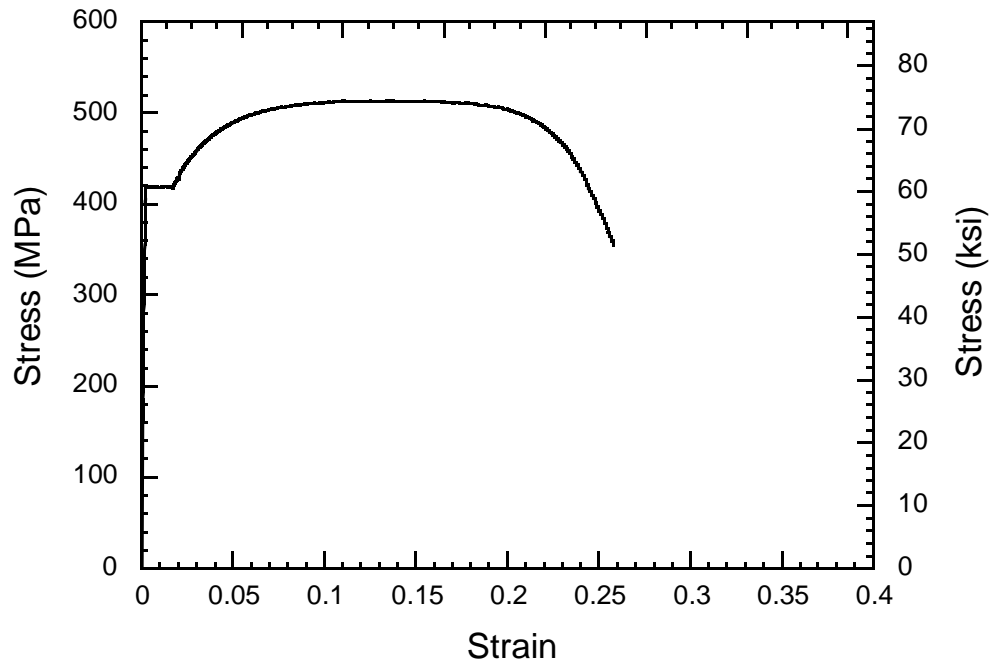
Figure 4-12   Stress-Strain Curve for Column C6

4.6.2.   Steel Plate

ASTM 1008 CS steel was specified for the plate test. This is cold-rolled commercial steel sheet with no mandatory mechanical properties. Typical yield strength and elongation are specified to be between 140 and 275 MPa (20 and 40 ksi), and more than 30% in 50 mm (2 in), respectively (ASTM, 2005). Coupons for tension testing complying with ASTM A370 (ASTM, 2005) were fabricated from the plate material. Specified plate thickness for the plate used was 0.76 mm (0.0299 in). The measured thickness of the plate was 0.77 mm (0.0303"). Mean coupon test result is presented in Figure 4-13. The measured yield and the measured Young's modulus were 239 MPa (34.7 ksi) and 184,890 MPa (26,809 ksi), respectively.

4.6.3.   Concrete

The compressive strength for the concrete used in the CFST was obtained from compression tests of concrete cylinders. Sets of three cylinders were tested at twenty eight days. Concrete slump and compressive strength results are presented in Table 3-1. Concrete compressive strength of circular columns on the day of blast load testing was predicted by the following relationships proposed by ACI Committee 211 (1992) since cylinder tests were not conducted on the test day:

$$f'_{c(t)} = f'_{c(28)}\left(\frac{t}{4 + 0.85t}\right) \tag{4-1}$$

where $f'_{c(t)}$ is the compressive strength at age t (days). The predicted compressive strengths on the test day were 43.2 MPa (6268 psi), 43.4 MPa (6292 psi) and 43.5 MPa (6313 psi) for Column B1-C4 and B1-C6, Column B1-C5 and B3-C4, and Column B2-C6 and B2-C5, respectively.
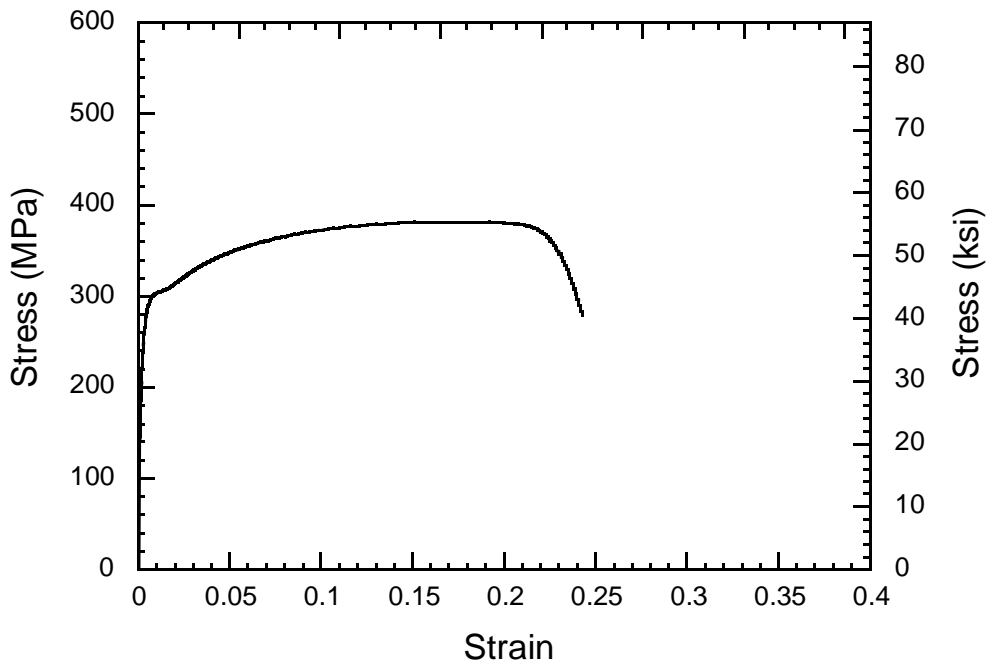
Figure 4-13   Stress-Strain Curve for Plate Test

Table 4-1   Measured Concrete Properties

Concrete Location	Concrete Slump mm (in)	Concrete Strength * MPa (psi)
Column	191 (7.5)	42.0 (6088)
Footing	216 (8.5)	30.0 (4349)

* Mean value at 28 days

4.7   Test Setup

Test specimens were fabricated in the facility of US Army Corps of Engineers, Vicksburg, Mississippi, where tests were performed. First, the C-channels of cap-beams and footings, columns and connection plates were assembled as shown in Figure 4-14. Note that the assemblies in Figure 4-14 were upside down with respect to the actual setting. Figure 4-15 shows the column-to-cap beam connection. Then, the beam and column assemblies were set at the test site and concrete of the footings was cast in the ground. Finally, non-shrink concrete and concrete were cast into the columns and the cap-beams, respectively.

Not that, for the plate test, 50.8 x 1219.2 x 3.2 bars were welded in the field along the Column B2-C5 and B2-C6 such that the 0.76 mm plate to be welded between these columns did not have to perfectly match the distance between the columns. These 3.2 mm thick bars to which the plate was welded are typically called "fish plate" in the context of steel shear wall design (Driver *et al*. 1997).

Figure 4-14   Assembly of C-channels, Columns and Connection Plates

The bent frames were braced in what would correspond to the bridge longitudinal direction at the level of the cap-beams. A reaction frame was built for this purpose. The cap-beams were not connected to the frame but in contact with the 6 x 6 x ¼ angles of the frame, such as to support the force from the cap-beam. The reaction frame was design to resist 400 kN (90 kip) of lateral force. Figure 4-16 illustrates plan and side views of the test setup for the series of column tests. Figure 4-17 through Figure 4-20 show general photographs of the specimens' setup.

Figure 4-15   Column-to-cap Beam Connection

L 6 x 6 x 1/4"

3673.5

Bent 2

Reaction Frame

Bent 1

Cap-beam

812.8   812.8

Cap-beam

1244.6

W 6 x 12"

Square HSS
4 x 4 x 1/4"

Foundation-beam

L 4 x 4 x 5/16"

Foundation-beam

1270

1270

Side View (1-1)

L 6 x 6 x 1/4"

Bent 2

Square HSS
4 x 4 x 1/4"

Bent 1

L 4 x 4 x 1/4"

Column C6

Column C6

Cap-beam

Cap-beam

2870.2

Column C5

Column C5

Column C4

Column C4

812.8   812.8

1

Reaction
Frame

1

South

East ——+—— West

3673.5

North

Plan View (2-2)
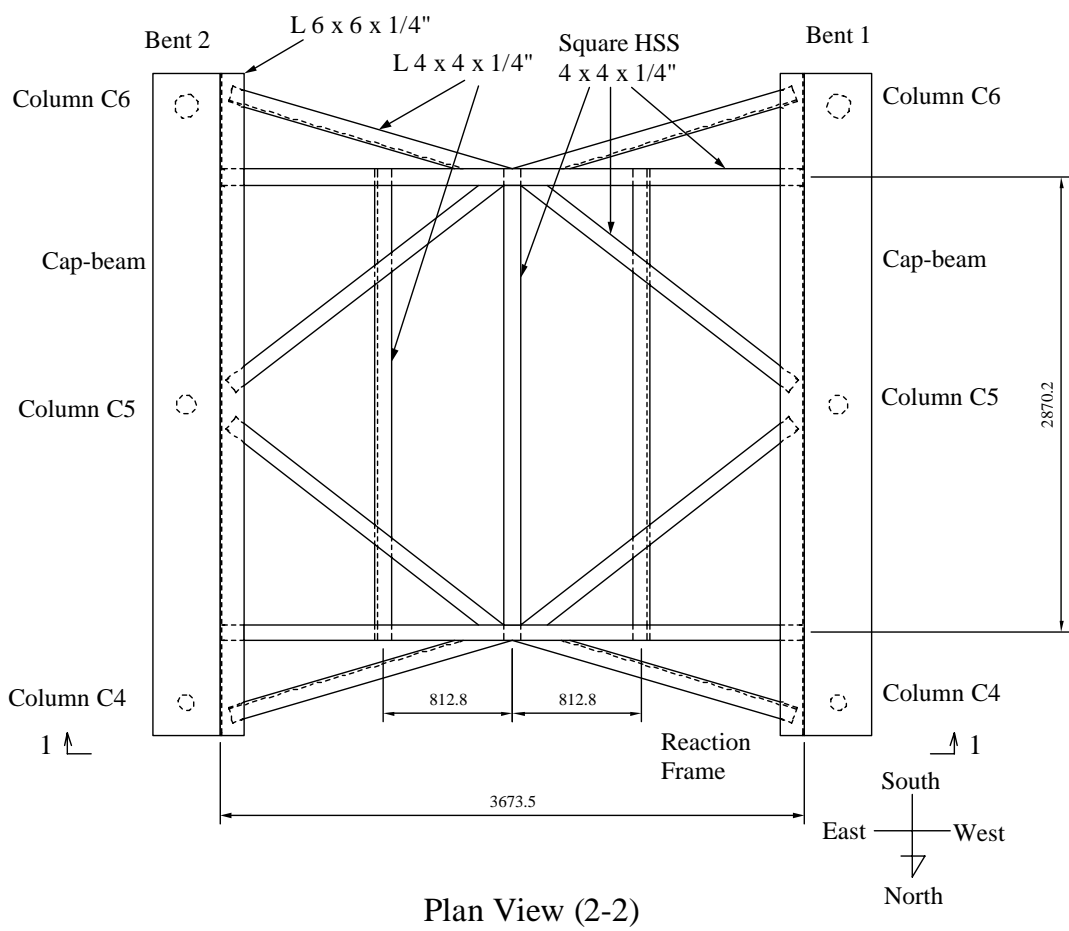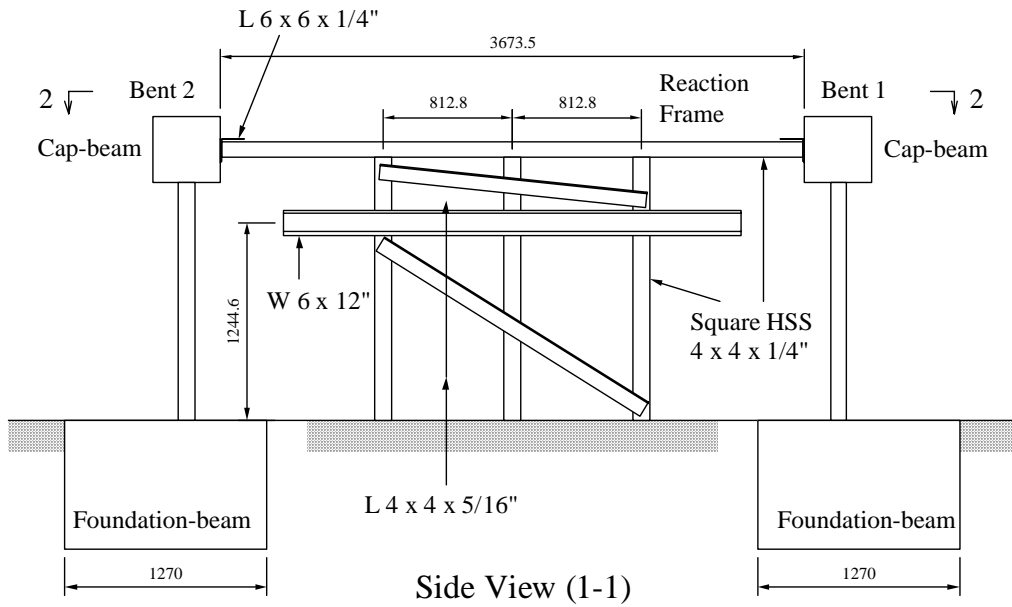
Figure 4-16   Test Setup (Bent 1 and 2)

75
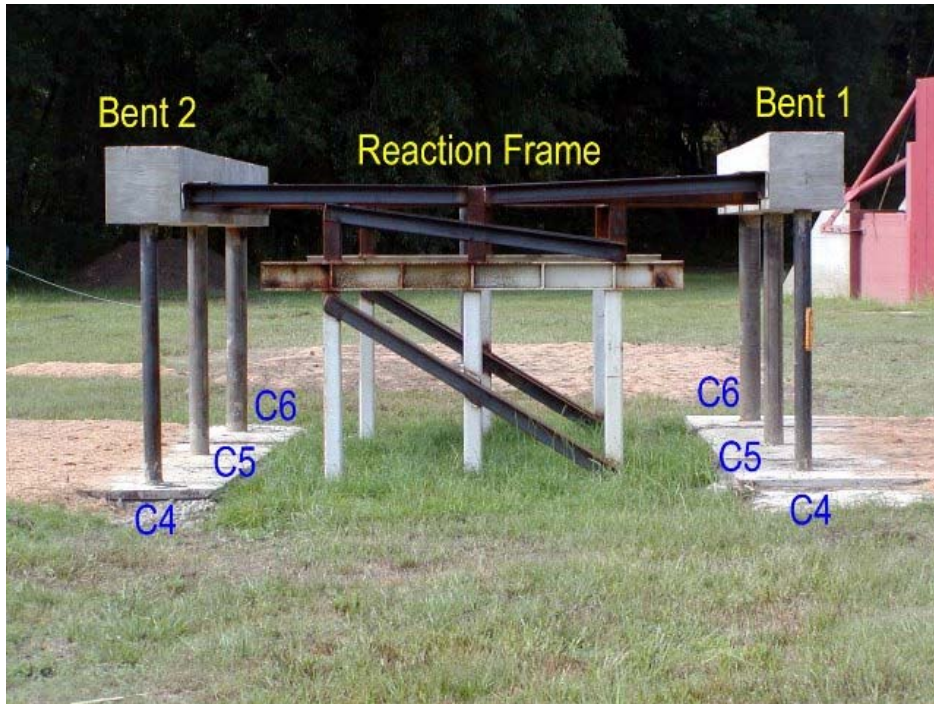
Figure 4-17   Test Setup from Side View
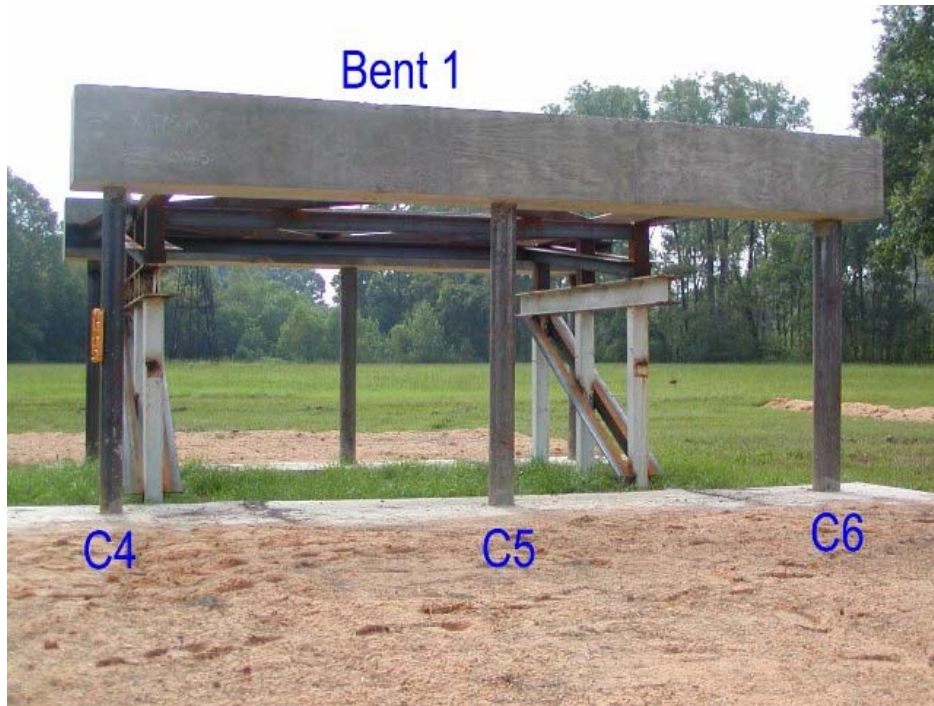
Figure 4-18   Test Setup from Bent 1 Front
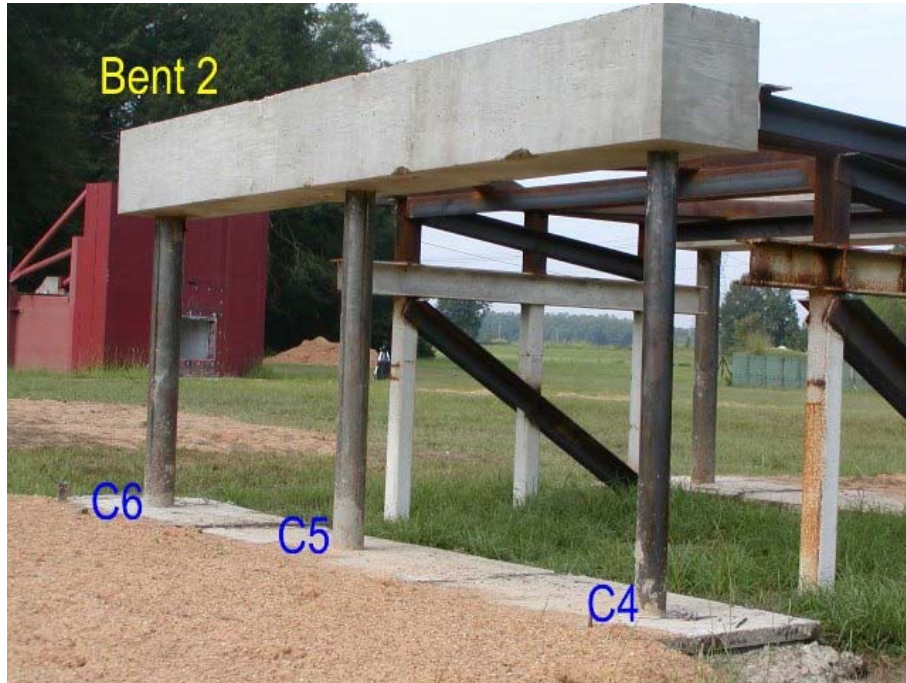
Figure 4-19   Test Setup from Bent 2 Front

Figure 4-20   Test Setup from Bent 2 Front

SECTION 5
EXPERIMENTAL CASES AND OBSERVATIONS

5.1 General

This section presents a description of the experimental cases and experimental observations made after a series of blast tests on CFST columns performed at the U.S. Army Corps of Engineers Research Facility in Vicksburg, Mississippi. Due to constraints in the maximum possible blast charge weight that could be used at the test site, test specimen dimensions were set to be 1/4 scale of the prototype bridge piers. Investigation of the core concrete of the columns is also presented along with the experimental observations.

5.2 Explosive Charge

The explosive charges used were nitromethane, which is widely used as a solvent in a variety of industrial applications. The actual charge mass is conventionally converted into a TNT equivalent mass, and the conversion factor is 1.1. For instance, a 10 kg charge of nitromethane converts to 11 kg of TNT. The charge was contained in a columnar plastic vessel with diameter of 2.5" (63.5 mm) or 6" (152.4 mm) depending on the charge volume. The standoff distance, x, height of charge, z, for the tests conducted are defined schematically shown in Figure 5-1. Standoff distance is taken as distance between the center of the charge and the closest point of the column to the charge, and height of charge is distance from ground level to the center of the charge.

5.3 Experimental Cases

Summary of the pier test cases is presented in Table 5-1. Summary of test objectives and target deformation of column tests are shown in Table 5-2 along with test results. Exact values of charge weights and stand off distances were omitted for security reason; instead these values were normalized and expressed in function of W and X respectively. In addition to the pier tests, a plate connected between two piers, Column B2-C5 and B2-C6, was also tested; test summary and result for this test are presented in Table 5-3. Three parameters were considered in deciding
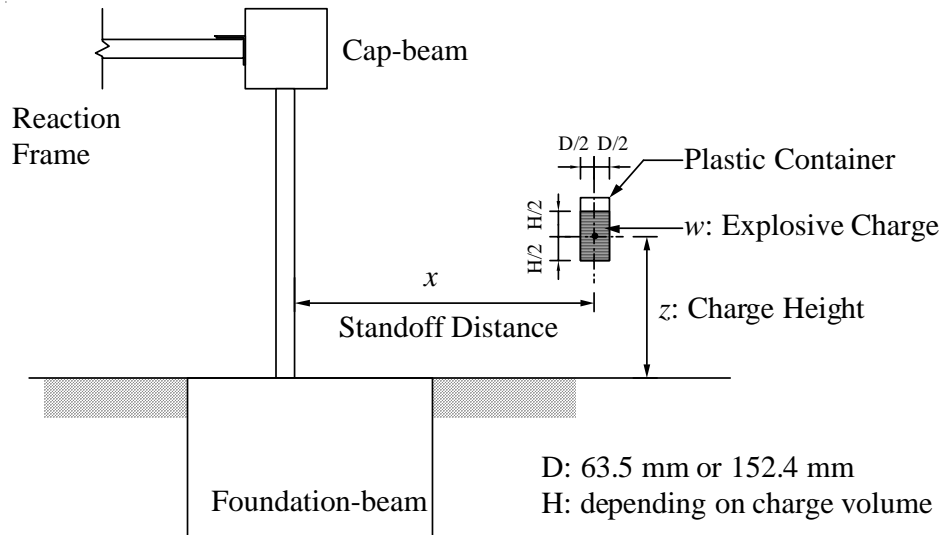
Side View
Figure 5-1   Explosive Charge Situation

test conditions, height of charge, z, standoff distance, x, and weight of charge, w. Height was chosen either to be a lower height (h = 250 mm) or a middle height (h = 750 mm) case. Lower height represented the height from the assumed blast scenario, which was 1 m for the prototype bridge. Middle height corresponds to the mid-height of the bridge column and was chosen because it was expected to provide the most severe damage to a column. The maximum blast charge was limited to W due to the constraints at the test site. Standoff distance and charge weight were determined such that maximum deformation due to the explosion was equal to maximum deformation capacity of the column. The maximum deformation caused by the explosion was predicted using the concept of impulsive response presented in Section 3.3. In brief, the response is assessed by equating the kinetic energy to the strain energy produced in the structure. The maximum deformation capacity was estimated according to the experimental results by Marson and Bruneau (2004), calculated as shown in Section 3.3, and the maximum rotation capacity was set to be 0.14 rad at middle span of the column for the cases with charges at mid-height, and 0.07 rad at the bottom of the column for the charges located at the lower height. The resulting target deformations for the mid-height cases (Test 2 to Test 5) and lower height case (Test 6) were 53 mm and 18 mm, respectively, as shown in Table 5-2.

Table 5-1   Summary of Column Test Cases

Test Num.	Bent	Column	Charge Weight, w	Standoff Distance, x	Charge Height, z (m)
Test 1	B1	C4	0.1 W	3 X	0.25
Test 2	B1	C4	0.55 W	3 X	0.75
Test 3	B1	C4	W	2 X	0.75
Test 4	B1	C6	W	1.1 X	0.75
Test 5	B1	C5	W	1.3 X	0.75
Test 6	B2	C4	W	1.6 X	0.25
Test 7	B2	C4	W	0.6 X	0.25
Test 9	B2	C6	W	0.8 X	0.25
Test 10	B2	C5	W	0.8 X	0.25

Table 5-2   Summary of Column Test Objectives, Target Deformation and Results

Test Num.	Column	Objective	Target Deformation (mm)	Maximum Deformation of Test (mm)
Test 1	B1-C4	Preliminary	0	0
Test 2	B1-C4	Maximum Deformation	53	0
Test 3	B1-C4		53	30
Test 4	B1-C6		53	46
Test 5	B1-C5		53	76
Test 6	B2-C4		18	24
Test 7	B2-C4	Fracture of Steel Shell	70	395
Test 9	B2-C6		23	45
Test 10	B2-C5		23	100

Table 5-3   Summary of Plate Test Case and Result

Test Num.	Bent	Column	Charge Weight, w	Standoff Distance, x	Charge Height, z (m)	Elongation (%)
Test 8	B2	C5, C6	0.06W	5 X	0.25	8.9 (Bottom) 4.2 (Top)

Since coupon tests of materials used in the specimen fabrication was conducted after the series of explosion tests, mechanical properties were assumed for design purposes to determine blast parameters for the tests. The material properties, dynamic magnification factors and overstrength factors were the same as the ones assumed for the design of the columns and the plate presented in Sections 4.2 and 4.3, respectively.

Owing to some uncertainty such as response of the cap-beam and behavior of concrete in the cap-beam subjected to blast load, the blast charge in the first test, Test 1, was selected to ensure that Column B1-C4 responded within the elastic range. Although Test 2 was originally intended to induce inelastic deformations, there was no damage to Column B1-C4, as the column again responded within the elastic range.

To obtain inelastic deformations, the predetermined testing program had to be revised – new test cases were developed by increasing blast charge, w, or/and decreasing standoff distance, x. As such, blast charge was increased to the maximum value W from 0.55W and standoff distance was decreased to 2X from 3X in Test 3. On the basis of the results of Test 3 in which inelastic deformations were obtained, the calculation procedure to predict column deformations was revised. It was postulated that effective pressures acting on the column were less than calculated due to the circular shape of the incidence surface. To account for this effect, a reduction factor β was proposed in Equation 3-3, and a value of 0.85 was adopted for Test 2 following the design procedure of Section 3.3. However, that 0.85 value was found to be too conservative on the basis of the test results. As a first step (by trial and error), by back-calibration with Test 3 results, a new estimated value of β was calculated to be 0.38. This factor of 0.38 was used to recalculate the blast charge parameters for all the remaining column tests. As such, the blast charge parameters shown in Table 5-1 are the recalculated values based on this factor of 0.38,

and these parameters are the ones actually used in the tests. This factor will be discussed in detail in subsequent section based on test results.

Test 4, 5 and 6 were conducted to verify that the target deformation could be achieved using the new value of β. As Test 4, 5 and 6 provided sufficient data on the ability to match the predicted target deformations, Test 7, 9 and 10 were conducted in an attempt to push the columns to their ultimate limit state, namely fracture of the steel tube, due to excessive plastic rotation.

5.4 Experimental Observations

This section describes, in detail, the observations on the series of ten tests, namely nine column tests and one plate test. Investigation of the post-test condition of the core concrete of the columns is also presented along with the experimental observations. The investigation of the core concrete was conducted for some of the columns that were cut out from the bents at the top and the bottom of the columns, and shipped to the Structural Engineering and Earthquake Simulation Laboratory (SEESL) at the University at Buffalo (UB). The columns were cut open using a grinding cutter to make two vertical cuts on diametrically opposed sides of the structural members and removing half of the steel shell to expose the concrete.

5.4.1. Test 1 and Test 2

No damage was observed in Column B1-C4 in Test 1 and Test 2. Figures 5-2 and 5-4 show the column after the tests. The column responded within elastic range in both tests. Note that no significant damage was suffered by the concrete cap-beam and foundation-beam as a result of the blast pressures. Figure 5-3 shows the blast fire ball during Test 2. This picture was taken by a high speed digital video camera at 1000 frames per 1 second. Bent 1 was engulfed in flames and the fire ball almost reached to Bent 2 on the other side of the test set-up.

5.4.2. Test 3

Figure 5-5 shows the blast fire ball for this test (also taken by the high speed digital video camera). Figure 5-6 shows the deformed Column B1-C4 after Test 3, and Figure 5-7 illustrates the deformed shape and residual displacements. To measure the deformation of the column, a string was attached to the top and bottom of the column, and the distance between the string and the column was measured using a tape measure, as shown in Figure 5-8. Note that the deformation of the column in the other test cases was also measured in this same manner. As

shown in Figure 5-7, the maximum deformation measured was 30 mm, occurring at the same height as the blast charge. Some pits were observed on the surface of the column around the same height of the blast charge, as seen in Figure 5-9. No damage of the concrete occurred at the cap-beam and foundation-beam as a result of the blast pressures. Figure 5-10 shows the core concrete observation after half the steel shell was removed. Cracks in the core concrete were only observed on the tension side around the mid-height of the column.

5.4.3. Test 4

Figures 5-11 and 5-12 show, respectively, Column B1-C6 after Test 4 and the measured deformations. Maximum deformation of 46 mm was observed at the same height of the blast charge as shown in Figures 5-12 and 5-13. This was deemed to be reasonably close to the target value of 53 mm. Figure 5-14 shows a 4 mm wide gap between the column and the foundation. Cracks were observed in both the cap-beam and foundation-beam as shown in Figures 5-14 to 5-16. Figure 5-17 shows the surface of the column around the height of the blast charge. Many pits and a notch are observed on that figure. These marks can be attributed to debris impacts, particularly to the disk attached at the mid-height of the blast charge container as it hit the column during the explosion. No spalling of the concrete was observed at the cap-beam and foundation-beam as a result of the blast pressures. Inspection of core concrete after removal of half of the steel shell (Figure 5-18) showed that cracks occurred at column mid-height on the tension side (as was also noted for B1-C4 after Test 3). In addition, some cracks developed at both the top and bottom of the column on the tension side of the negative moment due to the rigid boundary conditions. It should be added that although the cap-beams were not fixed to the reaction frames, the rotation of the cap-beam was partly restrained by the torsion resistance of the cap-beam and the other two columns in the pier-bent.

5.4.4. Test 5

Figures 5-19 and 5-20 show Column B1-C5 after Test 5 and the measured deformation, respectively. Maximum deformation of 76 mm was observed at the height of the blast charge, as shown in Figures 5-20 and 5-21. This was somewhat more than the expected target deformation. A gap of about 3 mm developed between the column and foundation, as shown in Figure 5-22. Cracks developed in the cap-beam radiating from top of the column as seen in Figure 5-23. Many pits and a notch were observed on the surface of the column around the height of the blast

charge, as seen in Figures 5-24 and 5-25. No damage of the concrete occurred at the cap-beam and foundation-beam as a result of the blast pressures. As Figure 5-26 indicates, the cracking pattern in the concrete core was very similar to the one seen in Column B1-C6 after Test 4.

5.4.5. Test 6

Figure 5-27 shows Column B2-C4 after Test 6. As shown in Figure 5-28, a maximum deformation of 24 mm was observed at 108 mm above the height of the blast charge. This was reasonably close to the expected target deformation. Figure 5-29 shows a gap of approximately 8mm between the column and the foundation. As seen in Figures 5-30 and 5-31, cratering was observed at the edge of the foundation-beam, but there was no damage at the cap-beam. Recall that, in this case, the blast charge was closer to the foundation-beam than the cap-beam.

5.4.6. Test 7

Test 7 was conducted as a retest of Column B2-C4, which had already experienced inelastic deformations in Test 6. A smaller stand-off distance of 0.6 X was used to induce fracture of the steel shell upon excessive plastic rotations. The 70 mm target deformation shown in Table 5-2 was calculated arbitrarily assuming that the onset of the fracture would occur at 80% of the maximum deformation capacity calculated by assuming a 0.07 rad rotation at the top of the column for the charge considered (low height case). The column was blown up from the bent by the explosion, as shown in Figures 5-32 and 5-33. The column landed about 34 m away in the direction of north to north-east of the test set-up, even though the blast charge was originally positioned east of the column (see orientation of cardinal directions with respect to the test set-up in Figure 3-16). Review of the video recorded during the test showed that the column first sheared off to the west and bounced off the reaction frame to the north to north-east direction. Figure 5-34 shows Column B2-C4 after Test 7, and Figure 5-35 illustrates the measured deformed shape. As shown in Figure 5-36, a maximum deformation of 140 mm was observed around the mid-height of the column. Figures 5-37 and 5-38 show the fractured sections of the column bottom and top, respectively, as found in the field. The foundation was heavily damaged and the concrete was locally crushed as shown in Figure 5-39. The rubble was removed from the foundation to inspect the depth of damage and reveal the location of the fracture. As seen in Figure 5-40, the column ruptured at the connection to the top plate of the embedded steel foundation. Figures 5-41 and 5-42 show the fracture surface of the column at that location. This

fracture surface of the steel tube was irregular and generally oriented at an angle from the longitudinal axis of the tube that was approximately 45 degree for large segments of the circular fracture surface. Fracture surface of the column under the cap-beam is presented in Figure 5-43.

Inspection of the core concrete after removal of the steel shell, as shown in Figure 5-44, revealed that cracking developed on the tension side of the region of significant bending of the deformed column. Figures 5-45 and 5-46 show a section and a side view of the column bottom, respectively. The 102 mm diameter circular section deformed into an elliptic shape with 114 mm height and 76 mm width under blast pressures. However, no concrete crushing was observed in the concrete core.

5.4.7. Test 8

Test 8 was performed with the plate welded to Column B2-C5 and Column B2-C6. Figures 5-47 and 5-48 show Plate B2-SP56 after the test from the front and back, respectively, and Figure 5-49 illustrates the measured out-of-plane deformations. The plate residual deformations were generally "pulled" toward the side where the blast charge was located, which could be attributed to the negative pressure that follows the maximum positive pressure. Fracture of the plate was observed at the bottom of the fish plates, and the fracture extended 248 mm and 394 mm from the bottom of Column C6 and Column C5, respectively. To estimate the total residual elongation of the plate, the deformed plate was pushed toward the reaction frame and the length of the plate at its bottom edge was measured using a measuring tape. The measured plate lengths were 1826 mm and 1746 mm at the bottom and top of the plate, respectively. Given the original plate length of 1676 mm, the resulting 150 mm and 70 mm elongation of the bottom and top of the plate corresponded to 8.9 % and 4.2 % elongation, respectively.

5.4.8. Test 9

Tests 9 and 10 were carried out after the plate of Test 8 was removed. These tests were aimed at inducing fracture of the steel shell without fully propagating the crack across the steel tube as in Test 7. Since the column was blown up out of the bent in Test 7, the target displacement was reduced from 70 mm to 23 mm, arbitrarily calculated assuming that onset of fracture occurs at 130% of the maximum deformation capacity corresponding to 0.07 rad rotation at the bottom of the column for the same low height charges. Being able to reach this onset of fracture would

allow defining the ultimate limit state of the specimen. The fish plate was left connected to the columns as their removal could not be accommodated within the test schedule. Test 8 produced no damage to B2-C6 and B2-C5 making it possible to test these columns using new blast scenarios. In these last two tests, the blast charge was set on the side of the bent rather than on the front. This was done partly because it was desired to have the fish plate on the back side of the column with respect to the blast location, and partly to investigate a boundary condition at the top of the columns different from the one for Test 1 through Test 7. Therefore, the column boundary condition in Test 9 and Test 10 was considered to be rigid, i.e. fixed-fixed.

Figure 5-52 shows Column B2-C6 after Test 9, and Figure 5-53 depicts the measured deformed shape. Maximum deformation of 45 mm was observed at about 310 mm above the foundation which was 60 mm higher than the height of the blast charge. Figures 5-55 and 5-56 show the damage to the foundation beam, where cratering of the concrete reached the embedded C-channels. There was no significant damage at the cap-beam as Figure 5-57 shows. Inspection of the core concrete (Figure 5-58) indicates that cracks were closely distributed on the tension side around the bottom part of the column where maximum deformation occurred.

5.4.9. Test 10

Figure 5-59 shows Column B2-C5 after Test 10 and Figure 5-60 illustrates the measured deformation. As shown in Figure 5-61, a maximum deformation of 100 mm was observed at about 327 mm above the foundation, which was 77 mm higher than the height of the blast charge. A discontinuity in the deformation of the column can be seen at the bottom of column as a result of partial fracture of the steel tube. The damage of the foundation beam is shown in Figures 5-62 and 5-63. The crater into the foundation reached the embedded C-channel connection. Note that the connection concept considered in this experiment performed successfully under blast loading, as the embedded C-channel connection and the C-channels did not suffer damage and allowed development of the full composite strength of the columns.

Buckling of the steel tube was observed near the height where maximum deformation occurred, as seen in Figure 5-64. Figures 5-65 and 5-66 show the steel tube fractured halfway around the base of the column. Figure 5-67 shows that crack distribution in the core concrete developed in the region of significant bending, and on the tension side of the deformed column. Figure 5-68

shows that there was no significant crushing of concrete at the location of buckling of the steel tube.

5.5 Summary

Bridge piers specimens, at 1/4 scale of the prototype bridge piers, were tested under blast loading. Nine CFST columns and one plate spanning between two columns were tested. The CFST columns exhibited a ductile behavior under blast load. No significant damage was suffered by the concrete cap-beam as a result of the blast pressures. The foundation connection concept applied in this experiment allowed to develop the composite strength of CFST column under blast loading.

Figure 5-2   Column B1-C4 after Test 1

Figure 5-3   Blast Fire Ball (Column B1-C4, Test 2)

Figure 5-4   Column B1-C4 after Test 2

Figure 5-5   Blast Fire Ball (Column B1-C4, Test 3)

Figure 5-6   Column B1-C4 after Test 3
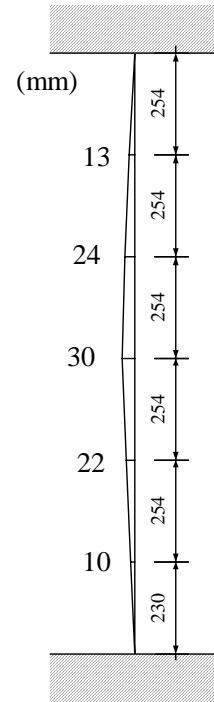
Figure 5-7   Deformation of Column B1-C4 after Test 3

Figure 5-8 Maximum Deformation (in) of Column B1-C4 after Test 3

Figure 5-9 Column Surface of Column B1-C4 after Test 3

Figure 5-10 Core Concrete of Column B1-C4 after Test 3

Figure 5-11   Column B1-C6 after Test 4
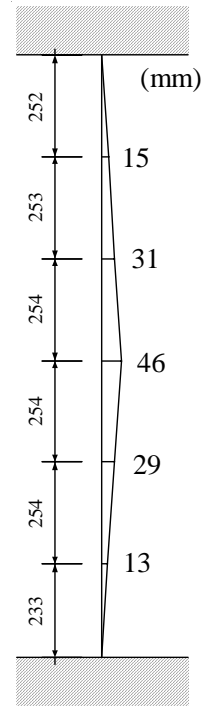
Figure 5-12   Deformation of Column B1-C6 after Test 4

Figure 5-13   Maximum Deformation (in) of Column B1-C6 after Test 4

Figure 5-14   Gap between Column and Foundation of Column B1-C6 after Test 4

Figure 5-15   Cracking at Cap-beam of Column B1-C6 after Test 4

Figure 5-16   Cracking at Cap-beam of Column B1-C6 after Test 4
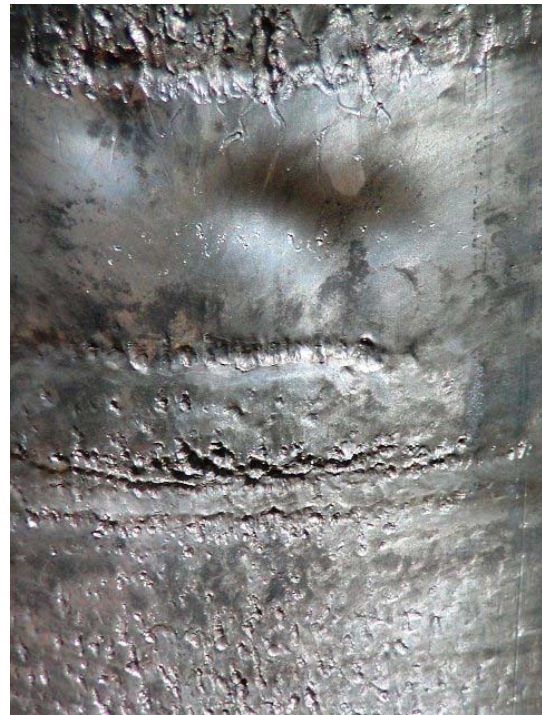
Figure 5-17   Column Surface of Column B1-C6 after Test 4

Figure 5-18   Core Concrete of Column B1-C6 after Test 4

Figure 5-19   Column B1-C5 after Test 5

(mm)

252

25

252

57

253

76

249

43

254

19

239
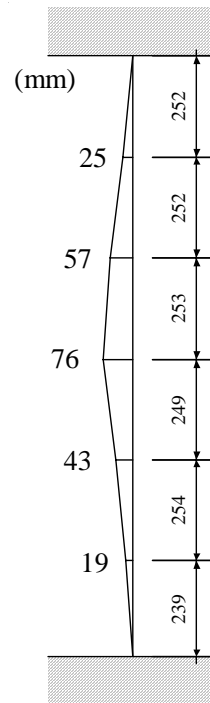
Figure 5-20   Deformation of Column B1-C5 after Test 5

Figure 5-21　Maximum Deformation (in) of Column B1-C5 after Test 5

Figure 5-22　Gap between Column and Foundation of Column B1-C5 after Test 5
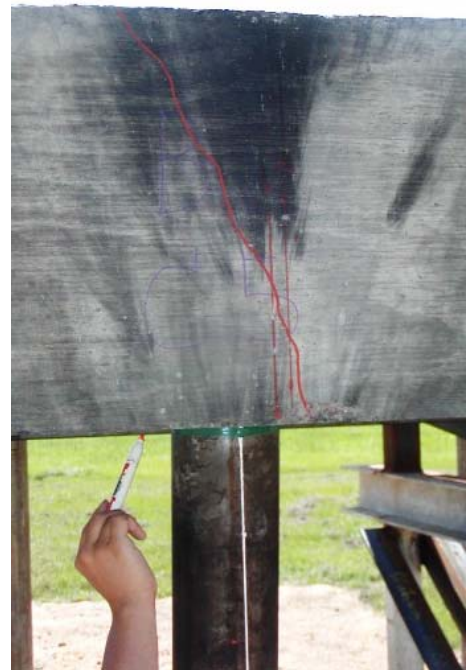
Figure 5-23　Cracking at Cap-beam of Column B1-C5 after Test 5

Figure 5-24　Column Surface of Column B1-C5 after Test 5

Figure 5-25　Column Surface of Column B1-C5 after Test 5

Figure 5-26　Core Concrete of Column B1-C5 after Test 5

Figure 5-27   Column B2-C4 after Test 6
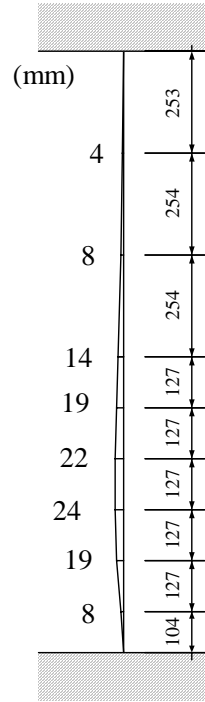
Figure 5-28   Deformation of Column B2-C4 after Test 6

Figure 5-29   Gap (in) between Column and Foundation of Column B2-C4 after Test 6

Figure 5-30   Damage at Foundation of Column B2-C4 after Test 6

Figure 5-31   No Damage at Cap-beam of Column B2-C4 after Test 6

Figure 5-32   Disappearance of Column B2-C4 after Test 7

Figure 5-33   Disappearance of Column B2-C4 after Test 7

Figure 5-34   Column B2-C4 after Test 7
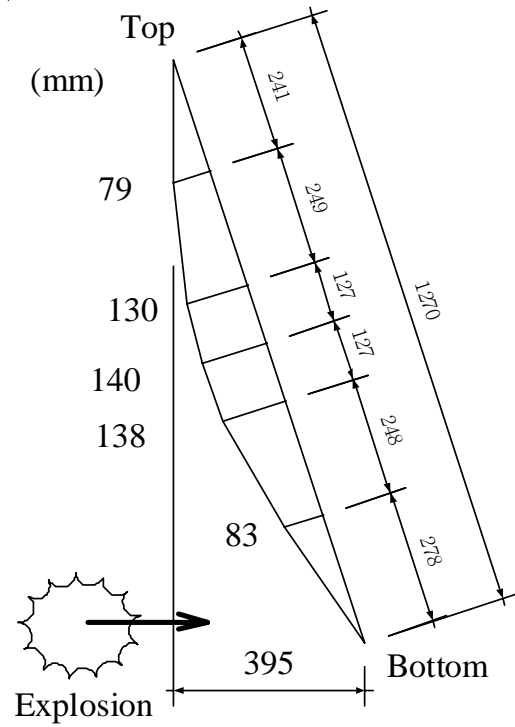
Figure 5-35   Deformation of Column B2-C4 after Test 7

Figure 5-36   Maximum Deformation (in) of Column B2-C4 after Test 7

Figure 5-37   Cut Section on Bottom of Column B2-C4 after Test 7

Figure 5-38   Cut Section on Top of Column B2-C4 after Test 7

Figure 5-39   Damage at Foundation of Column B2-C4 after Test 7

Figure 5-40   Foundation after Removal of Rubble (Column B2-C4, Test 7)

100

Figure 5-41   Fracture Surface of Column in Foundation (Column B2-C4, Test 7)

Figure 5-42   Fracture Surface of Column in Foundation (Column B2-C4, Test 7)

Figure 5-43   Fracture Surface of column under Cap-beam (Column B2-C4, Test 7)

Figure 5-44   Core Concrete of Column B2-C4 after Test 7

Figure 5-45   Section at Bottom of Column B2-C4 after Test 7

Figure 5-46   Bottom of Column B2-C4 after Test 7

Figure 5-47   Deformation of Plate B2-SP56 after Test 8 (Front Face)

Figure 5-48   Deformation of Plate B2-SP56 after Test 8 (Back Face)
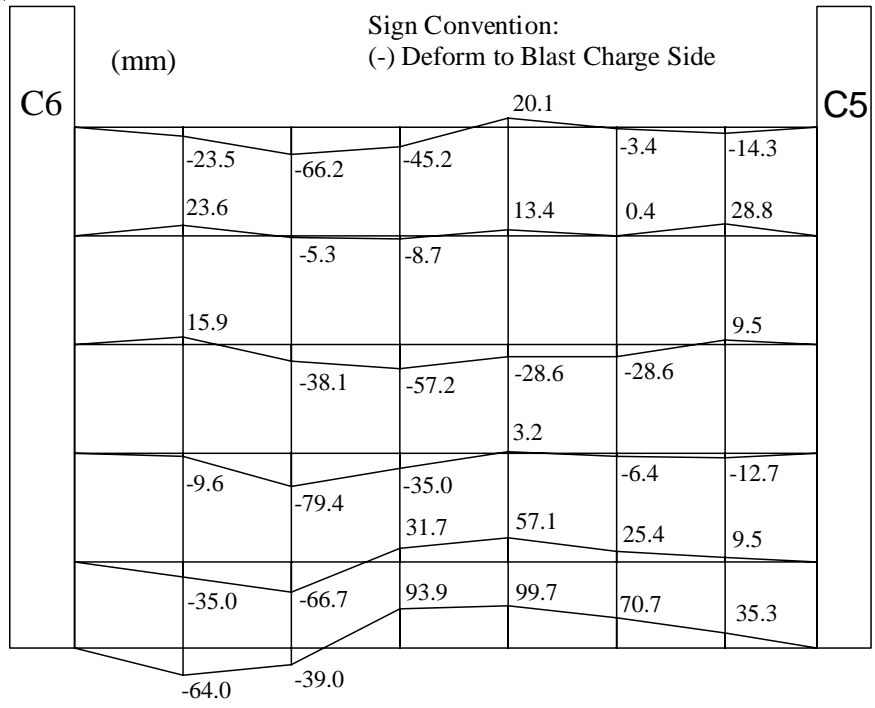
Figure 5-49   Deformation of Plate B2-SP56 after Test 8

Figure 5-50   Fracture of Plate at C5 Side (Plate B2-SP56 after Test 8)

Figure 5-51   Fracture of Plate at C6 Side (Plate B2-SP56 after Test 8)

Figure 5-52   Column B2-C6 after Test 9
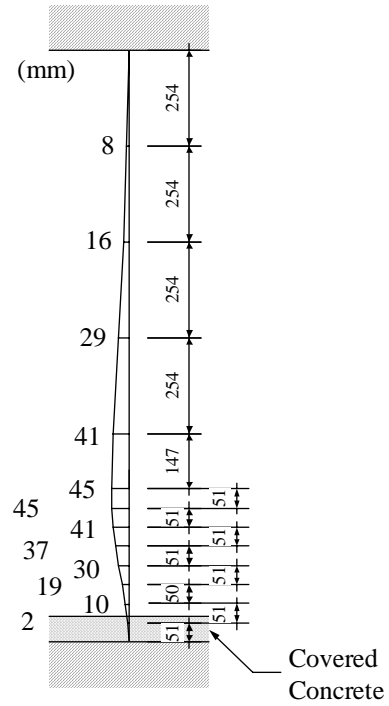
Figure 5-53   Deformation of Column B2-C6 after Test 9

Figure 5-54   Maximum Deformation (in) of Column B2-C6 after Test 9

Figure 5-55   Damage at Foundation of Column B2-C6 after Test 9

Figure 5-56   Damage at Foundation after Removal of Rubble (Column B2-C6, Test 9)
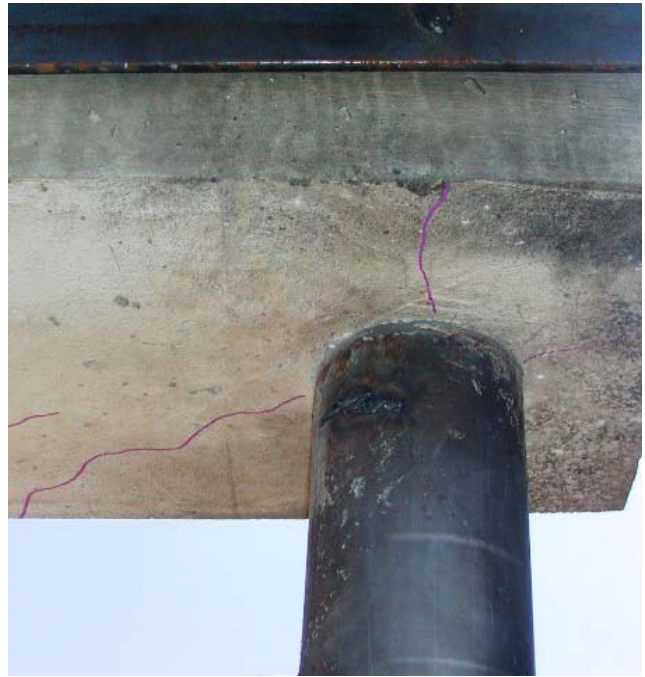
Figure 5-57   Damage at Cap-beam of Column B2-C6 after Test 9

Figure 5-58   Core Concrete of Column B2-C6 after Test 9

Figure 5-59   Column B2-C5 after Test 10
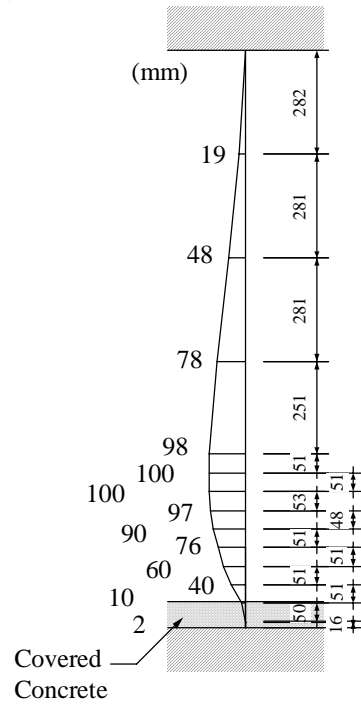
Figure 5-60   Deformation of Column B2-C5 after Test 10

Figure 5-61   Maximum Deformation (in) of Column B2-C5 after Test 10

Figure 5-62   Damage at Foundation Column B2-C5 after Test 10

108

Figure 5-63   Damage at Foundation After Removal of Rubble (Column B2-C5, After Test 10)

Figure 5-64   Buckling Surface (Column B2-C5, After Test 10)

Figure 5-65   Fracture of Column (Column B2-C5, After Test 10)

Figure 5-66   Fracture Surface (Column B2-C5, After Test 10)
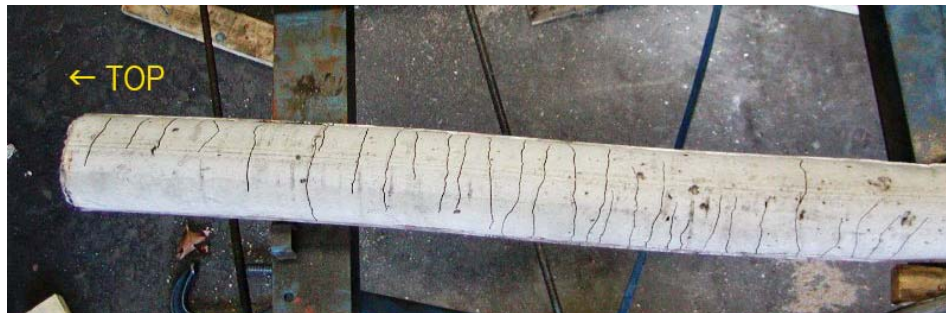
Figure 5-67   Core Concrete of Column B2-C5 after Test 10

Figure 5-68   Core Concrete at Steel Buckling of Column B2-C5 after Test 10

SECTION 6
EXPERIMENTAL RESULTS AND SIMPLIFIED ANALYSIS

6.1   General

This section describes the results of the blast experiments on the columns and the plate, and compares the observed behavior with the results from simplified analysis. First, experimentally obtained deformations of the columns are compared with the theoretical deformations of rigid-plastic columns having a plastic hinge and the maximum deformations at the height of the explosion. In addition, the columns maximum deformations and the plate elongation from the tests are compared with the ones calculated using simplified analysis. Next, P-delta effects due to the large deformations of the columns are examined analytically. Then, progression of damage in the columns as a function of blast charge is discussed by sequencing the data from the series of tests. Finally, a procedure for blast resistant design of CFST columns is suggested using the simplified analysis.

6.2   Deformation of Columns

In section 3.3, the concept of equivalent uniform peak pressure and equivalent uniform peak impulse were introduced to model the blast pressure and impulse applied to an equivalent SDOF system. The peak pressure and impulse were normalized by the deformed shape $\delta(z)$ of their respective column to get the equivalent uniform peak pressure and impulse. These were given by Equations 3-15 and 3-4, respectively, and reproduced here:

$$p_{eq} = \frac{\int_0^H p(z)\,\delta(z)\,dz}{\int_0^H \delta(z)\,dz} \tag{6-1}$$

$$i_{eq} = \frac{\int_0^H i(z)\,\delta(z)\,dz}{\int_0^H \delta(z)\,dz} \tag{6-2}$$

The assumed deformed shape $\delta(z)$ must closely match the actual deformation of the column for the equivalent uniform pressure and impulse to be accurate.

111

The deflected shape of a column in the elastic range is different from the one in the plastic range, but for the large blast charges relatively close to the columns that are considered here, the columns underwent significant plastic deformations (reported in Section 5.4). Experimentally obtained maximum deformations were also observed to occur around the height of the blast charge.

The deformations of the columns obtained from the test cases shown in Table 6-1 were compared with analytical results based on the above observations, in which plastic hinges (rigid-plastic model) occurred at top and bottom of each column and at the height of the blast charge. Figures 6-1 and 6-2 compare the corresponding experimentally and analytically obtained deformations for explosions at mid-height and low height, respectively. Figure 6-1 shows that when the explosion was located at mid-height, there was good agreement in deflected shape between the experiment and the rigid-plastic hinge model. In Figure 6-2, the assumed deflected shapes are shown to approximately match the deformations obtained experimentally even though the maximum deformations occurred at 60 mm to 108 mm above the blast height (depending on the case). This confirms that, for the simplified analysis, the deformed shape could be assumed to be linear between rigid-plastic hinges and that the maximum deformation can be reasonably assumed to occur at the height of the explosion.

Table 6-1   Summary of Column Test Cases and Analytical Results

Test Num	Column	Charge Weight	Standoff Distance	Height (m)	Equivalent Uniform Impulse, i_{eq} (MPa-msec)	Equivalent Uniform Pressure, p_{eq} (MPa)	t_m/t_d
Test 3	B1-C4	W	2 X	0.750	7.08	90.6	20.1
Test 4	B1-C6	W	1.1 X	0.750	13.91	215.7	26.1
Test 5	B1-C5	W	1.3 X	0.750	11.77	203.7	49.2
Test 6	B2-C4	W	1.6 X	0.250	9.08	128.1	15.6
Test 9	B2-C6	W	0.8 X	0.250	19.48	275.0	17.8
Test 10	B2-C5	W	0.8 X	0.250	19.48	275.0	34.4
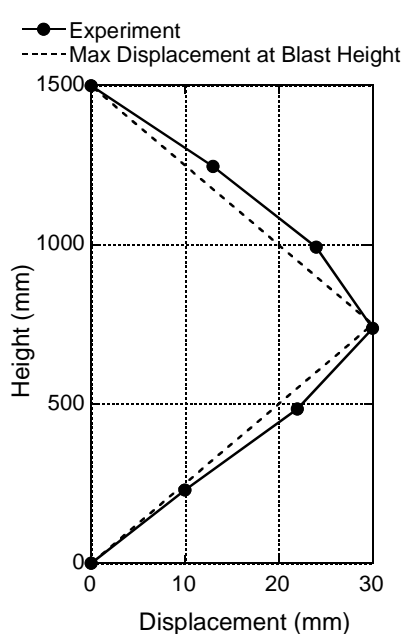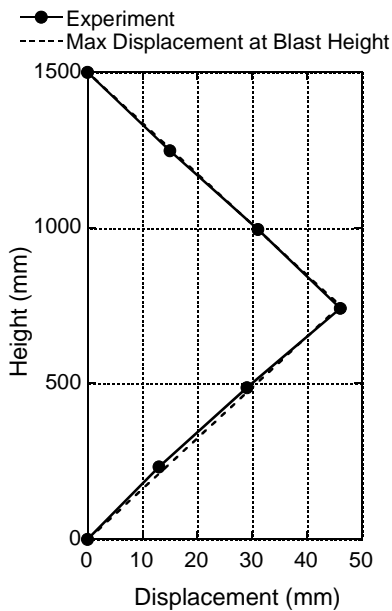
(a) Test 3, Column B1-C4   (b) Test 4, Column B1-C6   (c) Test 5, Column B1-C5

Figure 6-1   Comparison of Column Deformation (Blast at Mid-height)
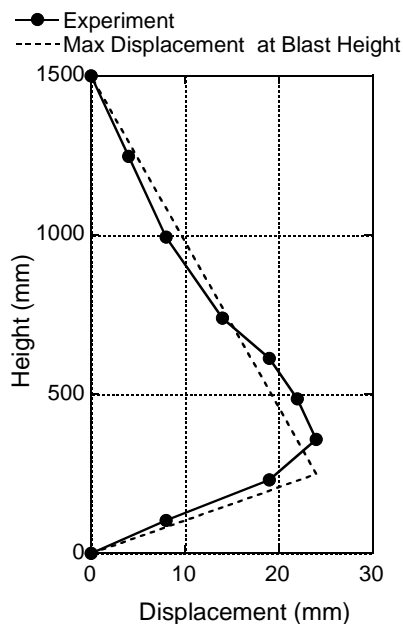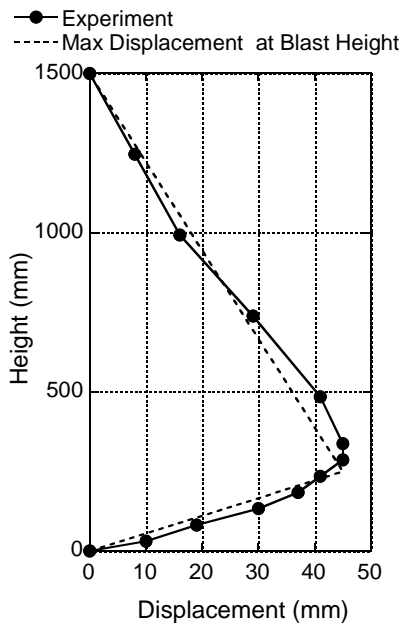
(a) Test 6, Column B2-C4   (b) Test 9, Column B2-C6   (c) Test 10, Column B2-C5
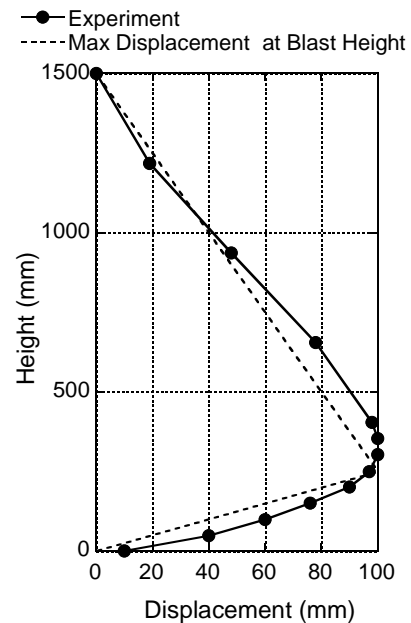
Figure 6-2   Comparison of Column Deformation (Blast at Low Height)

113

6.3 Comparison with Simplified Analysis for Column Tests

Experimentally obtained maximum plastic deformations of the piers were compared with the ones that can be calculated using simplified method of analysis. These simplified analyses were conducted using the strength values obtained from the compression tests of concrete cylinders and the tensile tests for the steel tubes from which the specimens were constructed. Furthermore, as considered in the column design (Section 4.2), concrete strength and yield stress of steel were multiplied by 1.25 and 1.2, respectively, to account for strain rate effects subjected to blast loading. As shown in Section 3.3, the maximum deformations due to blast loading are obtained considering an equivalent SDOF system having an elastic-perfectly-plastic behavior, and assuming that all the energy imparted to the system by the blast loading is converted into internal strain energy. The maximum deformation per this approach is given by Equation 3-2, reproduced here:

$$X_m = \frac{1}{2}\left(\frac{I_{eq}^2}{K_{LM}\ m\ R_u} + X_E\right) \tag{6-3}$$

The equivalent uniform impulse per unit area, I_{eq}, is given by:

$$I_{eq} = \beta\ D\ i_{eq} \tag{6-4}$$

also presented earlier as Equation 3-3. The equivalent uniform impulse per unit area, i_{eq}, in Equation 6-2, is based on the variation of the impulse, $i(z)$, along the height. Graphs from Figures 6-3 to 6-7 present the variations of the total impulse, $i(z)$, and the peak pressure, $p(z)$, along the height of the center line of the column for each test as generated by BEL. According to these variations of the impulse and the peak pressure, the equivalent uniform impulse and the equivalent uniform pressure respectively calculated by Equations 6-2 and 6-1 are presented in Table 6-1. Table 6-1 also presents the ratio of the time to reach maximum deflection, t_m, over the load duration of the positive phase of the impulse, t_d. Since $t_m/t_d > 3$ for each test, the energy imparted to the system by the blast loading can be evaluated by an impulse analysis.

β in Equation 6-4 is a factor to account for the reduction of pressures on the column due to its circular shape. For simplicity, a constant value of β was adopted considering the total impulse indicated by BEL at each point along the height. This value of β was originally taken as 0.85 for the design of the prototype bridge columns, described in Section 3.3. However, this value of

114

0.85 was found to be too conservative on the basis of the test results. Hence, it was revised based on the test results. Note that the maximum deformations measured after the tests were obtained without loading on the structure (i.e. after the blast load) and are actually residual plastic deformations, X_{test}. Therefore, the test results had to be compared with the calculated residual deformations whose values were $X_m - X_E$, where X_E and X_m respectively represent the elastic maximum deformations and the maximum deformations under blast loading. Following this approach by calibrating analysis with the test results, revised values for β for each test were calculated using the above equations. The resulting values for β are presented in Table 6-2 for the six test cases for which residual plastic deformations were obtained, along with the calculated elastic maximum deformations, the calculated maximum deformations under blast loadings, and the residual plastic deformations from the tests. It was found that the value of β for this type of circular columns is 0.45 (i.e. mean value of 0.450 and standard deviation of 0.020 from the six samples considered).

Incidentally for comparison purposes, for the wind loading, the total force on a circular surface cylinder would be calculated by:

$$F = q_z G C_f A_f \tag{6-5}$$

where q_z is the velocity pressure evaluated at height z, G is the gust-effect factor, C_f is the force coefficients and A_f is the projected area normal to the wind (ASCE 2006). There is a direct analogy between the β value above obtained from blast tests and the factor C_f used to calculate wind forces. The coefficient C_f for wind acting on a cylindrical tower depends on type of cross section, surface type of the structure, and h/D (where h is the height of the cylindrical structure and D is the diameter of its circular cross-section). By linearly interpolating the tabulated values in ASCE (2006), the coefficients C_f are 0.64, 0.63 and 0.62 (mean value of 0.63) for Column C4, C5 and C6, respectively. Therefore, the value accounting for the shape of the projected area for wind load in this case is approximately 0.63, which is significantly different from the value of 0.45 obtained for the blast loading. However, note that the 0.45 factor derived here is to be used in the context of near field explosions using the envelope of peak pressure in the design or analysis process. These peak pressure do not occur

115

along the column at the same time. Different pressure profiles would likely result from far field explosions as maximum pressure would hit the column more uniformly almost at the same time.

Table 6-2   Summary of Column Test and Analysis Results and Shape Factors

Test Num	Column	Shape Factor, β	Calculation			Test
			Maximum Elastic Deformation, X_E	Maximum Deformation, X_m	Maximum Residual Deformation, $X_m - X_E$	Maximum Residual Deformation X_{test}
			(mm)	(mm)	(mm)	(mm)
Test 3	B1-C4	0.472	6	36	30	30
Test 4	B1-C6	0.458	4	50	46	46
Test 5	B1-C5	0.447	3	79	76	76
Test 6	B2-C4	0.465	10	34	24	24
Test 9	B2-C6	0.440	6	51	45	45
Test 10	B2-C5	0.417	5	105	100	100
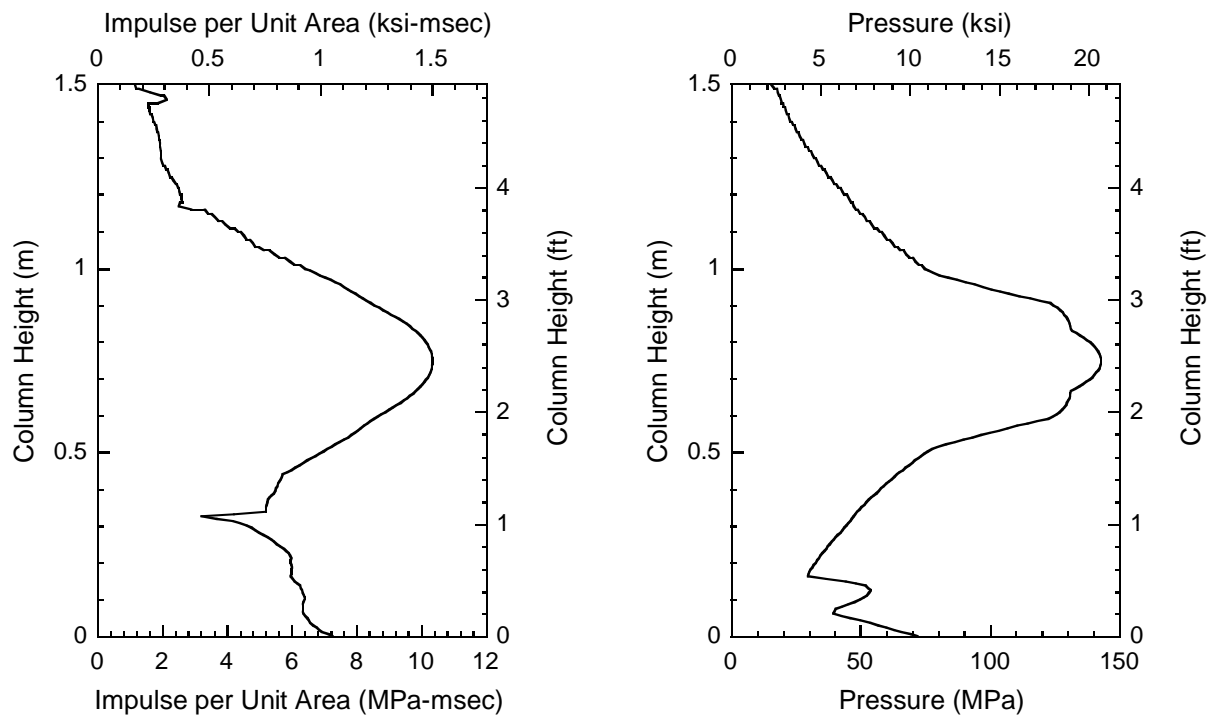
Figure 6-3   Variation of Impulse and Peak Pressure along Height of Column for Test 3 (Column B1-C4)

116
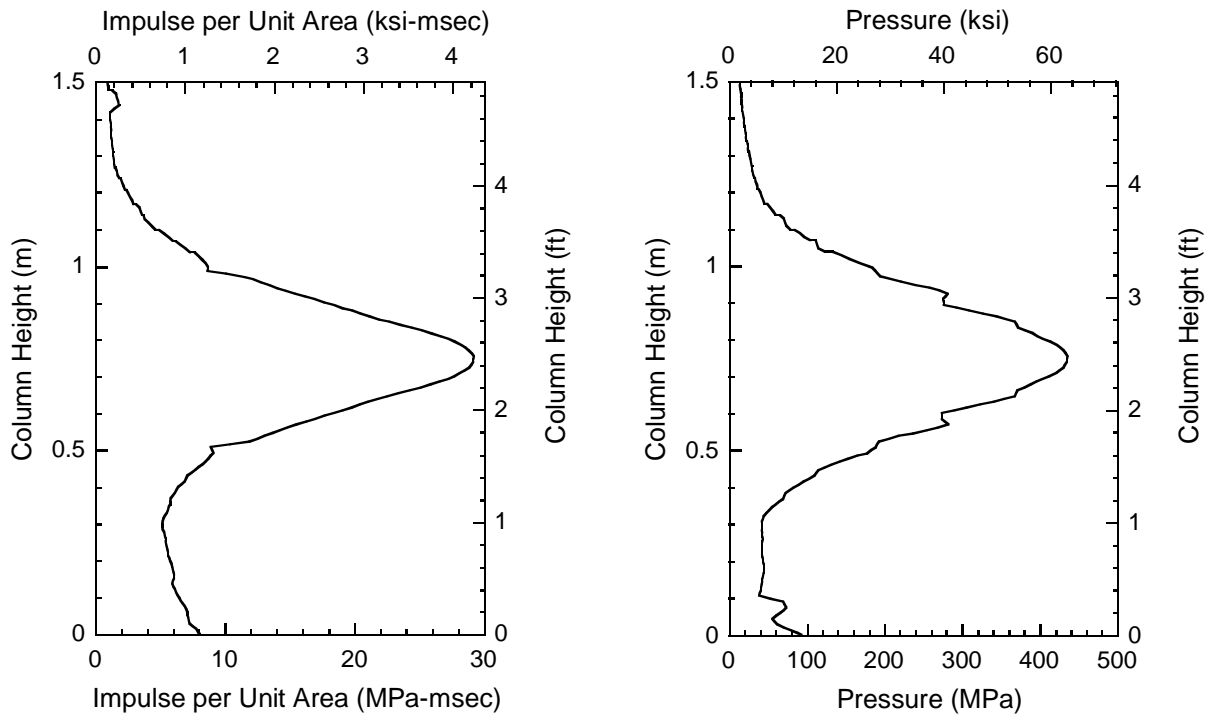
Figure 6-4   Variation of Impulse and Peak Pressure along Height of Column for Test 4 (Column B1-C6)
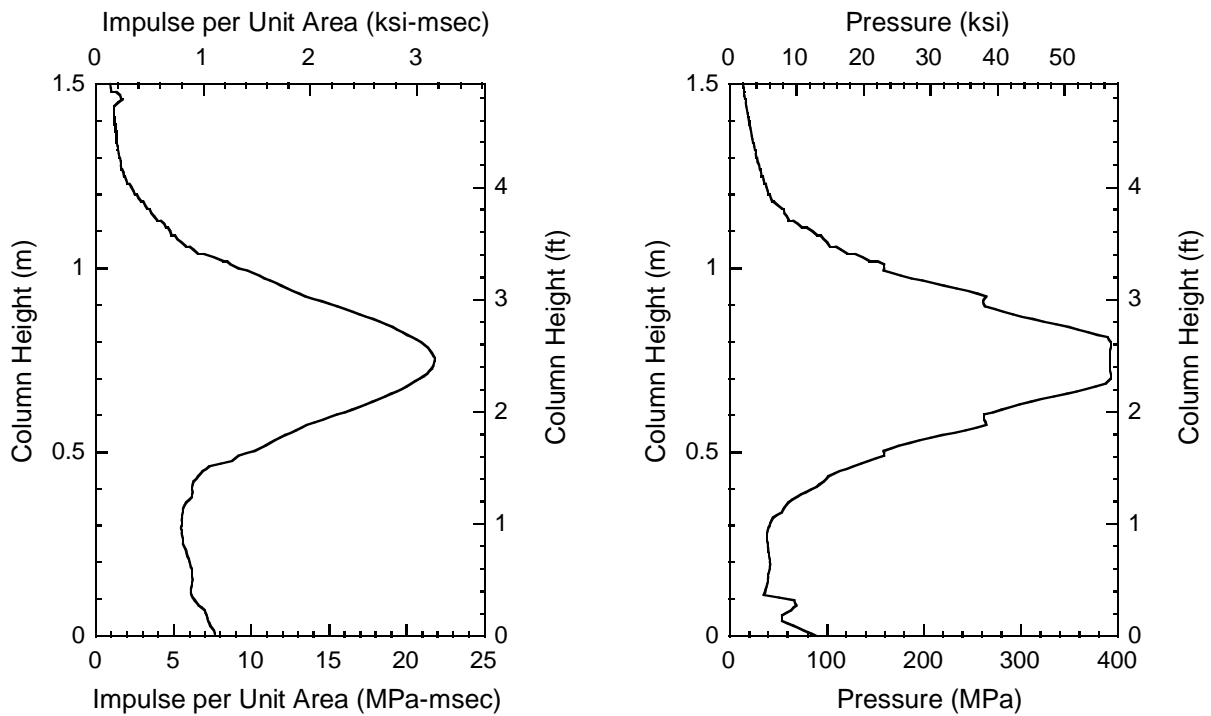
Figure 6-5   Variation of Impulse and Peak Pressure along Height of Column for Test 5 (Column B1-C5)

117
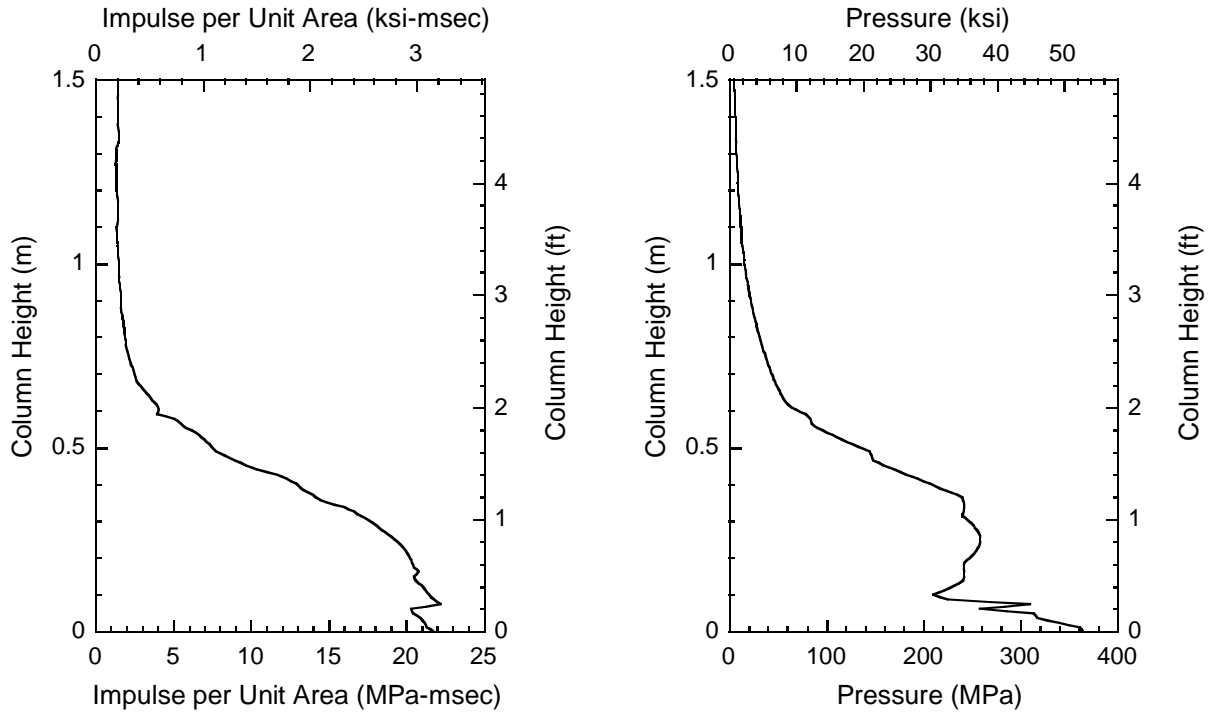
Figure 6-6   Variation of Impulse and Peak Pressure along Height of Column for Test 6 (Column B2-C4)
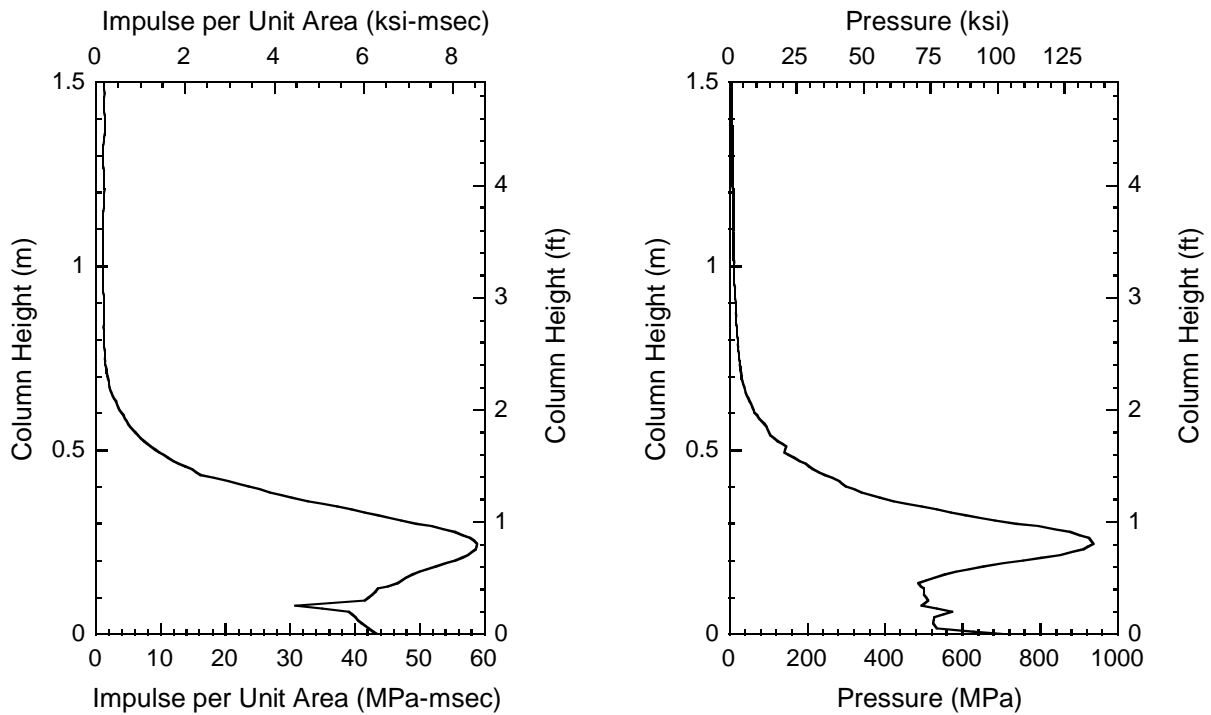
Figure 6-7   Variation of Impulse and Peak Pressure along Height of Column for Test 9 (Column B2-C6) and Test 10 (Column B2-C5)

6.4   Comparison with Simplified Analysis for Plate Test

Experimentally obtained plate elongation was compared with the one that can be calculated using the simplified method of analysis. As described in Section 3.3, the elongation of the plate was obtained by equating the kinetic energy of the blast impulsive loading to the absorbed internal plastic work of the plate. This simplified analysis was conducted using the strain rate effects considered in the plate design (Section 4.3) and the strength values obtained from the tensile tests for the steel plates for coupons taken from the same sheet as the specimen. Analytical and test results are summarized in Table 6-3. The maximum elongation measured after the test was 8.9 % and 4.2 % at the bottom and top of the plate, respectively, whereas the one from the analysis was 6.1 %. This difference can be explained considering that the simplified analysis assumed the plate to uniformly elongate along its height under an equivalent pressure uniformly applied over the entire plate (as described in Section 4.3) while, in the experiment, the bottom part of the plate stretched more than the upper part due to its closer proximity to the charge. Note that the elongation at the height of the charge obtained after the test could not easily be measured. However, on the basis of the deformations obtained along the height as shown in Figure 5-49, there are reasons to believe that the maximum elongation was the largest at the bottom of the plate.

Table 6-3   Summary of Analytical and Test Results of Plate Test

Test Num	Charge Weight	Standoff Distance	Height (m)	Equivalent Uniform Impulse, i_{eq} (MPa-msec)	Equivalent Uniform Pressure, p_{eq} (MPa)	Elongation	
						Test (%)	Analysis (%)
Test 8	0.06 W	5 X	0.25	7.08	90.6	8.9 (Bottom) 4.2 (Top)	6.1

6.5   P-delta Effects on Columns

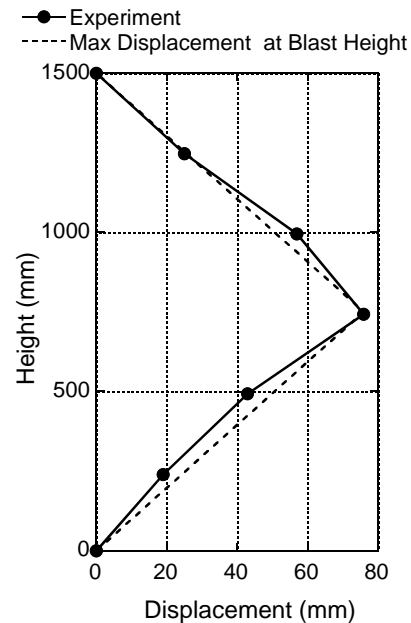Secondary moments are produced by the axial force due to the lateral deflections of the column (commonly referred to P-δ effects). These moments are negligible when the axial force or the deflections are relatively small. However, this effect needs to be considered for column severely deformed under blast load to determine whether the deformed columns can sustain the applied gravity loads. Here, because the blast tests were carried out without an axial force representative of the gravity loads applied to the bridge bent in the prototype, secondary moment effects were analytically examined for each of the columns in the experiments.

In such P-δ analysis or second-order analysis, the additional moment causes an additional deflection, and this deflection and the axial load result in further additional moments. As such, iterative calculations are required to obtain the total deflections until the solution converges (stable structure) or diverges (unstable system that would collapse under the applied gravity loads). The columns were modeled by beam elements having fixed boundary conditions at the top and bottom using the structural analysis program, SAP2000 (2005). An axial force of 85.4 kN was considered for the test columns which were 1/4 scale of the prototype bridge for which this force is equal to 1366 kN (both cases giving similar ratios of axial load to axial yield capacity). The flexural stiffness of the CFST columns was calculated as the equivalent flexural stiffness of the composite section by Equation 3-11.

Table 6-4 summarizes the resulting deformations from the second-order analysis (along with the maximum elastic deformations). Iteration details of calculations for the second-order deformations are presented in Appendix C. Figure 6-8 schematically illustrates a resistance-deflection curve at the maximum deflection point. As described previously, the maximum deformations measured after the tests were not the maximum deformations, X_m, but the residual plastic displacements, X_{test}. In other words, after reaching the maximum deformation due to the blast load (point A), a column subjected to blast load would rebound elastically to point B after the blast load. From that point, by considering the P-δ effects, it was calculated that the column would have actually returned to point C instead of point B. In addition, calculations show that the second-order deformations would be smaller than the maximum elastic deformations, X_m, that would correspond to loading from point B to point A for all test cases considered as shown

120

in Table 6-4. Therefore, these deformed columns subjected to blast load were stable against the axial force considered. Note that, if the second-order deformations due to the gravity forces exceeded the elastic deformation, X_E, the column would not return to point C after the blast load and instability would develop (point D).

Incidentally, it was decided to also conduct P-δ analysis considering larger axial force on the specimen columns, to investigate whether the proposed system would remain stable even under substantially greater axial loads than typically encountered in most bridge applications, such as to verify the suitability of the proposed concept for as broad a range of applications as possible. The axial force was arbitrarily selected to be 341.5 kN which was 4 times larger than the previously considered scaled axial force. This force is smaller than the buckling strength, P_n, that is 417, 605 and 822 kN for Column C4, C5 and C6 respectively, given by:

$$P_n = 0.85 \cdot A_s \cdot 0.658^{\lambda_c^{\,2}} F_m \tag{6-6}$$

where A_s is the gross area of steel tube, λ_c is the slenderness parameter for compression members and F_m is the modified yield stress (AISC 2001). The resulting deformations were 1.6, 0.6, 1.9, 0.7, 0.3 and 1.3 mm for Test 3, 4, 5, 6, 9 and 10, respectively. Since these deformations were smaller than the maximum elastic deformations shown in Table 6-4, the deformed columns subjected to blast load were also deemed stable, i.e., not subjected to P- δ failure.
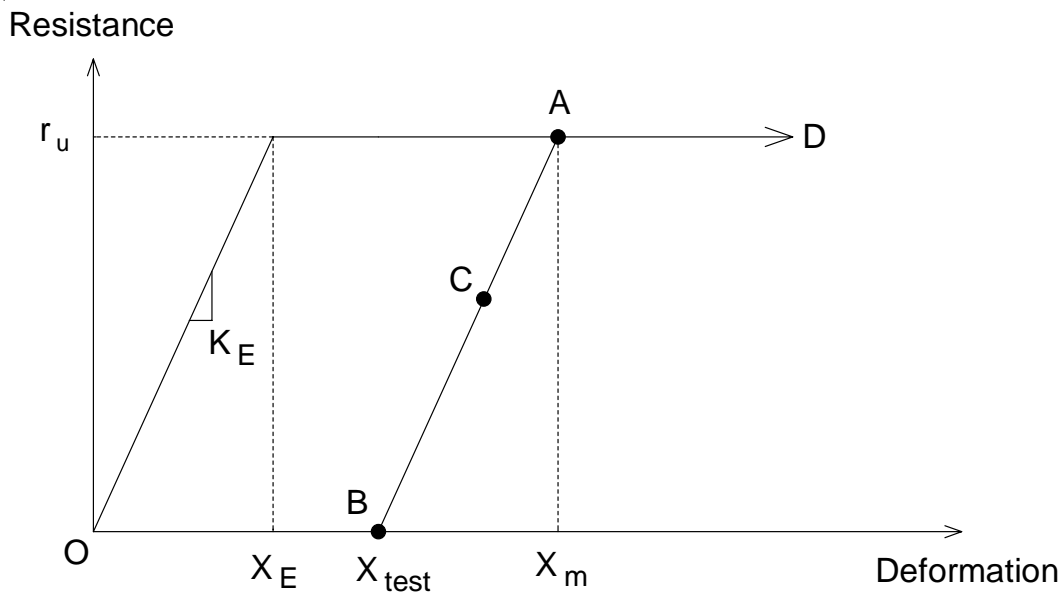
Resistance

Figure 6-8   Resistance versus Deflection at Maximum Deflection Point

Table 6-4   Summary of Maximum Second-order Deformations

Test Num	Column	Maximum Second-order Deformation (mm)	Maximum Elastic Deformation, X_E (mm)
Test 3	B1-C4	0.4	6
Test 4	B1-C6	0.1	4
Test 5	B1-C5	0.5	3
Test 6	B2-C4	0.2	10
Test 9	B2-C6	0.1	6
Test 10	B2-C5	0.3	5

6.6   Damage Progress of Columns

By sequencing the tests results as a function of increasing charge, the progress of damage along a typical column is presented in Figure 6-9 and Figure 6-10 for the blast charge located at low and mid-height, respectively. Although results presented in these figures are for columns having different diameters, they provide useful information on how the deformation of a column relates to the extent of damage. Results are presented corresponding to these damage states, namely; (1) plastic deformation, (2) on-set of fracture of the column and (3) post-fracture of the column. In each case, column deformations are shown along with the rotation at supports and maximum deformation, and the crack patterns of core concrete are sketched based on the observation of the core concrete performed after the test (see Section 5.4).

Figure 6-9 (3) shows the deformations obtained in Column B2-C5 at the onset of fracture. For that case, this limit state was observed to develop at a plastic rotation angle of approximately 0.297 rad (17.0 deg) at the bottom support, calculated as shown on that figure. It can be speculated that the plastic rotation angle for that limit state would have been sensibly similar for the other column. Figure 6-9 (4) shows the case for which the steel tube fractured fully. In this case, it is assumed that the complete fracture first occurred at the bottom end of the column. After it fractured under the applied pressures, the column behaved as a cantilever suspended from the top. Therefore, it developed the curvature in the direction reversed to what was observed for the other columns. Then, it eventually fractured at the top as this column was projected outside of its setup under the blast forces. One could approximate the plastic rotation that occurred when the top ruptured, to be 0.327 rad (18.7 degree) by the procedure graphically shown on Figure 6-9 (4). Note that the plastic rotation at the fracture of the lower part of the column can not be calculated as the short segment of the column was completely damaged at that location during the test and is actually missing. Also, note that all three test results for the blast charges at middle height of the columns produced plastic deformations (as presented in Figure 6-10), but the corresponding rotation angles calculated for the supports only reached 0.101 rad (5.8 deg). No onset of fracture or no complete fracture was observed with the limited data in this case.

(a) Column Deformation   (b) Crack Patterns of Core Concrete

(1) Plastic Deformation
(Test 6 : Column B2-C4)

(a) Column Deformation   (b) Crack Patterns of Core Concrete

(2) Plastic Deformation
(Test 9 : Column B2-C6)

(a) Column Deformation   (b) Crack Patterns of Core Concrete

(3) On-set of Fracture of Column
(Test 10 : Column B2-C5)

(a) Column Deformation   (b) Crack Patterns of Core Concrete

(4) Post-fracture of Column
(Test 7 : Column B2-C4)

Figure 6-9   Damage Progress of Column (Blast at Low Height)

124

(a) Column Deformation (b) Crack Patterns of Core Concrete
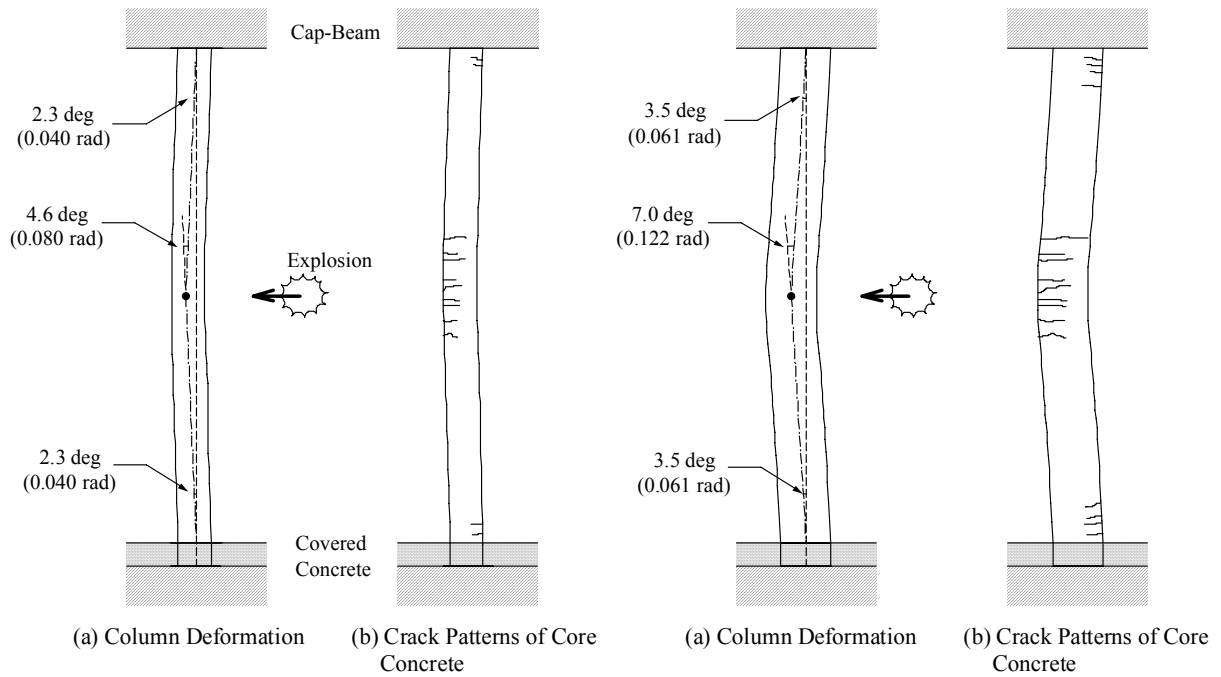
(1) Plastic Deformation
(Test 3 : Column B1-C4)

(a) Column Deformation (b) Crack Patterns of Core Concrete

(2) Plastic Deformation
(Test 4 : Column B1-C6)

(a) Column Deformation (b) Crack Patterns of Core Concrete
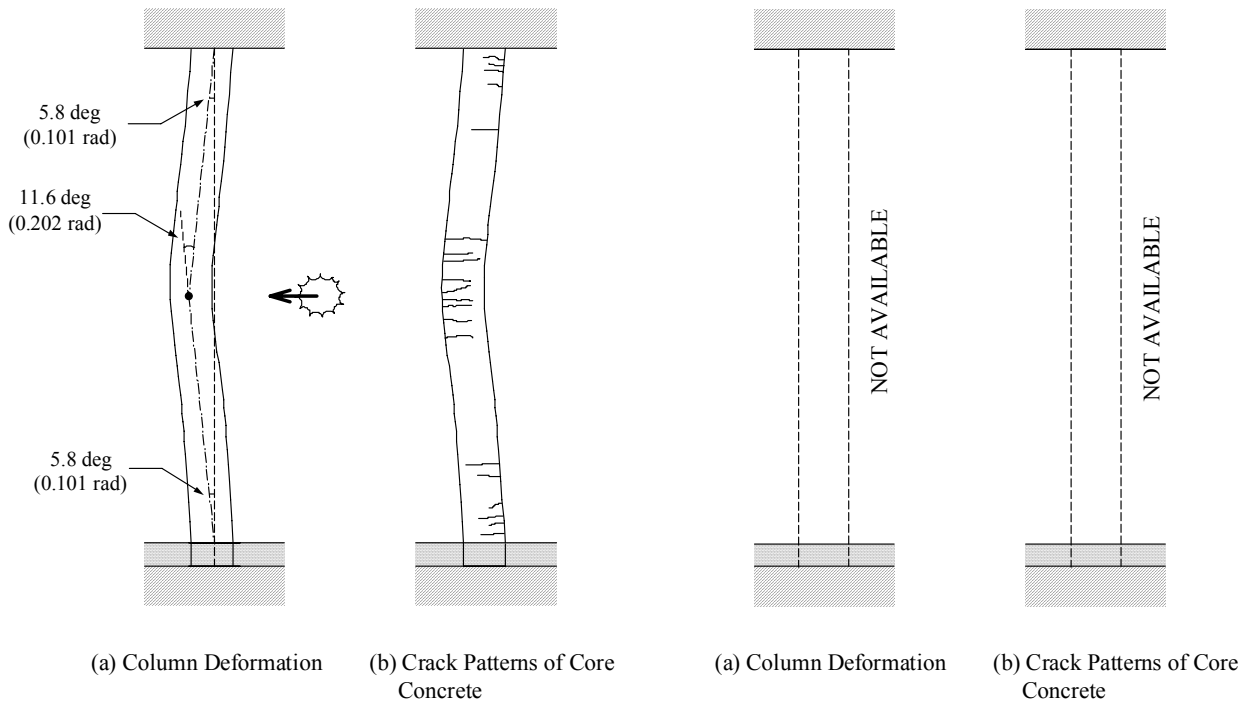
(3) Plastic Deformation
(Test 5 : Column B1-C5)

(a) Column Deformation (b) Crack Patterns of Core Concrete

(4) On-set of Fracture of Column and Post-fracture of Column

Figure 6-10   Damage Progress of Column (Blast at Middle Height)

125

6.7 Suggested Procedure for Blast Resistant Design of CFST Columns

Building upon the existing impulse-momentum approach commonly used in blast-resistant design and results from the series of experiments reported in earlier sections, a procedure for the blast resistant design of CFST columns is suggested as follows using a simplified analysis method described earlier. The flow chart corresponding to the suggested CFST column design procedure is shown in Figure 6-11, and the details of the design procedure are presented below.

(1) Step 1. Assume a blast scenario.

A credible blast scenario must be formulated through a risk assessment procedure considering the terrorist's purposes and tactics, the location of the target bridge, the method for carrying the explosives, and other relevant factors. It is beyond the scope of this report to provide guidance on such credible scenarios (see FEMA 2003 and Williamson and Winget 2005 for details). However, once such a scenario is selected, standoff distance, height and weight of the blast charge are determined.

(2) Step 2. Establish corresponding external loading.

(i) Calculate the distribution of peak impulse, $i(z)$, and peak pressure, $p(z)$, along the column height using a blast pressure generating software such as BEL.

(ii) Select a plastic deformation shape for the column, $\delta(z)$, assuming that maximum deformation occurs at the blast height and rigid-plastic material behavior.

(iii) Calculate the equivalent uniform peak impulse, $i_{eq}(z)$, and pressure, $p_{eq}(z)$, by:

$$i_{eq} = \frac{\int_0^H i(z)\,\delta(z)\,dz}{\int_0^H \delta(z)\,dz} \tag{6-7}$$

$$p_{eq} = \frac{\int_0^H p(z)\,\delta(z)\,dz}{\int_0^H \delta(z)\,dz} \tag{6-8}$$

where H is height of the column (USACE-ERDC 2004).

(3) Step 3. Calculate the plastic moment capacity, M_p, of the column by:

$$M_p = \left(Z - 2\,t\,h_n^2\right) f_s + \left[\frac{2}{5}\left(\frac{D}{2} - t\right)^3 - \left(\frac{D}{2} - t\right) h_n^2\right] f_c \tag{6-9}$$
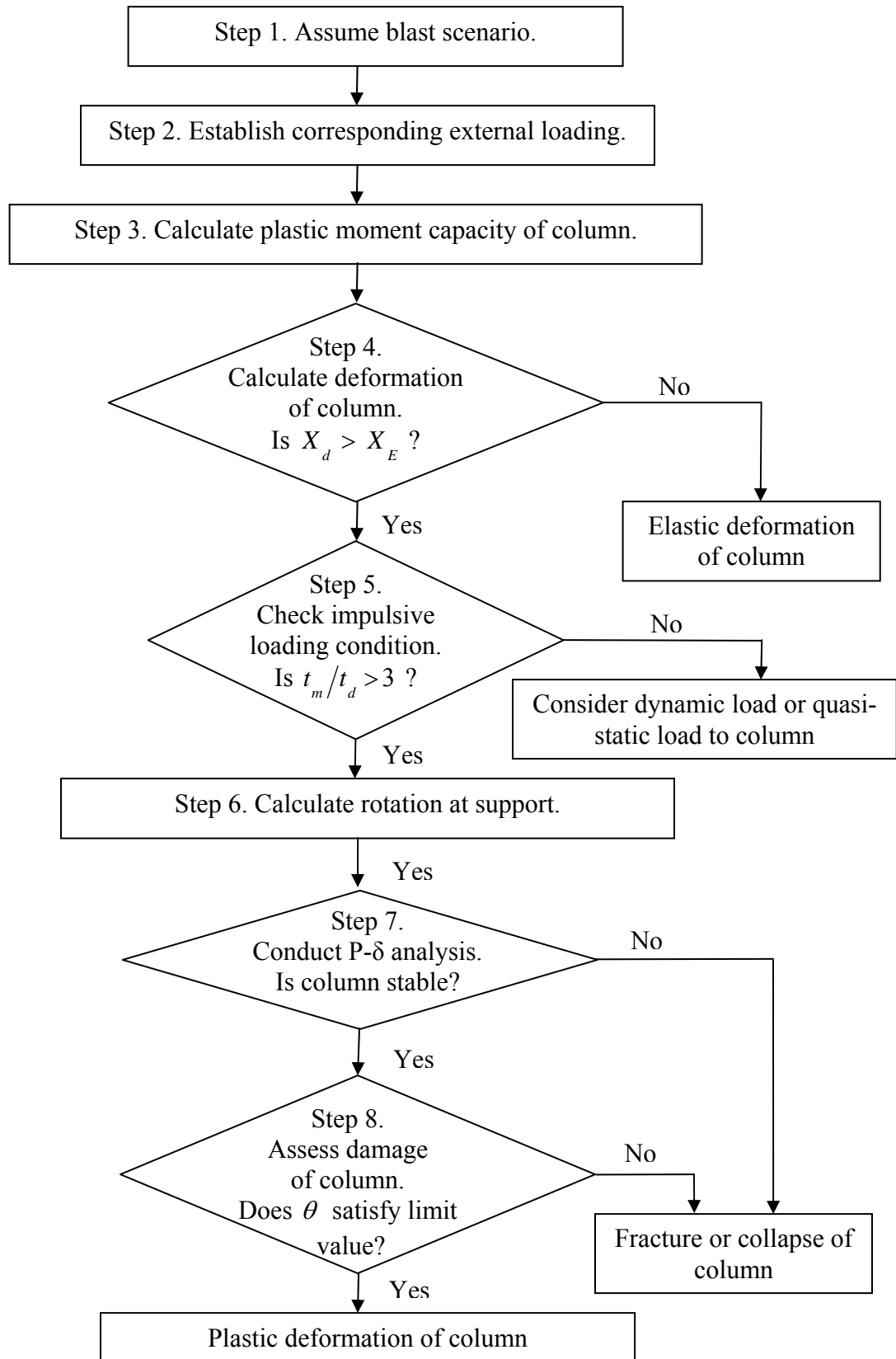
Figure 6-11   Flow Chart for Blast Resistant Design of CFST Column

127

where Z and t are the plastic modulus and thickness of the steel tube section, f_s is the yield strength of steel, f_c is the concrete strength and h_n is given by:

$$h_n = \frac{A_c \ f_c}{2 \ D \ f_c + 4 \ t \ (2 \ f_s - f_c)}$$ (6-10)

where A_c is the core concrete area (see Section 3.3 from Bruneau and Marson, 2004). Note that factors to account for strain rate effects need to be considered for the yield strength of steel and the concrete strength. The values of 1.25 and 1.2 for concrete strength and yield strength of steel, respectively, are provided in Mays and Smith (1995) as shown in Table 2-4 in Section 2.

(4) Step 4. Calculate deformation of the column, X_d.

(i) Calculate the equivalent flexural stiffness, EI_e, by:

$$EI_e = E_s \ I_s + 0.8 \ E_c \ I_c$$ (6-11)

where E_s, E_c are the Young's moduli of steel and concrete, and I_s, I_c are the moment of inertia of the steel tube section and core concrete section, respectively (Eurocode 4 1994).

(ii) Calculate the equivalent elastic stiffness per unit length, K_E.

(iii) Select the load-mass factor, K_{LM}, from Table 2-1 in Section 2 depending on the edge and loading conditions.

(iv) Calculate mass per unit length, m.

(v) Select ultimate resistance per unit length, r_u, from Table 2-2 in Section 2 depending on the edge and loading conditions.

(vi) Calculate elastic deflection at yielding, X_E, by:

$$X_E = \frac{r_u}{K_e}$$ (6-12)

(vii) Calculate effective impulse per unit length, I_{eq}, by:

$$I_{eq} = \beta \ D \ i_{eq}$$ (6-13)

where the β factor accounts for the reduction of pressures on the column due to its circular shape and is taken as 0.45 for the type of the column considered here.

(viii) Calculate maximum inelastic deformation, X_m, by:

$$X_m = \frac{1}{2}\left(\frac{I_{eq}^2}{K_{LM}\, m\, R_u} + X_E\right)$$ (6-14)

which was presented in Section 4.3 from USDA, 1990.

(5) Step 5. Check whether the loading condition can be considered as an impulsive load, which will be the case if:

$$\frac{t_m}{t_d} > 3$$ (6-15)

where t_m is the time at which the deformation reaches X_E given by:

$$t_m = \frac{I_{eq}}{R_u}$$ (6-16)

and t_d is the time at which blast pressures dissipate given by:

$$t_d = 2\,\frac{i_{eq}}{p_{eq}}$$ (6-17)

If $t_m/t_d < 3$, then the response of the column due to the blast loading must instead be evaluated by dynamic analysis or by the quasi-static load method. These were described in Section 2.3 from Mays and Smith, 1995. Note that this should be rarely the case for the type of bridge structure considered here.

(6) Step 6. Calculate rotation at the support, θ.

(7) Step 7. Conduct P-δ analysis to check that the gravity loads can be supported by the deformed column after blast (i.e. collapse prevention).

(8) Step 8. Assess the damage of the column as a result of the above design for the selected blast scenario. This limited testing program provided some evidence that fracture of steel tube will begin close to the plastic rotation of 0.3 rad (17.2 deg). However, in light of few numbers of tests conducted, it might be reasonable to limit the plastic rotations to a somewhat lesser value for design purposes. There are no specific rules to select what would be an appropriate value, and some judgment must come to play. There is evidence from the seismic testing of CFSTs that they can develop a cyclic plastic rotation of 0.07 rad (4.0 deg) at the column end before their fracture. And there is sufficient evidence from this test program that under blast induced

monotonic loading, larger plastic rotations can be developed. Given that at least three specimens have been respectively tested up to 0.101, 0.144 and 0.297 rad plastic rotations for Test 5, 9 and 10 at the column end, it appears reasonable to limit plastic rotations to 0.2 rad, understanding that this is an arbitrary chosen design recommendation at this point. In-span plastic hinges can develop twice that amount.

SECTION 7
CONCLUSIONS

7.1 General

In this study, a multi-hazard bridge pier concept to protect bridges from seismic and blast loading has been developed and experimentally validated. Reviewing existing systems known to provide satisfactory seismic performance, it was proposed that a multi-column pier-bent with CFST columns could meet the multi-hazard performance objectives. This satisfactory behavior is obtained partly because breaching and spalling of concrete are prevented to occur in CFST columns.

The specimens considered in this experimental program were designed per a simplified method of analysis that considered an equivalent SDOF system having an elastic-perfectly-plastic behavior and assuming that all the energy imparted to the system by the blast loading is converted into internal strain energy. Blast tests showed that CFST columns of bridge pier specimens exhibited a ductile behavior under blast loading. No significant damage was suffered by the concrete cap-beams as a result of the blast pressures. The foundation connection concept applied in this experiment allowed to develop the composite strength of CFST column under blast loading. Maximum deformation occurred along each column at the height of the explosion, and the deformed shape of the column was dominantly corresponding to a rigid-plastic mode in which plastic hinges occurred at the top and bottom of the column and at the height of the blast charge.

The results of the blast experiments were compared with the results from a simplified method of analysis considering an equivalent SDOF system. Comparison of the results from the blast tests with the results predicted by this simplified analysis showed that the blast effective pressures acting on a circular column are equal to 0.45 those acting on a flat surface. A procedure for the blast resistant design of CFST column was suggested using the simplified analysis.

7.2   Recommendations for Future Research

While this report has presented results from an experimental program to validate the proposed multi-hazard bridge pier concept, focus was predominantly on the experimental phase of the program and on correlating the results with a simplified analysis model. Future research could investigate the adequacy of finite element models to better understand the behavior of the system. The data provided by this experimental program could be used to calibrate the finite element models which then could be used for extended parametric studies. As part of these finite element parametric studies, time history analyses could also be performed using a combination of pressure-time history obtained from the restricted computer software BEL (Bridge Explosive Loading).

Because using CFST columns is not a common practice in bridge engineering (although they are used sometimes), questions may arise regarding the blast performance of comparable regular reinforced concrete columns or of reinforced concrete columns jacketed by steel shells. The latter case visually resembles the CFST that has been considered in this report, but is not providing composite action at the column top and base. At the initial stages of this project, while the effective pressure factor of 0.45 for circular columns was not known, analytical predictions showed that the jacketed columns would shear off at their base due to the lack of continuity of the steel shell and that the corresponding reinforced concrete columns would breach. Future research could investigate the performance of these systems in full knowledge of the effective pressure factor derived in this project. However, this is beyond the scope of this report.

SECTION 8

REFERENCES

Abramson, H. N. et al. (1999). *Improving surface transportation security: A research and development strategy*, Committee on R&D Strategies to Improve Surface Transportation Security, National Research Council, National Academy Press, Washington, D.C.

ACI (1992). *Standard Practice for Selecting Proportions for Normal, Heavyweight, and Mass Concrete*. ACI Manual of Concrete Practice, American Concrete Institute, Committee 211, Detroit.

AISC (1999). *LRFD Specifications for Structural Steel Buildings*, American Institute of Steel Construction, Chicago, IL.

AISC (2001). *LRFD Manual of Steel Construction*, American Institute of Steel Construction, Chicago, IL (3rd edition).

AISC (2005). *Seismic Provisions for Structural Steel Buildings*, American Institute of Steel Construction, Chicago, IL.

ARA (2004). *Anti-Terrorist Blast (AT-Blast) version 2.1*, Applied Research Associates, Albuquerque, NM.

ASCE (1997). *Design of Blast Resistant Buildings in Petrochemical Facilities*, Task Committee on Blast Resistant Design of the Petrochemical Committee, American Society of Civil Engineers, New York, NY.

ASCE (2006). *Minimum design loads for buildings and other structures*, ASCE Standard ASCE/SEI 7-05, Reston, Va.

ASCE Manual 42. (1985). *Design of Structures to Resist Nuclear Weapons Effects*, Committee on Dynamic Effects, American Society of Civil Engineers, New York, NY.

Baker W.E. (1973). *Explosions in Air*, University of Texas Press, Austin, Texas.

Baker W.E., Cox P.A., Westine, P.S., Kulesz, J.J. and Strehlow, R.A. (1983). *Explosion Hazards and Evaluation, Elsevier*, Amsterdam.

Brode, H.L. (1955). "Numerical Solution of Spherical Blast Waves." *Journal of Applied Physics*, No.6, June.

Bruneau M, Marson J (2004). "Seismic design of concrete-filled circular steel bridge piers", *Journal of Bridge Engineering*, 9(1), 24-34.

Bruneau M, Berman J, Lopez Garcia D, Vian D (2005). "Steel plate shear wall buildings: design requirements and research." *2005 North American Steel Construction Conference*, electronic paper, American Institute of Steel Construction, Chicago, USA.

Bulson, P.S. (1997). "Explosive Loading of Engineering Structures", E & FN SPON, London, UK.

Conrath, E.J., Krauthammer, T., Marchand, K.A. and Mlakar, P.F. (1999). *Structural Design for Physical Security: State of the Practice,* ASCE, Reston, Va.

Dicleli M, Bruneau M (1996). "Quantitative approach to rapid seismic evaluation of slab-on-girder steel highway bridges." *Journal of Structural Engineering*, 122(10), 1160-1168.

Driver, R.G., Kulak, G.L., Kennedy, D.J.L., and Elwi, A.E. (1997), "Seismic Behavior of Steel Plate Shear Walls", Structural Engineering Report No. 215, Department of Civil Engineering, University of Alberta, Edmonton, Alberta, Canada.

Defense Threat Reduction Agency (DTRA). (1997). *Design and Analysis of Hardened Structures to Conventional Weapons Effects*. Washington, D.C. (distribution limited to U.S. Government agencies and their contractors).

Eurocode 4. (1994). "Design of composite steel and concrete structures." Commission of the European Communities, Brussels.

FEMA. (2003). Reference Manual to Mitigate Potential Terrorist Attacks against Buildings (FEMA 426). Federal Emergency Management Agency, Washington, D.C.

FHWA. (1969). Standard Plans for Highway Bridges – Volume IV: Typical Continuous Bridges. Federal Highway Administration, Washington, DC.

FHWA. (2003). *Recommendations for bridge and tunnel security*. Prepared by the Blue Ribbon Panel on Bridge and Tunnel Security, Federal Highway Administration, Washington, D.C.

Glasstone, S. and Dolan, P.J. ed. (1977) *The Effects of Nuclear Weapons*. The United States Department of Defense and the United States Department of Energy.

Hopkinson, B. (1915). British Ordnance Board Minutes 13565.

Marchand, K., and Plenge, B. (1998). "Concrete hard target spall and breach model." *AFRL-MN-EG-TR-1998-7032*, *Technical Rep. Prepared for the Munitions Directorate of the Air Force Research Laboratory*, Eglin Air Force Base, Fla. (distribution limited to U.S. Government agencies and their contractors).

Marson J, Bruneau M (2004). "Cyclic testing of concrete-filled circular steel bridge piers having encased fixed-based detail." *Journal of Bridge Engineering*, **9**(1), 14-23.

Mays, G.C., Smith, P.D. (1995): *Blast effects on buildings*. Telford, London, UK.

Priestley M.J.N., Seible F., Calvi G.M. (1996). *Seismic Design and Retrofit of Bridges*, Wiley, New York, NY.

Rankin, W.J.M. (1870). "On the Thermodynamic Theory of Waves of Finite Longitudinal Disturbance." *Philosophical Transactions of the Royal Society of London*, Vol.160, 277-288

SAP2000. (2005). *SAP2000 ver 10.0.1*, Computers and Structures, Inc., CA.

Science Applications International Corporation (SAIC). (2002). "A guide to highway vulnerability assessment for critical asset identification and protection." Rep. Prepared for The American Association of State Highway and Transportation Officials' Security Task Force.

Science Applications International Corp. (SAIC). (2001). *BlastX version 4.2.3.0.*, San Diego, Calif. (distribution limited to U.S. government agencies and their contractors).

Smith, P.D. and Hetherington, J.D. (1994). *Blast and Ballistic Loading of Structures*, Butterworth-Heinemann.

USACE-OD. (2002). *SPAn32 version 1.2.7.2*. U.S. Army Corps of Engineers Omaha District, Omaha, Neb. (distribution limited to U.S. Government agencies and their contractors).

USACE-ERDC. (2004). *Bridge Explosive Loading (BEL) version 1.1.0.3*. US Army Corps of Engineers' Engineer Research and Development Center, Vicksburg, MS. (distribution limited to U.S. Government agencies and their contractors).

USDA. (1986). *Fundamentals of Protective Design for Conventional Weapons*, Technical Manual TM5-855-1, US Department of the Army, Washington, DC.

USDA. (1990). *Structures to Resist the Effects of Accidental Explosions*. Technical Manual TM 5-1300, US Department of the Army, Washington, DC.

United States Department of Homeland Security (USDHS). (2002). "Department of Homeland Security website." <http://www.whitehouse.gov/homeland/> (June 1, 2002).

United States Department of Justice (USDJ). (1995). "Vulnerability assessment of federal facilities." 444 DM 1. Study coordinated by the United States Marshals Service dated June 28, 1995.

Williamson EB, Winget DG (2005). "Risk management and design of critical bridges for terrorist attacks." *Journal of Bridge Engineering*, 10(1), 96-106.

Winget DG, Marchand KA, Williamson EB (2005). "Analysis and design of critical bridges subjected to blast loads." *Journal of Structural Engineering*, 131(8), 1243-1255.

APPENDIX A
COLUMN DESIGN

This appendix provides calculations of specimens' design for column C4, C5 and C6 according to the pier concept proposed in Section 3.3. The plastic moment capacity, M_p, of the column specimens was calculated using the approximate equation presented in Bruneau and Marson (2004). The plastic moment capacity of the column specimens resulted in 108.3 kip-in (12.2 kN-m), 169.4 kip-in (19.1 kN-m) and 242.2 kip-in (27.4 kN-m) for C4, C5 and C6, respectively.

--- Test Specimen ---

Design of C4, C5 and C6

Units: $kip := 1000 \cdot lbf$ $ksi := \dfrac{kip}{in^2}$ $msec := \dfrac{sec}{1000}$

           $kN := 1000 \cdot N$ $MPa := 1000000 \cdot Pa$

Factos: Dynamic increase factors: $DIF_{sy} := 1.20$ for structural steel yield

                                      $DIF_{su} := 1.05$ for structural steel ultimate

                                      $DIF_{c} := 1.25$ for structural concrete

         Overstrength factors: $R_{sy} := 1.0$ for structural steel yield

                                      $R_{su} := 1.0$ for structural steel ultimate

                                      $R_{c} := 1.0$ for structural concrete

Material properties

         Young modulus: Steel: $E_{s} := 200000 \cdot MPa$

                           Concrete: $E_{c} := 30000 \cdot MPa$

         Yield stress::   Steel (A500 Grade B): $f_{s} := DIF_{sy} \cdot R_{sy} \cdot 42 \cdot ksi$ $f_{s} = 50.4 \, ksi$

                                                   $f_{s1} := R_{sy} \cdot 42 \cdot ksi$ $f_{s1} = 42.0 \, ksi$

                           Concrete: $f_{c} := DIF_{c} \cdot R_{c} \cdot 40 \cdot MPa$ $f_{c} = 7.3 \, ksi$

                                             $f_{c1} := R_{c} \cdot 40 \cdot MPa$ $f_{c1} = 5.8 \, ksi$

Appendix A

(1) Column C4

Height of the column: $\qquad$ $L := 59\,in$

Outside diameter of the column: $\qquad$ $D := 4 \cdot in$
(HSS 4.000 x 0.125)

Wall thickness: $\qquad$ $t := 0.125 \cdot in$

Core concrete diameter: $\qquad D_c := D - 2 \cdot t \qquad\qquad D_c = 3.75\,in$

Concrete core area: $\qquad A_c := \pi \cdot \left(\dfrac{D_c}{2}\right)^2 \qquad\qquad A_c = 71\,cm^2$

Concrete core moment of inertia: $\quad I_c := \dfrac{\pi \cdot D_c^{\,4}}{64} \qquad\qquad I_c = 404\,cm^4$

Steel tube area: $\qquad A_s := \dfrac{\pi}{4} \cdot \left(D^2 - D_c^{\,2}\right) \qquad A_s = 10\,cm^2 \qquad A_s = 1.522\,in^2$

Steel tube moment of inertia: $\qquad I_s := \dfrac{\pi \cdot \left(D^4 - D_c^{\,4}\right)}{64} \qquad I_s = 119\,cm^4$

Compressive strength of the composite column (AISC's LRFD Specifications for Structural Steel Buildings, Chapter I):

Modified yield stress: $\qquad F_m := f_{s1} + \dfrac{0.85 \cdot f_{c1} \cdot A_c}{A_s} \qquad F_m = 536\,MPa$

Modified modulus of elasticity: $\quad E_m := E_s + \dfrac{0.4 \cdot E_c \cdot A_c}{A_s} \qquad E_m = 287097\,MPa$

Effective length factor: $\qquad K := 0.7$

Radius of gyration: $\qquad r := 0.25 \cdot \sqrt{D^2 + D_c^{\,2}} \qquad r = 3.48\,cm$

Slenderness factor: $\qquad \lambda_c := \dfrac{K \cdot L}{\pi \cdot r} \cdot \sqrt{\dfrac{F_m}{E_m}} \qquad \lambda_c = 0.41$

Compressive strength: $\qquad P_n := 0.85 \cdot A_s \cdot 0.658^{\lambda_c^{\,2}} \cdot F_m \qquad P_n = 417\,kN$

Plastic moment capacity (Bruneau and Marson 2004):

Factor h_n:

$$h_n := \frac{A_c \cdot f_c}{2 \cdot D \cdot f_c + 4 \cdot t \cdot (2 \cdot f_s - f_c)}$$

$$h_n = 1.94 \, cm$$

Plastic modulus of the steel tube: $Z := \dfrac{D^3 - D_c^{\,3}}{6}$

$$Z = 31 \, cm^3$$

Plastic moment capacity:

$$M_p := \left(Z - 2 \cdot t \cdot h_n^2 \right) \cdot f_s + \left[\frac{2}{5} \cdot \left(\frac{D}{2} - t \right)^3 - \left(\frac{D}{2} - t \right) \cdot h_n^2 \right] \cdot f_c$$

Plastic moment capacity of steel tube:

$$M_{ps} := Z \cdot f_s \qquad M_{ps} = 95 \, kip \cdot in$$

According to Bruneau and Marson (2004), the value of Mp given by the former equation should be multiplied by 1.1, hence

Revised plastic moment capacity: $\quad M_p := 1.1 \cdot M_p$

$$M_p = 12.2 \, kN \cdot m$$

$$M_p = 108.3 \, kip \cdot in$$

Appendix A

(2) Column C5

Height of the column: $L := 59\,\text{in}$

Outside diameter of the column: $D := 5\cdot\text{in}$
  (HSS 5.000 x 0.125)

Wall thickness: $t := 0.125\cdot\text{in}$

Core concrete diameter: $D_c := D - 2\cdot t$ $D_c = 4.75\,\text{in}$

Concrete core area: $A_c := \pi\cdot\left(\dfrac{D_c}{2}\right)^2$ $A_c = 114\,\text{cm}^2$

Concrete core moment of inertia: $I_c := \dfrac{\pi\cdot D_c^{\,4}}{64}$ $I_c = 1040\,\text{cm}^4$

Steel tube area: $A_s := \dfrac{\pi}{4}\cdot\left(D^2 - D_c^{\,2}\right)$ $A_s = 12\,\text{cm}^2 \quad A_s = 1.914\,\text{in}^2$

Steel tube moment of inertia: $I_s := \dfrac{\pi\cdot\left(D^4 - D_c^{\,4}\right)}{64}$ $I_s = 237\,\text{cm}^4$

Compressive strength of the composite column (AISC's LRFD Specifications for Structural Steel Buildings, Chapter I):

Modified yield stress: $F_m := f_{s1} + \dfrac{0.85\cdot f_{c1}\cdot A_c}{A_s}$ $F_m = 604\,\text{MPa}$

Modified modulus of elasticity: $E_m := E_s + \dfrac{0.4\cdot E_c\cdot A_c}{A_s}$ $E_m = 311077\,\text{MPa}$

Effective length factor: $K := 0.7$

Radius of gyration: $r := 0.25\cdot\sqrt{D^2 + D_c^{\,2}}$ $r = 4.38\,\text{cm}$

Slenderness factor: $\lambda_c := \dfrac{K\cdot L}{\pi\cdot r}\cdot\sqrt{\dfrac{F_m}{E_m}}$ $\lambda_c = 0.34$

Compressive strength: $P_n := 0.85\cdot A_s\cdot 0.658^{\lambda_c^{\,2}}\cdot F_m$ $P_n = 605\,\text{kN}$

Appendix A

Plastic moment capacity (Bruneau and Marson 2004):

Factor h_n:
$$h_n := \frac{A_c \cdot f_c}{2 \cdot D \cdot f_c + 4 \cdot t \cdot (2 \cdot f_s - f_c)} \qquad h_n = 2.74 \, cm$$

Plastic modulus of the steel tube: $Z := \dfrac{D^3 - D_c^3}{6} \qquad Z = 49 \, cm^3$

Plastic moment capacity:
$$M_p := \left(Z - 2 \cdot t \cdot h_n^2 \right) \cdot f_s + \left[\frac{2}{5} \cdot \left(\frac{D}{2} - t \right)^3 - \left(\frac{D}{2} - t \right) \cdot h_n^2 \right] \cdot f_c$$

Plastic moment capacity of steel tube: $\qquad M_{ps} := Z \cdot f_s \qquad M_{ps} = 150 \, kip \cdot in$

According to Bruneau and Marson (2004), the value of Mp given by the former equation should be multiplied by 1.1, hence

Revised plastic moment capacity: $\quad M_p := 1.1 \cdot M_p \qquad\qquad M_p = 19.1 \, kN \cdot m$

$$M_p = 169.4 \, kip \cdot in$$

Appendix A

(3) Column C6

Height of the column: $\qquad$ $L := 59 \text{in}$

Outside diameter of the column: $\qquad$ $D := 6 \cdot \text{in}$
(HSS 6.000 x 0.125)

Wall thickness: $\qquad$ $t := 0.125 \cdot \text{in}$

Core concrete diameter: $\quad D_c := D - 2 \cdot t$ $\qquad$ $D_c = 5.75 \text{ in}$

Concrete core area: $\quad A_c := \pi \cdot \left(\dfrac{D_c}{2} \right)^2$ $\qquad$ $A_c = 168 \text{ cm}^2$

Concrete core moment of inertia: $\quad I_c := \dfrac{\pi \cdot D_c^{\,4}}{64}$ $\qquad$ $I_c = 2233 \text{ cm}^4$

Steel tube area: $\quad A_s := \dfrac{\pi}{4} \cdot \left(D^2 - D_c^{\,2} \right)$ $\qquad$ $A_s = 15 \text{ cm}^2 \qquad A_s = 2.307 \text{ in}^2$

Steel tube moment of inertia: $\quad I_s := \dfrac{\pi \cdot \left(D^4 - D_c^{\,4} \right)}{64}$ $\qquad$ $I_s = 415 \text{ cm}^4$

Compressive strength of the composite column (AISC's LRFD Specifications for Structural Steel Buildings, Chapter I):

Modified yield stress: $\quad F_m := f_{s1} + \dfrac{0.85 \cdot f_{c1} \cdot A_c}{A_s}$ $\qquad$ $F_m = 672 \text{ MPa}$

Modified modulus of elasticity: $\quad E_m := E_s + \dfrac{0.4 \cdot E_c \cdot A_c}{A_s}$ $\qquad$ $E_m = 335064 \text{ MPa}$

Effective length factor: $\quad K := 0.7$

Radius of gyration: $\quad r := 0.25 \cdot \sqrt{D^2 + D_c^{\,2}}$ $\qquad$ $r = 5.28 \text{ cm}$

Slenderness factor: $\quad \lambda_c := \dfrac{K \cdot L}{\pi \cdot r} \cdot \sqrt{\dfrac{F_m}{E_m}}$ $\qquad$ $\lambda_c = 0.28$

Compressive strength: $\quad P_n := 0.85 \cdot A_s \cdot 0.658^{\lambda_c^{\,2}} \cdot F_m$ $\qquad$ $P_n = 822 \text{ kN}$

Appendix A

Plastic moment capacity (Bruneau and Marson 2004):

Factor h_n:
$$h_n := \frac{A_c \cdot f_c}{2 \cdot D \cdot f_c + 4 \cdot t \cdot (2 \cdot f_s - f_c)} \qquad h_n = 3.57 \, cm$$

Plastic modulus of the steel tube:
$$Z := \frac{D^3 - D_c^{\,3}}{6} \qquad Z = 71 \, cm^3$$

Plastic moment capacity:
$$M_p := \left(Z - 2 \cdot t \cdot h_n^2\right) \cdot f_s + \left[\frac{2}{5} \cdot \left(\frac{D}{2} - t\right)^3 - \left(\frac{D}{2} - t\right) \cdot h_n^2\right] \cdot f_c$$

Plastic moment capacity of steel tube:
$$M_{ps} := Z \cdot f_s \qquad M_{ps} = 217 \, kip \cdot in$$

According to Bruneau and Marson (2004), the value of Mp given by the former equation should be multiplied by 1.1, hence

Revised plastic moment capacity:
$$M_p := 1.1 \cdot M_p \qquad M_p = 27.4 \, kN \cdot m$$

$$M_p = 242.2 \, kip \cdot in$$

144

APPENDIX B
PLATE DESIGN

This appendix provides calculations of plate design for the plate test according to capacity design principles, such that the plate be able to reach its ultimate elongation before yielding of the columns to which the plate was welded. The structural response of the plate was idealized such that the plate dissipated all impulse provided by the blast loading. The kinetic energy of the blast impulsive loading was assumed to be absorbed as internal plastic work of the plate. The minimum available steel plate thickness of 22 gages (0.76 mm) and plate width of 48" (1219 mm) were selected in the final design. For this design, the maximum expected plate elongation became 8.6 %.

--- Test Specimen ---

Design of Plate (w = 0.06W, x = 5X, z = 0.25m)

Units: $kip := 1000 \cdot lbf$ $ksi := \dfrac{kip}{in^2}$ $msec := \dfrac{sec}{1000}$

$kN := 1000 \cdot N$ $MPa := 1000000 \cdot Pa$

Factos:

    Dynamic increase factors: $DIF_{sy} := 1.20$ for structural steel yield

        $DIF_{su} := 1.05$ for structural steel ultimate

        $DIF_{c} := 1.25$ for structural concrete

    Overstrength factors: $R_{sy} := 1.2$ for structural steel yield

        $R_{su} := 1.2$ for structural steel ultimate

        $R_{c} := 1.1$ for structural concrete

Material properties

    Young modulus: Steel: $E_s := 200000 \cdot MPa$

        Concrete: $E_c := 30000 \cdot MPa$

    Yield stress: Steel Plate (A36): $f_{sp} := DIF_{sy} \cdot R_{sy} \cdot 20 \cdot ksi$ $f_{sp} = 198.6 \, MPa$

        Steel Column (A500 Grade B): $f_s := DIF_{sy} \cdot R_{sy} \cdot 42 \cdot ksi$ $f_s = 417.0 \, MPa$

    Ultimate stress: Steel Plate (A36): $f_{sup} := DIF_{su} \cdot R_{su} \cdot 30 \cdot ksi$ $f_{sup} = 260.6 \, MPa$

        Concrete: $f_c := DIF_c \cdot R_c \cdot 40 \cdot MPa$ $f_c = 55.0 \, MPa$

    Unit weight: Steel: $\gamma_s := 7800 \cdot \dfrac{kg}{m^3}$

Appendix B

Geometry:	Plate height:		$H := 48in$
	Plate width:		$B := 68.5 \cdot in$
	Plate thickness:		$t_p := 0.76mm$
	Height of the column:		$L := 59in$
	Outside diameter of the column:		$D := 5 \cdot in$
	Column wall thickness:		$t := 0.125 \cdot in$
Boundary conditions:	Column:	Fixed at the bottom, fixed at the top.	
	Plate:	Pinned along the column.	

Plate design:

Plate thickness:
$$t_p = 0.760 \, mm$$

Yield stress:
$$f_{sp} = 198.6 \, MPa \qquad f_{sp} = 0.19857 \, \frac{kN}{mm^2}$$

UDL by yielding plate:
$$f_y := t_p \cdot f_{sp} \qquad f_y = 150.9 \, \frac{kN}{m}$$

UDL at ultimate:
$$f_u := t_p \cdot f_{sup} \qquad f_u = 198.1 \, \frac{kN}{m}$$

Elongation at yield:
$$x_{yp} := \frac{f_{sp}}{E_s} \cdot B \qquad x_{yp} = 1.7 \, mm \qquad \frac{x_{yp}}{B} = 0.099 \, \%$$

Elongation at the onset
of Strain Hardening:
$$x_{hp} := 15 \cdot x_{yp} \qquad x_{hp} = 26 \, mm \qquad \frac{x_{hp}}{B} = 1.49 \, \%$$

Elongation at ultimate:
$$x_{up} := B \cdot 0.20 \qquad x_{up} = 348.0 \, mm$$

Internal work at yield:
$$W_{iyp} := \frac{1}{2} f_{sp} \cdot t_p \cdot H \cdot x_{yp} \qquad W_{iyp} = 0.16 \, kN \cdot m$$

Internal work at the onset of Strain
Hardening elongation:
$$W_{ihp} := f_{sp} \cdot t_p \cdot H \cdot (x_{hp} - x_{yp}) + W_{iyp} \qquad W_{ihp} = 4.61 \, kN \cdot m$$

Internal work at 10% elongation:

$$W_{i10p} := \frac{1}{2} \left[(f_{sup} - f_{sp}) \cdot \frac{(B \cdot 0.20 - x_{hp})}{(B \cdot 0.20 - x_{hp})} \right] \cdot t_p \cdot H \cdot (B \cdot 0.10 - x_{hp}) + f_{sp} \cdot t_p \cdot H \cdot (B \cdot 0.10 - x_{yp}) + W_{iyp}$$

$$W_{i10p} = 36.11 \, kN \cdot m$$

Appendix B

Blast load parameters: (these parameters were obtained using BEL for w = 0.06W at x = 5X)

Equivalent uniform pressure: $\qquad p_r := 173 \cdot psi$

Equivalent uniform impulse: $\qquad i_r := 47.09 \cdot psi \cdot msec$

Time parameter: $\qquad t_d := \dfrac{i_r \cdot 2}{p_r} \qquad t_d = 0.54\,msec$

Kinetic Energy by Impulse:

Load - mass factor: $\qquad K_{LM} := 0.66$

Section area of the plate: $\qquad A_p := H \cdot t_p \qquad A_p = 926.59\,mm^2$

Mass per unit length: $\qquad mass := \gamma_s \cdot A_p \qquad mass = 7.23 \dfrac{kg}{m}$

Impulse per unit length: $\qquad i := H \cdot i_r$

Kinetic energy: $\qquad KE := \dfrac{i^2}{2 \cdot K_{LM} \cdot mass} \cdot B \qquad KE = 28.58\,kN \cdot m$

Find elongation of plate due to blast:

$$f(\varepsilon) := \frac{1}{2}\left[\left(f_{sup} - f_{sp}\right) \cdot \frac{\left(B \cdot \varepsilon - x_{hp}\right)}{\left(B \cdot 0.20 - x_{hp}\right)}\right] \cdot t_p \cdot H \cdot \left(B \cdot \varepsilon - x_{hp}\right) + f_{sp} \cdot t_p \cdot H \cdot \left(B \cdot \varepsilon - x_{yp}\right) + W_{iyp} - \frac{i^2}{2 \cdot K_{LM} \cdot \left[\gamma_s \cdot \left(H \cdot t_p\right)\right]} \cdot$$

$$sol := root(f(\varepsilon), \varepsilon) \qquad sol = 0.086$$

Appendix B

Geometry of the composite column:

Core concrete diameter: $D_c := D - 2 \cdot t$ $\qquad D_c = 4.75\,\text{in}$

Concrete core area: $A_c := \pi \cdot \left(\dfrac{D_c}{2}\right)^2$ $\qquad A_c = 114\,\text{cm}^2$

Concrete core moment of inertia: $I_c := \dfrac{\pi \cdot D_c^{\,4}}{64}$ $\qquad I_c = 1040\,\text{cm}^4$

Steel tube area: $A_s := \dfrac{\pi}{4} \cdot \left(D^2 - D_c^{\,2}\right)$ $\qquad A_s = 12\,\text{cm}^2$

Steel tube moment of inertia: $I_s := \dfrac{\pi \cdot \left(D^4 - D_c^{\,4}\right)}{64}$ $\qquad I_s = 237\,\text{cm}^4$

Compressive strength of the composite column (AISC's LRFD Specifications for Structural Steel Buildings, Chapter I):

Modified yield stress: $F_m := f_s + \dfrac{0.85 \cdot f_c \cdot A_c}{A_s}$ $\qquad F_m = 850\,\text{MPa}$

Modified modulus of elasticity: $E_m := E_s + \dfrac{0.4 \cdot E_c \cdot A_c}{A_s}$ $\qquad E_m = 311077\,\text{MPa}$

Effective length factor: $K := 0.7$

Radius of gyration: $r := 0.25 \cdot \sqrt{D^2 + D_c^{\,2}}$ $\qquad r = 4.38\,\text{cm}$

Slenderness factor: $\lambda_c := \dfrac{K \cdot L}{\pi \cdot r} \cdot \sqrt{\dfrac{F_m}{E_m}}$ $\qquad \lambda_c = 0.40$

Compressive strength: $P_n := 0.85 \cdot A_s \cdot 0.658^{\lambda_c^{\,2}} \cdot F_m$ $\qquad P_n = 835\,\text{kN}$

Plastic moment capacity (Bruneau and Marson 2004):

Factor h_n:
$$h_n := \frac{A_c \cdot f_c}{2 \cdot D \cdot f_c + 4 \cdot t \cdot (2 \cdot f_s - f_c)} \qquad h_n = 2.63\,cm$$

Plastic modulus of the steel tube:
$$Z := \frac{D^3 - D_c^3}{6} \qquad Z = 49\,cm^3$$

Plastic moment capacity:
$$M_p := \left(Z - 2 \cdot t \cdot h_n^2\right) \cdot f_s + \left[\frac{2}{5} \cdot \left(\frac{D}{2} - t\right)^3 - \left(\frac{D}{2} - t\right) \cdot h_n^2\right] \cdot f_c$$

According to Bruneau and Marson (2004), the value of Mp given by the former equation should be multiplied by 1.1, hence

Revised plastic moment capacity:
$$M_p := 1.1 \cdot M_p \qquad M_p = 23.09\,kN \cdot m \qquad M_p = 204\,kip \cdot in$$

Column Check:

Equivalent flexural stiffness:
$$EI_e := E_s \cdot I_s + 0.8 \cdot E_c \cdot I_c \qquad EI_e = 723\,kN \cdot m^2$$

Equivalent elastic stiffness per unit length:
$$K_e := \frac{384 \cdot EI_e}{L^4} \qquad K_e = 55074\,\frac{kN}{m^2}$$

Equivalent elastic stiffness per unit length:
$$K_E := \frac{307 \cdot EI_e}{L^4} \qquad K_E = 44031\,\frac{kN}{m^2}$$

Load - mass factor:
$$K_{LM} := 0.66$$

Mass per unit length:
$$mass := A_s \cdot 7800 \cdot \frac{kg}{m^3} + A_c \cdot 2400 \cdot \frac{kg}{m^3} \qquad mass = 37.07\,\frac{kg}{m}$$

Equivalent elastic UDL:
$$r_y := \frac{12 \cdot M_p}{L^2} \qquad r_y = 123.4\,\frac{kN}{m}$$

Equivalent plastic UDL:
$$r_p := \frac{16 \cdot M_p}{L^2} \qquad r_p = 164.5\,\frac{kN}{m} \qquad > \qquad f_y = 150.9\,\frac{kN}{m} \qquad OK$$

UDL by yielding plate

Equivalent ultimate UDL:
$$r_u := 1.3 \cdot r_p \qquad r_u = 213.9\,\frac{kN}{m} \qquad > \qquad f_u = 198.1\,\frac{kN}{m} \qquad OK$$

UDL at ultimate

APPENDIX C

P-DELTA ANALYSIS

This appendix provides results of iterations for the P-δ analysis of the test CFST columns. The columns were modeled by beam elements having fixed boundary conditions at the top and bottom using the structural analysis program, SAP2000. An axial force of 85.4 kN was considered for the test columns to calculate deflections due to P-δ effects. This corresponds to 13, 12 and 6 % of the axial strength for Column C4, C5 and C6, respectively, given by:

$$P = f_s A_s + 0.85 f_c' A_c \tag{C-1}$$

where f_s is the yield stress of steel, f_c' is compressive strength of concrete, and A_c and A_s are, respectively, area of concrete and steel (AISC 2001). These axial forces are smaller than that of the typical bridge which is about 15 % of the yield axial force. The flexural stiffness of the CFST columns was calculated as the equivalent flexural stiffness of the composite section. The resulting maximum second-order deformations were 0.4, 0.1, 0.5, 0.2, 0.1 and 0.3 mm for Test 3, 4, 5, 6, 9 and 10, respectively. Obviously, these are small numbers given by the low axial forces applied to the columns.

Test 3: Column B1-C4
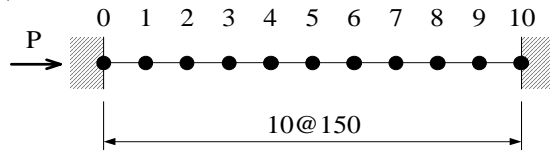
Axial Force P =   85.375   kN

(0) Initial Condition

Location	0	1	2	3	4	5	6	7	8	9	10
δ_0 (mm)	0	6.0	12.0	18.0	24.0	30.0	24.0	18.0	12.0	6.0	0
M (kN mm)	0	512	1025	1537	2049	2561	2049	1537	1025	512	0

(1) 1st Iteration

Location	0	1	2	3	4	5	6	7	8	9	10
δ (mm)	0	0.04	0.13	0.24	0.34	0.38	0.34	0.24	0.13	0.04	0
δ_0 (mm)	0	6	12	18	24	30	24	18	12	6	0
$\delta + \delta_0$ (mm)	0	6.04	12.1325	18.2425	24.335	30.375	24.335	18.2425	12.1325	6.04	0
M (kN mm)	0	516	1036	1557	2078	2593	2078	1557	1036	516	0

(2) 2nd Iteration

Location	0	1	2	3	4	5	6	7	8	9	10
δ (mm)	0	0.04	0.14	0.26	0.36	0.40	0.36	0.26	0.14	0.04	0
δ_0 (mm)	0	6	12	18	24	30	24	18	12	6	0
$\delta + \delta_0$ (mm)	0	6.04	12.14	18.2575	24.355	30.395	24.355	18.2575	12.14	6.04	0
M (kN mm)	0	516	1036	1559	2079	2595	2079	1559	1036	516	0

(3) 3rd Iteration

Location	0	1	2	3	4	5	6	7	8	9	10
δ (mm)	0	0.04	0.14	0.26	0.36	0.40	0.36	0.26	0.14	0.04	0

Test 4: Column B1-C6
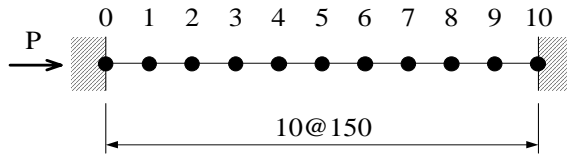
Axial Force P =   85.375   kN

(0) Initial Condition

Location	0	1	2	3	4	5	6	7	8	9	10
δ_0 (mm)	0	9.2	18.4	27.6	36.8	46.0	36.8	27.6	18.4	9.2	0
M (kN mm)	0	785	1571	2356	3142	3927	3142	2356	1571	785	0

(1) 1st Iteration

Location	0	1	2	3	4	5	6	7	8	9	10
δ (mm)	0	0.02	0.05	0.09	0.12	0.14	0.12	0.09	0.05	0.02	0
δ_0 (mm)	0	9.2	18.4	27.6	36.8	46.0	36.8	27.6	18.4	9.2	0.0
$\delta + \delta_0$ (mm)	0	9.22	18.45	27.69	36.92	46.14	36.92	27.69	18.45	9.22	0
M (kN mm)	0	787	1575	2364	3152	3939	3152	2364	1575	787	0

(2) 2nd Iteration

Location	0	1	2	3	4	5	6	7	8	9	10
δ (mm)	0	0.02	0.05	0.09	0.13	0.14	0.13	0.09	0.05	0.02	0
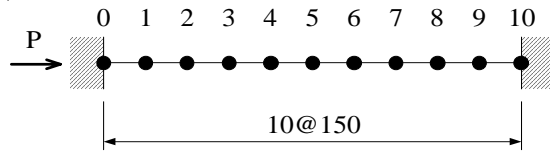
Test 5: Column B1-C5

Axial Force P = 85.375 kN

(0) Initial Condition

Location	0	1	2	3	4	5	6	7	8	9	10
δ_0 (mm)	0	15.2	30.4	45.6	60.8	76.0	60.8	45.6	30.4	15.2	0
M (kN mm)	0	1298	2595	3893	5191	6489	5191	3893	2595	1298	0

(1) 1st Iteration

Location	0	1	2	3	4	5	6	7	8	9	10
δ (mm)	0	0.05	0.16	0.29	0.41	0.45	0.41	0.29	0.16	0.05	0
δ_0 (mm)	0	15.2	30.4	45.6	60.8	76.0	60.8	45.6	30.4	15.2	0.0
$\delta + \delta_0$ (mm)	0	15.25	30.56	45.89	61.21	76.45	61.21	45.89	30.56	15.25	0
M (kN mm)	0	1302	2609	3918	5225	6527	5225	3918	2609	1302	0

(2) 2nd Iteration

Location	0	1	2	3	4	5	6	7	8	9	10
δ (mm)	0	0.05	0.16	0.30	0.42	0.47	0.42	0.30	0.16	0.05	0
δ_0 (mm)	0	15.2	30.4	45.6	60.8	76.0	60.8	45.6	30.4	15.2	0.0
$\delta + \delta_0$ (mm)	0	15.25	30.56	45.90	61.22	76.47	61.22	45.90	30.56	15.25	0
M (kN mm)	0	1302	2609	3919	5226	6528	5226	3919	2609	1302	0

(3) 3rd Iteration

Location	0	1	2	3	4	5	6	7	8	9	10
δ (mm)	0	0.05	0.16	0.30	0.42	0.47	0.42	0.30	0.16	0.05	0

Test 6: Column B2-C4
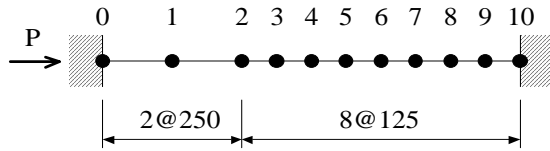
Axial Force P =   85.375   kN

(0) Initial Condition

Location	0	1	2	3	4	5	6	7	8	9	10
δ_0 (mm)	0	4.8	9.6	12.0	14.4	16.8	19.2	21.6	24.0	12.0	0
M (kN mm)	0	410	820	1025	1229	1434	1639	1844	2049	1025	0

(1) 1st Iteration

Location	0	1	2	3	4	5	6	7	8	9	10
δ (mm)	0	0.03	0.09	0.12	0.14	0.16	0.16	0.14	0.09	0.03	0
δ_0 (mm)	0	4.8	9.6	12.0	14.4	16.8	19.2	21.6	24.0	12.0	0.0
$\delta + \delta_0$ (mm)	0	4.83	9.69	12.12	14.54	16.96	19.36	21.74	24.09	12.03	0
M (kN mm)	0	412	827	1034	1241	1448	1652	1856	2057	1027	0

(2) 2nd Iteration

Location	0	1	2	3	4	5	6	7	8	9	10
δ (mm)	0	0.03	0.09	0.12	0.15	0.16	0.16	0.14	0.10	0.03	0
δ_0 (mm)	0	4.8	9.6	12.0	14.4	16.8	19.2	21.6	24.0	12.0	0.0
$\delta + \delta_0$ (mm)	0	4.83	9.69	12.12	14.55	16.96	19.36	21.74	24.10	12.03	0
M (kN mm)	0	412	827	1035	1242	1448	1653	1856	2057	1027	0

(3) 3rd Iteration

Location	0	1	2	3	4	5	6	7	8	9	10
δ (mm)	0	0.03	0.09	0.12	0.15	0.16	0.16	0.14	0.10	0.03	0

Test 9: Column B2-C6
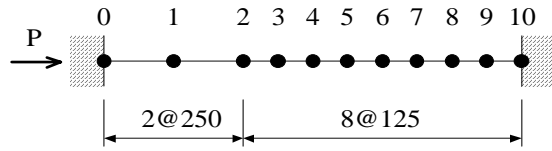
Axial Force P = 85.375 kN

(0) Initial Condition

Location	0	1	2	3	4	5	6	7	8	9	10
δ_0 (mm)	0	9.0	18.0	22.5	27.0	31.5	36.0	40.5	45.0	22.5	0
M (kN mm)	0	768	1537	1921	2305	2689	3074	3458	3842	1921	0

(1) 1st Iteration

Location	0	1	2	3	4	5	6	7	8	9	10
δ (mm)	0	0.01	0.04	0.05	0.06	0.07	0.07	0.06	0.04	0.02	0
δ_0 (mm)	0	9.0	18.0	22.5	27.0	31.5	36.0	40.5	45.0	22.5	0.0
$\delta + \delta_0$ (mm)	0	9.01	18.04	22.55	27.06	31.57	36.07	40.56	45.04	22.52	0
M (kN mm)	0	769	1540	1925	2310	2695	3079	3463	3846	1922	0

(2) 2nd Iteration

Location	0	1	2	3	4	5	6	7	8	9	10
δ (mm)	0	0.01	0.04	0.05	0.06	0.07	0.07	0.06	0.04	0.02	0

Appendix C

Test 10: Column B2-C5
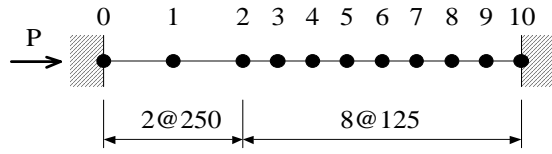
0 1 2 3 4 5 6 7 8 9 10

P

2@250   8@125

Axial Force P = 85.375 kN

(0) Initial Condition

Location	0	1	2	3	4	5	6	7	8	9	10
δ_0 (mm)	0	20.0	40.0	50.0	60.0	70.0	80.0	90.0	100.0	50.0	0
M (kN mm)	0	1708	3415	4269	5123	5976	6830	7684	8538	4269	0

(1) 1st Iteration

Location	0	1	2	3	4	5	6	7	8	9	10
δ (mm)	0	0.05	0.17	0.23	0.28	0.31	0.31	0.27	0.19	0.07	0
δ_0 (mm)	0	20.0	40.0	50.0	60.0	70.0	80.0	90.0	100.0	50.0	0.0
$\delta + \delta_0$ (mm)	0	20.05	40.17	50.23	60.28	70.31	80.31	90.27	100.19	50.07	0
M (kN mm)	0	1712	3429	4288	5146	6003	6856	7707	8553	4274	0

(2) 2nd Iteration

Location	0	1	2	3	4	5	6	7	8	9	10
δ (mm)	0	0.05	0.17	0.24	0.29	0.32	0.32	0.27	0.19	0.07	0
δ_0 (mm)	0	20.0	40.0	50.0	60.0	70.0	80.0	90.0	100.0	50.0	0.0
$\delta + \delta_0$ (mm)	0	20.05	40.17	50.24	60.29	70.32	80.32	90.27	100.19	50.07	0
M (kN mm)	0	1712	3430	4289	5147	6003	6857	7707	8554	4275	0

(3) 3rd Iteration

Location	0	1	2	3	4	5	6	7	8	9	10
δ (mm)	0	0.05	0.17	0.24	0.29	0.32	0.32	0.28	0.19	0.07	0

MCEER Technical Reports

MCEER publishes technical reports on a variety of subjects written by authors funded through MCEER. These reports are available from both MCEER Publications and the National Technical Information Service (NTIS). Requests for reports should be directed to MCEER Publications, MCEER, University at Buffalo, State University of New York, Red Jacket Quadrangle, Buffalo, New York 14261. Reports can also be requested through NTIS, 5285 Port Royal Road, Springfield, Virginia 22161. NTIS accession numbers are shown in parenthesis, if available.

NCEER-87-0001 "First-Year Program in Research, Education and Technology Transfer," 3/5/87, (PB88-134275, A04, MF-A01).

NCEER-87-0002 "Experimental Evaluation of Instantaneous Optimal Algorithms for Structural Control," by R.C. Lin, T.T. Soong and A.M. Reinhorn, 4/20/87, (PB88-134341, A04, MF-A01).

NCEER-87-0003 "Experimentation Using the Earthquake Simulation Facilities at University at Buffalo," by A.M. Reinhorn and R.L. Ketter, to be published.

NCEER-87-0004 "The System Characteristics and Performance of a Shaking Table," by J.S. Hwang, K.C. Chang and G.C. Lee, 6/1/87, (PB88-134259, A03, MF-A01). This report is available only through NTIS (see address given above).

NCEER-87-0005 "A Finite Element Formulation for Nonlinear Viscoplastic Material Using a Q Model," by O. Gyebi and G. Dasgupta, 11/2/87, (PB88-213764, A08, MF-A01).

NCEER-87-0006 "Symbolic Manipulation Program (SMP) - Algebraic Codes for Two and Three Dimensional Finite Element Formulations," by X. Lee and G. Dasgupta, 11/9/87, (PB88-218522, A05, MF-A01).

NCEER-87-0007 "Instantaneous Optimal Control Laws for Tall Buildings Under Seismic Excitations," by J.N. Yang, A. Akbarpour and P. Ghaemmaghami, 6/10/87, (PB88-134333, A06, MF-A01). This report is only available through NTIS (see address given above).

NCEER-87-0008 "IDARC: Inelastic Damage Analysis of Reinforced Concrete Frame - Shear-Wall Structures," by Y.J. Park, A.M. Reinhorn and S.K. Kunnath, 7/20/87, (PB88-134325, A09, MF-A01). This report is only available through NTIS (see address given above).

NCEER-87-0009 "Liquefaction Potential for New York State: A Preliminary Report on Sites in Manhattan and Buffalo," by M. Budhu, V. Vijayakumar, R.F. Giese and L. Baumgras, 8/31/87, (PB88-163704, A03, MF-A01). This report is available only through NTIS (see address given above).

NCEER-87-0010 "Vertical and Torsional Vibration of Foundations in Inhomogeneous Media," by A.S. Veletsos and K.W. Dotson, 6/1/87, (PB88-134291, A03, MF-A01). This report is only available through NTIS (see address given above).

NCEER-87-0011 "Seismic Probabilistic Risk Assessment and Seismic Margins Studies for Nuclear Power Plants," by Howard H.M. Hwang, 6/15/87, (PB88-134267, A03, MF-A01). This report is only available through NTIS (see address given above).

NCEER-87-0012 "Parametric Studies of Frequency Response of Secondary Systems Under Ground-Acceleration Excitations," by Y. Yong and Y.K. Lin, 6/10/87, (PB88-134309, A03, MF-A01). This report is only available through NTIS (see address given above).

NCEER-87-0013 "Frequency Response of Secondary Systems Under Seismic Excitation," by J.A. HoLung, J. Cai and Y.K. Lin, 7/31/87, (PB88-134317, A05, MF-A01). This report is only available through NTIS (see address given above).

NCEER-87-0014 "Modelling Earthquake Ground Motions in Seismically Active Regions Using Parametric Time Series Methods," by G.W. Ellis and A.S. Cakmak, 8/25/87, (PB88-134283, A08, MF-A01). This report is only available through NTIS (see address given above).

NCEER-87-0015 "Detection and Assessment of Seismic Structural Damage," by E. DiPasquale and A.S. Cakmak, 8/25/87, (PB88-163712, A05, MF-A01). This report is only available through NTIS (see address given above).

NCEER-87-0016   "Pipeline Experiment at Parkfield, California," by J. Isenberg and E. Richardson, 9/15/87, (PB88-163720, A03, MF-A01). This report is available only through NTIS (see address given above).

NCEER-87-0017   "Digital Simulation of Seismic Ground Motion," by M. Shinozuka, G. Deodatis and T. Harada, 8/31/87, (PB88-155197, A04, MF-A01). This report is available only through NTIS (see address given above).

NCEER-87-0018   "Practical Considerations for Structural Control: System Uncertainty, System Time Delay and Truncation of Small Control Forces," J.N. Yang and A. Akbarpour, 8/10/87, (PB88-163738, A08, MF-A01). This report is only available through NTIS (see address given above).

NCEER-87-0019   "Modal Analysis of Nonclassically Damped Structural Systems Using Canonical Transformation," by J.N. Yang, S. Sarkani and F.X. Long, 9/27/87, (PB88-187851, A04, MF-A01).

NCEER-87-0020   "A Nonstationary Solution in Random Vibration Theory," by J.R. Red-Horse and P.D. Spanos, 11/3/87, (PB88-163746, A03, MF-A01).

NCEER-87-0021   "Horizontal Impedances for Radially Inhomogeneous Viscoelastic Soil Layers," by A.S. Veletsos and K.W. Dotson, 10/15/87, (PB88-150859, A04, MF-A01).

NCEER-87-0022   "Seismic Damage Assessment of Reinforced Concrete Members," by Y.S. Chung, C. Meyer and M. Shinozuka, 10/9/87, (PB88-150867, A05, MF-A01). This report is available only through NTIS (see address given above).

NCEER-87-0023   "Active Structural Control in Civil Engineering," by T.T. Soong, 11/11/87, (PB88-187778, A03, MF-A01).

NCEER-87-0024   "Vertical and Torsional Impedances for Radially Inhomogeneous Viscoelastic Soil Layers," by K.W. Dotson and A.S. Veletsos, 12/87, (PB88-187786, A03, MF-A01).

NCEER-87-0025   "Proceedings from the Symposium on Seismic Hazards, Ground Motions, Soil-Liquefaction and Engineering Practice in Eastern North America," October 20-22, 1987, edited by K.H. Jacob, 12/87, (PB88-188115, A23, MF-A01). This report is available only through NTIS (see address given above).

NCEER-87-0026   "Report on the Whittier-Narrows, California, Earthquake of October 1, 1987," by J. Pantelic and A. Reinhorn, 11/87, (PB88-187752, A03, MF-A01). This report is available only through NTIS (see address given above).

NCEER-87-0027   "Design of a Modular Program for Transient Nonlinear Analysis of Large 3-D Building Structures," by S. Srivastav and J.F. Abel, 12/30/87, (PB88-187950, A05, MF-A01). This report is only available through NTIS (see address given above).

NCEER-87-0028   "Second-Year Program in Research, Education and Technology Transfer," 3/8/88, (PB88-219480, A04, MF-A01).

NCEER-88-0001   "Workshop on Seismic Computer Analysis and Design of Buildings With Interactive Graphics," by W. McGuire, J.F. Abel and C.H. Conley, 1/18/88, (PB88-187760, A03, MF-A01). This report is only available through NTIS (see address given above).

NCEER-88-0002   "Optimal Control of Nonlinear Flexible Structures," by J.N. Yang, F.X. Long and D. Wong, 1/22/88, (PB88-213772, A06, MF-A01).

NCEER-88-0003   "Substructuring Techniques in the Time Domain for Primary-Secondary Structural Systems," by G.D. Manolis and G. Juhn, 2/10/88, (PB88-213780, A04, MF-A01).

NCEER-88-0004   "Iterative Seismic Analysis of Primary-Secondary Systems," by A. Singhal, L.D. Lutes and P.D. Spanos, 2/23/88, (PB88-213798, A04, MF-A01).

NCEER-88-0005   "Stochastic Finite Element Expansion for Random Media," by P.D. Spanos and R. Ghanem, 3/14/88, (PB88-213806, A03, MF-A01).

NCEER-88-0006 "Combining Structural Optimization and Structural Control," by F.Y. Cheng and C.P. Pantelides, 1/10/88, (PB88-213814, A05, MF-A01).

NCEER-88-0007 "Seismic Performance Assessment of Code-Designed Structures," by H.H-M. Hwang, J-W. Jaw and H-J. Shau, 3/20/88, (PB88-219423, A04, MF-A01). This report is only available through NTIS (see address given above).

NCEER-88-0008 "Reliability Analysis of Code-Designed Structures Under Natural Hazards," by H.H-M. Hwang, H. Ushiba and M. Shinozuka, 2/29/88, (PB88-229471, A07, MF-A01). This report is only available through NTIS (see address given above).

NCEER-88-0009 "Seismic Fragility Analysis of Shear Wall Structures," by J-W Jaw and H.H-M. Hwang, 4/30/88, (PB89-102867, A04, MF-A01).

NCEER-88-0010 "Base Isolation of a Multi-Story Building Under a Harmonic Ground Motion - A Comparison of Performances of Various Systems," by F-G Fan, G. Ahmadi and I.G. Tadjbakhsh, 5/18/88, (PB89-122238, A06, MF-A01). This report is only available through NTIS (see address given above).

NCEER-88-0011 "Seismic Floor Response Spectra for a Combined System by Green's Functions," by F.M. Lavelle, L.A. Bergman and P.D. Spanos, 5/1/88, (PB89-102875, A03, MF-A01).

NCEER-88-0012 "A New Solution Technique for Randomly Excited Hysteretic Structures," by G.Q. Cai and Y.K. Lin, 5/16/88, (PB89-102883, A03, MF-A01).

NCEER-88-0013 "A Study of Radiation Damping and Soil-Structure Interaction Effects in the Centrifuge," by K. Weissman, supervised by J.H. Prevost, 5/24/88, (PB89-144703, A06, MF-A01).

NCEER-88-0014 "Parameter Identification and Implementation of a Kinematic Plasticity Model for Frictional Soils," by J.H. Prevost and D.V. Griffiths, to be published.

NCEER-88-0015 "Two- and Three- Dimensional Dynamic Finite Element Analyses of the Long Valley Dam," by D.V. Griffiths and J.H. Prevost, 6/17/88, (PB89-144711, A04, MF-A01).

NCEER-88-0016 "Damage Assessment of Reinforced Concrete Structures in Eastern United States," by A.M. Reinhorn, M.J. Seidel, S.K. Kunnath and Y.J. Park, 6/15/88, (PB89-122220, A04, MF-A01). This report is only available through NTIS (see address given above).

NCEER-88-0017 "Dynamic Compliance of Vertically Loaded Strip Foundations in Multilayered Viscoelastic Soils," by S. Ahmad and A.S.M. Israil, 6/17/88, (PB89-102891, A04, MF-A01).

NCEER-88-0018 "An Experimental Study of Seismic Structural Response With Added Viscoelastic Dampers," by R.C. Lin, Z. Liang, T.T. Soong and R.H. Zhang, 6/30/88, (PB89-122212, A05, MF-A01). This report is available only through NTIS (see address given above).

NCEER-88-0019 "Experimental Investigation of Primary - Secondary System Interaction," by G.D. Manolis, G. Juhn and A.M. Reinhorn, 5/27/88, (PB89-122204, A04, MF-A01).

NCEER-88-0020 "A Response Spectrum Approach For Analysis of Nonclassically Damped Structures," by J.N. Yang, S. Sarkani and F.X. Long, 4/22/88, (PB89-102909, A04, MF-A01).

NCEER-88-0021 "Seismic Interaction of Structures and Soils: Stochastic Approach," by A.S. Veletsos and A.M. Prasad, 7/21/88, (PB89-122196, A04, MF-A01). This report is only available through NTIS (see address given above).

NCEER-88-0022 "Identification of the Serviceability Limit State and Detection of Seismic Structural Damage," by E. DiPasquale and A.S. Cakmak, 6/15/88, (PB89-122188, A05, MF-A01). This report is available only through NTIS (see address given above).

NCEER-88-0023 "Multi-Hazard Risk Analysis: Case of a Simple Offshore Structure," by B.K. Bhartia and E.H. Vanmarcke, 7/21/88, (PB89-145213, A05, MF-A01).

NCEER-88-0024   "Automated Seismic Design of Reinforced Concrete Buildings," by Y.S. Chung, C. Meyer and M. Shinozuka, 7/5/88, (PB89-122170, A06, MF-A01). This report is available only through NTIS (see address given above).

NCEER-88-0025   "Experimental Study of Active Control of MDOF Structures Under Seismic Excitations," by L.L. Chung, R.C. Lin, T.T. Soong and A.M. Reinhorn, 7/10/88, (PB89-122600, A04, MF-A01).

NCEER-88-0026   "Earthquake Simulation Tests of a Low-Rise Metal Structure," by J.S. Hwang, K.C. Chang, G.C. Lee and R.L. Ketter, 8/1/88, (PB89-102917, A04, MF-A01).

NCEER-88-0027   "Systems Study of Urban Response and Reconstruction Due to Catastrophic Earthquakes," by F. Kozin and H.K. Zhou, 9/22/88, (PB90-162348, A04, MF-A01).

NCEER-88-0028   "Seismic Fragility Analysis of Plane Frame Structures," by H.H-M. Hwang and Y.K. Low, 7/31/88, (PB89-131445, A06, MF-A01).

NCEER-88-0029   "Response Analysis of Stochastic Structures," by A. Kardara, C. Bucher and M. Shinozuka, 9/22/88, (PB89-174429, A04, MF-A01).

NCEER-88-0030   "Nonnormal Accelerations Due to Yielding in a Primary Structure," by D.C.K. Chen and L.D. Lutes, 9/19/88, (PB89-131437, A04, MF-A01).

NCEER-88-0031   "Design Approaches for Soil-Structure Interaction," by A.S. Veletsos, A.M. Prasad and Y. Tang, 12/30/88, (PB89-174437, A03, MF-A01). This report is available only through NTIS (see address given above).

NCEER-88-0032   "A Re-evaluation of Design Spectra for Seismic Damage Control," by C.J. Turkstra and A.G. Tallin, 11/7/88, (PB89-145221, A05, MF-A01).

NCEER-88-0033   "The Behavior and Design of Noncontact Lap Splices Subjected to Repeated Inelastic Tensile Loading," by V.E. Sagan, P. Gergely and R.N. White, 12/8/88, (PB89-163737, A08, MF-A01).

NCEER-88-0034   "Seismic Response of Pile Foundations," by S.M. Mamoon, P.K. Banerjee and S. Ahmad, 11/1/88, (PB89-145239, A04, MF-A01).

NCEER-88-0035   "Modeling of R/C Building Structures With Flexible Floor Diaphragms (IDARC2)," by A.M. Reinhorn, S.K. Kunnath and N. Panahshahi, 9/7/88, (PB89-207153, A07, MF-A01).

NCEER-88-0036   "Solution of the Dam-Reservoir Interaction Problem Using a Combination of FEM, BEM with Particular Integrals, Modal Analysis, and Substructuring," by C-S. Tsai, G.C. Lee and R.L. Ketter, 12/31/88, (PB89-207146, A04, MF-A01).

NCEER-88-0037   "Optimal Placement of Actuators for Structural Control," by F.Y. Cheng and C.P. Pantelides, 8/15/88, (PB89-162846, A05, MF-A01).

NCEER-88-0038   "Teflon Bearings in Aseismic Base Isolation: Experimental Studies and Mathematical Modeling," by A. Mokha, M.C. Constantinou and A.M. Reinhorn, 12/5/88, (PB89-218457, A10, MF-A01). This report is available only through NTIS (see address given above).

NCEER-88-0039   "Seismic Behavior of Flat Slab High-Rise Buildings in the New York City Area," by P. Weidlinger and M. Ettouney, 10/15/88, (PB90-145681, A04, MF-A01).

NCEER-88-0040   "Evaluation of the Earthquake Resistance of Existing Buildings in New York City," by P. Weidlinger and M. Ettouney, 10/15/88, to be published.

NCEER-88-0041   "Small-Scale Modeling Techniques for Reinforced Concrete Structures Subjected to Seismic Loads," by W. Kim, A. El-Attar and R.N. White, 11/22/88, (PB89-189625, A05, MF-A01).

NCEER-88-0042   "Modeling Strong Ground Motion from Multiple Event Earthquakes," by G.W. Ellis and A.S. Cakmak, 10/15/88, (PB89-174445, A03, MF-A01).

NCEER-88-0043 "Nonstationary Models of Seismic Ground Acceleration," by M. Grigoriu, S.E. Ruiz and E. Rosenblueth, 7/15/88, (PB89-189617, A04, MF-A01).

NCEER-88-0044 "SARCF User's Guide: Seismic Analysis of Reinforced Concrete Frames," by Y.S. Chung, C. Meyer and M. Shinozuka, 11/9/88, (PB89-174452, A08, MF-A01).

NCEER-88-0045 "First Expert Panel Meeting on Disaster Research and Planning," edited by J. Pantelic and J. Stoyle, 9/15/88, (PB89-174460, A05, MF-A01).

NCEER-88-0046 "Preliminary Studies of the Effect of Degrading Infill Walls on the Nonlinear Seismic Response of Steel Frames," by C.Z. Chrysostomou, P. Gergely and J.F. Abel, 12/19/88, (PB89-208383, A05, MF-A01).

NCEER-88-0047 "Reinforced Concrete Frame Component Testing Facility - Design, Construction, Instrumentation and Operation," by S.P. Pessiki, C. Conley, T. Bond, P. Gergely and R.N. White, 12/16/88, (PB89-174478, A04, MF-A01).

NCEER-89-0001 "Effects of Protective Cushion and Soil Compliancy on the Response of Equipment Within a Seismically Excited Building," by J.A. HoLung, 2/16/89, (PB89-207179, A04, MF-A01).

NCEER-89-0002 "Statistical Evaluation of Response Modification Factors for Reinforced Concrete Structures," by H.H-M. Hwang and J-W. Jaw, 2/17/89, (PB89-207187, A05, MF-A01).

NCEER-89-0003 "Hysteretic Columns Under Random Excitation," by G-Q. Cai and Y.K. Lin, 1/9/89, (PB89-196513, A03, MF-A01).

NCEER-89-0004 "Experimental Study of `Elephant Foot Bulge' Instability of Thin-Walled Metal Tanks," by Z-H. Jia and R.L. Ketter, 2/22/89, (PB89-207195, A03, MF-A01).

NCEER-89-0005 "Experiment on Performance of Buried Pipelines Across San Andreas Fault," by J. Isenberg, E. Richardson and T.D. O'Rourke, 3/10/89, (PB89-218440, A04, MF-A01). This report is available only through NTIS (see address given above).

NCEER-89-0006 "A Knowledge-Based Approach to Structural Design of Earthquake-Resistant Buildings," by M. Subramani, P. Gergely, C.H. Conley, J.F. Abel and A.H. Zaghw, 1/15/89, (PB89-218465, A06, MF-A01).

NCEER-89-0007 "Liquefaction Hazards and Their Effects on Buried Pipelines," by T.D. O'Rourke and P.A. Lane, 2/1/89, (PB89-218481, A09, MF-A01).

NCEER-89-0008 "Fundamentals of System Identification in Structural Dynamics," by H. Imai, C-B. Yun, O. Maruyama and M. Shinozuka, 1/26/89, (PB89-207211, A04, MF-A01).

NCEER-89-0009 "Effects of the 1985 Michoacan Earthquake on Water Systems and Other Buried Lifelines in Mexico," by A.G. Ayala and M.J. O'Rourke, 3/8/89, (PB89-207229, A06, MF-A01).

NCEER-89-R010 "NCEER Bibliography of Earthquake Education Materials," by K.E.K. Ross, Second Revision, 9/1/89, (PB90-125352, A05, MF-A01). This report is replaced by NCEER-92-0018.

NCEER-89-0011 "Inelastic Three-Dimensional Response Analysis of Reinforced Concrete Building Structures (IDARC-3D), Part I - Modeling," by S.K. Kunnath and A.M. Reinhorn, 4/17/89, (PB90-114612, A07, MF-A01). This report is available only through NTIS (see address given above).

NCEER-89-0012 "Recommended Modifications to ATC-14," by C.D. Poland and J.O. Malley, 4/12/89, (PB90-108648, A15, MF-A01).

NCEER-89-0013 "Repair and Strengthening of Beam-to-Column Connections Subjected to Earthquake Loading," by M. Corazao and A.J. Durrani, 2/28/89, (PB90-109885, A06, MF-A01).

NCEER-89-0014 "Program EXKAL2 for Identification of Structural Dynamic Systems," by O. Maruyama, C-B. Yun, M. Hoshiya and M. Shinozuka, 5/19/89, (PB90-109877, A09, MF-A01).

NCEER-89-0015   "Response of Frames With Bolted Semi-Rigid Connections, Part I - Experimental Study and Analytical Predictions," by P.J. DiCorso, A.M. Reinhorn, J.R. Dickerson, J.B. Radziminski and W.L. Harper, 6/1/89, to be published.

NCEER-89-0016   "ARMA Monte Carlo Simulation in Probabilistic Structural Analysis," by P.D. Spanos and M.P. Mignolet, 7/10/89, (PB90-109893, A03, MF-A01).

NCEER-89-P017   "Preliminary Proceedings from the Conference on Disaster Preparedness - The Place of Earthquake Education in Our Schools," Edited by K.E.K. Ross, 6/23/89, (PB90-108606, A03, MF-A01).

NCEER-89-0017   "Proceedings from the Conference on Disaster Preparedness - The Place of Earthquake Education in Our Schools," Edited by K.E.K. Ross, 12/31/89, (PB90-207895, A012, MF-A02). This report is available only through NTIS (see address given above).

NCEER-89-0018   "Multidimensional Models of Hysteretic Material Behavior for Vibration Analysis of Shape Memory Energy Absorbing Devices, by E.J. Graesser and F.A. Cozzarelli, 6/7/89, (PB90-164146, A04, MF-A01).

NCEER-89-0019   "Nonlinear Dynamic Analysis of Three-Dimensional Base Isolated Structures (3D-BASIS)," by S. Nagarajaiah, A.M. Reinhorn and M.C. Constantinou, 8/3/89, (PB90-161936, A06, MF-A01). This report has been replaced by NCEER-93-0011.

NCEER-89-0020   "Structural Control Considering Time-Rate of Control Forces and Control Rate Constraints," by F.Y. Cheng and C.P. Pantelides, 8/3/89, (PB90-120445, A04, MF-A01).

NCEER-89-0021   "Subsurface Conditions of Memphis and Shelby County," by K.W. Ng, T-S. Chang and H-H.M. Hwang, 7/26/89, (PB90-120437, A03, MF-A01).

NCEER-89-0022   "Seismic Wave Propagation Effects on Straight Jointed Buried Pipelines," by K. Elhmadi and M.J. O'Rourke, 8/24/89, (PB90-162322, A10, MF-A02).

NCEER-89-0023   "Workshop on Serviceability Analysis of Water Delivery Systems," edited by M. Grigoriu, 3/6/89, (PB90-127424, A03, MF-A01).

NCEER-89-0024   "Shaking Table Study of a 1/5 Scale Steel Frame Composed of Tapered Members," by K.C. Chang, J.S. Hwang and G.C. Lee, 9/18/89, (PB90-160169, A04, MF-A01).

NCEER-89-0025   "DYNA1D: A Computer Program for Nonlinear Seismic Site Response Analysis - Technical Documentation," by Jean H. Prevost, 9/14/89, (PB90-161944, A07, MF-A01). This report is available only through NTIS (see address given above).

NCEER-89-0026   "1:4 Scale Model Studies of Active Tendon Systems and Active Mass Dampers for Aseismic Protection," by A.M. Reinhorn, T.T. Soong, R.C. Lin, Y.P. Yang, Y. Fukao, H. Abe and M. Nakai, 9/15/89, (PB90-173246, A10, MF-A02). This report is available only through NTIS (see address given above).

NCEER-89-0027   "Scattering of Waves by Inclusions in a Nonhomogeneous Elastic Half Space Solved by Boundary Element Methods," by P.K. Hadley, A. Askar and A.S. Cakmak, 6/15/89, (PB90-145699, A07, MF-A01).

NCEER-89-0028   "Statistical Evaluation of Deflection Amplification Factors for Reinforced Concrete Structures," by H.H.M. Hwang, J-W. Jaw and A.L. Ch'ng, 8/31/89, (PB90-164633, A05, MF-A01).

NCEER-89-0029   "Bedrock Accelerations in Memphis Area Due to Large New Madrid Earthquakes," by H.H.M. Hwang, C.H.S. Chen and G. Yu, 11/7/89, (PB90-162330, A04, MF-A01).

NCEER-89-0030   "Seismic Behavior and Response Sensitivity of Secondary Structural Systems," by Y.Q. Chen and T.T. Soong, 10/23/89, (PB90-164658, A08, MF-A01).

NCEER-89-0031   "Random Vibration and Reliability Analysis of Primary-Secondary Structural Systems," by Y. Ibrahim, M. Grigoriu and T.T. Soong, 11/10/89, (PB90-161951, A04, MF-A01).

NCEER-89-0032   "Proceedings from the Second U.S. - Japan Workshop on Liquefaction, Large Ground Deformation and Their Effects on Lifelines, September 26-29, 1989," Edited by T.D. O'Rourke and M. Hamada, 12/1/89, (PB90-209388, A22, MF-A03).

NCEER-89-0033   "Deterministic Model for Seismic Damage Evaluation of Reinforced Concrete Structures," by J.M. Bracci, A.M. Reinhorn, J.B. Mander and S.K. Kunnath, 9/27/89, (PB91-108803, A06, MF-A01).

NCEER-89-0034   "On the Relation Between Local and Global Damage Indices," by E. DiPasquale and A.S. Cakmak, 8/15/89, (PB90-173865, A05, MF-A01).

NCEER-89-0035   "Cyclic Undrained Behavior of Nonplastic and Low Plasticity Silts," by A.J. Walker and H.E. Stewart, 7/26/89, (PB90-183518, A10, MF-A01).

NCEER-89-0036   "Liquefaction Potential of Surficial Deposits in the City of Buffalo, New York," by M. Budhu, R. Giese and L. Baumgrass, 1/17/89, (PB90-208455, A04, MF-A01).

NCEER-89-0037   "A Deterministic Assessment of Effects of Ground Motion Incoherence," by A.S. Veletsos and Y. Tang, 7/15/89, (PB90-164294, A03, MF-A01).

NCEER-89-0038   "Workshop on Ground Motion Parameters for Seismic Hazard Mapping," July 17-18, 1989, edited by R.V. Whitman, 12/1/89, (PB90-173923, A04, MF-A01).

NCEER-89-0039   "Seismic Effects on Elevated Transit Lines of the New York City Transit Authority," by C.J. Costantino, C.A. Miller and E. Heymsfield, 12/26/89, (PB90-207887, A06, MF-A01).

NCEER-89-0040   "Centrifugal Modeling of Dynamic Soil-Structure Interaction," by K. Weissman, Supervised by J.H. Prevost, 5/10/89, (PB90-207879, A07, MF-A01).

NCEER-89-0041   "Linearized Identification of Buildings With Cores for Seismic Vulnerability Assessment," by I-K. Ho and A.E. Aktan, 11/1/89, (PB90-251943, A07, MF-A01).

NCEER-90-0001   "Geotechnical and Lifeline Aspects of the October 17, 1989 Loma Prieta Earthquake in San Francisco," by T.D. O'Rourke, H.E. Stewart, F.T. Blackburn and T.S. Dickerman, 1/90, (PB90-208596, A05, MF-A01).

NCEER-90-0002   "Nonnormal Secondary Response Due to Yielding in a Primary Structure," by D.C.K. Chen and L.D. Lutes, 2/28/90, (PB90-251976, A07, MF-A01).

NCEER-90-0003   "Earthquake Education Materials for Grades K-12," by K.E.K. Ross, 4/16/90, (PB91-251984, A05, MF-A05). This report has been replaced by NCEER-92-0018.

NCEER-90-0004   "Catalog of Strong Motion Stations in Eastern North America," by R.W. Busby, 4/3/90, (PB90-251984, A05, MF-A01).

NCEER-90-0005   "NCEER Strong-Motion Data Base: A User Manual for the GeoBase Release (Version 1.0 for the Sun3)," by P. Friberg and K. Jacob, 3/31/90 (PB90-258062, A04, MF-A01).

NCEER-90-0006   "Seismic Hazard Along a Crude Oil Pipeline in the Event of an 1811-1812 Type New Madrid Earthquake," by H.H.M. Hwang and C-H.S. Chen, 4/16/90, (PB90-258054, A04, MF-A01).

NCEER-90-0007   "Site-Specific Response Spectra for Memphis Sheahan Pumping Station," by H.H.M. Hwang and C.S. Lee, 5/15/90, (PB91-108811, A05, MF-A01).

NCEER-90-0008   "Pilot Study on Seismic Vulnerability of Crude Oil Transmission Systems," by T. Ariman, R. Dobry, M. Grigoriu, F. Kozin, M. O'Rourke, T. O'Rourke and M. Shinozuka, 5/25/90, (PB91-108837, A06, MF-A01).

NCEER-90-0009   "A Program to Generate Site Dependent Time Histories: EQGEN," by G.W. Ellis, M. Srinivasan and A.S. Cakmak, 1/30/90, (PB91-108829, A04, MF-A01).

NCEER-90-0010   "Active Isolation for Seismic Protection of Operating Rooms," by M.E. Talbott, Supervised by M. Shinozuka, 6/8/9, (PB91-110205, A05, MF-A01).

NCEER-90-0011   "Program LINEARID for Identification of Linear Structural Dynamic Systems," by C-B. Yun and M. Shinozuka, 6/25/90, (PB91-110312, A08, MF-A01).

NCEER-90-0012   "Two-Dimensional Two-Phase Elasto-Plastic Seismic Response of Earth Dams," by A.N. Yiagos, Supervised by J.H. Prevost, 6/20/90, (PB91-110197, A13, MF-A02).

NCEER-90-0013   "Secondary Systems in Base-Isolated Structures: Experimental Investigation, Stochastic Response and Stochastic Sensitivity," by G.D. Manolis, G. Juhn, M.C. Constantinou and A.M. Reinhorn, 7/1/90, (PB91-110320, A08, MF-A01).

NCEER-90-0014   "Seismic Behavior of Lightly-Reinforced Concrete Column and Beam-Column Joint Details," by S.P. Pessiki, C.H. Conley, P. Gergely and R.N. White, 8/22/90, (PB91-108795, A11, MF-A02).

NCEER-90-0015   "Two Hybrid Control Systems for Building Structures Under Strong Earthquakes," by J.N. Yang and A. Danielians, 6/29/90, (PB91-125393, A04, MF-A01).

NCEER-90-0016   "Instantaneous Optimal Control with Acceleration and Velocity Feedback," by J.N. Yang and Z. Li, 6/29/90, (PB91-125401, A03, MF-A01).

NCEER-90-0017   "Reconnaissance Report on the Northern Iran Earthquake of June 21, 1990," by M. Mehrain, 10/4/90, (PB91-125377, A03, MF-A01).

NCEER-90-0018   "Evaluation of Liquefaction Potential in Memphis and Shelby County," by T.S. Chang, P.S. Tang, C.S. Lee and H. Hwang, 8/10/90, (PB91-125427, A09, MF-A01).

NCEER-90-0019   "Experimental and Analytical Study of a Combined Sliding Disc Bearing and Helical Steel Spring Isolation System," by M.C. Constantinou, A.S. Mokha and A.M. Reinhorn, 10/4/90, (PB91-125385, A06, MF-A01). This report is available only through NTIS (see address given above).

NCEER-90-0020   "Experimental Study and Analytical Prediction of Earthquake Response of a Sliding Isolation System with a Spherical Surface," by A.S. Mokha, M.C. Constantinou and A.M. Reinhorn, 10/11/90, (PB91-125419, A05, MF-A01).

NCEER-90-0021   "Dynamic Interaction Factors for Floating Pile Groups," by G. Gazetas, K. Fan, A. Kaynia and E. Kausel, 9/10/90, (PB91-170381, A05, MF-A01).

NCEER-90-0022   "Evaluation of Seismic Damage Indices for Reinforced Concrete Structures," by S. Rodriguez-Gomez and A.S. Cakmak, 9/30/90, PB91-171322, A06, MF-A01).

NCEER-90-0023   "Study of Site Response at a Selected Memphis Site," by H. Desai, S. Ahmad, E.S. Gazetas and M.R. Oh, 10/11/90, (PB91-196857, A03, MF-A01).

NCEER-90-0024   "A User's Guide to Strongmo: Version 1.0 of NCEER's Strong-Motion Data Access Tool for PCs and Terminals," by P.A. Friberg and C.A.T. Susch, 11/15/90, (PB91-171272, A03, MF-A01).

NCEER-90-0025   "A Three-Dimensional Analytical Study of Spatial Variability of Seismic Ground Motions," by L-L. Hong and A.H.-S. Ang, 10/30/90, (PB91-170399, A09, MF-A01).

NCEER-90-0026   "MUMOID User's Guide - A Program for the Identification of Modal Parameters," by S. Rodriguez-Gomez and E. DiPasquale, 9/30/90, (PB91-171298, A04, MF-A01).

NCEER-90-0027   "SARCF-II User's Guide - Seismic Analysis of Reinforced Concrete Frames," by S. Rodriguez-Gomez, Y.S. Chung and C. Meyer, 9/30/90, (PB91-171280, A05, MF-A01).

NCEER-90-0028   "Viscous Dampers: Testing, Modeling and Application in Vibration and Seismic Isolation," by N. Makris and M.C. Constantinou, 12/20/90 (PB91-190561, A06, MF-A01).

NCEER-90-0029   "Soil Effects on Earthquake Ground Motions in the Memphis Area," by H. Hwang, C.S. Lee, K.W. Ng and T.S. Chang, 8/2/90, (PB91-190751, A05, MF-A01).

NCEER-91-0001   "Proceedings from the Third Japan-U.S. Workshop on Earthquake Resistant Design of Lifeline Facilities and Countermeasures for Soil Liquefaction, December 17-19, 1990," edited by T.D. O'Rourke and M. Hamada, 2/1/91, (PB91-179259, A99, MF-A04).

NCEER-91-0002   "Physical Space Solutions of Non-Proportionally Damped Systems," by M. Tong, Z. Liang and G.C. Lee, 1/15/91, (PB91-179242, A04, MF-A01).

NCEER-91-0003   "Seismic Response of Single Piles and Pile Groups," by K. Fan and G. Gazetas, 1/10/91, (PB92-174994, A04, MF-A01).

NCEER-91-0004   "Damping of Structures: Part 1 - Theory of Complex Damping," by Z. Liang and G. Lee, 10/10/91, (PB92-197235, A12, MF-A03).

NCEER-91-0005   "3D-BASIS - Nonlinear Dynamic Analysis of Three Dimensional Base Isolated Structures: Part II," by S. Nagarajaiah, A.M. Reinhorn and M.C. Constantinou, 2/28/91, (PB91-190553, A07, MF-A01). This report has been replaced by NCEER-93-0011.

NCEER-91-0006   "A Multidimensional Hysteretic Model for Plasticity Deforming Metals in Energy Absorbing Devices," by E.J. Graesser and F.A. Cozzarelli, 4/9/91, (PB92-108364, A04, MF-A01).

NCEER-91-0007   "A Framework for Customizable Knowledge-Based Expert Systems with an Application to a KBES for Evaluating the Seismic Resistance of Existing Buildings," by E.G. Ibarra-Anaya and S.J. Fenves, 4/9/91, (PB91-210930, A08, MF-A01).

NCEER-91-0008   "Nonlinear Analysis of Steel Frames with Semi-Rigid Connections Using the Capacity Spectrum Method," by G.G. Deierlein, S-H. Hsieh, Y-J. Shen and J.F. Abel, 7/2/91, (PB92-113828, A05, MF-A01).

NCEER-91-0009   "Earthquake Education Materials for Grades K-12," by K.E.K. Ross, 4/30/91, (PB91-212142, A06, MF-A01). This report has been replaced by NCEER-92-0018.

NCEER-91-0010   "Phase Wave Velocities and Displacement Phase Differences in a Harmonically Oscillating Pile," by N. Makris and G. Gazetas, 7/8/91, (PB92-108356, A04, MF-A01).

NCEER-91-0011   "Dynamic Characteristics of a Full-Size Five-Story Steel Structure and a 2/5 Scale Model," by K.C. Chang, G.C. Yao, G.C. Lee, D.S. Hao and Y.C. Yeh," 7/2/91, (PB93-116648, A06, MF-A02).

NCEER-91-0012   "Seismic Response of a 2/5 Scale Steel Structure with Added Viscoelastic Dampers," by K.C. Chang, T.T. Soong, S-T. Oh and M.L. Lai, 5/17/91, (PB92-110816, A05, MF-A01).

NCEER-91-0013   "Earthquake Response of Retaining Walls; Full-Scale Testing and Computational Modeling," by S. Alampalli and A-W.M. Elgamal, 6/20/91, to be published.

NCEER-91-0014   "3D-BASIS-M: Nonlinear Dynamic Analysis of Multiple Building Base Isolated Structures," by P.C. Tsopelas, S. Nagarajaiah, M.C. Constantinou and A.M. Reinhorn, 5/28/91, (PB92-113885, A09, MF-A02).

NCEER-91-0015   "Evaluation of SEAOC Design Requirements for Sliding Isolated Structures," by D. Theodossiou and M.C. Constantinou, 6/10/91, (PB92-114602, A11, MF-A03).

NCEER-91-0016   "Closed-Loop Modal Testing of a 27-Story Reinforced Concrete Flat Plate-Core Building," by H.R. Somaprasad, T. Toksoy, H. Yoshiyuki and A.E. Aktan, 7/15/91, (PB92-129980, A07, MF-A02).

NCEER-91-0017   "Shake Table Test of a 1/6 Scale Two-Story Lightly Reinforced Concrete Building," by A.G. El-Attar, R.N. White and P. Gergely, 2/28/91, (PB92-222447, A06, MF-A02).

NCEER-91-0018   "Shake Table Test of a 1/8 Scale Three-Story Lightly Reinforced Concrete Building," by A.G. El-Attar, R.N. White and P. Gergely, 2/28/91, (PB93-116630, A08, MF-A02).

NCEER-91-0019   "Transfer Functions for Rigid Rectangular Foundations," by A.S. Veletsos, A.M. Prasad and W.H. Wu, 7/31/91, to be published.

NCEER-91-0020   "Hybrid Control of Seismic-Excited Nonlinear and Inelastic Structural Systems," by J.N. Yang, Z. Li and A. Danielians, 8/1/91, (PB92-143171, A06, MF-A02).

NCEER-91-0021   "The NCEER-91 Earthquake Catalog: Improved Intensity-Based Magnitudes and Recurrence Relations for U.S. Earthquakes East of New Madrid," by L. Seeber and J.G. Armbruster, 8/28/91, (PB92-176742, A06, MF-A02).

NCEER-91-0022   "Proceedings from the Implementation of Earthquake Planning and Education in Schools: The Need for Change - The Roles of the Changemakers," by K.E.K. Ross and F. Winslow, 7/23/91, (PB92-129998, A12, MF-A03).

NCEER-91-0023   "A Study of Reliability-Based Criteria for Seismic Design of Reinforced Concrete Frame Buildings," by H.H.M. Hwang and H-M. Hsu, 8/10/91, (PB92-140235, A09, MF-A02).

NCEER-91-0024   "Experimental Verification of a Number of Structural System Identification Algorithms," by R.G. Ghanem, H. Gavin and M. Shinozuka, 9/18/91, (PB92-176577, A18, MF-A04).

NCEER-91-0025   "Probabilistic Evaluation of Liquefaction Potential," by H.H.M. Hwang and C.S. Lee," 11/25/91, (PB92-143429, A05, MF-A01).

NCEER-91-0026   "Instantaneous Optimal Control for Linear, Nonlinear and Hysteretic Structures - Stable Controllers," by J.N. Yang and Z. Li, 11/15/91, (PB92-163807, A04, MF-A01).

NCEER-91-0027   "Experimental and Theoretical Study of a Sliding Isolation System for Bridges," by M.C. Constantinou, A. Kartoum, A.M. Reinhorn and P. Bradford, 11/15/91, (PB92-176973, A10, MF-A03).

NCEER-92-0001   "Case Studies of Liquefaction and Lifeline Performance During Past Earthquakes, Volume 1: Japanese Case Studies," Edited by M. Hamada and T. O'Rourke, 2/17/92, (PB92-197243, A18, MF-A04).

NCEER-92-0002   "Case Studies of Liquefaction and Lifeline Performance During Past Earthquakes, Volume 2: United States Case Studies," Edited by T. O'Rourke and M. Hamada, 2/17/92, (PB92-197250, A20, MF-A04).

NCEER-92-0003   "Issues in Earthquake Education," Edited by K. Ross, 2/3/92, (PB92-222389, A07, MF-A02).

NCEER-92-0004   "Proceedings from the First U.S. - Japan Workshop on Earthquake Protective Systems for Bridges," Edited by I.G. Buckle, 2/4/92, (PB94-142239, A99, MF-A06).

NCEER-92-0005   "Seismic Ground Motion from a Haskell-Type Source in a Multiple-Layered Half-Space," A.P. Theoharis, G. Deodatis and M. Shinozuka, 1/2/92, to be published.

NCEER-92-0006   "Proceedings from the Site Effects Workshop," Edited by R. Whitman, 2/29/92, (PB92-197201, A04, MF-A01).

NCEER-92-0007   "Engineering Evaluation of Permanent Ground Deformations Due to Seismically-Induced Liquefaction," by M.H. Baziar, R. Dobry and A-W.M. Elgamal, 3/24/92, (PB92-222421, A13, MF-A03).

NCEER-92-0008   "A Procedure for the Seismic Evaluation of Buildings in the Central and Eastern United States," by C.D. Poland and J.O. Malley, 4/2/92, (PB92-222439, A20, MF-A04).

NCEER-92-0009   "Experimental and Analytical Study of a Hybrid Isolation System Using Friction Controllable Sliding Bearings," by M.Q. Feng, S. Fujii and M. Shinozuka, 5/15/92, (PB93-150282, A06, MF-A02).

NCEER-92-0010   "Seismic Resistance of Slab-Column Connections in Existing Non-Ductile Flat-Plate Buildings," by A.J. Durrani and Y. Du, 5/18/92, (PB93-116812, A06, MF-A02).

NCEER-92-0011   "The Hysteretic and Dynamic Behavior of Brick Masonry Walls Upgraded by Ferrocement Coatings Under Cyclic Loading and Strong Simulated Ground Motion," by H. Lee and S.P. Prawel, 5/11/92, to be published.

NCEER-92-0012   "Study of Wire Rope Systems for Seismic Protection of Equipment in Buildings," by G.F. Demetriades, M.C. Constantinou and A.M. Reinhorn, 5/20/92, (PB93-116655, A08, MF-A02).

NCEER-92-0013   "Shape Memory Structural Dampers: Material Properties, Design and Seismic Testing," by P.R. Witting and F.A. Cozzarelli, 5/26/92, (PB93-116663, A05, MF-A01).

NCEER-92-0014   "Longitudinal Permanent Ground Deformation Effects on Buried Continuous Pipelines," by M.J. O'Rourke, and C. Nordberg, 6/15/92, (PB93-116671, A08, MF-A02).

NCEER-92-0015   "A Simulation Method for Stationary Gaussian Random Functions Based on the Sampling Theorem," by M. Grigoriu and S. Balopoulou, 6/11/92, (PB93-127496, A05, MF-A01).

NCEER-92-0016   "Gravity-Load-Designed Reinforced Concrete Buildings: Seismic Evaluation of Existing Construction and Detailing Strategies for Improved Seismic Resistance," by G.W. Hoffmann, S.K. Kunnath, A.M. Reinhorn and J.B. Mander, 7/15/92, (PB94-142007, A08, MF-A02).

NCEER-92-0017   "Observations on Water System and Pipeline Performance in the Limón Area of Costa Rica Due to the April 22, 1991 Earthquake," by M. O'Rourke and D. Ballantyne, 6/30/92, (PB93-126811, A06, MF-A02).

NCEER-92-0018   "Fourth Edition of Earthquake Education Materials for Grades K-12," Edited by K.E.K. Ross, 8/10/92, (PB93-114023, A07, MF-A02).

NCEER-92-0019   "Proceedings from the Fourth Japan-U.S. Workshop on Earthquake Resistant Design of Lifeline Facilities and Countermeasures for Soil Liquefaction," Edited by M. Hamada and T.D. O'Rourke, 8/12/92, (PB93-163939, A99, MF-E11).

NCEER-92-0020   "Active Bracing System: A Full Scale Implementation of Active Control," by A.M. Reinhorn, T.T. Soong, R.C. Lin, M.A. Riley, Y.P. Wang, S. Aizawa and M. Higashino, 8/14/92, (PB93-127512, A06, MF-A02).

NCEER-92-0021   "Empirical Analysis of Horizontal Ground Displacement Generated by Liquefaction-Induced Lateral Spreads," by S.F. Bartlett and T.L. Youd, 8/17/92, (PB93-188241, A06, MF-A02).

NCEER-92-0022   "IDARC Version 3.0: Inelastic Damage Analysis of Reinforced Concrete Structures," by S.K. Kunnath, A.M. Reinhorn and R.F. Lobo, 8/31/92, (PB93-227502, A07, MF-A02).

NCEER-92-0023   "A Semi-Empirical Analysis of Strong-Motion Peaks in Terms of Seismic Source, Propagation Path and Local Site Conditions, by M. Kamiyama, M.J. O'Rourke and R. Flores-Berrones, 9/9/92, (PB93-150266, A08, MF-A02).

NCEER-92-0024   "Seismic Behavior of Reinforced Concrete Frame Structures with Nonductile Details, Part I: Summary of Experimental Findings of Full Scale Beam-Column Joint Tests," by A. Beres, R.N. White and P. Gergely, 9/30/92, (PB93-227783, A05, MF-A01).

NCEER-92-0025   "Experimental Results of Repaired and Retrofitted Beam-Column Joint Tests in Lightly Reinforced Concrete Frame Buildings," by A. Beres, S. El-Borgi, R.N. White and P. Gergely, 10/29/92, (PB93-227791, A05, MF-A01).

NCEER-92-0026   "A Generalization of Optimal Control Theory: Linear and Nonlinear Structures," by J.N. Yang, Z. Li and S. Vongchavalitkul, 11/2/92, (PB93-188621, A05, MF-A01).

NCEER-92-0027   "Seismic Resistance of Reinforced Concrete Frame Structures Designed Only for Gravity Loads: Part I - Design and Properties of a One-Third Scale Model Structure," by J.M. Bracci, A.M. Reinhorn and J.B. Mander, 12/1/92, (PB94-104502, A08, MF-A02).

NCEER-92-0028   "Seismic Resistance of Reinforced Concrete Frame Structures Designed Only for Gravity Loads: Part II - Experimental Performance of Subassemblages," by L.E. Aycardi, J.B. Mander and A.M. Reinhorn, 12/1/92, (PB94-104510, A08, MF-A02).

NCEER-92-0029   "Seismic Resistance of Reinforced Concrete Frame Structures Designed Only for Gravity Loads: Part III - Experimental Performance and Analytical Study of a Structural Model," by J.M. Bracci, A.M. Reinhorn and J.B. Mander, 12/1/92, (PB93-227528, A09, MF-A01).

NCEER-92-0030   "Evaluation of Seismic Retrofit of Reinforced Concrete Frame Structures: Part I - Experimental Performance of Retrofitted Subassemblages," by D. Choudhuri, J.B. Mander and A.M. Reinhorn, 12/8/92, (PB93-198307, A07, MF-A02).

NCEER-92-0031   "Evaluation of Seismic Retrofit of Reinforced Concrete Frame Structures: Part II - Experimental Performance and Analytical Study of a Retrofitted Structural Model," by J.M. Bracci, A.M. Reinhorn and J.B. Mander, 12/8/92, (PB93-198315, A09, MF-A03).

NCEER-92-0032   "Experimental and Analytical Investigation of Seismic Response of Structures with Supplemental Fluid Viscous Dampers," by M.C. Constantinou and M.D. Symans, 12/21/92, (PB93-191435, A10, MF-A03). This report is available only through NTIS (see address given above).

NCEER-92-0033   "Reconnaissance Report on the Cairo, Egypt Earthquake of October 12, 1992," by M. Khater, 12/23/92, (PB93-188621, A03, MF-A01).

NCEER-92-0034   "Low-Level Dynamic Characteristics of Four Tall Flat-Plate Buildings in New York City," by H. Gavin, S. Yuan, J. Grossman, E. Pekelis and K. Jacob, 12/28/92, (PB93-188217, A07, MF-A02).

NCEER-93-0001   "An Experimental Study on the Seismic Performance of Brick-Infilled Steel Frames With and Without Retrofit," by J.B. Mander, B. Nair, K. Wojtkowski and J. Ma, 1/29/93, (PB93-227510, A07, MF-A02).

NCEER-93-0002   "Social Accounting for Disaster Preparedness and Recovery Planning," by S. Cole, E. Pantoja and V. Razak, 2/22/93, (PB94-142114, A12, MF-A03).

NCEER-93-0003   "Assessment of 1991 NEHRP Provisions for Nonstructural Components and Recommended Revisions," by T.T. Soong, G. Chen, Z. Wu, R-H. Zhang and M. Grigoriu, 3/1/93, (PB93-188639, A06, MF-A02).

NCEER-93-0004   "Evaluation of Static and Response Spectrum Analysis Procedures of SEAOC/UBC for Seismic Isolated Structures," by C.W. Winters and M.C. Constantinou, 3/23/93, (PB93-198299, A10, MF-A03).

NCEER-93-0005   "Earthquakes in the Northeast - Are We Ignoring the Hazard? A Workshop on Earthquake Science and Safety for Educators," edited by K.E.K. Ross, 4/2/93, (PB94-103066, A09, MF-A02).

NCEER-93-0006   "Inelastic Response of Reinforced Concrete Structures with Viscoelastic Braces," by R.F. Lobo, J.M. Bracci, K.L. Shen, A.M. Reinhorn and T.T. Soong, 4/5/93, (PB93-227486, A05, MF-A02).

NCEER-93-0007   "Seismic Testing of Installation Methods for Computers and Data Processing Equipment," by K. Kosar, T.T. Soong, K.L. Shen, J.A. HoLung and Y.K. Lin, 4/12/93, (PB93-198299, A07, MF-A02).

NCEER-93-0008   "Retrofit of Reinforced Concrete Frames Using Added Dampers," by A. Reinhorn, M. Constantinou and C. Li, to be published.

NCEER-93-0009   "Seismic Behavior and Design Guidelines for Steel Frame Structures with Added Viscoelastic Dampers," by K.C. Chang, M.L. Lai, T.T. Soong, D.S. Hao and Y.C. Yeh, 5/1/93, (PB94-141959, A07, MF-A02).

NCEER-93-0010   "Seismic Performance of Shear-Critical Reinforced Concrete Bridge Piers," by J.B. Mander, S.M. Waheed, M.T.A. Chaudhary and S.S. Chen, 5/12/93, (PB93-227494, A08, MF-A02).

NCEER-93-0011   "3D-BASIS-TABS: Computer Program for Nonlinear Dynamic Analysis of Three Dimensional Base Isolated Structures," by S. Nagarajaiah, C. Li, A.M. Reinhorn and M.C. Constantinou, 8/2/93, (PB94-141819, A09, MF-A02).

NCEER-93-0012   "Effects of Hydrocarbon Spills from an Oil Pipeline Break on Ground Water," by O.J. Helweg and H.H.M. Hwang, 8/3/93, (PB94-141942, A06, MF-A02).

NCEER-93-0013   "Simplified Procedures for Seismic Design of Nonstructural Components and Assessment of Current Code Provisions," by M.P. Singh, L.E. Suarez, E.E. Matheu and G.O. Maldonado, 8/4/93, (PB94-141827, A09, MF-A02).

NCEER-93-0014   "An Energy Approach to Seismic Analysis and Design of Secondary Systems," by G. Chen and T.T. Soong, 8/6/93, (PB94-142767, A11, MF-A03).

NCEER-93-0015   "Proceedings from School Sites: Becoming Prepared for Earthquakes - Commemorating the Third Anniversary of the Loma Prieta Earthquake," Edited by F.E. Winslow and K.E.K. Ross, 8/16/93, (PB94-154275, A16, MF-A02).

NCEER-93-0016   "Reconnaissance Report of Damage to Historic Monuments in Cairo, Egypt Following the October 12, 1992 Dahshur Earthquake," by D. Sykora, D. Look, G. Croci, E. Karaesmen and E. Karaesmen, 8/19/93, (PB94-142221, A08, MF-A02).

NCEER-93-0017   "The Island of Guam Earthquake of August 8, 1993," by S.W. Swan and S.K. Harris, 9/30/93, (PB94-141843, A04, MF-A01).

NCEER-93-0018   "Engineering Aspects of the October 12, 1992 Egyptian Earthquake," by A.W. Elgamal, M. Amer, K. Adalier and A. Abul-Fadl, 10/7/93, (PB94-141983, A05, MF-A01).

NCEER-93-0019   "Development of an Earthquake Motion Simulator and its Application in Dynamic Centrifuge Testing," by I. Krstelj, Supervised by J.H. Prevost, 10/23/93, (PB94-181773, A-10, MF-A03).

NCEER-93-0020   "NCEER-Taisei Corporation Research Program on Sliding Seismic Isolation Systems for Bridges: Experimental and Analytical Study of a Friction Pendulum System (FPS)," by M.C. Constantinou, P. Tsopelas, Y-S. Kim and S. Okamoto, 11/1/93, (PB94-142775, A08, MF-A02).

NCEER-93-0021   "Finite Element Modeling of Elastomeric Seismic Isolation Bearings," by L.J. Billings, Supervised by R. Shepherd, 11/8/93, to be published.

NCEER-93-0022   "Seismic Vulnerability of Equipment in Critical Facilities: Life-Safety and Operational Consequences," by K. Porter, G.S. Johnson, M.M. Zadeh, C. Scawthorn and S. Eder, 11/24/93, (PB94-181765, A16, MF-A03).

NCEER-93-0023   "Hokkaido Nansei-oki, Japan Earthquake of July 12, 1993, by P.I. Yanev and C.R. Scawthorn, 12/23/93, (PB94-181500, A07, MF-A01).

NCEER-94-0001   "An Evaluation of Seismic Serviceability of Water Supply Networks with Application to the San Francisco Auxiliary Water Supply System," by I. Markov, Supervised by M. Grigoriu and T. O'Rourke, 1/21/94, (PB94-204013, A07, MF-A02).

NCEER-94-0002   "NCEER-Taisei Corporation Research Program on Sliding Seismic Isolation Systems for Bridges: Experimental and Analytical Study of Systems Consisting of Sliding Bearings, Rubber Restoring Force Devices and Fluid Dampers," Volumes I and II, by P. Tsopelas, S. Okamoto, M.C. Constantinou, D. Ozaki and S. Fujii, 2/4/94, (PB94-181740, A09, MF-A02 and PB94-181757, A12, MF-A03).

NCEER-94-0003   "A Markov Model for Local and Global Damage Indices in Seismic Analysis," by S. Rahman and M. Grigoriu, 2/18/94, (PB94-206000, A12, MF-A03).

NCEER-94-0004   "Proceedings from the NCEER Workshop on Seismic Response of Masonry Infills," edited by D.P. Abrams, 3/1/94, (PB94-180783, A07, MF-A02).

NCEER-94-0005   "The Northridge, California Earthquake of January 17, 1994: General Reconnaissance Report," edited by J.D. Goltz, 3/11/94, (PB94-193943, A10, MF-A03).

NCEER-94-0006   "Seismic Energy Based Fatigue Damage Analysis of Bridge Columns: Part I - Evaluation of Seismic Capacity," by G.A. Chang and J.B. Mander, 3/14/94, (PB94-219185, A11, MF-A03).

NCEER-94-0007   "Seismic Isolation of Multi-Story Frame Structures Using Spherical Sliding Isolation Systems," by T.M. Al-Hussaini, V.A. Zayas and M.C. Constantinou, 3/17/94, (PB94-193745, A09, MF-A02).

NCEER-94-0008   "The Northridge, California Earthquake of January 17, 1994: Performance of Highway Bridges," edited by I.G. Buckle, 3/24/94, (PB94-193851, A06, MF-A02).

NCEER-94-0009   "Proceedings of the Third U.S.-Japan Workshop on Earthquake Protective Systems for Bridges," edited by I.G. Buckle and I. Friedland, 3/31/94, (PB94-195815, A99, MF-A06).

NCEER-94-0010   "3D-BASIS-ME: Computer Program for Nonlinear Dynamic Analysis of Seismically Isolated Single and Multiple Structures and Liquid Storage Tanks," by P.C. Tsopelas, M.C. Constantinou and A.M. Reinhorn, 4/12/94, (PB94-204922, A09, MF-A02).

NCEER-94-0011   "The Northridge, California Earthquake of January 17, 1994: Performance of Gas Transmission Pipelines," by T.D. O'Rourke and M.C. Palmer, 5/16/94, (PB94-204989, A05, MF-A01).

NCEER-94-0012   "Feasibility Study of Replacement Procedures and Earthquake Performance Related to Gas Transmission Pipelines," by T.D. O'Rourke and M.C. Palmer, 5/25/94, (PB94-206638, A09, MF-A02).

NCEER-94-0013   "Seismic Energy Based Fatigue Damage Analysis of Bridge Columns: Part II - Evaluation of Seismic Demand," by G.A. Chang and J.B. Mander, 6/1/94, (PB95-18106, A08, MF-A02).

NCEER-94-0014   "NCEER-Taisei Corporation Research Program on Sliding Seismic Isolation Systems for Bridges: Experimental and Analytical Study of a System Consisting of Sliding Bearings and Fluid Restoring Force/Damping Devices," by P. Tsopelas and M.C. Constantinou, 6/13/94, (PB94-219144, A10, MF-A03).

NCEER-94-0015   "Generation of Hazard-Consistent Fragility Curves for Seismic Loss Estimation Studies," by H. Hwang and J-R. Huo, 6/14/94, (PB95-181996, A09, MF-A02).

NCEER-94-0016   "Seismic Study of Building Frames with Added Energy-Absorbing Devices," by W.S. Pong, C.S. Tsai and G.C. Lee, 6/20/94, (PB94-219136, A10, A03).

NCEER-94-0017   "Sliding Mode Control for Seismic-Excited Linear and Nonlinear Civil Engineering Structures," by J. Yang, J. Wu, A. Agrawal and Z. Li, 6/21/94, (PB95-138483, A06, MF-A02).

NCEER-94-0018   "3D-BASIS-TABS Version 2.0: Computer Program for Nonlinear Dynamic Analysis of Three Dimensional Base Isolated Structures," by A.M. Reinhorn, S. Nagarajaiah, M.C. Constantinou, P. Tsopelas and R. Li, 6/22/94, (PB95-182176, A08, MF-A02).

NCEER-94-0019   "Proceedings of the International Workshop on Civil Infrastructure Systems: Application of Intelligent Systems and Advanced Materials on Bridge Systems," Edited by G.C. Lee and K.C. Chang, 7/18/94, (PB95-252474, A20, MF-A04).

NCEER-94-0020   "Study of Seismic Isolation Systems for Computer Floors," by V. Lambrou and M.C. Constantinou, 7/19/94, (PB95-138533, A10, MF-A03).

NCEER-94-0021   "Proceedings of the U.S.-Italian Workshop on Guidelines for Seismic Evaluation and Rehabilitation of Unreinforced Masonry Buildings," Edited by D.P. Abrams and G.M. Calvi, 7/20/94, (PB95-138749, A13, MF-A03).

NCEER-94-0022   "NCEER-Taisei Corporation Research Program on Sliding Seismic Isolation Systems for Bridges: Experimental and Analytical Study of a System Consisting of Lubricated PTFE Sliding Bearings and Mild Steel Dampers," by P. Tsopelas and M.C. Constantinou, 7/22/94, (PB95-182184, A08, MF-A02).

NCEER-94-0023   "Development of Reliability-Based Design Criteria for Buildings Under Seismic Load," by Y.K. Wen, H. Hwang and M. Shinozuka, 8/1/94, (PB95-211934, A08, MF-A02).

NCEER-94-0024   "Experimental Verification of Acceleration Feedback Control Strategies for an Active Tendon System," by S.J. Dyke, B.F. Spencer, Jr., P. Quast, M.K. Sain, D.C. Kaspari, Jr. and T.T. Soong, 8/29/94, (PB95-212320, A05, MF-A01).

NCEER-94-0025   "Seismic Retrofitting Manual for Highway Bridges," Edited by I.G. Buckle and I.F. Friedland, published by the Federal Highway Administration (PB95-212676, A15, MF-A03).

NCEER-94-0026   "Proceedings from the Fifth U.S.-Japan Workshop on Earthquake Resistant Design of Lifeline Facilities and Countermeasures Against Soil Liquefaction," Edited by T.D. O'Rourke and M. Hamada, 11/7/94, (PB95-220802, A99, MF-E08).

NCEER-95-0001   "Experimental and Analytical Investigation of Seismic Retrofit of Structures with Supplemental Damping: Part 1 - Fluid Viscous Damping Devices," by A.M. Reinhorn, C. Li and M.C. Constantinou, 1/3/95, (PB95-266599, A09, MF-A02).

NCEER-95-0002   "Experimental and Analytical Study of Low-Cycle Fatigue Behavior of Semi-Rigid Top-And-Seat Angle Connections," by G. Pekcan, J.B. Mander and S.S. Chen, 1/5/95, (PB95-220042, A07, MF-A02).

NCEER-95-0003   "NCEER-ATC Joint Study on Fragility of Buildings," by T. Anagnos, C. Rojahn and A.S. Kiremidjian, 1/20/95, (PB95-220026, A06, MF-A02).

NCEER-95-0004   "Nonlinear Control Algorithms for Peak Response Reduction," by Z. Wu, T.T. Soong, V. Gattulli and R.C. Lin, 2/16/95, (PB95-220349, A05, MF-A01).

NCEER-95-0005   "Pipeline Replacement Feasibility Study: A Methodology for Minimizing Seismic and Corrosion Risks to Underground Natural Gas Pipelines," by R.T. Eguchi, H.A. Seligson and D.G. Honegger, 3/2/95, (PB95-252326, A06, MF-A02).

NCEER-95-0006   "Evaluation of Seismic Performance of an 11-Story Frame Building During the 1994 Northridge Earthquake," by F. Naeim, R. DiSulio, K. Benuska, A. Reinhorn and C. Li, to be published.

NCEER-95-0007   "Prioritization of Bridges for Seismic Retrofitting," by N. Basöz and A.S. Kiremidjian, 4/24/95, (PB95-252300, A08, MF-A02).

NCEER-95-0008   "Method for Developing Motion Damage Relationships for Reinforced Concrete Frames," by A. Singhal and A.S. Kiremidjian, 5/11/95, (PB95-266607, A06, MF-A02).

NCEER-95-0009   "Experimental and Analytical Investigation of Seismic Retrofit of Structures with Supplemental Damping: Part II - Friction Devices," by C. Li and A.M. Reinhorn, 7/6/95, (PB96-128087, A11, MF-A03).

NCEER-95-0010   "Experimental Performance and Analytical Study of a Non-Ductile Reinforced Concrete Frame Structure Retrofitted with Elastomeric Spring Dampers," by G. Pekcan, J.B. Mander and S.S. Chen, 7/14/95, (PB96-137161, A08, MF-A02).

NCEER-95-0011   "Development and Experimental Study of Semi-Active Fluid Damping Devices for Seismic Protection of Structures," by M.D. Symans and M.C. Constantinou, 8/3/95, (PB96-136940, A23, MF-A04).

NCEER-95-0012   "Real-Time Structural Parameter Modification (RSPM): Development of Innervated Structures," by Z. Liang, M. Tong and G.C. Lee, 4/11/95, (PB96-137153, A06, MF-A01).

NCEER-95-0013   "Experimental and Analytical Investigation of Seismic Retrofit of Structures with Supplemental Damping: Part III - Viscous Damping Walls," by A.M. Reinhorn and C. Li, 10/1/95, (PB96-176409, A11, MF-A03).

NCEER-95-0014   "Seismic Fragility Analysis of Equipment and Structures in a Memphis Electric Substation," by J-R. Huo and H.H.M. Hwang, 8/10/95, (PB96-128087, A09, MF-A02).

NCEER-95-0015   "The Hanshin-Awaji Earthquake of January 17, 1995: Performance of Lifelines," Edited by M. Shinozuka, 11/3/95, (PB96-176383, A15, MF-A03).

NCEER-95-0016   "Highway Culvert Performance During Earthquakes," by T.L. Youd and C.J. Beckman, available as NCEER-96-0015.

NCEER-95-0017   "The Hanshin-Awaji Earthquake of January 17, 1995: Performance of Highway Bridges," Edited by I.G. Buckle, 12/1/95, to be published.

NCEER-95-0018   "Modeling of Masonry Infill Panels for Structural Analysis," by A.M. Reinhorn, A. Madan, R.E. Valles, Y. Reichmann and J.B. Mander, 12/8/95, (PB97-110886, MF-A01, A06).

NCEER-95-0019   "Optimal Polynomial Control for Linear and Nonlinear Structures," by A.K. Agrawal and J.N. Yang, 12/11/95, (PB96-168737, A07, MF-A02).

NCEER-95-0020 "Retrofit of Non-Ductile Reinforced Concrete Frames Using Friction Dampers," by R.S. Rao, P. Gergely and R.N. White, 12/22/95, (PB97-133508, A10, MF-A02).

NCEER-95-0021 "Parametric Results for Seismic Response of Pile-Supported Bridge Bents," by G. Mylonakis, A. Nikolaou and G. Gazetas, 12/22/95, (PB97-100242, A12, MF-A03).

NCEER-95-0022 "Kinematic Bending Moments in Seismically Stressed Piles," by A. Nikolaou, G. Mylonakis and G. Gazetas, 12/23/95, (PB97-113914, MF-A03, A13).

NCEER-96-0001 "Dynamic Response of Unreinforced Masonry Buildings with Flexible Diaphragms," by A.C. Costley and D.P. Abrams," 10/10/96, (PB97-133573, MF-A03, A15).

NCEER-96-0002 "State of the Art Review: Foundations and Retaining Structures," by I. Po Lam, to be published.

NCEER-96-0003 "Ductility of Rectangular Reinforced Concrete Bridge Columns with Moderate Confinement," by N. Wehbe, M. Saiidi, D. Sanders and B. Douglas, 11/7/96, (PB97-133557, A06, MF-A02).

NCEER-96-0004 "Proceedings of the Long-Span Bridge Seismic Research Workshop," edited by I.G. Buckle and I.M. Friedland, to be published.

NCEER-96-0005 "Establish Representative Pier Types for Comprehensive Study: Eastern United States," by J. Kulicki and Z. Prucz, 5/28/96, (PB98-119217, A07, MF-A02).

NCEER-96-0006 "Establish Representative Pier Types for Comprehensive Study: Western United States," by R. Imbsen, R.A. Schamber and T.A. Osterkamp, 5/28/96, (PB98-118607, A07, MF-A02).

NCEER-96-0007 "Nonlinear Control Techniques for Dynamical Systems with Uncertain Parameters," by R.G. Ghanem and M.I. Bujakov, 5/27/96, (PB97-100259, A17, MF-A03).

NCEER-96-0008 "Seismic Evaluation of a 30-Year Old Non-Ductile Highway Bridge Pier and Its Retrofit," by J.B. Mander, B. Mahmoodzadegan, S. Bhadra and S.S. Chen, 5/31/96, (PB97-110902, MF-A03, A10).

NCEER-96-0009 "Seismic Performance of a Model Reinforced Concrete Bridge Pier Before and After Retrofit," by J.B. Mander, J.H. Kim and C.A. Ligozio, 5/31/96, (PB97-110910, MF-A02, A10).

NCEER-96-0010 "IDARC2D Version 4.0: A Computer Program for the Inelastic Damage Analysis of Buildings," by R.E. Valles, A.M. Reinhorn, S.K. Kunnath, C. Li and A. Madan, 6/3/96, (PB97-100234, A17, MF-A03).

NCEER-96-0011 "Estimation of the Economic Impact of Multiple Lifeline Disruption: Memphis Light, Gas and Water Division Case Study," by S.E. Chang, H.A. Seligson and R.T. Eguchi, 8/16/96, (PB97-133490, A11, MF-A03).

NCEER-96-0012 "Proceedings from the Sixth Japan-U.S. Workshop on Earthquake Resistant Design of Lifeline Facilities and Countermeasures Against Soil Liquefaction, Edited by M. Hamada and T. O'Rourke, 9/11/96, (PB97-133581, A99, MF-A06).

NCEER-96-0013 "Chemical Hazards, Mitigation and Preparedness in Areas of High Seismic Risk: A Methodology for Estimating the Risk of Post-Earthquake Hazardous Materials Release," by H.A. Seligson, R.T. Eguchi, K.J. Tierney and K. Richmond, 11/7/96, (PB97-133565, MF-A02, A08).

NCEER-96-0014 "Response of Steel Bridge Bearings to Reversed Cyclic Loading," by J.B. Mander, D-K. Kim, S.S. Chen and G.J. Premus, 11/13/96, (PB97-140735, A12, MF-A03).

NCEER-96-0015 "Highway Culvert Performance During Past Earthquakes," by T.L. Youd and C.J. Beckman, 11/25/96, (PB97-133532, A06, MF-A01).

NCEER-97-0001 "Evaluation, Prevention and Mitigation of Pounding Effects in Building Structures," by R.E. Valles and A.M. Reinhorn, 2/20/97, (PB97-159552, A14, MF-A03).

NCEER-97-0002 "Seismic Design Criteria for Bridges and Other Highway Structures," by C. Rojahn, R. Mayes, D.G. Anderson, J. Clark, J.H. Hom, R.V. Nutt and M.J. O'Rourke, 4/30/97, (PB97-194658, A06, MF-A03).

NCEER-97-0003   "Proceedings of the U.S.-Italian Workshop on Seismic Evaluation and Retrofit," Edited by D.P. Abrams and G.M. Calvi, 3/19/97, (PB97-194666, A13, MF-A03).

NCEER-97-0004   "Investigation of Seismic Response of Buildings with Linear and Nonlinear Fluid Viscous Dampers," by A.A. Seleemah and M.C. Constantinou, 5/21/97, (PB98-109002, A15, MF-A03).

NCEER-97-0005   "Proceedings of the Workshop on Earthquake Engineering Frontiers in Transportation Facilities," edited by G.C. Lee and I.M. Friedland, 8/29/97, (PB98-128911, A25, MR-A04).

NCEER-97-0006   "Cumulative Seismic Damage of Reinforced Concrete Bridge Piers," by S.K. Kunnath, A. El-Bahy, A. Taylor and W. Stone, 9/2/97, (PB98-108814, A11, MF-A03).

NCEER-97-0007   "Structural Details to Accommodate Seismic Movements of Highway Bridges and Retaining Walls," by R.A. Imbsen, R.A. Schamber, E. Thorkildsen, A. Kartoum, B.T. Martin, T.N. Rosser and J.M. Kulicki, 9/3/97, (PB98-108996, A09, MF-A02).

NCEER-97-0008   "A Method for Earthquake Motion-Damage Relationships with Application to Reinforced Concrete Frames," by A. Singhal and A.S. Kiremidjian, 9/10/97, (PB98-108988, A13, MF-A03).

NCEER-97-0009   "Seismic Analysis and Design of Bridge Abutments Considering Sliding and Rotation," by K. Fishman and R. Richards, Jr., 9/15/97, (PB98-108897, A06, MF-A02).

NCEER-97-0010   "Proceedings of the FHWA/NCEER Workshop on the National Representation of Seismic Ground Motion for New and Existing Highway Facilities," edited by I.M. Friedland, M.S. Power and R.L. Mayes, 9/22/97, (PB98-128903, A21, MF-A04).

NCEER-97-0011   "Seismic Analysis for Design or Retrofit of Gravity Bridge Abutments," by K.L. Fishman, R. Richards, Jr. and R.C. Divito, 10/2/97, (PB98-128937, A08, MF-A02).

NCEER-97-0012   "Evaluation of Simplified Methods of Analysis for Yielding Structures," by P. Tsopelas, M.C. Constantinou, C.A. Kircher and A.S. Whittaker, 10/31/97, (PB98-128929, A10, MF-A03).

NCEER-97-0013   "Seismic Design of Bridge Columns Based on Control and Repairability of Damage," by C-T. Cheng and J.B. Mander, 12/8/97, (PB98-144249, A11, MF-A03).

NCEER-97-0014   "Seismic Resistance of Bridge Piers Based on Damage Avoidance Design," by J.B. Mander and C-T. Cheng, 12/10/97, (PB98-144223, A09, MF-A02).

NCEER-97-0015   "Seismic Response of Nominally Symmetric Systems with Strength Uncertainty," by S. Balopoulou and M. Grigoriu, 12/23/97, (PB98-153422, A11, MF-A03).

NCEER-97-0016   "Evaluation of Seismic Retrofit Methods for Reinforced Concrete Bridge Columns," by T.J. Wipf, F.W. Klaiber and F.M. Russo, 12/28/97, (PB98-144215, A12, MF-A03).

NCEER-97-0017   "Seismic Fragility of Existing Conventional Reinforced Concrete Highway Bridges," by C.L. Mullen and A.S. Cakmak, 12/30/97, (PB98-153406, A08, MF-A02).

NCEER-97-0018   "Loss Asssessment of Memphis Buildings," edited by D.P. Abrams and M. Shinozuka, 12/31/97, (PB98-144231, A13, MF-A03).

NCEER-97-0019   "Seismic Evaluation of Frames with Infill Walls Using Quasi-static Experiments," by K.M. Mosalam, R.N. White and P. Gergely, 12/31/97, (PB98-153455, A07, MF-A02).

NCEER-97-0020   "Seismic Evaluation of Frames with Infill Walls Using Pseudo-dynamic Experiments," by K.M. Mosalam, R.N. White and P. Gergely, 12/31/97, (PB98-153430, A07, MF-A02).

NCEER-97-0021   "Computational Strategies for Frames with Infill Walls: Discrete and Smeared Crack Analyses and Seismic Fragility," by K.M. Mosalam, R.N. White and P. Gergely, 12/31/97, (PB98-153414, A10, MF-A02).

NCEER-97-0022 "Proceedings of the NCEER Workshop on Evaluation of Liquefaction Resistance of Soils," edited by T.L. Youd and I.M. Idriss, 12/31/97, (PB98-155617, A15, MF-A03).

MCEER-98-0001 "Extraction of Nonlinear Hysteretic Properties of Seismically Isolated Bridges from Quick-Release Field Tests," by Q. Chen, B.M. Douglas, E.M. Maragakis and I.G. Buckle, 5/26/98, (PB99-118838, A06, MF-A01).

MCEER-98-0002 "Methodologies for Evaluating the Importance of Highway Bridges," by A. Thomas, S. Eshenaur and J. Kulicki, 5/29/98, (PB99-118846, A10, MF-A02).

MCEER-98-0003 "Capacity Design of Bridge Piers and the Analysis of Overstrength," by J.B. Mander, A. Dutta and P. Goel, 6/1/98, (PB99-118853, A09, MF-A02).

MCEER-98-0004 "Evaluation of Bridge Damage Data from the Loma Prieta and Northridge, California Earthquakes," by N. Basoz and A. Kiremidjian, 6/2/98, (PB99-118861, A15, MF-A03).

MCEER-98-0005 "Screening Guide for Rapid Assessment of Liquefaction Hazard at Highway Bridge Sites," by T. L. Youd, 6/16/98, (PB99-118879, A06, not available on microfiche).

MCEER-98-0006 "Structural Steel and Steel/Concrete Interface Details for Bridges," by P. Ritchie, N. Kauhl and J. Kulicki, 7/13/98, (PB99-118945, A06, MF-A01).

MCEER-98-0007 "Capacity Design and Fatigue Analysis of Confined Concrete Columns," by A. Dutta and J.B. Mander, 7/14/98, (PB99-118960, A14, MF-A03).

MCEER-98-0008 "Proceedings of the Workshop on Performance Criteria for Telecommunication Services Under Earthquake Conditions," edited by A.J. Schiff, 7/15/98, (PB99-118952, A08, MF-A02).

MCEER-98-0009 "Fatigue Analysis of Unconfined Concrete Columns," by J.B. Mander, A. Dutta and J.H. Kim, 9/12/98, (PB99-123655, A10, MF-A02).

MCEER-98-0010 "Centrifuge Modeling of Cyclic Lateral Response of Pile-Cap Systems and Seat-Type Abutments in Dry Sands," by A.D. Gadre and R. Dobry, 10/2/98, (PB99-123606, A13, MF-A03).

MCEER-98-0011 "IDARC-BRIDGE: A Computational Platform for Seismic Damage Assessment of Bridge Structures," by A.M. Reinhorn, V. Simeonov, G. Mylonakis and Y. Reichman, 10/2/98, (PB99-162919, A15, MF-A03).

MCEER-98-0012 "Experimental Investigation of the Dynamic Response of Two Bridges Before and After Retrofitting with Elastomeric Bearings," by D.A. Wendichansky, S.S. Chen and J.B. Mander, 10/2/98, (PB99-162927, A15, MF-A03).

MCEER-98-0013 "Design Procedures for Hinge Restrainers and Hinge Sear Width for Multiple-Frame Bridges," by R. Des Roches and G.L. Fenves, 11/3/98, (PB99-140477, A13, MF-A03).

MCEER-98-0014 "Response Modification Factors for Seismically Isolated Bridges," by M.C. Constantinou and J.K. Quarshie, 11/3/98, (PB99-140485, A14, MF-A03).

MCEER-98-0015 "Proceedings of the U.S.-Italy Workshop on Seismic Protective Systems for Bridges," edited by I.M. Friedland and M.C. Constantinou, 11/3/98, (PB2000-101711, A22, MF-A04).

MCEER-98-0016 "Appropriate Seismic Reliability for Critical Equipment Systems: Recommendations Based on Regional Analysis of Financial and Life Loss," by K. Porter, C. Scawthorn, C. Taylor and N. Blais, 11/10/98, (PB99-157265, A08, MF-A02).

MCEER-98-0017 "Proceedings of the U.S. Japan Joint Seminar on Civil Infrastructure Systems Research," edited by M. Shinozuka and A. Rose, 11/12/98, (PB99-156713, A16, MF-A03).

MCEER-98-0018 "Modeling of Pile Footings and Drilled Shafts for Seismic Design," by I. PoLam, M. Kapuskar and D. Chaudhuri, 12/21/98, (PB99-157257, A09, MF-A02).

MCEER-99-0001   "Seismic Evaluation of a Masonry Infilled Reinforced Concrete Frame by Pseudodynamic Testing," by S.G. Buonopane and R.N. White, 2/16/99, (PB99-162851, A09, MF-A02).

MCEER-99-0002   "Response History Analysis of Structures with Seismic Isolation and Energy Dissipation Systems: Verification Examples for Program SAP2000," by J. Scheller and M.C. Constantinou, 2/22/99, (PB99-162869, A08, MF-A02).

MCEER-99-0003   "Experimental Study on the Seismic Design and Retrofit of Bridge Columns Including Axial Load Effects," by A. Dutta, T. Kokorina and J.B. Mander, 2/22/99, (PB99-162877, A09, MF-A02).

MCEER-99-0004   "Experimental Study of Bridge Elastomeric and Other Isolation and Energy Dissipation Systems with Emphasis on Uplift Prevention and High Velocity Near-source Seismic Excitation," by A. Kasalanati and M. C. Constantinou, 2/26/99, (PB99-162885, A12, MF-A03).

MCEER-99-0005   "Truss Modeling of Reinforced Concrete Shear-flexure Behavior," by J.H. Kim and J.B. Mander, 3/8/99, (PB99-163693, A12, MF-A03).

MCEER-99-0006   "Experimental Investigation and Computational Modeling of Seismic Response of a 1:4 Scale Model Steel Structure with a Load Balancing Supplemental Damping System," by G. Pekcan, J.B. Mander and S.S. Chen, 4/2/99, (PB99-162893, A11, MF-A03).

MCEER-99-0007   "Effect of Vertical Ground Motions on the Structural Response of Highway Bridges," by M.R. Button, C.J. Cronin and R.L. Mayes, 4/10/99, (PB2000-101411, A10, MF-A03).

MCEER-99-0008   "Seismic Reliability Assessment of Critical Facilities: A Handbook, Supporting Documentation, and Model Code Provisions," by G.S. Johnson, R.E. Sheppard, M.D. Quilici, S.J. Eder and C.R. Scawthorn, 4/12/99, (PB2000-101701, A18, MF-A04).

MCEER-99-0009   "Impact Assessment of Selected MCEER Highway Project Research on the Seismic Design of Highway Structures," by C. Rojahn, R. Mayes, D.G. Anderson, J.H. Clark, D'Appolonia Engineering, S. Gloyd and R.V. Nutt, 4/14/99, (PB99-162901, A10, MF-A02).

MCEER-99-0010   "Site Factors and Site Categories in Seismic Codes," by R. Dobry, R. Ramos and M.S. Power, 7/19/99, (PB2000-101705, A08, MF-A02).

MCEER-99-0011   "Restrainer Design Procedures for Multi-Span Simply-Supported Bridges," by M.J. Randall, M. Saiidi, E. Maragakis and T. Isakovic, 7/20/99, (PB2000-101702, A10, MF-A02).

MCEER-99-0012   "Property Modification Factors for Seismic Isolation Bearings," by M.C. Constantinou, P. Tsopelas, A. Kasalanati and E. Wolff, 7/20/99, (PB2000-103387, A11, MF-A03).

MCEER-99-0013   "Critical Seismic Issues for Existing Steel Bridges," by P. Ritchie, N. Kauhl and J. Kulicki, 7/20/99, (PB2000-101697, A09, MF-A02).

MCEER-99-0014   "Nonstructural Damage Database," by A. Kao, T.T. Soong and A. Vender, 7/24/99, (PB2000-101407, A06, MF-A01).

MCEER-99-0015   "Guide to Remedial Measures for Liquefaction Mitigation at Existing Highway Bridge Sites," by H.G. Cooke and J. K. Mitchell, 7/26/99, (PB2000-101703, A11, MF-A03).

MCEER-99-0016   "Proceedings of the MCEER Workshop on Ground Motion Methodologies for the Eastern United States," edited by N. Abrahamson and A. Becker, 8/11/99, (PB2000-103385, A07, MF-A02).

MCEER-99-0017   "Quindío, Colombia Earthquake of January 25, 1999: Reconnaissance Report," by A.P. Asfura and P.J. Flores, 10/4/99, (PB2000-106893, A06, MF-A01).

MCEER-99-0018   "Hysteretic Models for Cyclic Behavior of Deteriorating Inelastic Structures," by M.V. Sivaselvan and A.M. Reinhorn, 11/5/99, (PB2000-103386, A08, MF-A02).

MCEER-99-0019 "Proceedings of the 7th U.S.- Japan Workshop on Earthquake Resistant Design of Lifeline Facilities and Countermeasures Against Soil Liquefaction," edited by T.D. O'Rourke, J.P. Bardet and M. Hamada, 11/19/99, (PB2000-103354, A99, MF-A06).

MCEER-99-0020 "Development of Measurement Capability for Micro-Vibration Evaluations with Application to Chip Fabrication Facilities," by G.C. Lee, Z. Liang, J.W. Song, J.D. Shen and W.C. Liu, 12/1/99, (PB2000-105993, A08, MF-A02).

MCEER-99-0021 "Design and Retrofit Methodology for Building Structures with Supplemental Energy Dissipating Systems," by G. Pekcan, J.B. Mander and S.S. Chen, 12/31/99, (PB2000-105994, A11, MF-A03).

MCEER-00-0001 "The Marmara, Turkey Earthquake of August 17, 1999: Reconnaissance Report," edited by C. Scawthorn; with major contributions by M. Bruneau, R. Eguchi, T. Holzer, G. Johnson, J. Mander, J. Mitchell, W. Mitchell, A. Papageorgiou, C. Scaethorn, and G. Webb, 3/23/00, (PB2000-106200, A11, MF-A03).

MCEER-00-0002 "Proceedings of the MCEER Workshop for Seismic Hazard Mitigation of Health Care Facilities," edited by G.C. Lee, M. Ettouney, M. Grigoriu, J. Hauer and J. Nigg, 3/29/00, (PB2000-106892, A08, MF-A02).

MCEER-00-0003 "The Chi-Chi, Taiwan Earthquake of September 21, 1999: Reconnaissance Report," edited by G.C. Lee and C.H. Loh, with major contributions by G.C. Lee, M. Bruneau, I.G. Buckle, S.E. Chang, P.J. Flores, T.D. O'Rourke, M. Shinozuka, T.T. Soong, C-H. Loh, K-C. Chang, Z-J. Chen, J-S. Hwang, M-L. Lin, G-Y. Liu, K-C. Tsai, G.C. Yao and C-L. Yen, 4/30/00, (PB2001-100980, A10, MF-A02).

MCEER-00-0004 "Seismic Retrofit of End-Sway Frames of Steel Deck-Truss Bridges with a Supplemental Tendon System: Experimental and Analytical Investigation," by G. Pekcan, J.B. Mander and S.S. Chen, 7/1/00, (PB2001-100982, A10, MF-A02).

MCEER-00-0005 "Sliding Fragility of Unrestrained Equipment in Critical Facilities," by W.H. Chong and T.T. Soong, 7/5/00, (PB2001-100983, A08, MF-A02).

MCEER-00-0006 "Seismic Response of Reinforced Concrete Bridge Pier Walls in the Weak Direction," by N. Abo-Shadi, M. Saiidi and D. Sanders, 7/17/00, (PB2001-100981, A17, MF-A03).

MCEER-00-0007 "Low-Cycle Fatigue Behavior of Longitudinal Reinforcement in Reinforced Concrete Bridge Columns," by J. Brown and S.K. Kunnath, 7/23/00, (PB2001-104392, A08, MF-A02).

MCEER-00-0008 "Soil Structure Interaction of Bridges for Seismic Analysis," I. PoLam and H. Law, 9/25/00, (PB2001-105397, A08, MF-A02).

MCEER-00-0009 "Proceedings of the First MCEER Workshop on Mitigation of Earthquake Disaster by Advanced Technologies (MEDAT-1), edited by M. Shinozuka, D.J. Inman and T.D. O'Rourke, 11/10/00, (PB2001-105399, A14, MF-A03).

MCEER-00-0010 "Development and Evaluation of Simplified Procedures for Analysis and Design of Buildings with Passive Energy Dissipation Systems," by O.M. Ramirez, M.C. Constantinou, C.A. Kircher, A.S. Whittaker, M.W. Johnson, J.D. Gomez and C. Chrysostomou, 11/16/01, (PB2001-105523, A23, MF-A04).

MCEER-00-0011 "Dynamic Soil-Foundation-Structure Interaction Analyses of Large Caissons," by C-Y. Chang, C-M. Mok, Z-L. Wang, R. Settgast, F. Waggoner, M.A. Ketchum, H.M. Gonnermann and C-C. Chin, 12/30/00, (PB2001-104373, A07, MF-A02).

MCEER-00-0012 "Experimental Evaluation of Seismic Performance of Bridge Restrainers," by A.G. Vlassis, E.M. Maragakis and M. Saiid Saiidi, 12/30/00, (PB2001-104354, A09, MF-A02).

MCEER-00-0013 "Effect of Spatial Variation of Ground Motion on Highway Structures," by M. Shinozuka, V. Saxena and G. Deodatis, 12/31/00, (PB2001-108755, A13, MF-A03).

MCEER-00-0014 "A Risk-Based Methodology for Assessing the Seismic Performance of Highway Systems," by S.D. Werner, C.E. Taylor, J.E. Moore, II, J.S. Walton and S. Cho, 12/31/00, (PB2001-108756, A14, MF-A03).

MCEER-01-0001 "Experimental Investigation of P-Delta Effects to Collapse During Earthquakes," by D. Vian and M. Bruneau, 6/25/01, (PB2002-100534, A17, MF-A03).

MCEER-01-0002 "Proceedings of the Second MCEER Workshop on Mitigation of Earthquake Disaster by Advanced Technologies (MEDAT-2)," edited by M. Bruneau and D.J. Inman, 7/23/01, (PB2002-100434, A16, MF-A03).

MCEER-01-0003 "Sensitivity Analysis of Dynamic Systems Subjected to Seismic Loads," by C. Roth and M. Grigoriu, 9/18/01, (PB2003-100884, A12, MF-A03).

MCEER-01-0004 "Overcoming Obstacles to Implementing Earthquake Hazard Mitigation Policies: Stage 1 Report," by D.J. Alesch and W.J. Petak, 12/17/01, (PB2002-107949, A07, MF-A02).

MCEER-01-0005 "Updating Real-Time Earthquake Loss Estimates: Methods, Problems and Insights," by C.E. Taylor, S.E. Chang and R.T. Eguchi, 12/17/01, (PB2002-107948, A05, MF-A01).

MCEER-01-0006 "Experimental Investigation and Retrofit of Steel Pile Foundations and Pile Bents Under Cyclic Lateral Loadings," by A. Shama, J. Mander, B. Blabac and S. Chen, 12/31/01, (PB2002-107950, A13, MF-A03).

MCEER-02-0001 "Assessment of Performance of Bolu Viaduct in the 1999 Duzce Earthquake in Turkey" by P.C. Roussis, M.C. Constantinou, M. Erdik, E. Durukal and M. Dicleli, 5/8/02, (PB2003-100883, A08, MF-A02).

MCEER-02-0002 "Seismic Behavior of Rail Counterweight Systems of Elevators in Buildings," by M.P. Singh, Rildova and L.E. Suarez, 5/27/02. (PB2003-100882, A11, MF-A03).

MCEER-02-0003 "Development of Analysis and Design Procedures for Spread Footings," by G. Mylonakis, G. Gazetas, S. Nikolaou and A. Chauncey, 10/02/02, (PB2004-101636, A13, MF-A03, CD-A13).

MCEER-02-0004 "Bare-Earth Algorithms for Use with SAR and LIDAR Digital Elevation Models," by C.K. Huyck, R.T. Eguchi and B. Houshmand, 10/16/02, (PB2004-101637, A07, CD-A07).

MCEER-02-0005 "Review of Energy Dissipation of Compression Members in Concentrically Braced Frames," by K.Lee and M. Bruneau, 10/18/02, (PB2004-101638, A10, CD-A10).

MCEER-03-0001 "Experimental Investigation of Light-Gauge Steel Plate Shear Walls for the Seismic Retrofit of Buildings" by J. Berman and M. Bruneau, 5/2/03, (PB2004-101622, A10, MF-A03, CD-A10).

MCEER-03-0002 "Statistical Analysis of Fragility Curves," by M. Shinozuka, M.Q. Feng, H. Kim, T. Uzawa and T. Ueda, 6/16/03, (PB2004-101849, A09, CD-A09).

MCEER-03-0003 "Proceedings of the Eighth U.S.-Japan Workshop on Earthquake Resistant Design f Lifeline Facilities and Countermeasures Against Liquefaction," edited by M. Hamada, J.P. Bardet and T.D. O'Rourke, 6/30/03, (PB2004-104386, A99, CD-A99).

MCEER-03-0004 "Proceedings of the PRC-US Workshop on Seismic Analysis and Design of Special Bridges," edited by L.C. Fan and G.C. Lee, 7/15/03, (PB2004-104387, A14, CD-A14).

MCEER-03-0005 "Urban Disaster Recovery: A Framework and Simulation Model," by S.B. Miles and S.E. Chang, 7/25/03, (PB2004-104388, A07, CD-A07).

MCEER-03-0006 "Behavior of Underground Piping Joints Due to Static and Dynamic Loading," by R.D. Meis, M. Maragakis and R. Siddharthan, 11/17/03, (PB2005-102194, A13, MF-A03, CD-A00).

MCEER-03-0007 "Seismic Vulnerability of Timber Bridges and Timber Substructures," by A.A. Shama, J.B. Mander, I.M. Friedland and D.R. Allicock, 12/15/03.

MCEER-04-0001 "Experimental Study of Seismic Isolation Systems with Emphasis on Secondary System Response and Verification of Accuracy of Dynamic Response History Analysis Methods," by E. Wolff and M. Constantinou, 1/16/04 (PB2005-102195, A99, MF-E08, CD-A00).

MCEER-04-0002   "Tension, Compression and Cyclic Testing of Engineered Cementitious Composite Materials," by K. Kesner and S.L. Billington, 3/1/04, (PB2005-102196, A08, CD-A08).

MCEER-04-0003   "Cyclic Testing of Braces Laterally Restrained by Steel Studs to Enhance Performance During Earthquakes," by O.C. Celik, J.W. Berman and M. Bruneau, 3/16/04, (PB2005-102197, A13, MF-A03, CD-A00).

MCEER-04-0004   "Methodologies for Post Earthquake Building Damage Detection Using SAR and Optical Remote Sensing: Application to the August 17, 1999 Marmara, Turkey Earthquake," by C.K. Huyck, B.J. Adams, S. Cho, R.T. Eguchi, B. Mansouri and B. Houshmand, 6/15/04, (PB2005-104888, A10, CD-A00).

MCEER-04-0005   "Nonlinear Structural Analysis Towards Collapse Simulation: A Dynamical Systems Approach," by M.V. Sivaselvan and A.M. Reinhorn, 6/16/04, (PB2005-104889, A11, MF-A03, CD-A00).

MCEER-04-0006   "Proceedings of the Second PRC-US Workshop on Seismic Analysis and Design of Special Bridges," edited by G.C. Lee and L.C. Fan, 6/25/04, (PB2005-104890, A16, CD-A00).

MCEER-04-0007   "Seismic Vulnerability Evaluation of Axially Loaded Steel Built-up Laced Members," by K. Lee and M. Bruneau, 6/30/04, (PB2005-104891, A16, CD-A00).

MCEER-04-0008   "Evaluation of Accuracy of Simplified Methods of Analysis and Design of Buildings with Damping Systems for Near-Fault and for Soft-Soil Seismic Motions," by E.A. Pavlou and M.C. Constantinou, 8/16/04, (PB2005-104892, A08, MF-A02, CD-A00).

MCEER-04-0009   "Assessment of Geotechnical Issues in Acute Care Facilities in California," by M. Lew, T.D. O'Rourke, R. Dobry and M. Koch, 9/15/04, (PB2005-104893, A08, CD-A00).

MCEER-04-0010   "Scissor-Jack-Damper Energy Dissipation System," by A.N. Sigaher-Boyle and M.C. Constantinou, 12/1/04 (PB2005-108221).

MCEER-04-0011   "Seismic Retrofit of Bridge Steel Truss Piers Using a Controlled Rocking Approach," by M. Pollino and M. Bruneau, 12/20/04 (PB2006-105795).

MCEER-05-0001   "Experimental and Analytical Studies of Structures Seismically Isolated with an Uplift-Restraint Isolation System," by P.C. Roussis and M.C. Constantinou, 1/10/05 (PB2005-108222).

MCEER-05-0002   "A Versatile Experimentation Model for Study of Structures Near Collapse Applied to Seismic Evaluation of Irregular Structures," by D. Kusumastuti, A.M. Reinhorn and A. Rutenberg, 3/31/05 (PB2006-101523).

MCEER-05-0003   "Proceedings of the Third PRC-US Workshop on Seismic Analysis and Design of Special Bridges," edited by L.C. Fan and G.C. Lee, 4/20/05, (PB2006-105796).

MCEER-05-0004   "Approaches for the Seismic Retrofit of Braced Steel Bridge Piers and Proof-of-Concept Testing of an Eccentrically Braced Frame with Tubular Link," by J.W. Berman and M. Bruneau, 4/21/05 (PB2006-101524).

MCEER-05-0005   "Simulation of Strong Ground Motions for Seismic Fragility Evaluation of Nonstructural Components in Hospitals," by A. Wanitkorkul and A. Filiatrault, 5/26/05 (PB2006-500027).

MCEER-05-0006   "Seismic Safety in California Hospitals: Assessing an Attempt to Accelerate the Replacement or Seismic Retrofit of Older Hospital Facilities," by D.J. Alesch, L.A. Arendt and W.J. Petak, 6/6/05 (PB2006-105794).

MCEER-05-0007   "Development of Seismic Strengthening and Retrofit Strategies for Critical Facilities Using Engineered Cementitious Composite Materials," by K. Kesner and S.L. Billington, 8/29/05 (PB2006-111701).

MCEER-05-0008   "Experimental and Analytical Studies of Base Isolation Systems for Seismic Protection of Power Transformers," by N. Murota, M.Q. Feng and G-Y. Liu, 9/30/05 (PB2006-111702).

MCEER-05-0009   "3D-BASIS-ME-MB: Computer Program for Nonlinear Dynamic Analysis of Seismically Isolated Structures," by P.C. Tsopelas, P.C. Roussis, M.C. Constantinou, R. Buchanan and A.M. Reinhorn, 10/3/05 (PB2006-111703).

MCEER-05-0010   "Steel Plate Shear Walls for Seismic Design and Retrofit of Building Structures," by D. Vian and M. Bruneau, 12/15/05 (PB2006-111704).

MCEER-05-0011   "The Performance-Based Design Paradigm," by M.J. Astrella and A. Whittaker, 12/15/05 (PB2006-111705).

MCEER-06-0001   "Seismic Fragility of Suspended Ceiling Systems," H. Badillo-Almaraz, A.S. Whittaker, A.M. Reinhorn and G.P. Cimellaro, 2/4/06 (PB2006-111706).

MCEER-06-0002   "Multi-Dimensional Fragility of Structures," by G.P. Cimellaro, A.M. Reinhorn and M. Bruneau, 3/1/06 (PB2007-106974, A09, MF-A02, CD A00).

MCEER-06-0003   "Built-Up Shear Links as Energy Dissipators for Seismic Protection of Bridges," by P. Dusicka, A.M. Itani and I.G. Buckle, 3/15/06 (PB2006-111708).

MCEER-06-0004   "Analytical Investigation of the Structural Fuse Concept," by R.E. Vargas and M. Bruneau, 3/16/06 (PB2006-111709).

MCEER-06-0005   "Experimental Investigation of the Structural Fuse Concept," by R.E. Vargas and M. Bruneau, 3/17/06 (PB2006-111710).

MCEER-06-0006   "Further Development of Tubular Eccentrically Braced Frame Links for the Seismic Retrofit of Braced Steel Truss Bridge Piers," by J.W. Berman and M. Bruneau, 3/27/06 (PB2007-105147).

MCEER-06-0007   "REDARS Validation Report," by S. Cho, C.K. Huyck, S. Ghosh and R.T. Eguchi, 8/8/06 (PB2007-106983).

MCEER-06-0008   "Review of Current NDE Technologies for Post-Earthquake Assessment of Retrofitted Bridge Columns," by J.W. Song, Z. Liang and G.C. Lee, 8/21/06 06 (PB2007-106984).

MCEER-06-0009   "Liquefaction Remediation in Silty Soils Using Dynamic Compaction and Stone Columns," by S. Thevanayagam, G.R. Martin, R. Nashed, T. Shenthan, T. Kanagalingam and N. Ecemis, 8/28/06 06 (PB2007-106985).

MCEER-06-0010   "Conceptual Design and Experimental Investigation of Polymer Matrix Composite Infill Panels for Seismic Retrofitting," by W. Jung, M. Chiewanichakorn and A.J. Aref, 9/21/06 (PB2007-106986).

MCEER-06-0011   "A Study of the Coupled Horizontal-Vertical Behavior of Elastomeric and Lead-Rubber Seismic Isolation Bearings," by G.P. Warn and A.S. Whittaker, 9/22/06 (PB2007-108679).

MCEER-06-0012   "Proceedings of the Fourth PRC-US Workshop on Seismic Analysis and Design of Special Bridges: Advancing Bridge Technologies in Research, Design, Construction and Preservation," Edited by L.C. Fan, G.C. Lee and L. Ziang, 10/12/06.

MCEER-06-0013   "Cyclic Response and Low Cycle Fatigue Characteristics of Plate Steels," by P. Dusicka, A.M. Itani and I.G. Buckle, 11/1/06 06 (PB2007-106987).

MCEER-06-0014   "Proceedings of the Second US-Taiwan Bridge Engineering Workshop," edited by W.P. Yen, J. Shen, J-Y. Chen and M. Wang, 11/15/06.

MCEER-06-0015   "User Manual and Technical Documentation for the REDARS™ Import Wizard," by S. Cho, S. Ghosh, C.K. Huyck and S.D. Werner, 11/30/06.

MCEER-06-0016   "Hazard Mitigation Strategy and Monitoring Technologies for Urban and Infrastructure Public Buildings: Proceedings of the China-US Workshops," edited by X.Y. Zhou, A.L. Zhang, G.C. Lee and M. Tong, 12/12/06.

MCEER-07-0001   "Static and Kinetic Coefficients of Friction for Rigid Blocks," by C. Kafali, S. Fathali, M. Grigoriu and A.S. Whittaker, 3/20/07.

MCEER-07-0002   "Hazard Mitigation Investment Decision Making: Organizational Response to Legislative Mandate," by L.A. Arendt, D.J. Alesch and W.J. Petak, 4/9/07.

MCEER-07-0003 "Seismic Behavior of Bidirectional-Resistant Ductile End Diaphragms with Unbonded Braces in Straight or Skewed Steel Bridges," by O. Celik and M. Bruneau, 4/11/07.

MCEER-07-0004 "Modeling Pile Behavior in Large Pile Groups Under Lateral Loading," by A.M. Dodds and G.R. Martin, 4/16/07.

MCEER-07-0005 "Experimental Investigation of Blast Performance of Seismically Resistant Concrete-Filled Steel Tube Bridge Piers," by S. Fujikura, M. Bruneau and D. Lopez-Garcia, 4/20/07.